Physico-Chemical Characteristics and Radiative Properties of Aerosols over Indian Coastal and Marine Environment

Thesis submitted to

Cochin University of Science and Technology

in partial fulfilment for the award of the Degree of

Doctor of Philosophy
in
Physics

UNDER THE FACULTY OF SCIENCE

by

Aryasree S

SPACE PHYSICS LABORATORY
VIKRAM SARABHAI SPACE CENTRE
THIRUVANANTHAPURAM-695 022
KERALA, INDIA

AUGUST 2016

Dedicated to...

My parents

DECLARATION

I hereby declare that the Ph.D. thesis work titled, ***"Physico-Chemical Characteristics and Radiative Properties of Aerosols over Indian Coastal and Marine Environment"*** is based on the original work carried out by me under the supervision of Dr**. Prabha R Nair,** at Space Physics Laboratory, Vikram Sarabhai Space centre, Thiruvananthapuram and has not been included in any other thesis submitted previously for the award of any degree.

Thiruvananthapuram — Aryasree S

23August 2016 — (Author)

Certified

Dr. Prabha R Nair

Thesis supervisor

Head ACTG & Scientist SG

Space Physics Laboratory

भारत सरकार
अंतरिक्ष विभाग
विक्रम साराभाई अंतरिक्ष केन्द्र
तिरुवनन्तपुरम-695 022
केरल, भारत
फोन : 91-471-2563927
फैक्स : +91-471-2706535
तार/Gram:SPACE

सत्यमेव जयते

Government of India
Department of Space
Vikram Sarabhai Space Centre
Thiruvananthapuram-695 022
Kerala, INDIA
Telephone : +91-471-2563927
Fax : +91-471-2706535
ई-मेल/e-mail: prabha_nair @vssc.gov.in

SPACE PHYSICS LABORATORY

CERTIFICATE

Certified that the thesis titled ***"Physico-Chemical Characteristics and Radiative Properties of Aerosols over Indian Coastal and Marine Environment"*** submitted by **Ms. Aryasree S** in partial fulfilment of the requirements for the Degree of Doctor of Philosophy at Cochin University of Science and Technology carried out by her under my supervision at Space Physics Laboratory, Vikram Sarabhai Space Centre, Thiruvananthapuram is an authentic record of research work and has not been included in any other thesis submitted previously for the award of any degree.

Dr. Prabha R Nair
(Thesis Supervisor)

Thiruvananthapuram
23 August, 2016

भारत सरकार
अंतरिक्ष विभाग
विक्रम साराभाई अंतरिक्ष केन्द्र
तिरुवनन्तपुरम-695 022
केरल, भारत
फोन : 91-471-2563927
फैक्स : +91-471-2706535
तार/Gram:SPACE

सत्यमेव जयते

Government of India
Department of Space
Vikram Sarabhai Space Centre
Thiruvananthapuram-695 022
Kerala, INDIA
Telephone : +91-471-2563927
Fax : +91-471-2706535
ई-मेल/e-mail: prabha_nair @vssc.gov.in

SPACE PHYSICS LABORATORY

CERTIFICATE

Certified that all the relevant corrections and modifications suggested by the audience during the Pre-synopsis seminar and recommended by the Doctoral Committee of the candidate have been incorporated in this thesis.

Dr. Prabha R Nair
(Thesis Supervisor)

Thiruvananthapuram
23 August, 2016

Acknowledgements

It has been a very long journey and there is no word to describe how much I am indebted to those who followed, travelled hand in hand and went ahead along the way. I take this opportunity to express my gratitude for their love support and care.

First and foremost, I am obliged to Dr. Prabha R. Nair, my mentor, for her guidance, wholehearted support and encouragement at each stage of my research. It is her ideas and guidance which helped to cast this thesis in the final form. I am deeply indebted to her for all the knowledge and experience that I have gained from her during this work. I express my deep sense of gratitude to her family for their support during the course of this work.

I would like to thank Dr. Anil Bhardwaj, Director, SPL for his advices and support, as Academic committee chairman during my tenure as research fellow and by providing the facilities for the work at SPL.

I want to extend gratitude to former directors of SPL, Dr. K. Krishna Moorthy, and Prof. R. Sridharan for their valuable suggestions and constant encouragement.

It is my great pleasure to express my deep and sincere thanks to the Academic committee and doctoral committee of SPL for their feedbacks and advices which helped me to evolve in this field. I would like to thank Dr. K. Parameswaran, Dr. Mannil Mohan, Dr. Sudha Ravindran (late), Dr. Radhika Ramachandran, Dr. K. Rajeev, Dr. Geetha Ramkumar, Dr. C. Suresh Raju, Dr. Tarun Kumar Pant, Dr. Rajkumar Choudhary, , Dr. K. Kishore Kumar, Dr. Suresh Babu, Dr. S. V. Sunil Kumar, Dr Siji Kumar, Dr. D. Bala Subrahmanyam, Dr. Kiran Kumar Dr. Siddharth, Dr. Satheesh, Dr. G. Manju, Dr. Sandhya and Dr. Vipin for their feedbacks, advices and criticism especially during the annual reviews which helped me in shaping my thesis better.

It is my pleasure to thank the doctoral committee members from CUSAT, Dr. B Pradeep, Dr. CA Babu, Dr. K Mohan Kumar, Dr Godfrey Loius, Dr Kurian Sajan, Dr Santhosh Raghavan and Head of physics department for their advices and encouragement.

I would like to thank the Atmospheric Technology Division of SPL, particularly, Mr. S. V. Mohan Kumar, Mr. P. Pradeep Kumar, Ms. Sreelatha, Mr. T. P. Das, Mr. Dinakar Prasad, Mr. Pramod, Mr. Ajeesh, Mr. Anumod, Mr. Sam Das, Mrs. Santhi for their wholehearted support and care extended throughout. Special thanks to, Dr. Vijayakumar, Dr. Vineeth, Dr. Mukunda Gogoi, Dr Adityya, Dr Megha, Mr Shobhan Kumar, Mr. Manoj. K Mishra, Ms Mridula, Ms Dhanya, Ms Neha, Dr Uma, Mr Santhosh Muraleedharan , Mr Kandula Subrahmanyam and all the other scientists in SPL for their help and directions at the times I needed.

Special thanks to Dr Prashanth Hegde and Mr Girach Imran for their valuable advices, help and company during my research period. I gratefully remember my seniors cum roommates Dr. Sherine and Dr. Liji M David for their support and love.

Sincere thanks to the library staff of VSSC for the service rendered for literature collection during my research work. I thank Ms. Geetha C., Ms. Suseela, Ms. Sisira, Ms. Shalini, Ms. Prameela, Mr. Watson, Mr. T. K. Vijayan, and all others in office for the administrative and logistic support I have received during my research tenure. I also acknowledge Mr. Asoka Kumar G. S. for his help. I thank Mr. Hari VS and Ms. Indu KR for their sincere and dedicated help in lab and collecting data.

I am extremely thankful to ISRO Geosphere Biosphere Programme for conducting the ICARB campaigns and Indian Climate Research Program for CTCZ campaign, which forms the major dataset for this study. I am thankful to the NOAA for the NCEP data available from their website, http://www.esrl.noaa.gov/psd, the NOAA Air Resources Laboratory for the provision of the HYSPLIT transport and dispersion model (http://www.arl.noaa.gov/ready.html), MODIS Science team of NASA through http://ladsweb.nascom.nasa.gov/, GSFC and TRMM data for the accumulated daily rainfall which have been extensively used in this thesis. I am also grateful to Dr. Sanbhu Namboodiri and Mr. Dileep of the Meteorological Facility of Vikram Sarabhai Space Centre, Thiruvananthapuram, for providing the relevant meteorological data used in this study.

I thankfully remember my seniors Dr. Susan, Dr. Meenu, Dr. Marina, Dr. Bijoy, Dr. Naseema, Dr. Sreeja, Dr. Jai, Dr Sonal, Dr. Lijo, Dr. Veena, Dr Anish, Dr. Raghuram, Dr. Prijith, Dr. Sumod, Asha, Arun, Dr. Tinu, Dr. Anu for their help, care and support. My hearty thanks to my batchmates Madhav, Abhinaw, Neethu, Renju, and Manoj for their encouragement and help. I thank my juniors Lakshmi, Ashok, Ajesh, Muhsin, Jayachandran, Aneesh, Vrinda, Sneha, Freddy, Maria, Lavanya, Ashwathy, Govind, Nalini, Roshny, Edwin and Koushik for their friendship, help and company. I appreciate the support of Ms Sreedevi, Dr Ambili, Ms Kavitha, Ms Aswini, and Mr Nithin. I gratefully remember my teachers and friends during college and school. I cannot forget my friends Surej, Jethin, Athul, Anton, Madhavi, Krishnaraj, Poornima and Kiran for their love and support.

I sincerely thank the Indian Space Research Organization for providing the fellowship to carry out the research activities at Space Physics Laboratory, Vikram Sarabhai Space Centre, Thiruvananthapuram. I warmly thank VSSC library, accounts, transport, canteen and all other supporting facilities.

Above all I thank my parents Sudha and Raju for having faith in me and supporting me in all my endeavors.

Thanks to god almighty for giving me this great opportunity and showing his grace throughout this journey.

Aryasree S
Author

List of Publications

Peer-Reviewed Journals

- Prabha R.Nair, Liji Mary David, **S Aryasree**, and K.Susan George, "Distribution of ozone in the marine boundary layer of Arabian sea prior to monsoon: Prevailing airmass and effect of aerosols "Atmos Environ., 74 (2013)18-28.
- Nair, P. R., S. K. George**, S. Aryasree**, and S. Jacob (2014), Chemical composition of aerosols over Bay of Bengal during pre-monsoon: Dominance of anthropogenic sources, J. Atmos. Sol. Terr. Phys., 109, doi:10.1016/201401004.
- Bindu G, Prabha R Nair, **S Aryasree** and Salu Jacob, 2015, Pattern of aerosol mass loading and chemical composition over the atmospheric environment of an urban coastal station, Journal of Atmospheric and Solar-Terrestrial Physics, 138-139(2016) 121–135, doi.org/10.1016/ j.jastp.2016.01.004
- **S Aryasree**, P. R. Nair, I. A. Girach, and S. Jacob (2015), "Winter time chemical characteristics of aerosols over the Bay of Bengal: Continental influence", Environ. Sci. Pollut. Res., doi:10.1007/s11356-015-4700-7.
- **S Aryasree**, Prabha R Nair, Girach Imran Asatar and Salu Jacob. "Seasonal variations of aerosol chemical composition over the marine environment of Bay of Bengal. J. Geophys. Res (Atmospheres), doi:10.1002/2015JD023418.

Proceedings of Symposia

- **S Aryasree**., Girach Imran A, and Prabha R Nair, Continental influence on aerosols over Bay of Bengal during pre-monsoon and winter, IASTA Bulletin, Vol. 20, 2012.
- **S Aryasree**., Prabha R. Nair, Girach, I. A., and Salu Jacob, Seasonal variation of aerosol chemical characteristics over Bay of Bengal: A Multi Campaign Analysis, IASTA Bulletin vol. 21, ISSN 09714510, Varanasi, 45-48, 2014.
- **S Aryasree** and Prabha R. Nair., Size characteristics of aerosols at a tropical coastal station and association with mesospheric circulation, IASTA Bulletin vol. 21, ISSN 09714510, 42-45, 2014.

Symposium Presentations (National and International)

- Girach Imran Asatar, Prabha R Nair, S Sijikumar and **S Aryasree**, "Trace gases at coastal station and over marine environment: Close association with meteorology",

Indo-US Conference-cum-Workshop on Air Quality and Climate Research, Hyderabad, March 14-24, 2011.

- **S Aryasree**, Prabha.R.Nair and Salu Jacob, "Size distribution and chemical composition of aerosols at the coastal environment of Trivandrum" Poster presented at NSSS, Tirupati, February 2012.
- Prabha.R.Nair, Liji.M.David, **S Aryasree**, Girach Imran Asatar, and S SijiKumar "Role of Mesoscale dynamics in modifying the diurnal variation of trace gases and aerosols at a coastal environment" presented at COSPAR, Mysore, July2012.
- **S Aryasree**, Girach Imran Asatar, Prabha. R. Nair, and Salu Jacob, "Continental influence of aerosols over Bay of Bengal during pre-monsoon and winter" Paper presented at IASTA, Bombay, December 2012.
- **S Aryasree** and Prabha.R.Nair,"Size characteristics of aerosols at a tropical coastal station and association with mesoscale circulation" IASTA, Varanasi, November 2014.
- **S Aryasree**, Prabha.R.Nair, G. I. Asatar and Salu Jacob, "Seasonal Variation of Aerosol chemical characteristics over Bay of Bengal: A multi campaign analysis" IASTA, Varanasi, November 2014.
- **S Aryasree**, Prabha.R.Nair and Salu Jacob, Analytical procedures for measurement of inorganic species in atmospheric Aerosols, ISAS Conference, Kochi, 2014.
- I. A. Girach, Prabha R. Nair, N. Ojha, P. Hegde and **S Aryasree**., Variations in near-surface Ozone over Bay of Bengal during summer-monsoon, 19th NSSS VSSC , Thirvananthapuram, Feb-09-12, 2016.
- Prabha R Nair, Liji Mary David, **S Aryasree** and Kavitha M, Temporal trends of climatically significant atmospheric constituents over Indian region**,** International Conference on Climate Change and Disaster Management, Thiruvananthapuram, India, February 26-28, 2015.
- **S Aryasree**, Prabha. R. Nair, I.A Girach and Salu Jacob, Seasonal variation of near-surface and columnar properties of aerosols over Bay of Bengal, 19th NSSS VSSC , Thirvananthapuram, Feb-09-12, 2016.

.

Contents

Chapter 3- Temporal Changes in Physical, Chemical and Radiative Properties of Near-Surface Aerosols at the Coastal Site Thiruvananthapuram: Role of Changing Sources and Meteorology

Preface

Atmospheric aerosols, the tiny solid or liquid particles of 1nm to 100μm in size, suspended in air, play key roles in weather, climate, hydrological cycle, atmospheric chemistry, the living environment and public health. By scattering and absorbing the incoming solar radiation as well as the outgoing terrestrial radiation, the aerosols alter the radiation balance of the earth-atmosphere system and hence influence the climate. Acting as cloud condensation nuclei, they control the cloud formation processes, cloud microphysical properties and precipitation patterns. Based on their concentration levels and chemical composition, aerosols cause adverse effects on the environment affecting plants, animals, human beings and materials. For the quantitative assessment of the radiative and environmental impacts of aerosols, comprehensive information on their physical and chemical characteristics is essential. Produced by a large variety of natural and anthropogenic sources spread all over the globe and in the atmosphere, their physical and chemical properties exhibit large spatio-temporal heterogeneity. This demands region specific and concurrent measurements of physical and chemical characteristics which is highly limited, particularly over Asian region. In fact the largest uncertainty in assessing the anthropogenic radiative forcing in the earth-atmosphere system arises due to lack of aerosol data on regional scales (IPCC 2013). In this thesis, it is attempted to make simultaneous and collocated measurements of aerosol physical characteristics like aerosol number density, size distribution, mass loading and chemical composition at the tropical coastal site Thiruvananthapuram and the oceanic environments of Arabian Sea (AS) and Bay of Bengal (BoB) to understand their seasonal features, source characteristics, role of meteorology and radiative properties. Based on this in situ measured data, the radiative characteristics such as scattering coefficient, absorption coefficient, extinction coefficient, single scattering albedo and phase functions were estimated for the first time for the study regions. A detailed analysis of the association between the in situ measured near-surface aerosol characteristics and satellite measured columnar properties and their seasonal changes over the chemically and dynamically active oceanic environment of BoB was also carried out.

The thesis is organized in seven chapters. Chapter 1 gives an overview of atmospheric aerosols with emphasis on their sources and production mechanisms, sinks/removal processes along with their physical and chemical characteristics and radiative impacts. A brief review of the various experimental techniques employed for

aerosol characterization also is included in this chapter. This chapter also contains an overview of the studies carried out on the physical, chemical and radiative properties by various investigators all over the globe and in the Indian context. In Chapter 2 is given a detailed description of the various instruments and analytical techniques used for the present study. This chapter also gives details of supporting data used in this work.

Chapter 3 gives the results of a detailed study on the total aerosol number density, size distribution, mass loading of aerosols at Thiruvananthapuram (8.5ºN, 77ºE) giving diurnal changes, seasonal patterns and their association with mesoscale and synoptic scale meteorology. An account of the corresponding changes in chemical composition of aerosols are also provided. Certain interesting inferences made out of the simultaneous measurement of size resolved number density and the mass concentrations of various chemical species, are also presented. Employing the technique of Principal Component Analysis, the seasonally active sources of aerosols were identified and discussed. Based on the measured chemical compositions, chemical models were evolved. Giving these models as the realistic inputs for the Optical Properties of Aerosols and Clouds (OPAC) model, the radiative characteristics of the aerosol system over this tropical coastal site has been computed on seasonal basis for the first time. This chapter ends with an account of the decadal changes in the aerosol number density, size distribution, mass loading and chemical composition from 2003 to 2013.

Chapter 4 deals with the spatial variation of the physical characteristics like total aerosol number density, size distribution and mass loading of aerosols along with their chemical composition over the marine environments of BoB and AS during pre-monsoon months as observed during the ship-based Integrated Campaign for Aerosols gases & Radiation Budget (ICARB) conducted under ISRO-GBP during March-May 2006. All the analysis carried out for the coastal site TVM were repeated for these oceanic regions and quantitative results on the spatial patterns of size-dependent aerosol number density are presented. The regional differences in number size distribution, size dependence of aerosol chemical species and wind dependence of aerosol number density are also discussed. The contributions of natural and anthropogenic components in aerosols were delineated. The region specific chemical models and the corresponding radiative properties over AS and BoB are also presented along with a comparison between the two.

Chapter 5 focuses on the winter time physical, chemical and radiative characteristics of aerosols over BoB including south-east BoB for the first time as

measured on board ship during the ICARB conducted in the winter period, December 2008 to January 2009. The spatial variation of total aerosol mass loading and mass concentration of various chemical species in aerosols were addressed with a view to identify the major sources over this oceanic environment, the transport pathways leading to the observed spatial distribution and to delineate the natural and anthropogenic contributions. A case study of wind induced production of marine aerosols and rain deposition of various species during a rain event occurred during the cruise is also addressed here. Based on the measurements, the region-specific chemical models for the BoB region for this particular season were evolved and the radiative properties estimated for the winter season.

In Chapter 6 is presented the results of a comprehensive study on the spatial and seasonal changes in the in-situ measured near-surface physical and chemical characteristics of aerosols over the marine environment of BoB and the satellite-measured columnar properties. The e^{-1} scale distance for aerosols intruding into the marine region in terms of total mass loading as well as mass concentration of various chemical species are also estimated and presented. Most importantly, apart from the spatial and seasonal behavior of near-surface aerosol characteristics and the columnar properties of aerosols, their mutual dependence were also investigated and results presented.

Chapter 7 presents a brief summary of the work presented in the previous chapters highlighting the major results. In this chapter is also outlined the future scope of the present study and its applications.

Chapter 1

Atmospheric Aerosols: An Overview

1.1 Introduction

In atmospheric science, the term aerosol refers to the solid, liquid or mixed phase (e.g. solid core with liquid shell) particles, suspended in the atmosphere, with sizes ranging from 0.001μm to ~100μm. Atmospheric aerosols are produced by a variety of natural and anthropogenic sources and comprise of sea salt, soil dust, volcanic emissions, meteoric dust, fly ash, fog, smog, haze, smoke, biogenic particles, bacteria, virus, etc. In the atmosphere, aerosols exhibit large heterogeneity in size, shape, chemical composition, production mechanisms, removal processes and their residence time. The annual mean global production of aerosols is estimated to be ~2600 to 12000Tg yr^{-1} [*IPCC, 2013*]. The contribution of aerosols to atmospheric mass is only few parts per billion and forming a minor constituent in the atmosphere, but playing crucial roles in the earth-atmosphere system.

By scattering and/or absorbing the incoming solar radiation and the outgoing terrestrial radiation, aerosols alter the radiation budget of the earth-atmosphere system and thus affect the climate [*Haywood and Boucher*, 2000; *IPCC*, 2013]. Aerosols also act as cloud condensation nuclei (CCN) facilitating cloud formation, influence the cloud distribution and their microphysical properties [*Twomey*, 1977; *Wilson* et al., 2015]. Moreover, scattering of radiation by aerosols cause reduction in visibility, leading to severe traffic problems, particularly during winter.

The aerosol particles are small masses with large surface area upon which many chemical reactions can take place. The role of aerosols in the formation of Arctic haze, Polar Stratospheric Clouds (PSCs) in the Antarctic and their role in the depletion of stratospheric ozone are well established [*Cariolle et al*., 1989; *Achtert et al*., 2012]. Depending on the ability of the aerosol to penetrate the respiratory system and the chemical composition, it often becomes hazardous to human health. Acid rain is another environmental problem resulting from heavy atmospheric loading of acidic species and causing damage to plants and materials. Aerosols also affect the electrical conductivity of the atmosphere by altering the mobility of ions [*Wallace and Hobbs*, 1977]. All the above discussed effects of aerosols depend on their physical as well as chemical properties and the prevailing meteorological conditions.

1.2 Aerosol production mechanisms

Aerosols are formed in the atmosphere by two basic mechanisms namely (1) Bulk-to-particle conversion or mechanical disintegration process and (2) Gas-to-particle conversion. Based on these formation mechanisms, aerosols are classified as primary aerosols and secondary aerosols.

1.2.1 Bulk-to-particle conversion

In Bulk-to-Particle Conversion (BPC) mechanism, aerosol particles are produced from the bulk of materials like soil, rock, water or vegetation and includes processes such as weathering, soil re-suspension, sea spray, volcanic eruption, biological litter, etc. [*Hidy*, 1984]. The exposed materials are chemically or mechanically disintegrated by the action of wind, water or temperature variations. It is well established that the mechanism by which soil dust or crustal material becomes airborne is mainly due to the action of wind [*Gillette et al*; 1978; *Pruppacher and Klett*, 1997; *Kok et al*., 2011]. Another type of mechanical disintegration is the formation of sea salt aerosols from the sea water due to the action of wind on the sea surface. Large quantities of organic materials such as pollen grains, seeds, waxes, spores and leaf fragments released by the plants are also considered to be formed by this mechanism. A significant part of the volcanic aerosols is also the result of mechanical disintegration. Most of these aerosols are emitted directly into the atmosphere and hence called **primary aerosols**.

1.2.2 Gas-to-particle conversion

Gas-to-Particle Conversion (GPC) includes production of particulate matter/aerosols from the gaseous precursors produced mainly as a result of industrial activities, vehicular emissions, biomass burning, plant emissions etc. [*Weber*, 1998; K*erminen, 2008*]. In this process, the phase change occurs either by direct nucleation and condensation of vapour or through chemical reactions between various gaseous substances.

The nucleation processes are basically of three types: (a) homogenous homo-molecular nucleation (b) homogenous hetero-molecular reaction and (c) heterogeneous hetero-molecular reaction [*Prospero et al*., 1983; *Seinfeld and Pandis*, 2006]. The former mechanism involves the formation of new, liquid or solid ultra-fine particles from a gas phase consisting of a single gas species only. The second process involves

the formation of new particles from gas phase consisting of two or more gaseous species. In the third process, growth of pre-existing particles takes place due to condensation of gaseous species on them. A very high super saturation ratio is required for homogenous nucleation whereas relatively low super saturation is sufficient for heterogeneous nucleation. Laboratory estimates [*Whitby*, 1978; *Hegg et al*., 1991] show that >80% of the particle mass production is through condensation on existing particles. Formation of sulphates from SO_2, nitrate from NO_2 and aldehydes, carboxylic acids, dicarboxylic acids, etc. from non-methane hydrocarbons are examples of GPC. Aerosols formed from the condensation of atmospheric gas-phase species are designated as **secondary aerosols**.

1.3 Physical characteristics of aerosols

The radiative, environmental and biological effects of atmospheric aerosols strongly depend on their physical properties such as size, shape, number density and mass concentration [*Seinfeld and Pandis*, 2006]. Aerosols exhibit large variety of sizes covering several orders in magnitude and arbitrary shapes.

1.3.1 Shape

In a strict sense, aerosols are complex 3-dimensional objects with arbitrary shape and they cannot be fully described by a single dimension such as a radius or diameter. In terms of the shapes, aerosols are broadly classified as [*Reist*,1993; *Hinds*, 1999] (a) Isometric particles having all three dimensions equal, like spheres (b) fibres with large length in one dimension and much smaller dimensions in the other two like threads or mineral fibres (c) Platelets having two long dimensions compared to the third dimension, like leaf fragments.

In general, the particles in liquid phase and those formed through GPC are spherical in shape, but those formed by mechanical disintegration processes deviate from spherical shape. In order to simplify the measurement process, it is often convenient to define the particle size using the concept of equivalent spheres. In this case, the particle size is defined by the diameter of an equivalent sphere having the same property as the actual particle, such as volume, mass, settling velocity, electrical mobility etc. [*Harrison and Van Grieken*, 1998]. Two commonly used parameters in this context are the aerodynamic diameter and the Stoke's diameter.

Aerodynamic diameter (d_{ae}) of a particle is defined as the diameter of a sphere of unit density having the same settling velocity as that of the particle. This suggests

that the particles of any shape or density will have same aerodynamic diameter if their settling velocity is same. It is related to the true (geometrical) diameter (d) of the particle through the relation [*Mark*, 1998]

$$d_{ae} = d\left(\frac{\rho}{\rho^*}\right)^{0.5} \qquad 1.1$$

where ρ refers to the density of the particle and ρ^*, density of water droplets. For non-spherical particles, the relation for aerodynamic diameter is given as,

$$d_{ae} = d_v\left\{\frac{\rho\ C_n \mathrm{Re}_p^*}{\rho^* C_n^* \mathrm{Re}_p \phi}\right\} \qquad 1.2$$

where d_v is the diameter of a sphere that has the same volume as that of the non-spherical particle in question, C_n is the Cunningham slip correction factor for the particle, Re_p the particle Reynolds number and ϕ the dynamic shape factor. The terms marked with * refer to the spherical water droplet. **Stokes diameter** is the diameter of a sphere of the same density as the particle in question having the same settling velocity as the particle. The shape critically controls the optical properties of the particle. Non-spherical particles have increased lateral scattering than spherical ones. In almost all theoretical estimation of aerosol effects, they are treated as homogeneous spheres. This assumption simplifies the mathematical treatment of atmospheric effects of aerosols, at the same time providing adequate description of the effects reasonably.

1.3.2 Size

Being originated from various sources and through different formation mechanisms, aerosol sizes vary six orders in magnitude from 10^{-3}µm to 10^{2}µm [*Junge*, 1983; *Prospero et al*., 1983]. Particles greater than 100µm do not remain suspended in the air for long time due to gravitational settling. Aerosol system with all particles having the same size is called **monodisperse**. Aerosol system in which particles of different sizes co-exist is called **poly disperse**. Atmospheric aerosols are poly disperse in nature.

1.3.2.1 Aerosol size distribution

The size distribution of aerosols is a key parameter in the study of aerosol effects on atmospheric processes as well as their adverse impact on environment and human health [*d'Almeida et al*., 1991; *Pope et al*., 2011]. The aerosol size distribution is generally expressed in terms of number density versus size spectrum. The number

distribution n(r), expressed as the number of particles of dN(r) per unit interval of radius and per unit volume, is defined as

$$n(r) = dN(r)/dr \quad 1.3a$$

where dN(r) is the number density of the particles in the radius range dr centred around r. Since the size of aerosols vary over several orders of magnitude, the particle radius is usually expressed in logarithmic scale. The aerosol size distribution in the logarithmic scale is expressed as

$$n^*(r) = dN/d(\ln r) \quad 1.3b$$

where n*(r) represents the number of particles per unit logarithmic radius interval d(lnr) centred on r. The aerosol size distribution is also defined in terms of surface area, mass and volume distribution. The surface area, volume and mass size distributions are expressed as [*Jaenicke, 1984;Curtius,* 2006]

$$S(r) = 4\pi r^2 n(r)dr \quad 1.4$$

$$V(r) = (4/3)\pi r^3 n(r)\, dr \quad 1.5$$

$$M(r) = \rho V(r) \quad 1.6$$

where S(r) is the surface concentration ($cm^2\ cm^{-3}$), V (r) is the volume concentration ($cm^3\ cm^{-3}$) and M(r) is the mass concentration ($g\ cm^{-3}$) and ρ is the bulk density of the particles ($g\ cm^{-3}$). Aerosols number size distributions can be mathematically expressed using different analytical functions such as, inverse power law, modified gamma distribution, log-normal distribution, etc.

1.3.2.1.1 Inverse power law distribution

Junge in 1952 put forward a simple analytic function - the inverse power law- in logarithmic scales to illustrate the number size distribution also called Junge distribution expressed as,

$$n(r) = \frac{dN}{d(\ln r)} = Cr^{-\nu} \quad 1.7$$

Where C is a constant, ν is the power law index which indicates the dominance of larger aerosols over smaller ones with values of ν ranging from 2 to 5 for ambient aerosols [*Jaenicke, 1984*; *Pruppacher and Klett*, 1997]. Power law size distribution suggests that the number of aerosols decreases monotonically with an increase in size.

1.3.2.1.2 Log normal distribution

Most commonly used function to describe ambient aerosol distribution is the lognormal distribution function [*Deepak and Box,* 1982; *d'Almeida et al.,* 1991] given by

$$n(r) = \frac{1}{\sqrt{2\pi}\sigma_m r} \exp\left[\frac{-\left(\ln r - \ln r_m\right)^2}{2\sigma_m^2}\right] \quad 1.8$$

where r_m is the mode radius, σ_m is the standard deviation.

When the size distribution is characterized by multiple modes, it can be represented as

$$n(r) = \sum_{i=1}^{n} \frac{1}{\sqrt{2\pi} r \sigma_{mi}} \exp\left(\left[-\frac{(\ln r - \ln r_{mi})^2}{2\sigma_{mi}{}^2}\right]\right. \quad 1.9$$

Where r_{mi} is the mode radius, σ_{mi} is the standard deviation, for the i^{th} mode. Different modes represent the contributions from different aerosol sources.

1.3.2.1.3 Modified gamma distribution

Another distribution which is widely accepted to describe haze and cloud particles is the modified Gamma distribution function by *Deirmendjian,* [1969] is given by,

$$n(r) = Ar^{k1}\exp(-Br^{k2}) \quad 1.10$$

where A, B, k_1 and k_2 are positive constants. A is the number concentration of particles, B and k_1 represents the fitting parameters. k_2 is an additional parameter determining the shape of the distribution.

Considering the production and removal processes and also the various effects produced by the aerosols in different sizes, they are also divided into three categories as [*Whitby*, 1978],

1. Nucleation mode (Aitken particles) with particle radius $r \leq 0.1\mu m$
2. Accumulation mode (Large particle) with $0.1 \leq r \leq 1\mu m$
3. Coarse mode (Giant particles) with $r > 1\mu m$

In general, particles in the nucleation mode (Aitken particles) are formed by GPC. The Aitken particles play important role in atmospheric electricity [*Twomey*, 1977; *Elias et al.,* 2009]. Particles in the size range 0.1 to 1μm are considered to be in accumulation mode (large particles) which is considered as the most stable size range of atmospheric aerosols. Particles in the nucleation mode eventually get incorporated

into accumulation mode through coagulation or condensation processes. The most important removal mechanism for these particles is the wet removal. In the accumulation mode the particle sizes are comparable to the wavelength of visible light. Hence these particles are optically most effective. Particles in the coarse mode (giant particles) are larger than 1µm and generally smaller than 100µm. These particles are formed by the mechanical disintegration of bulk materials like action of wind on soil or sea water. Figure 1.1 illustrates the different modes (idealized) discussed above.

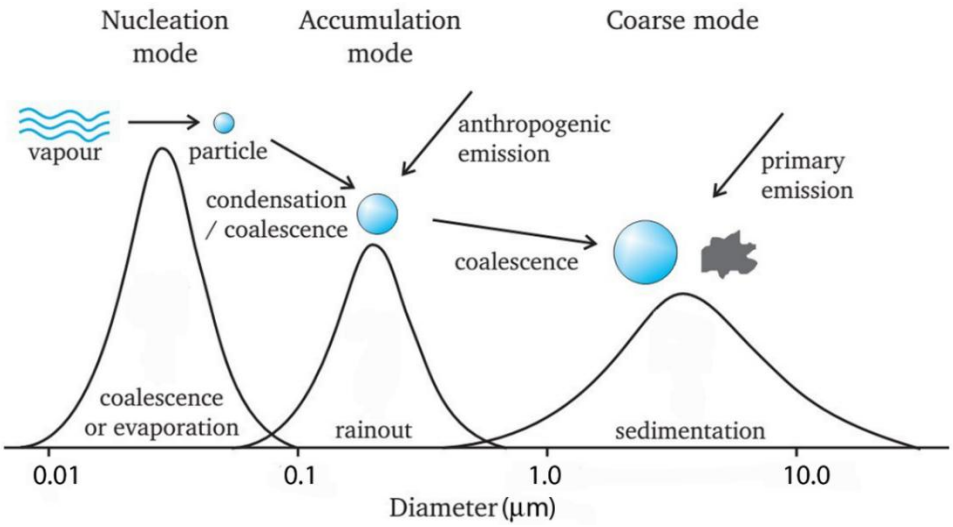

Figure 1.1. *Different modes of aerosols existing in atmosphere along with their respective deposition mechanisms.*

The respiratory system is the most frequently affected organ system by aerosols (also called Particulate Matter). Numerous epidemiological studies show that fine mode aerosols and traffic-related air pollution are correlated with severe health effects, including enhanced mortality, cardio-vascular, respiratory and allergic diseases [*Dockery et al*., 1993; *Ramanathan and Feng*, 2005; *Anderson*, 2009]. In this context, particle size is an important factor [*Englert*, 2004] and hence classified according to the efficiency with which they enter the body through the respiratory system. Particulate Matter (PM) with aerodynamic diameter upto 1µm, 2.5µm and10µm (referred as PM1, PM2.5, PM10) are of biological importance in this context [*Hidy*, 1984; *Pope et al*., 2006, 2011]. The large-sized particles (aerodynamic dia>10µm) entering the nasal passages mostly impinge on the mucous membranes and are removed before reaching larynx and will not pause health hazards. The capture efficiency decreases with decreasing particles size. Particles between 2.5 and 1µm in aerodynamic diameter (PM2.5and PM1 respectively) are capable of getting deposited, in the upper respiratory

tract. Particles with aerodynamic dia≤ 1μm are capable of reaching upto alveoli from where they enter the blood stream and hence are considered as most hazardous.

The aerosol number density and mass concentration exhibit large variation in different environments [*Koepke et al.,* 1997]. In the lower troposphere, the total particle number concentration typically varies in the range of about 10^2–$10^5 cm^{-3}$, and typical mass concentration varies between 1 and 100μg m^{-3}. Aerosol concentrations in the free troposphere are typically 1–2 orders of magnitude lower than in the atmospheric boundary layer. Clean continental air contains less than $3{,}000 cm^{-3}$, polluted continental air typically $50{,}000 cm^{-3}$, and Urban air typically contains $160{,}000 cm^{-3}$. Desert air has about $2{,}300 cm^{-3}$. Clean marine air generally has about $1{,}500 cm^{-3}$. The lowest sea-level values occur over the oceans near the subtropical highs ($600 cm^{-3}$on average, but occasionally below $300 cm^{-3}$). Arctic air has about $6600 cm^{-3}$ and on the Antarctic plateau only $43 cm^{-3}$occur.

1.3.3 Aerosol density

It is the mass per unit volume of aerosol particles. It is a crucial factor in deciding the optical and radiative effects of aerosols. Density of droplets and particles formed from BPC is same as the parent material. Density of the basic materials of aerosols range from ~2.0g cm^{-3} for soot, 2.25g cm^{-3} for sea spray to >2.6g cm^{-3} for minerals [*Hess et al*., 1998; *Hand and Kreidenweis*, 2002; *Seinfeld and Pandis*, 2006].

1.4 Removal mechanisms/Sinks

The particles that are placed continually in the atmosphere are removed from the atmosphere at about the same rate as they are produced (under equilibrium conditions), depending on their sizes by two main processes namely dry deposition and wet removal [*Junge*, 1963; *Slinn and Slinn,* 1980; *Prospero et al*., 1983; *Jaenicke*, 1984]. In addition to this, due to the process of coagulation, particles in certain size range are continuously transformed to another size.

1.4.1 Dry deposition

Dry deposition is the group of deposition mechanisms that transport aerosol particles directly to the surface. In this process the removal of aerosol is caused by gravitational settling, turbulent diffusion and through impaction on vegetation, building and other objects. The main external force acting on the particle is gravity. The dry

deposition of particles takes place in three steps [*Wu et al.,* 1992]. In the first step, particles are transported from the atmosphere down to the viscous sublayer that envelops all surfaces. In the second step, the particles are transported across the viscous sublayer by Brownian diffusion, phoretic effects, interception and inertial forces such as impaction and sedimentation. Finally, the particles interact with the surface: they may adhere or they may bounce off. The dry deposition process is dependent on the aerodynamic characteristics of the particles and the near surface boundary layer features [*Stull et al*., 1988].

The deposition velocity (V_d) defined for aerosol particles as the deposition flux F divided by airborne concentration C_0

$$V_d = -F/C_0 \qquad 1.11$$

The minus sign is required since the downward flux is negative, whereas the dry deposition velocity is defined as positive. This is expressed in units of cm s^{-1}.

The deposition velocity and diffusion coefficient are basic parameters which determine the dry removal rate which is given by [*Harrison and van Grieken*, 1998],

$$V_d = mgB = (4/3)\pi r^3 \rho g \qquad 1.12$$

m is the particle mass, g is the acceleration due to gravity and B is the particle mobility (B=D/kT, D is the diffusion coefficient and k the Boltzmann constant). Thus larger and heavier particles have higher fall velocity compared to the finer ones. The dry deposition process also depends on atmospheric conditions and surface characteristics.

1.4.2 Wet removal

Wet removal of aerosol particle involves two processes [*Seinfeld and Pandis,* 2006] (*i*) below-cloud scavenging (wash out) and (*ii*) in-cloud scavenging (nucleation scavenging or rain out). The capture of aerosol by the falling hydrometeors (rain, snow, cloud and fog drops) is called below cloud scavenging. In-cloud processes consist of activation of aerosols as cloud condensation nuclei (CCN), attachment of aerosols to the pre-existing cloud drops and removal of aerosol containing cloud droplets produced by the first two processes by large falling hydrometeors. Wet removal is one of the most important removal mechanisms of aerosols in the size range of 0.05 to 3µm [*Jaenicke*, 1984]. These processes are important in lower troposphere where cloud formation take place. The aerosol mass removed by wash out is significantly lower in magnitude than that by nucleation scavenging [*Flossman et al*., 1985; *Flossman and*

Pruppacher,1988]. Wet removal is 30 times more efficient than dry deposition in removing aerosol mass from the atmosphere *Jaencike,* [1984].

1.4.3 Coagulation

Coagulation is the process by which aerosol particles undergoing random motion collide and coalesce to form larger particles. Thus coagulation leads to a transformation of particles from small sizes to larger ones. Any mechanism which induces a relative velocity between particles causes coagulation. Such processes include Brownian motion, shearing flow of fluid, turbulent motions and differential particle motion associated with external force fields. Particles undergoing Brownian motion have a finite probability of colliding and sticking together. This sticking probability is a function of their shape, surface condition, relative humidity of air, presence of foreign vapours in air and several other factors. This process is primarily important for particles in the size range 0.1 to 1μm [*Junge*, 1963; *Seinfeld and Pandis*, 2006]. Coagulation is more effective for large population of small particles rather than small population of large particles.

1.5 Aerosol residence time

Residence time of aerosols indicates the time for which the aerosol particle is suspended as entity. It also accounts for the measure of the time the particle spends chemically in the atmosphere, and the measure of the spatial and temporal variation of that species. It is also defined as the ratio of steady state mass of aerosol to the rate of mean input or output or as the ratio of the number of particles present to the rate of production/loss at a given time under steady state. The production mechanism as well as the removal mechanism control the residence time of aerosols in the atmosphere [*Jaenicke*, 1984]. The mathematical formulation for residence time for a first order removal process is,

$$\tau_R = M/S \qquad 1.13$$

where τ is the residence time, M is vertically-integrated aerosol concentration (also called the aerosol burden or column), *S* is the source flux and *R* is the removal or sink flux. If the source and sink terms are averaged over a long period, they should be balanced. Hence the residence time can be computed using S or R. But as the aerosol particle is moved to another size bin by transformation processes like coagulation, condensation or evaporation, its influence on atmospheric processes changes.

[*Jaenicke*, 1984] developed, an empirical size-dependent model from a combination of individual estimates.

$$\frac{1}{\tau} = \frac{1}{C_c}\left(\frac{D}{D_{max}}\right)^2 + \frac{1}{C_d}\left(\frac{D}{D_{max}}\right)^{-2} + \frac{1}{\tau_{wet}} \qquad 1.14$$

Where *Cc* and *Cd* are constants associated with coagulation and sedimentation having a value of 1.28 $\times 10^8$s, *D* is the particle diameter, *Dmax*= 0.6μm is the diameter of particle with maximum residence time and τ_{wet} is the residence time for wet removal of particles, which depends mainly on the altitude.

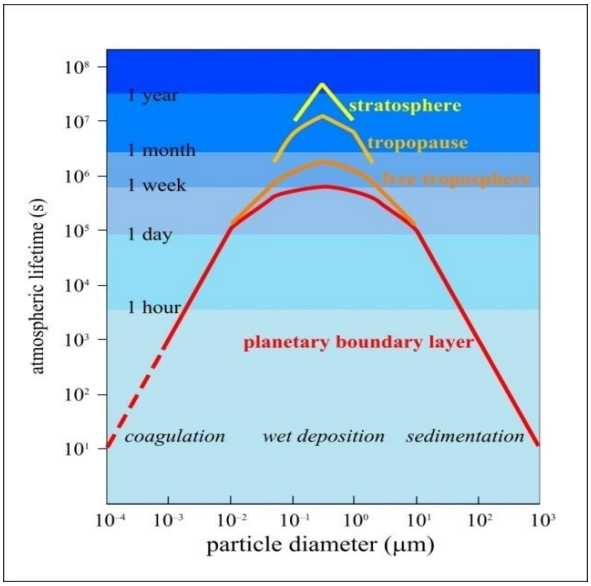

Figure 1.2.*Schematic illustrating the size dependent residence time of aerosols as a function of altitude [Jaenicke,1984].*

Figure 1.2 shows a schematic illustrating the size dependent residence time of aerosols as a function of altitude in the atmosphere. In the troposphere, the smallest and largest aerosols have residence times of hours to days, while the bulk of the aerosols in the intermediate size range have residence times of days to 1–2weeks. Shortest residence times are encountered in the planetary boundary layer and longest in stratosphere. The particles in the radius range 0.1-1.0μm remains airborne for longer time and have longer residence time. Based on the residence time, the possible horizontal displacement is estimated as ~ 8km for aerosols with radius ~ 0.001μm and ~ 8000km for those in the radius in the range of 0.1-1.0μm [*Jaenicke*, 1984].

1.6 Aerosol sources

Atmospheric aerosols originate from a wide variety of natural and anthropogenic sources. The natural sources include oceans, soil/earth's crust,

volcanoes, forest fires, meteors, extra-terrestrial dust, vegetation and other biological species. Industrial activities, vehicular emissions, fossil fuel burning, agricultural activities and associated biomass burning constitute major anthropogenic sources.

1.6.1 Natural sources

1.6.1.1 Oceanic aerosols

Oceans covering 70% of the earth's surface form largest source of natural aerosols [*Warneck*, 1988] with the annual emission varying from 1400-6800Tg [*IPCC,* 2013]. Oceanic aerosols are primarily composed of in-situ generated sea salt particles, produced by the action of wind on the sea surface [*Exton et al.*, 1985], and non-sea salt particles, formed as a result of oceanic biogenic activities [*Charlson et al.*, 1987; *Savoie et al.*, 1989]. Sea-salt aerosols are produced through wind stress on the ocean surface resulting in the direct injection of sea-spray aerosols into the atmosphere through bursting bubbles and/or wind tearing off the wave crests [*Lewis and Schwartz*, 2004]. Depending on their production mechanism, there are three sources for seaspray aerosols, namely film drops, jet drops, and spume drops [*Blanchard*, 1983; *Monahan et al*., 1982; *Wu*, 1993]. As wind blows over the ocean, waves break and entrain air into the water forming clouds of bubbles. Once formed these bubbles start rising to the surface due to their buoyancy and break up and form small droplets called film droplets which evaporate and particles are formed generally with diameters less than ~0.3μm [*Wu*, 1993; *Andreae*, 2002]. The bursting of an air bubble at the water surface also produces a jet of water that rises rapidly from the bottom of the collapsing bubble cavity, which break up into a number of jet drops [*Andreae*, 2002] which also evaporate forming sea-salt particles. At higher wind speeds, above $9ms^{-1}$, the tearing of wave crests results in the injection of ultra-large spume sea-salt particles [*Monahan et al*., 1982; *Smith et al*., 1989; *Wu*,1993] into the marine boundary layer. The sea salt production is strongly dependent on wind speed [*Exton et al*., 1985; *O'Dowd and Smith*, 1993]. Depending on the RH, the particles exist either as solution droplet or solid particles which constitute the sea salt aerosols.

When formed the sea-salt aerosols have the composition of sea water (Figure 1.3). But eventually they undergo several physical and chemical transformations. The major chemical compositions of sea salt aerosols are NaCl, KCl, $CaSO_4$, $(NH_4)_2SO_4$ etc. [*Lewis and Schwartz*, 2004]. Sea salt aerosols can uptake water and grow in size also.

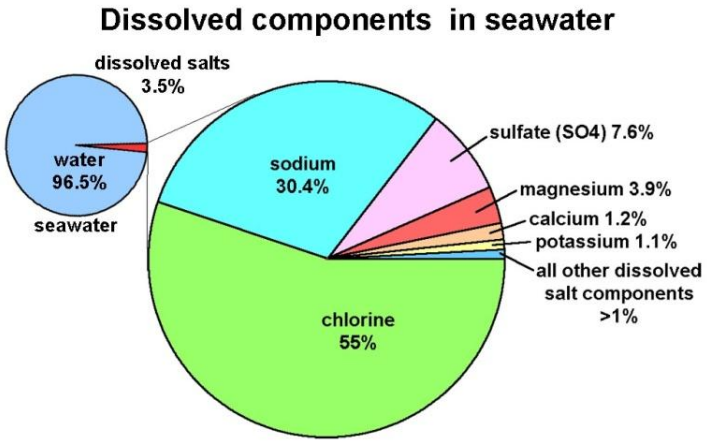

Figure 1.3.*Chemical composition of sea water.*

1.6.1.2 Oceanic non-sea salt aerosols

The dimethyl sulphide (DMS) produced by the marine phytoplankton forms a major precursor for the formation of non-sea salt aerosols in the marine environment [*Charlson et al*., 1987; *Savoie et al.*, 2002; *O'Dowd*, 2011]. Solar induced heating of oceanic surface layers boost the phytoplankton activity and the DMS produced gets oxidized by radicals like OH, in presence of solar UV to form SO_2 which in turn is transformed to sulphate aerosols and methane sulphonate [*Charlson et al*., 1987; *Quinn and Bates*, 2011]. The non-sea-salt sulphate particles thus formed in the marine boundary layer are hygroscopic (water active) in nature. Acting as CCN, these sulphate aerosols increase the earth's albedo, thus induce dimming and as a result, less sunlight reaches the ocean surface and hence temperatures drops. As a result, the phytoplankton activity decreases, DMS production falls and clouds dissolve. Thus DMS, acts as a feedback mechanism that operates between ocean ecosystems and the Earth's climate that keeps ground-level temperature within a range suitable for life. This is called CLAW hypothesis in the name of Charlson, Lovelock, Andreae and Warren who formulated this [*Charlson et al*., 1987]. Oceans also directly inject significant amount of organic aerosols depending on biological activity in ocean waters and the global emission rate has been estimated to lie in the range 2 to 20Tg yr^{-1} [*Gantt et al*., 2011].

1.6.1.3 Windblown soil/mineral dust

The soil particles are produced mainly by disintegration of aggregates of larger soil/rock particles due to weathering and mobilized by strong winds [*Kok et al.,* 2011]. These particles consist of materials derived from the earth's crust, and are therefore rich

in oxides of iron, calcium, and aluminium and hence referred as mineral dust. Factors determining whether soil particles can be aerosolized includes wind velocity and surface conditions of the terrain [*Gillette,* 1978 *Usher et al*., 2003; *Kurosaki and Mikami*, 2007]. Major sources of mineral dusts are deserts, dry lakebeds, semi-arid desert fringes and drier regions where vegetation is less or tilled soil surfaces [*Choobari et al*., 2013]. Wind speeds exceeding 0.5ms^{-1} are capable of lifting soil particles as large as ~2μm in size [*Gillete, 1978*; *Kok et al.,* 2011]. About 75% of the global mineral dust emissions are found to be of natural origin, while 25% are related to anthropogenic (primarily agricultural) emissions *Ginoux et al*., [2012]. The northern hemisphere generates ~90% of global dust where it is deposited as well [*Ginoux et al*.,2012]. The long-range transport of mineral dust by convection currents and general circulation systems make these particles present at locations far from their sources [*Choobari et al*., 2013 and reference therein]. For example transport of mineral dust from Africa to South Indian Ocean, from West Asia (Arabian region, Afghanistan etc.) to Arabian Sea, from China across the Pacific, from Australia over to Indian Ocean, are identified [*Prospero et al.,*1983; *Tyson et al.*,1996; *Satheesh and Srinivasan*,2002; *Mishra et al*., 2013].

The transports of mineral dust over to the pristine marine environments and the subsequent contamination have resulted in regional radiative forcing over these regions [*Dey et al*.,2004; *Sicard et al*., 2014]. It is estimated that on an average 1000-4000Tg of mineral aerosol are emitted into the atmosphere annually [*IPCC,* 2013]. Since these particles are generated at the earth's surface and are mostly large-sized, they are mostly confined within the troposphere.

In general, soil dust is rich in oxides of Fe, Ca, Al, silica and many other minerals depending on the region of their origin. Generally Fe and Al are considered as tracers for mineral dust and aerosols of crustal origin. On a global scale the major sources of mineral dust include Sahara Desert and Thar Desert which lie along the tropical belt.

1.6.1.4 Volcanic aerosols

Volcanic eruptions inject enormous quantities of gases and particulate matter/aerosols in the atmosphere. Contrary to the other aerosol sources, volcanic aerosols often reach up to stratospheric altitudes and are capable of producing long term climate impacts [*Hoffmann*, 1988; *Sato et al*., 1993]. Primary particles ejected from volcanic eruptions are mainly crustal materials and ash. In addition, huge amounts

of sulphur bearing gases like SO_2, COS, H_2S and F, Cl, water vapour get injected into the atmosphere upto stratospheric regions where they get converted to particles like H_2SO_4 droplets [*Vernier et al.,* 2011]. The plume of the eruption of Pinatubo in 1991 has reached 40km height. Particles and gases that enter the stratosphere remains there for a long time (several years) and hence have a strong impact on climate [*Nagai,* 2010]. Eruption of Mt. Pinatubo in 1991 has produced an average global cooling of about 0.5K [*Timmreck,* 2012].

1.6.1.5 Bio aerosols

Bio aerosols are of biological origin and include viable (living) and non-viable (dead) cells. Primary biogenic aerosol consists of plant debris (cuticular waxes, leaf fragments, etc.), humic matter, and microbial particles (bacteria, fungi, viruses, algae, pollen, spores, etc.). Vegetation also emit vapours of Volatile Organic Compounds (VOCs) which condense and form particles. These emissions include a wide range of hydrocarbons like terpenes, isoprenes, α-pinene, β-pinene, etc., which get oxidized to form organic aerosols [*Prospero*, 2002]. Plants, soil, water, and animals (including humans) all serve as sources of bio aerosols. Some bio aerosols, when breathed in, can cause serious health issues.

1.6.1.6 Extra-terrestrial Dust

The extra-terrestrial dust form one of the principal components in the natural background level of aerosols in upper atmosphere with an influx of 10Tg yr^{-1} [*d'Almeida*, 1991]. These particles originate from the debris of meteor showers, comets and inter planetary medium that enter the atmosphere. Even though their contribution to the total aerosol mass in the atmosphere amounts to be only a few percent, it is significant at higher altitudes. Their presence is visualized as the zodiacal light caused by the scattering of sunlight at high altitudes. The residence time of these particles ranges from several months to years. These particles can also reach the troposphere through processes like sedimentation/gravity settling. Extra-terrestrial/interplanetary dust consists of solid particles ranging from ~0.01 to 100 μm in diameter. Elemental composition analysis of extra-terrestrial or meteoritic dust showed the presence of Fe, Si, Mg, S, Ar, Ca, Ni, Al, Na, Cr, Mn, Cl, K, Ti and Co [*Morlok et al.*, 2006].

1.6.2 Anthropogenic aerosols

Aerosols are emitted from a wide range of man-made sources, the most significant sources being vehicular traffic, fossil fuel combustion, industrial activities,

residential combustion, agricultural slash burning, human induced forest fires, public power generation, wind erosion of tilled land, use of fertilizers and pesticides and waste incineration [*Wolf and Hidy*, 1997;*Wallace and Hobbs*1977; *Hidy,* 1984]. After industrial revolution, a sudden increase is seen in the anthropogenic emissions [IPCC 2007; 2013]. Generally, anthropogenic activities produce a wide variety of aerosol precursor gases like NO_x, SO_2, NH_4, and VOC's which get converted to aerosols. Hence most of the anthropogenic aerosols are produced through the GPC mechanism and particles formed are in fine mode (dia<1μm). Major anthropogenic contributions to aerosols include sulphates, organic species, black carbon, nitrates and trace metals/minerals, details of which are given in section 1.7.

1.6.2.1 Biomass Burning

Biomass refers to materials produced by living organisms like vegetation, dead wood, animal dung, peat, etc. Biomass burning includes (1) naturally occurring forest fires and lightning-induced fires that release particulate matter in the atmosphere and (2) burning of the world's living and dead vegetation including forests, savannas for land clearing, land use change, agricultural lands after harvesting, use of wood and dung for heating, cooking, production of charcoal etc. [*Cachier et al.,* 1995; *Liu et al.,* 2000]. The emissions depend generally on the type of ecosystem, the moisture content of the vegetation, and the nature of the fire. About 49.1Tg of biomass burning aerosols are emitted globally [IPCC 2013; *Grainer*, 2011]. Biomass burning produces primary aerosols in the form of ash, charcoal and secondary aerosols consisting of soot, SO_4, NO_3 and organics [*Schwartz et al*.,1995; *Tsigaridis et al*., 2006; *Liu and Wang*, 2010]. Majority (>90%) of biomass burning is human initiated and it has increased significantly over the last 100 years. It is established that the periodically occurring Indonesian fires increase the aerosols levels several times [*Ott et al.,* 2009].

1.6.2.2 Radioactive Aerosols

Radioactive aerosol refers to a radioactive dispersed phase of particle in air with natural or artificial origin. Natural radioactive aerosols form as a result of the decay of radon isotopes emitted from the soil surface into the atmosphere, as well as during the interaction of particles of cosmic radiation with the atoms of elements in the air [*Papastefanou*, 2008]. The radioactive atoms thus formed precipitate onto particles of non-radioactive atmospheric dust. In addition, dust containing radioactive isotopes of potassium, uranium, and thorium is carried from the soil surface into the atmosphere by

winds. A small quantity of radioactive aerosols enters the atmosphere with cosmic dust and meteorites [*Schery*, 2001]. Artificial radioactive aerosols contain fission products and radioactive isotopes with induced radioactivity which are formed from nuclear explosions [*Ogorodnikov*, 2002], nuclear power plants, industrial or accidental radioactive emissions at atomic industry plants, in uranium mines and enrichment plants.

Aerosol Type	Emission flux (per year)
Natural primary aerosols	
Desert dust	1000-4000Tg
Sea spray	1400-6800Tg
Biomass burning aerosols	20-35Tg
Terrestrial primary biogenic aerosols	Order of 1000Tg
Including bacteria	40-1800Gg
Including spores	30Tg
Precursors of natural secondary aerosols	
Dimethylsulphide (DMS)	20-40Tg S
Volcanic SO_2	6-20Tg S
Terpenes	40-400Tg
Anthropogenic primary aerosols	
Industrial dust	40-130Tg
Biomass burning aerosols	50-90Tg
Black carbon (from fossil fuel)	6-10Tg
Organic carbon (from fossil fuel)	20-30Tg
Secondary Organic Aerosol	20-380Tg

Table 1.1. *The major aerosol sources and their emission fluxes (IPCC 2007;2013).*

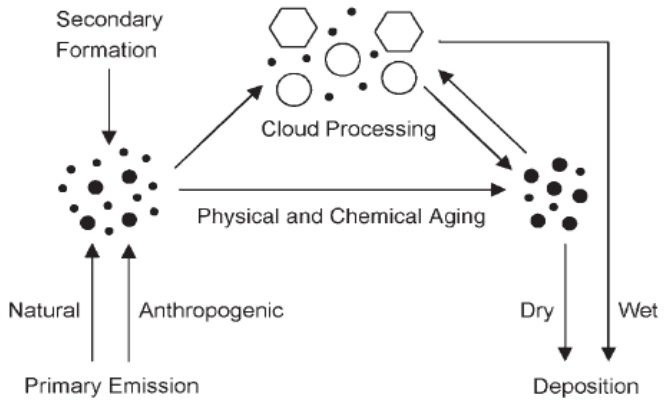

Figure 1.4. *Schematic of aerosols undergoing various physical and chemical interactions and transformations [Poschl,2005].*

In the atmosphere, aerosols undergo various physical and chemical interactions and transformations like changes of particle size, structure, and composition called

atmospheric aging (Figure 1.4). On a global scale the natural aerosols accounts three to four times larger than anthropogenic ones, but regionally anthropogenic emissions are significant [*Charlson et al*., 1992*;* IPCC, 2013] and often exceeds that of natural ones. The major aerosol sources and their emission fluxes per year as from IPCC 2013 are given in Table 1.1.

1.7 Chemical Composition of aerosols

Chemical composition of aerosols system is the most crucial parameter in deciding the radiative, climatic and biological impacts of aerosols. Aerosols comprise of large number of inorganic and organic components. In general, the predominant chemical components in atmospheric aerosols are sulphates, nitrates, sea salts, mineral dust, ammonium compounds, organic species, black carbon or elemental carbon and other carbonaceous particles, each of which typically contribute about 10–30% of the overall mass load [*Colbeck*, 2008]. Brief accounts on the formation mechanism of major species are given below.

1.7.1 Sulphates

SO_2 is the major source for sulphates produced by GPC which is formed in atmosphere naturally as well as anthropogenically. The major contributor to the sulphate burden is anthropogenic emissions. Sulphates are formed by the homogeneous gas phase oxidation of SO_2 by OH radical through various reactions. Other sulphur bearing gases like H_2S, CS_2, Di-Methyl Sulphide (DMS) also gets converted to SO_2 which is further oxidized photochemically to sulphuric acid which in turn forms sulphates. The reaction sequence is as follows [*Pitts and Pitts*, 2000]:

$$\begin{aligned} SO_2 + OH + M &\rightarrow HSO_3 + M \\ HSO_3 + O_2 &\rightarrow SO_3 + HO_2 \\ SO_3 + H_2O &\rightarrow H_2SO_4 \end{aligned} \qquad 1.15$$

Over continental regions where gaseous NH_4^+ is present H_2SO_4 transforms to ammonium sulphate and ammonium bisulphate. Over marine environment the non-sea-salt sulphates are formed through the oxidation of DMS [*Charlson et al*., 1987].

1.7.2 Nitrates

Nitrate is the end product of wide variety of reactions in the atmosphere involving trace gases like NO_x, N_2O, N_2O_3, NH_3, N_2O_4, etc. The most common particulate form of nitrate is ammonium nitrate (NH_4NO_3) [*Andreae et al*., 2000] and in

sea salt rich environment it exists as $NaNO_3$.The most common precursor of nitrates are NOx (NO+NO2), produced anthropogenically from fossil fuel combustion or naturally by thermo-chemical production from lightning discharges and emissions from soil [*Price et al.*, 1997]. About 50% of this NOx becomes oxidized to nitric acid by reacting with OH radical during day time or with water vapour during night time [*d'Almeida, et al., 1991*].

$$\begin{aligned} NO_2 + OH &\rightarrow HNO_3 \quad \text{(Day time)} \\ NO_2 + O_3 &\rightarrow NO_3 + O_3 \\ NO_3 + NO_2 &\leftrightarrow N_2O_5 \quad \text{(Night time)} \\ N_2O_5 + H_2O &\leftrightarrow 2HNO_3 \end{aligned} \qquad 1.16$$

1.7.3 Carbonaceous aerosols

Carbonaceous aerosols can be categorised as (1) Organic aerosols (2) Elemental carbon or Black carbon and (3) the inorganic carbonates. Traditionally the Total Carbon (TC) is defined as the sum of Organic Carbon (OC) and Elemental Carbon (EC). Carbonaceous aerosols account for 18 to 80% of atmospheric aerosols and exhibit a wide range of molecular structures, [*Pitts and Pitts*, 2000; *Gelencser*, 2004; *Orellena et al.*, 2011].

The natural sources of OC include disintegration and dispersion of bulk plant/algal material while industry and vehicular emission constitute the anthropogenic source. The contribution of natural organic compounds varies from 20-90% depending on the source [*Zhang et al.*, 2007]. Depending on their origin, OC components also classified as primary or secondary. Primary organic aerosol (POA) components are directly emitted in the condensed phase (liquid or solid particles) or as semi-volatile vapours, which are condensable under atmospheric conditions. The main sources of POA particles and components are natural and anthropogenic biomass burning, fossil-fuel combustion and wind-driven or traffic-related suspension of soil and road dust, biological materials, sea spray, and spray from other surface waters with dissolved organic compounds [*Kanakidou et al,* 2005]. Primary production also includes biological microbes such as bacteria, viruses, and fungal spores mostly produced on surface of plants. Secondary organic aerosol (SOA) components are formed by chemical reaction and gas-to-particle conversion of volatile organic compounds (VOCs) in the atmosphere, which may proceed through different pathways [*Poschl*, 2005; *Kroll and Seinfeld*, 2008]. Organic aerosols include both water-soluble organic

carbon (WSOC) and water-insoluble organic carbon WIOC. In the atmosphere WSOC amounts to 30-80 % of OC [*Kondo et al*., 2007].

Elemental Carbon (EC)/Black carbon (BC) is the product of incomplete combustion of hydrocarbon or pyrolysis and have graphite-like structure [*Chow et al*., 2004; *Jacobsen et al*, 2000; *Poschl et al.,* 2005; *Colbeck*, 2008]. The absorbing nature of BC makes it a potential climate forcing agent, estimated to be the second largest contributor to global warming after carbon dioxide (CO_2) on a global scale [*Jacobson* et al., 2000; *Hansen et al.*, 2000]. OC/BC or OC/EC ratio is used to identify their sources. In fossil fuel combustion, the OC/BC ratio is closer to unity and for biomass burning, this ratio ranges from 3 to 9 [*Turpin and Lim,* 2001].

1.7.4 Trace Metals

In polluted environments, considerable quantities of trace metals are observed. The major sources include combustion of fossil fuels, incineration of municipal and industrial hazardous wastes, smelters, refineries and other metallurgical industries. Quantitative estimates of trace element emissions like Cd, Cu, Pb, Mn, Hg, Ni, Ti, V, Zn, etc. from anthropogenic sources have been reported from various locations [e.g. *Pacyna*, et al., 2007; *Witt et al*., 2002]. Among the trace elements, Pb shows large spatial variability. It is formed mainly from leaded gasoline, manufacturing of ceramics, pigments, paints, glass, plastics, etc. and storage batteries and certain alloys like brass, solder, etc. Trace metals are formed from soil dust also.

As a result of coagulation between particles of different composition and due to the uptake of gases into pre-existing nuclei, particles of mixed composition are formed in the atmosphere. Depending on their mechanism of formation, aerosols can be grouped as externally mixed or internally mixed. While the "*external mixture*" refers to non-homogeneity in the chemical composition of the particle, the "*internal mixture*" refers to a homogeneous mixture of different chemical species in the same particle.

1.8 Refractive indices

The refractive index of aerosols depends on their chemical composition. Refractive index of aerosols is generally expressed as a complex number and is wavelength dependent. For non-absorbing aerosol particles, the imaginary part is zero and refractive index is a real number. For absorbing aerosols, refractive index is represented by a complex number with significant imaginary part. For the commonly observed aerosol components in the atmosphere, real part of the refractive index is in the visible

and near IR wavelength is between 1.3 and 1.8, whereas imaginary part lies in the range 5×10^{-9} to 5×10^{-1} [*Shettle and Fenn*, 1979]. The imaginary part of the refractive index is found to be maximum for soot or BC and minimum for sea salt particles.

1.9 Radiative impacts of aerosols

Atmospheric aerosols interact with the incoming solar short wave radiation and the outgoing terrestrial long wave radiation through the two basic processes of absorption and scattering [*McCartney*, 1976]. The effects of these processes range from the degradation of visibility to changes in the radiation budget of the earth-atmosphere system.

Absorption is the process in which the incident radiation is fully or partially extracted by the interacting particle, which is generally followed by emission. Absorption is spectrally selective and discrete. The absorption of radiation by aerosols results in heating of the atmosphere. The main absorbers of solar radiation are carbonaceous particles, particularly the BC. Certain minerals like Fe, Ti, Si etc. also show absorption characteristics [*Usher et al*., 2003].

Scattering is the process by which a particle in the path of an electromagnetic radiation extracts energy from the incident wave and reradiates that energy in all the directions. The scattering process depends on the size, shape and chemical composition of aerosols as well as the wavelength of incident radiation. Depending on the size of the particle relative to the wavelength (λ) of incident radiation, a dimensionless size parameter (α) is defined as,

$$\alpha=2\pi r/\lambda \qquad 1.17$$

(where r is the radius of the scatterer). Scattering by atmospheric particles are mainly is of two types namely Rayleigh scattering and Mie scattering [*McCartney, 1976]*.

1.9.1 Rayleigh scattering

When the particles interacting with the electromagnetic radiation are homogenous spheres with size much smaller than that of the wavelength of incident radiation (α <<1), the scattering process is termed as Rayleigh scattering. In the atmosphere, the chief Rayleigh scatterers are the air molecules and hence this type of scattering is also called molecular scattering. In this type of scattering, the intensity of scattered radiation also varies inversely as the fourth power of wavelength. Intensity of the scattered radiation also depends on the polarization characteristics of the incident

light. The scattered light intensity in Rayleigh scattering for unpolarized light is proportional to (1 + cos2θ) where θ is the scattering angle, i.e. the angle between the directions of the incident and scattered rays. The angular scattering pattern for unpolarized light is shown in Figure 1.5.

1.9.2 Mie scattering

Atmospheric aerosols are comparable or larger in size compared to wavelength in the visible or IR region. The characteristic features of scattering of electromagnetic radiation by particles with sizes comparable to the wavelength of incident radiation or when α~1, are described by Mie theory [*Mie*,1908]. Mie Theory assumes the particles to be isotropic and spherical with arbitrary size and refractive index [*Bulrich*, 1964; *McCartney*, 1976]. The scattering pattern essentially depends on particle size and refractive index. The main features of Mie scattering include increase of forward scattering with increase in particles size and weak wavelength dependence of scattering as the particle size increases [*Bulrich*, 1964; *McCartney*, 1976]. Mie scattering theory provides a generalized approach, has no particle size limitations and converges to the limit of geometric optics at large particle sizes.

Based on the theory of Mie, the differential scattering cross sections σ_{sc} are defined in terms of the angular intensity functions i_1 and i_2, as given by [*Bulrich*, 1964; *Born and Wolf* 1996],

$$\sigma_{sc}= \frac{\lambda^4}{8\pi^2}(i_1 + i_2) \qquad 1.18$$

where

$$i_1=\left|\sum_{n=1}^{\infty}\frac{2n+1}{n(n+1)}[a_n\pi_n(\cos\theta)+ b_n\tau_n(\cos\theta)]\right|^2 \qquad 1.19$$

$$i_2 =\left|\sum_{n=1}^{\infty}\frac{2n+1}{n(n+1)}[a_n\,\tau_n(\cos\theta) +\ b_n\pi_n(\cos\theta)]\right|^2 \qquad 1.20$$

In terms of Mie coefficients a_n and b_n, σ_{sc} is expressed as,

$$\sigma_{sc}= \frac{\lambda^2}{2\pi}\sum_{n=0}^{\infty}(2n + 1)\,(|a_n|^2+|b_n|^2) \qquad 1.21$$

The scattering coefficient β_{sc} is defined as the ratio of the energy scattered in all directions by unit volume of gas to the incident energy. In terms of scattering cross section and aerosol number density, β_{sc} is given as,

$$\beta_{sc} = \sigma_{sc}N \qquad 1.22$$

where N is the number of aerosols per unit volume. It can be written in the form of scattering efficiency factor (Q_{sc}) which is defined as ratio of scattering cross section to geometric cross section of the particle given as

$$Q_{sc}=\sigma_{sc}/\pi\ r^2 \qquad 1.23$$

where r represents the size (radius) of monodispersion.

For a polydisperse system of aerosols

$$\beta_{sc}=\int_{r1}^{r2}\pi r^2 Q_{sc} n(r)dr \qquad 1.24$$

where n(r)dr denote the size distribution function. Combined effect of absorption and scattering is called extinction. The extinction coefficient is given as,

$$\beta_{ext}=\beta_{sc}+\beta_{ab} \qquad 1.25$$

where β_{ab} and β_{sc} denotes the absorption coefficient and scattering coefficient respectively.

1.9.2.1 Optical thickness or optical depth

Aerosol optical depth τ an important parameter in the estimation of radiative effects/forcing due to aerosols. It is defined as the integrated extinction due to a unit column of the atmosphere given as

$$\tau=\int_0^h \beta_{ex} n(h)dh \qquad 1.26$$

where n(h)dh denote the altitude distribution function of aerosols. Optical depth due to entire atmospheric column is the sum of optical depths due to scattering and absorption by molecules and aerosols.

1.9.2.2 Single scattering albedo(ω)

The effectiveness of scattering relative to extinction or the relative importance of scattering over absorption is quantitatively expressed by single scattering albedo (ω) defined as,

$$\omega=\beta_{sc}/(\beta_{sc}+\beta_{ab}) \qquad 1.27$$

For an aerosol system of non-absorbing aerosols, $\omega=1$. Presence of absorbing aerosols reduces ω and hence as $\omega<1$. Weakly absorbing aerosols ($\omega\sim1$) scatter radiation and produce cooling. Absorbing aerosols ($\omega<0.8$) tend to reduce the solar energy lost from the earth atmosphere system by absorbing the radiation. This increases the energy input to the system and produces warming. Smaller the value of ω, more

likely is the layer to decrease planetary albedo. The albedo of the underlying surface also affects the radiative effects.

1.9.2.3 Phase function P(θ)

Phase function expresses the angular dependence of scattered radiation and defined as the ratio of energy scattered per unit solid angle in a given direction to the average energy scattered per unit solid angle in all directions. This definition requires that the integral of the phase function be normalized to unity. In terms of the angular scattering coefficient $\beta_{sc}(\theta)$ it is defined as,

$$P(\theta) = \frac{\beta_{sc}(\theta)}{\frac{1}{4\pi}\int_0^{4\pi} \beta_{sc}(\theta) d\psi} \qquad 1.28$$

1.9.2.4 Asymmetry parameter G (λ)

It is defined as the integrated measure denoting the fraction of light scattered in the forward to that scattered in the backward direction and given by,

$$g(\lambda) = \frac{\int_0^{4\pi} \cos(\theta) P(\lambda,\theta) d(Cos\theta)}{\int_0^{4\pi} P(\lambda,\theta) d(Cos\theta)} \qquad 1.29$$

g takes values 1, 0 and -1 depending on scattering direction. g = 1 for light scattered totally in the forward direction and g = -1 for complete backscattered radiation and g = 0 for isotropic scattering (e.g.gases). Globally, g values are highly heterogeneous, and it varies from 0.5 (polluted) to 0.75 (dusty/sea salt dominated) for aerosols and above 0.8 for clouds [*Boucher*, 1998].

Figure 1.5 shows the scattering patterns for different types of scattering. The greater the particle size, the more of the light is scattered in the forward direction.

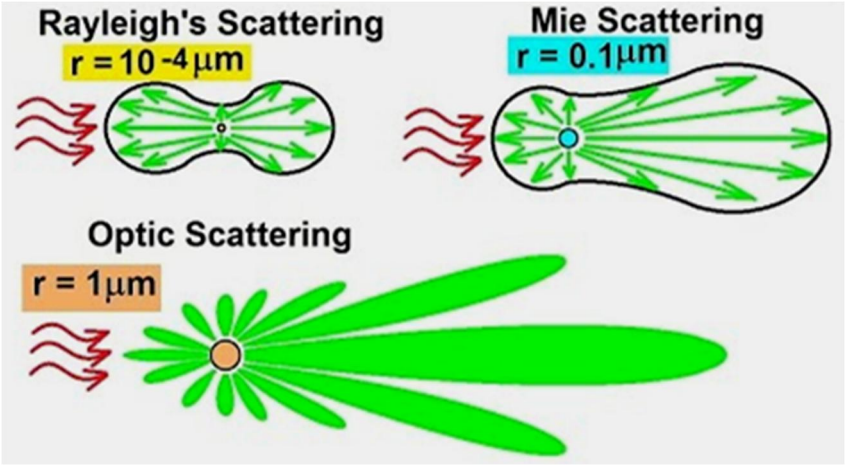

Figure 1.5.*Scattering patterns for Rayleigh and Mie scattering (small and large particles).*

Atmospheric aerosols affect the earth's radiation budget of the earth-atmosphere system through three processes. The radiative effects of aerosols are classified as direct effect, indirect effect and semi direct effect.

1.9.3 Direct effect

In the direct effect, aerosols scatter and or absorb the incoming solar radiation thereby altering the radiative balance of the earth-atmosphere system [*Haywood and Boucher, 2000; IPCC 2007;2013*]. Non-absorbing aerosols will increase the albedo of the atmosphere by scattering or reflecting back the solar radiation, thus reducing the amount of solar radiation reaching the surface. Hence scattering produces cooling in the atmosphere and earth's surface. On the other hand, the absorbing aerosols cause warming. Aerosols have a tendency to cool when they are over a low albedo surface and to warm when they are over high albedo surfaces such as snow [*Hadley and Kirchster*, 2012].

1.9.4 Indirect effect

Clouds play a significant role in the Earth-Atmospheric radiation balance by reflecting solar radiation back [*Twomey,*1977; *Derman et al.,* 2007; IPCC, 2013]. Aerosols act as cloud condensation nuclei and hence modify cloud microphysical properties. An increase in aerosol concentration causes an increase in cloud droplet concentration and a decrease in droplet size for fixed amount of liquid water content. This makes the clouds more reflective (brighter), which causes increase in cloud albedo resulting in negative radiative forcing or cooling (Twomey effect) [*Twomey,* 1977]. In the second indirect effect, the reduction of cloud droplet size affects the precipitation efficiency, which causes an increase in cloud lifetime [*Eastman and Warren*, 2013], and cloud optical thickness. The number of cloud droplets is regulated by the concentration of CCN which are generally hygroscopic aerosol particles (sulphates, dicarboxylic acids etc.).

1.9.5 Semi direct effect

This effect is associated with the absorption of solar radiation by aerosols like soot or BC in clouds. Solar heating by absorbing aerosols can evaporate low clouds resulting in the decrease of cloud cover. [*Hansen et al*.,1997; *Ackerman et al.*, 2000; *Jacobson*, 2012]. If present in high concentration, this can enhance the daytime clearing

of cloud. This warming can partially offset the cooling due to the indirect aerosol effect.

1.9.6 Radiative forcing (RF)

The term radiative forcing has been employed to denote an externally imposed perturbation in the radiative energy budget of the earth's climate system [*IPCC* 2007, 2013]. The instantaneous RF refers to an instantaneous change in net (down minus up) radiative flux (shortwave plus long wave; expressed in W m^{-2}) due to an imposed change in atmosphere. This forcing is usually defined in terms of flux changes at the top of the atmosphere (TOA) or at the climatological tropopause, with the latter being a better indicator of the global mean surface temperature response. Figure 1.6 shows the global average RF in 2011 relative to 1750, for the major climate drivers like greenhouse gases, aerosols, albedo change etc. [*IPCC*, 2013]. The confidence levels in the estimate of RF due to different climate drivers are also given in the figure.

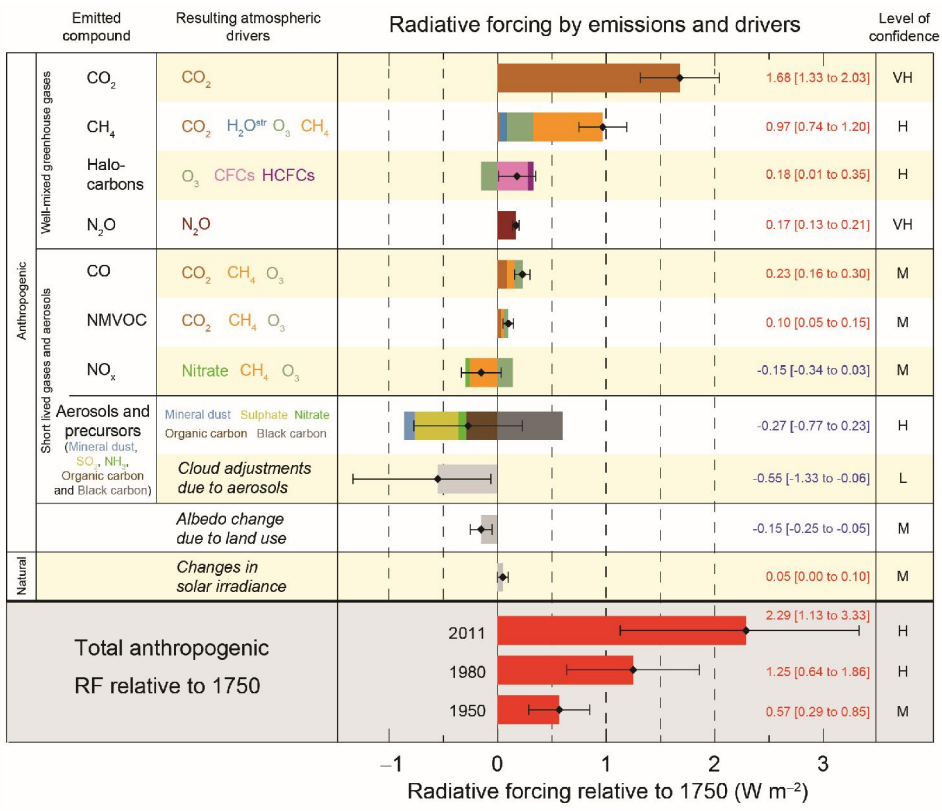

Figure 1.6.*Global average radiative forcing estimates in 2011 relative to 1750 for the main climate change drivers. Confidence levels are denoted by VH-very high, H-medium, L-low, VL-very low (adapted from IPCC 2013).*

Overall, the current aerosol radiative forcing due to scattering aerosols is estimated to be around 0.94Wm^{-2}, as opposed to a greenhouse gas forcing of about

+2.4Wm^{-2} (IPCC, 2013). The mean radiative forcing for the major aerosol species as reported by IPCC 2013 is –0.4 (–0.6 to –0.2)W m^{-2} for sulphate aerosol; black carbon aerosol as +0.4 (+0.05 to +0.8)W m^{-2}; and primary and secondary organic aerosol – 0.12 (–0.4 to +0.1)W m^{-2}; –0.11 (–0.3 to –0.03)Wm^{-2} for nitrate aerosol; and a contribution from mineral dust of –0.1 (–0.3 to +0.1)W m^{-2} that may not be entirely anthropogenic in origin.

1.10 Spatio-temporal variation of aerosols and transport

The spatial and temporal distribution of aerosols depend on the distribution of sources and sinks and the prevailing dynamics. Since majority of the aerosol sources are on the earth's surface, these particles are confined to the source regions and lower layers of the atmosphere. Aerosol properties exhibit diurnal, day-to-day, seasonal as well as interannual variations owing to variations in the intensity of sources/sinks and in response to variations in the meteorological conditions and transport. Aerosol properties also evolve during atmospheric transport [*Dentener, et al*., 1996; *Usher et al*., 2003]. The concentrations and properties of aerosols also vary with altitude in the atmosphere.

1.11 Altitude profile of aerosols

For computing the altitude dependent and columnar radiative properties and for assessing the radiative forcing, knowledge on vertical distribution of aerosols (altitude profile) is essential. Since most of the aerosol sources are located at the Earth's surface, it is assumed that aerosol concentrations decrease with height. Concentrations are generally larger in the atmospheric boundary layer than in the free troposphere. However, vertical transport and associated dynamics causes deviations from this structure. Often aerosol plumes get lifted into the free troposphere forming stratified layers. In addition to this, aerosols also form layers associated with temperature inversions, wind shear etc. There exists a local maximum of concentrations in the stratosphere called Junge layer where sink mechanisms are less efficient [*Junge et al*., 1961].

1.12 Aerosol measurement techniques

Measurements of aerosol properties are carried out by *in situ* and *remote sensing* techniques. In situ measurements make direct measurements of the parameters at their location or being in physical contact with them. In remote sensing the

parameters are deduced by measuring the impact of an electro-magnetic radiation, interacting with the particle but without being in physical contact.

1.12.1 Number density-Size distribution measurements

Particle sizing and number density measurements have been carried out using a variety of techniques. Optical particle counters, Differential mobility analysers, aerodynamic particle sizers are the widely used instruments for particle sizing and counting.

Optical particle counters (OPCs) are the most common method for counting and sizing of aerosols in the size range 0.1μm to 20μm. The basic principle of OPCs is to measure the amount of light scattered by individual particles as they traverse through focused beam of light. The light scattering efficiency depends on the size and refractive index of the particles [*McCartney*, 1976]. Most of the OPCs use laser light as the illuminating radiation. The scattered light from each particle is directed to a photodetector, where it is converted to a voltage pulse. Particle size is determined from the magnitude of this voltage pulse by using a calibration curve obtained from measurements using spherical particles of known sizes and refractive index. Pulse height and area are the commonly used measures of pulse magnitude. Size distributions are obtained by measuring the distribution of pulse magnitudes obtained from a representative population of particles. **Condensation nuclei counters** (CNC) also referred to as condensation particle counters or Aitken Nuclei Counters are used for the measurement of total aerosol number concentration. Particles are grown by condensation in CNCs until they are sufficiently large to be detected optically. The diameter growth factors are as large as 100 to 1000. CNCs can detect particles as small as 0.003 μm. In earlier instruments the counting was done using microscope. Currently, CNCs use automated single-particle counting achieved by measuring light attenuation or scattering by the particles.

Electrical mobility analyzers classify particles according to the electrical mobility [*Hinds*, 1999]. Conductivity depends on gas properties, particle charge and the geometric particle size but is independent of other particle properties such as density. Later the Electrical mobility analyser has been replaced by the differential mobility particle sizer (DMPS). The DMPS includes a differential mobility analyzer (DMA, also referred to as the electrostatic classifier) [*Mc Murray et al., 2000*] and a particle detector, like CNC.

The ***aerodynamic particle sizers*** are used for simultaneous counting and sizing particles. As an aerosol particle is rapidly accelerated through a nozzle into a partially evacuated chamber, particles tend to lag behind the carrier gas due to inertia. The difference between the particle and gas speeds increases with size and density since inertia increases with these properties. Aerodynamic size of the particle is inferred from particle velocity, which is determined by measuring the time of flight taken by the particle to travel a known distance.

1.12.2 Aerosol mass concentration measurements

Aerosol sampling for mass concentration measurements involves the collection of the aerosols on suitable collection media for subsequent gravimetric and chemical analysis. Traditionally aerosol sampling is done by drawing ambient air through suitable collection substrates like membrane or fiber filters, inertial impaction plates, thermal or electrostatic precipitation plates or in a liquid or wet media using a pump [*Chow*, 1995].Based on the size range of aerosols collected, the samplers are of two types namely Total Suspended Particulate (TSP) sampler or size selective sampler like PM10, PM2.5, PM1, etc. The latter needs a size-selective inlet and efficient flow control methods. The ideal aerosol sampling inlet would draw in 100% of the particles in a specified size range and would transport them to the collection media without altering their properties. The efficiency with which particles enter the inlet varies with particle size, wind speed, and direction. Depending on the flow rate, the samplers are classified as low volume and high volume samplers.

Particle collection on filters is achieved by three different processes: diffusion, direct interception and impaction [*Mark*, 1998] as illustrated in Figure 1.7. Diffusion refers to the net migration of particles from regions of high concentration to low concentration and this process is controlled by Brownian motion. Because particle diffusivities increase with decreasing size, collection efficiencies increase as size drops below ~0.1μm. Particles larger than about 0.5μm are collected by interception and impaction. Collection efficiencies in these mechanisms increase with increasing size. This mechanism is more effective in the case of particles with sizes < 0.1μ. Particles with the same order of size as the obstacle (e.g. pore size), gets collected by interception.

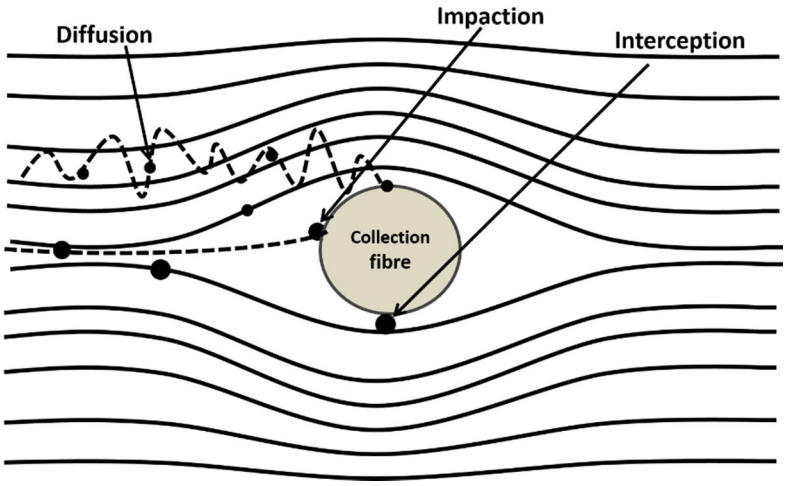

Figure 1.7. *Schematic of different deposition processes like diffusion, impaction and interception.*

Impaction is the most commonly used mechanism for particles in a wide size range. When the direction of airflow containing particles is distorted by the presence of a bent or obstacle, because of inertia, the particles tend to continue along their original path and get deposited on the obstacle (the filter medium in the case of sampling). Collection efficiencies by these mechanisms increase with increasing size above 0.5µm. Size-selective inlets use inertial classification to remove particles larger than a specified aerodynamic size, the most commonly used techniques being impaction and cyclonic separation.

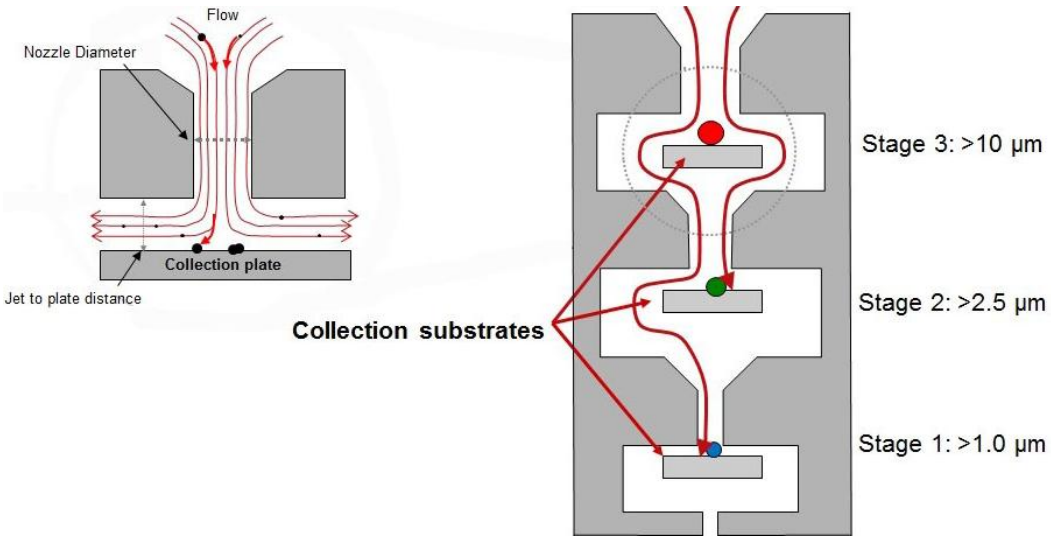

Figure1.8. *Mechanism of particles deposited in a cascaded impactor.*

The dimensionless parameter that determines whether particles are collected by an impactor is the Stokes number, St, defined as [*Mc Murray, 2002*]

$$St = \frac{\tau U_0}{(D_{nozzle})/2} = \frac{\rho_p D_p^2 C U_0}{9\mu D_{nozzle}} \qquad 1.30$$

Where τ is particle relaxation time, U_0 is the mean velocity through the accelerating nozzle, D_{nozzle} is the diameter of the accelerating nozzle, ρ_p is particle density, D_p is particle diameter, C is the slip correction factor and μ is the absolute viscosity of the gas. In practice, impactors collect particles that have Stokes numbers larger than a critical value typically in the range 0.21 to 0.23. Cascade impactors with a series of stages, each with a successively smaller cut point, are commonly used to collect size-resolved aerosols (Figure 1.8). Virtual impactors are also used as size-selective inlets.

Cyclones are cone-shaped devices in which the sampled aerosol enters tangentially, rotates several times about the axis, and exits vertically through an opening located on the axis at the top. Particles are transported to the wall by centrifugal force. Liquid particles adhere to the wall, while solid particles settle into a collecting cup located at the bottom of the cyclone. The performance of the cyclone (e.g. cut off size) is determined empirically.

Electrostatic **precipitation** is another technique which applies a potential difference across a sample airflow, which leads to the ionization of the gas column resulting in collisions between particles and ions to produce electrostatically charged particles. Subsequently passage of these charged particles through an electric field results in their collection at an oppositely charged electrode. The method has 100% efficiency for particles with diameter ranging from 0.2 to 10μm. In **thermal precipitators**, a gas containing suspended particles is brought into contact with a heated surface, the thermal force causes particles to migrate from a zone of high temperature to the zone of lower temperature. Automated methods for measurements of aerosol mass concentrations include the beta gauge, piezoelectric crystals, and the oscillating element instruments.

1.12.3 Measurement of Optical/radiative properties

Techniques of nephelometry and photoacoustic spectroscopy are used for measurement of absorption and scattering coefficients. The ***integrating nephelometer*** is used worldwide to measure the scattering coefficients of suspended particulate matter [*McMurry et al.,* 2000]. It works on the principle of attenuation of light passing

through a medium. Particle scattering coefficients for a given wavelength λ can be expressed as the integral over scattering angle θ of the particulate volume scattering function. The integration covers scattering angles from near forward to near backward. When equipped with a photon-counting detector, the integrating nephelometer can measure the particle light scattering coefficients less than $0.1Mm^{-1}$. Absorption coefficients are inferred from measurements on particles collected on filters. Aethalometer make use of this technique for measurement of BC. However, the viability of conducting in-situ measurements using **photoacoustic spectrometry** has also been demonstrated.

1.12.4 Chemical composition measurements

Several analytical techniques are available for identification and quantification of various chemical species in the aerosol samples. The most accepted techniques are Ion chromatography (IC) atomic absorption spectroscopy, atomic emission spectroscopy, High Performance Liquid Chromatography (HPLC), Gas Chromatography (GC), Inductively Coupled Plasma-Mass Spectrometry (ICP-MS), and Neutron Activation(NA).Scanning electron microscopy (SEM) and transmission electron microscopy (TEM) are also used for the measurement of particle morphology and elemental composition. Online monitoring of bio aerosols is carried out based on aerodynamic sizing and fluorescence spectroscopy. Brief descriptions of the major techniques relevant in the context of the present work and their underlying principle of operation are outlined below.

Chromatography refers to a group of analytical techniques that enables the separation, identification and quantification of the components of a complex mixture. This technique makes use of a stationary phase and a mobile phase. Components of the mixture are carried through the stationary phase by the flow of the mobile phase. Separation of components is based on the difference in migration rates among them which depends on the fraction of time it spends in the stationary phase. Different variants of this technique like Ion Chromatography (IC), Gas Chromatography (GC), High Pressure Liquid Chromatography (HPLC) are widely used for the analytical separation of complex mixtures. A detailed account of IC is given in Chapter 2.

Atomic spectroscopy involves the absorption, emission or fluorescence of radiation characteristic of the particular atom under analysis. Based on the specific mechanism of absorption, emission or fluorescence that is being used for analysis, the different methods are named as Atomic Absorption Spectroscopy (AAS), Atomic

Emission Spectroscopy (AES) and Atomic Fluorescence Spectroscopy (AFS). In AAS, the sample is atomized and the free atoms in ground state absorb radiation of specific wavelength characteristic of the species and get excited to higher levels. The wavelength at which absorption takes place and amount of attenuation occurs to the source intensity are used for identifying and quantifying the constituents in the sample. In AES, the elements or atoms are excited to higher energy levels by external sources and as they fall down to lower energy level, characteristic radiation of the atom is emitted, which is measured to quantify the respective species.

Neutron Activation Analysis (NAA) is the most commonly used technique for identifying and measuring trace amounts of specific nuclides in materials. In this technique the, isotopes of the element of interest – radio nuclides –are produced. The radiation emitted from this while decaying is detected and used for the quantification of the sample. The technique is capable of analyzing multiple elements present in the sample.

X-Ray Fluorescence (XRF) technique is used for analysis of metallic species with atomic number from 11 to 92. The filter deposit is irradiated by high energy X-rays which eject inner shell electrons from the atoms of each element in the sample. When a higher energy electron drops into the vacant lower energy orbital, a fluorescent X-ray photon, characteristic of the element, is released. The number of photons is proportional to the concentration of each element. Commonly used techniques are: 1) wavelength dispersive XRF (WDXRF), which utilizes crystal diffraction for observation of fluorescent X-rays and 2) energy dispersive XRF (EDXRF), which uses a silicon semiconductor detector. In the **Proton-Induced X-Ray Emission (PIXE)** analysis, the sample is bombarded with high energy protons to remove inner shell electrons.

For the quantification of carbonaceous aerosols, **thermal techniques** are widely accepted. The total carbon is estimated as the sum of elemental carbon (EC) or Black carbon (BC) and OC. TC, OC and EC can be determined by thermo chemical oxidation or thermal combustion of the sample and measurement of the evolved CO_2. The carbon content in each (OC or EC) gets oxidised at different temperatures characteristic of the component. BC is also estimated using optical absorption methods. **Photoacoustic spectroscopy** makes direct measurements of light absorption by aerosol particles and quantify the BC concentrations.

Mass spectrometry is an analytical technique that identifies the chemical composition of a sample based on the mass-to-charge ratio of charged particles. In this

technique, individual molecules in a sample are converted to ions and these charged particles are subjected to electric and magnetic fields. The deflection of a charged particle depends on its mass to charge ratio. The sample to be analyzed is ionized either thermally or with the help of a radio frequency spark/laser ion source and then separated according to their mass-to-charge ratio. **Scanning Electron microscope** also provides information on particle morphology and elemental composition. With this approach, particles are collected on a filter or impaction substrate and are irradiated by electrons under vacuum conditions. Information on elemental composition is achieved by measuring the X-ray energy spectrum produced by interactions of the electrons with the particles.

1.13 Remote sensing techniques

Atmospheric remote sensing, involves the detection of changes in electromagnetic radiation reaching the observer after interacting with atmospheric constituents such as gases, water vapour, aerosols, clouds by using appropriate inversion technique. Basically remote sensing techniques are of two types, namely active and passive.

Active remote sensing employs a radiation source generated by artificial means such as the lasers used in LIght Detection And Ranging (LIDAR), the microwaves used in RAdio Detection And Ranging (RADAR) or sound waves in SOund Navigation And Ranging (SONAR). **Passive remote sensing** utilizes the natural radiation sources such as Sun, Moon or the Earth-atmosphere system and is carried out from ground-based, ship-borne, air-borne, and space-borne platforms. Passive remote sensing devices include sun photometers/solar radiometers, and spectro- radiometers, etc.

1.13.1 Satellite Remote sensing of aerosols

In this technique, satellite sensors measure the top of the atmosphere (TOA) radiance which is emitted, reflected or scattered. For a cloud-free atmosphere, the TOA radiance is caused by scattering by molecules and aerosols, and by reflectance from the earth's surface. The satellite received radiances are analysed to extract the aerosol properties using appropriate inversion methodologies. However, for the retrievals, several assumptions on aerosol properties have to be made which include the nature of the aerosol size distribution, their refractive index, and reflectance of the underlying surface. In spite of this limitation, satellite remote sensing has the advantage of regional and global coverage.

The first applications of satellite remote sensing of aerosols began in the mid-1970s with the detection of desert aerosols above the ocean using LANDSAT, GOES, and AVHRR data [*Fraser,* 1976; *Mekler et al*; 1977; *Carlson and Wendling*, 1977; *Norton et al*; 1980].Long term aerosol product over land, is produced using ATSR-2 (Along Track Scanning Radiometer) [*Veefkind et al*. 1998] and AATSR (Advanced Along Track Scanning Radiometer) measurements [*Grey et al*. 2006]. Total ozone mapping Spectrometer (TOMS) provides the Absorbing Aerosol Index. The dedicated instruments for aerosol retrieval are POLarization and Directionality of the Earth's Reflectances (POLDER) which measures the spectral, directional and polarized light reflected by the Earth-Atmosphere system [*Tanre et al*. 2011], Moderate Resolution Imaging Spectroradiometer (MODIS)[*Levy et al.,* 2013] and the Multi-angle Imaging Spectro-Radiometer (MISR)[*Diner et al.,* 1998]. Another milestone was the launch of the space-borne lidar Cloud-Aerosol LIdar with Orthogonal Polarization (CALIOP) on CALIPSO (Cloud Aerosol Lidar and Infrared Pathfinder Satellite Observations) [*Young andVaughen*, 2009].

The Stratospheric Aerosol Measurement instrument (SAM) launched in 1978 [*McCormick et al.,* 1989] and the SAGE series Stratospheric Aerosol and Gas Experiment (SAGE) focussed on stratospheric aerosols and gases.

Radiative transfer (RT) calculations form an essential part of retrieval of aerosol parameters. Since RT calculations are highly time consuming, they are used outside the actual retrieval algorithm to prepare Look Up Tables (LUTs) for a wide variety of aerosol conditions. The LUTs are generated for a set of aerosol models which are representative for a certain area [*Remer et al.,* 2005; *Levy et al*. 2013] using RT codes. Aerosol parameters are retrieved by comparing the radiation received by an instrument at TOA with that calculated using a RT model for the same geometry and atmospheric conditions, for a range of aerosol models. The best fit model is selected to provide the retrieval solution.

1.14 Global scenario

Due to the growing scientific interest in atmospheric aerosols and their environmental and climatic impacts, and the tremendous advances in measurement technologies, the understanding of their physical properties, chemical composition and atmospheric processes has increased enormously during the last three decades. Before 1950's most of the aerosol research focused on atmospheric conductivity [*Barren and Willeke*, 2001]. The physical and chemical characteristion of aerosols was initiated by

Junge, [1963]. Since then, focused research in the area of aerosol science using sophisticated instruments, techniques and measurements in campaign mode have gained momentum all over the world. *Prospero et al.,* [1983] have given a detailed account on the physical and chemical characteristics of aerosols and highlighted the need for a comprehensive measurement of aerosol properties. This section gives a brief overview of the major studies on the physical, chemical and radiative characteristics of aerosols conducted all over the globe.

The fixed station measurements and the campaign-mode experiments conducted worldwide during last few decade have brought out the spatial and temporal heterogeneities in the physico-chemical characteristics of aerosols. The major land campaigns include Megacity Impact on Regional and Global Environments field experiment (MILAGRO) [*Paredes-Miranda et al*., 2009], Geostationary Earth Radiation Budget Inter-comparisons of Longwave and Shortwave (GERBILS)[*Christopher et al*., 2009], the Amazonian Aerosol Characterization Experiment 2008 (AMAZE-08), the Integrated project on Aerosol Cloud Climate and Air Quality interactions (EUCAARI) [*Kulmala et al.,* 2011] and Atmospheric Brown Clouds (ABC, *Nakajima et al.,* 2007),South AMerican Biomass Burning Analysis (SAMBA) over South America [*Brito et al*, 2014]; Intercontinental Chemical Transport Experiment (INTEX)[*Bergstrom et al*., 2010], African Monsoon Multidisciplinary Analysis AMMA over West Africa [*Matsuki et al*., 2010] and Southern African Fires and Atmosphere Research Initiative(SAFARI-92) over southern Atlantic and southern Africa [*Lindesay et al.,* 1996] and Ganges Valley Aerosol Experiment (GVAX)all of which improved our understanding of the regional properties of aerosols.

As part of GAW (Global Aerosol Watch), there are aerosol networks, regional or global in scope. In US several networks are operational since 1970s. Most of the network stations measure aerosol mass concentrations, chemical compositions and optical depths. Data from Interagency Monitoring of Protected Visual Environment (*IMPROVE*) network [*Malm et al*., 1994, *Hand et al.,* 2012] and other stations in US [*Quinn et al.*, 2002; *Bates et al.*, 2006], measurements from Arabian Peninsula [*Reid et al.,* 2008],China [*Li et al*., 2007] and West Africa [*Haywood et al.,* 2008] have produced several new results in aerosol science. Long term $PM_{2.5}$ measurements over the IMPROVE network sites showed significant downward trends (4.0%/yr), and that of PM10 was ~ 3.1%/yr for 2000–2009. *Hidy and Pennell* [2010] observed a similar declining trend of PM2.5 and sulphates in Canada. Similarly aerosol number concentrations [*Asmi et al*., 2013] are declining significantly at most sites in Europe,

the Pacific and the Caribbean, but increasing at South Pole based on a study of 17 globally distributed remote sites [IPCC, 2013].

Systematic long term measurements of physical and chemical characteristics of aerosols are being carried out from large number of stations in Europe [*Coe et al., 2006; Philippin et al.,2009; Putaud et al*., 2010], USA [*Asmi et al.,* 2011]. *Ford and Herald*, [2013] observed strong seasonality in aerosols over the Southeastern United States based on satellite data and surface network sites. Aerosol characteristics and their impacts on air quality and climate are being investigated over China and many other Asian countries [*Li et al.,* 2013, 2016; *Stone et al.,* 2013, *Sanderson et al*., 2014, *Ho et al*., 2015; *Ding et al.,* 2016].

Realizing the role of sea salt aerosols in cloud formation and regional climate, several laboratory and campaign mode measurements were initiated since 1950. The production mechanisms of sea salt aerosols from breaking waves and white caps and their wind speed dependence were postulated several decades ago [*Monahan et al*.,1982;*Exton*, et al., 1985and *De Leeuw* 1986].Studies have shown that the fine particle mode (r <0.25μm) in clean marine air is composed predominantly of nss-sulfate derived from the dimethylsulphide (DMS) [*Charlson et al*., 1987].The sea-salt, non-sea-salt and organic aerosols exists in ultrafine, fine and coarse modes over oceans. Extensive reviews on marine aerosols are also available in literature [*Fitzgerald*, 1991; *Heitzenberg* et al., 2000; *Gantt and Meskhidze*, 2013].

The major ship-based campaigns conducted over oceanic regions for marine aerosol characterisation include Transport and Chemical Evolution over the Pacific (TRACE)-A over the southern Atlantic [*Fishman et al.,* 1992], Aerosol Characterisaion Experiment ACE-1 and 2 over Southern Oceans and Atlantic [*Bates et al*, 1998; *Raes et al*., 2000],Tropospheric Aerosol Radiative Forcing Experiment TARFOX over north-western Atlantic [*Russell et al*, 1999], Aerosols99 over Atlantic [*Bates et al*, 2001], INDian Ocean Experiment (INDOEX) over Indian Ocean [*Ramanathan et al.*, 2001], TRACE-P over east Asia and north-western Pacific [*Jacob et al.*, 2003], ACE-Asia over east Asia and northwest Pacific [*Huebert et al.*, 2003] and Integrated Campaign for Aerosols, gases and Radiation Budget (ICARB; *Moorthy et al.,* 2008).

Significant contribution of soil dust particles have been reported in numerous studies conducted in Europe [*Pio et al.,* 2007], North-America [*Owega et al*. 2004], Asia [*Chen et al.,* 2004] and Australia [*Chan et al.,* 1999]. Mineral dust transported from arid continental areas through the atmosphere to remote marine regions has size ranges varying from 0.03μmto >75μm diameter [*Jaenicke and Schu¨tz*, 1978; *Maring et*

al., 2000]. Elaborate studies were carried out on the chemical composition of mineral dust from Sahara and Gobi deserts [*Kurosaki and Mikami* et al., 2007].The radiative effects of the Saharan dust on the Asian monsoon [*Chinnam et al.*, 2006; *Lau and Kim*, 2010;] and the West African monsoon are documented [*Lau et al*., 2009].

Anthropogenic aerosols including traffic-related pollutants and industrial emissions have an adverse effects on human health. Roads are one of the largest emitters of aerosols, in particular, the mineral components in many urban areas [*Ruellan and Cachier,* 2001, *Manoli et al*. 2002). *Hildemann et al.,* (1991) have reported that road dust in fine (<2μm) mode consists of 27% SiO_2, 17% organics, 11% Al_2O_3, 9% Fe_2O_3, and 4% Ca and contribute to a major anthropogenic dust source. It is found that road dust was heavily enriched in Cu, Zn and Pb, that are associated with vehicular emissions. Motor vehicles are found to be responsible for up to 30% of the $PM_{2.5}$ mass in industrial areas [*Fraser et al*., 2003]. *Dillner et al*., [2006] studied size segregated particulate composition over Beijing and found that fine mode particles including nitrates and sulphates are higher during industrial pollution events than dust events. Anthropogenic aerosol concentrations are much lower in the Southern Hemisphere than in the Northern Hemi- sphere [*Rotstayen et al.,* 2008]. Biomass burning is considered to be the largest source of primary carbonaceous aerosol particles into the Earth's atmosphere [*Virkula et al., 2014 and references therein*]. In view of this several studies were carried out to characterize the physiochemical and radiative properties of particulate emissions from biomass burning and forest fires.

In view of the importance of chemical composition of aerosols in radiative, climatic, environmental and health impacts, chemical characterization became part of aerosols science. The efforts for aerosol chemical characterization were initiated way back in the middle of twentieth century starting with the analysis of inorganic ions. Quality checked long-term chemical composition data of aerosols is available from several sites in US and Europe [*Putaud et al.,* 2010]. But data is limited over Asian region. However in recent years, several studies were conducted over China, Japan, Korea and Indian region[*Chun et al* 2001;*Takami et al*., 2005; *Nair et al.*, 2008; *Geng et al*., 2011; *Stone et al.*, 2011;*Ho et al*., 2015; *Ding et al.,* 2016; *Li et al.,*2016]. Even though, studies on inorganic aerosols are extensively done all over the world, the organic aerosol analysis was still limited. However, studies on black carbon/elemental carbon and other primary biological aerosols have advanced significantly in last one decade.

The radiative forcing capability of aerosols are also addressed extensively [*Charlson et al*., 1987; *Hansen et al.,* 1997, *Haywood and Boucher*, 2000] with model simulations [*Zhuang et al*., 2013; *Shindell et al*., 2013] long-term measurements and satellite based retrievals. The estimated direct radiative forcing showed a wide range of values [*Ramanathan et al.,* 2001; *Satheesh et al.*, 2002;*Markowicz et al*., 2008; *Zhuang et al.,* 2013]. Accurate measurement of absorbing aerosols is a major challenge even now. Even with the state of the art measurement techniques and modelling capabilities, the uncertainties in the assessment of regional radiative forcing due to aerosols remain large (IPCC, 2013).

1.15 Indian scenario

Indian research in the field of atmospheric aerosols was initiated in 1950s under India Meteorological Department (IMD) [*Sikka*, 2000]. Earlier studies were based on rain water chemistry, solar radiation measurements and atmospheric turbidity. Analysis of rain water analysis was extensively used for inferring the water soluble components of the atmospheric aerosols and to understand the aerosol characteristics [*Murty and Ramanamurty,*1969; *Kapoor et al.* 1972; *Khemani et al*., 1985; *Mahadevan et al.*,1989]. These studies revealed seasonality in aerosol composition with a significant signature of marine aerosols (Cl and Na) during monsoon season and sulphate aerosols and soil-derived metallic species during winter (Al, Fe, Mn and Ca) over Indian region.

One of the pioneering Indian works in aerosol research was based on the pyrheliometric measurements at various locations during 1966–1967 and the estimation of Angstrom turbidity coefficients [*Mani et al.,* 1969]. In 1970s IMD established the Background Air Pollution Monitoring Network (*BAPMoN*) of ten stations covering urban, semi-urban and remote island regions for atmospheric turbidity measurements using sunphotometers and rain water analysis [*Soni and Sarkar 2006*].Subsequently, high-volume air samplers and cascade impactors were used to collect ambient aerosols from different geographic environments and analyse them in the laboratory [*Rastogi and Sarin*, 2005; *George et al.,* 2011; *Kulshrestha et al*., 2013]. Systematic investigations of the physico-chemical properties of aerosols, their temporal and spatial heterogeneities, spectral characteristics, size distribution, and modulation by regional mesoscale, and synoptic meteorological processes commenced in early 1980s when lidars and multi-wavelength solar radiometers became operational [*Parameswaran et al*.,1994; *Devara et al.,*1995;*Jayaraman et al*., 1996; *Jayaraman et al*., 1998, *Moorthy et al*., 1999]. Under ISRO-GBP, aerosol research gained momentum and currently

aerosol optical depth and BC measurements are being done from a network of Stations spread all over India [*Gogoi et al*., 2009; *Babu et al.,* 2013]. The first time measurements of altitude profile of aerosols from Indian region were carried out from Thiruvananthapuram using lidar systems [*Parameswaran et al*., 1994, 1998, 2004].

With the establishment of AERONET stations over different locations of IGB, quantitative results on the AOD in fine and coarse modes have been brought out [*Dey et al*., 2004; *Srivastava et al*., 2012; *Tiwari et al*., 2013; *Kaskoutis et al*., 2013]. Aerosol mass concentration over Pune was found to be bimodal in nature with one peak in fine particle mode (0.04-0.05μm) and other in coarse mode (5-6μm) [*Safai et al*., 2004, 2005]. At Delhi, the summer time PM_{10} loading was 8% higher than that of $PM_{2.5}$ during August 2007 to October 2008 [*Tiwari et al*., 2012]. Aerosol characteristics over Indian region exhibits large variabilities and are strongly influenced by monsoon activity and changing air mass types [*Hegde et al.,* 2007; *George et al.,* 2008].

The chemical composition of aerosols also depict large regional variations over India [*Nair et al*.,2006; *George et al.,* 2008, 2011]. The concentration of mineral dust and combustion aerosols were found to dominate at Bombay affecting air quality and health [*Sadasivan and Negi*, 1990; *Nambi et al.* 1997; *Bhanarkar et al.* 2005]. Vehicular emissions show profound influence on the chemical composition of aerosols at urban areas like Pune [*Safai et al*., 2004]. The seasonal changes in aerosol chemical properties at TVM during under sea breeze conditions, their source characteristics and association with synoptic scale meteorology are given by *George et al.,* [2008]. At another site Cochin, the observed aerosol mass loading and mass concentrations of anthropogenic species were significantly higher than that at TVM [*Bindu et al.,* 2015]. Large contribution from crustal material/road dust followed by metallurgical and industrial emissions were observed at Tirupati [*Mouli et al.* 2006]. The chemical composition of PM10 aerosols including inorganic and carbonaceous aerosols at Chennai is given by *Mouli et al*., [2011].

During pre-monsoon seasons, the IGB receives heavier loading of natural dust aerosols, transported from the neighbouring Desert regions (Thar Desert) of western Rajasthan in India [*Dey et al*., 2004; *Pandithurai et al*., 2008; *Gautham et al*., 2009; *Srivastava et al*., 2010]. Information on the carbonaceous aerosols over IGB and Agra are also available [*Pachauri et al*., 2012 and *Singh et al*., 2016]. Studies over high altitude regions Hisar, Manora Peak, Mt. Abu and several other locations from middle Himalayan region have brought out annual changes in chemical composition of natural

and anthropogenic aerosols including carbonaceous species [*Shrestha et al*., 2010; *Rengarajan et al*., 2007; *Ram et al.,* 2008; *Hegde et al*., 2012; *Sudheer et al.*, 2015].

Emission of carbonaceous aerosols from various fuels used in India and their budgets were estimated by *Parashar et al.,*[2005] and *Venkataraman et al.,*(2005).The mass concentrations of inorganic ions and metallic species in aerosols from varying geographic locations like TVM, Ahmedabad, Kanpur are available and oceanic regions of AS, BoB and IO are available [*Kumar et al.*, 2008; *George et al*., 2011; *Ram and Sarin* 2012; *Nair et al.*, 2014], even though long term studies are limited. The OC measurements are sparingly done over Indian region except from few stations like Nainital [*Hegde et al*., 2015] and Ahmedabad [*Rastogi et al*., 2009]. Two major land campaigns were organized under ISRO-GBP for the characterization of aerosols during 2004 brought out significant regional variations in aerosol physical, chemical and optical properties over Indian region. As a part of the Land campaign I measurements of aerosol mass loading, optical depth and chemical composition have been carried out over peninsular India during the winter month of February 2004 [*Singh et al*., 2006; *Nair et al*., 2006; *Niranjan et al*., 2005; *Jayaraman et al.,* 2006]. Extensive information on the winter time aerosol properties over the IGP emerged as a result of the Land Campaign II conducted during December 2004. Which provided a comprehensive database on the optical, microphysical and chemical properties of aerosols over the Indo-Gangetic Plains [*Ganguly et al*., 2005; *Nair et al*., 2007; *Nair et al*., 2009; *George et al*., 2011]. Winter-time properties of aerosols over the urban site of Kanpur and rural location Kharagpur in the context of fog/haze events were investigated by various teams [*George et al*., 2008; *Nair et al*., 2009]. In situ measured data on aerosol number - density size distribution -a major input needed for RF estimation from Indian region is also limited except for the few measurements done on campaign mode [*Pant et al*., 2006; *Nair et al*., 2009].

Several campaigns were conducted over the Arabian Sea, Indian Ocean and BoB in the last few decades. Among these, the INDOEX campaign was a great step in bringing out a comprehensive picture on the physical, chemical and radiative characteristics of aerosols over the oceanic environments surrounding Indian subcontinent [*Satheesh et al*., 1999; *Rajeev et al*., 2000; *Ramanathan et al*., 2001]. A model for the natural and anthropogenic aerosols over the cruise region was evolved for the first time from the studies conducted during the INDOEX [*Satheesh et al.,*1999]. The mean single scattering albedo values were found to be 0.88 for coastal India, 0.93 for AS and 0.99 for the Indian Ocean. However, aerosol characterizations over the BoB

were rather limited confining to the north-western and north-BoB [*Vinoj et al.,* 2004; *Sumanth et al.,* 2005].

Another campaign, the Arabian Sea Monsoon Experiment (ARMEX) was conducted in inter monsoon season of 2002 and 2003 over Arabian Sea and characterized the physical properties of aerosols and assessed their radiative impacts [*Babu et al.,* 2004]. The ICARB campaigns conceived under Indian Geosphere Biosphere Programme and conducted over the Arabian Sea, Bay of Bengal and northern Indian Ocean [*Moorthy et al*., 2008; *George et al*., 2009; *Nair et al*., 2010; *Nair et al*., 2014; *Aryasree et al.,* 2015] has been a major step in aerosol characterisation over Indian region. As compared to Arabian Sea, measurements were less over the Bay of Bengal. The major cruise-based measurements conducted in this region are BOBMEX (Bay of Bengal Monsoon Experiment in July-August 1999 [*Bhat et al.,* 2001] and ICARB conducted in two phases. Apart from this, during the CTCZ (Continental Tropical Convergence Zone) campaign also aerosol measurements were carried out.

These campaigns provided a wealth of data on the chemical, physical and optical properties of aerosols over this region. Details on the earlier studies on aerosol characteristics (over the present study regions) based on in-situ measurements, along with few major studies over other regions are given in Table 1.2. Apart from the data from limited campaigns, majority of studies on aerosols over the marine environments of AS, IO and BoB made use of satellite-based AOD data [*Nair et al*., 2009; *Rajeev et al.*, 2010]. MODIS data of AOD, fine mode fraction are extensively used for aerosol characterization. Satellite data is also used with RT models for estimations of regional Radiative Forcing and their effects on atmospheric dynamics. Most of the studies on long-term trends on aerosol physical and optical properties over Indian region are based on satellite-based datasets [*Dey and Di Girolamo*, 2011; *Ramachandran et al*., 2013], Aerosol Robotic NETwork (AERONET) measurement stations [*Dey and Tripathi*, 2008], and ARFINET stations [*Moorthy et al*., 2013; *Babu et al*., 2013]. In spite of all these measurements and studies, size distribution measurements, chemical composition, in particular the size segregated chemical composition are insufficient for arriving at a comprehensive, region-specific picture of aerosols and realistic estimation of their radiative characteristics.

1.16 Scope of the present study

Aerosol research is fuelled by the impact of these minor species in earth's radiation budget, climate, air quality, visibility, remote sensing, atmospheric chemistry, environment and public health. For the quantitative assessment of any of the above impacts of aerosols, comprehensive understanding on their physical and chemical characteristics is essential. In general most of the studies focus on either their physical properties like, size, number density and mass concentration or their chemical characteristics. Aerosol optical depth, a measure of the radiative impact of aerosols, is also measured. But, simultaneous and collocated measurements of the physical and chemical properties which is crucial in the estimation of radiative impacts are highly limited and scarce over Indian region. This causes large uncertainties in all model based estimates of radiative forcing due to aerosols and the consequent climate impacts [IPCC 2013]. Moreover, due to the large spatio-temporal heterogeneities in the aerosol sources, sinks and transport processes, region-specific studies on the above aspects become highly essential. With this background, the present work has been carried out with the following major objectives.

(1) Simultaneous and collocated measurement of aerosol number density, size distribution, mass loading and chemical composition of near surface aerosols at the coastal site Thiruvananthapuram and the oceanic environment of Arabian Sea and Bay of Bengal (2) Model based estimation of radiative characteristics of aerosols over these environments making use of the in-situ measured data. (3) Understanding the role of mesoscale and synoptic scale meteorology in the spatio-temporal behavior of aerosols and to identify the transport pathways and (4) Seasonal changes in in-situ measured near surface properties and satellite-retrieved columnar characteristics of aerosols over the dynamically active BoB region.

Table 1.2. List of major studies on aerosol characteristics carried out at the present study location based on in-situ measurements, along with those conducted over various regions over the globe.

Region of Study	Aerosol Parameters measured	References
Thiruvananthapuram	Mass loading/distribution	*Pillai et al* 2001; *George et al*., 2011
	Inorganic Species	*George et al*., 2011
	Black carbon and optical properties	*Babu*, 2004; *Moorthy et al*., 1999
	Boundary layer Number density	*Parameswaran et al*., 1994
Bay of Bengal	Physical properties (Mass loading)	*Bhat et al*., 2001; *Nair et al*., 2010
	Chemical composition	*Kumar et al*., 2008; *Sudheer and Sarin 2008*; *Nair et al*., 2014; *Aryasree et al*., 2015
	Black carbon and Optical properties	*Satheesh et al*., 2006; *Nair et al*., 2010
Arabian Sea	Physical properties (Mass loading)	*Tindele and Pease 1999; Babu, et al*., 2004; *Satheesh et al*., 2002 ; *Nair et al.,* 2006; *Kumar et al*., 2008; *George et al*., 2009
	Chemical composition	
	Black carbon and Optical properties	*Ramanathan et al.,* 2001; *Babu et al*., 2004; *Satheesh et al.,* 1999; *Nair et al*., 2008
Europe	Physical and chemical and radiative properties	*Coe et al*., 2006; *Pio et al.,* 2007; *Pacyna et al*., 2007; *Putaud et al*., 2010; *Kulmala et al.,* 2011
US	Physical and chemical and radiative properties	*Malm et al.,* 1994; *Quinn et al.,* 2002; *Quinn and Bates*, 2005; *Remer et al.,* 1997; *Owega et al*., 2004; *Hand et al.,* 2012; *Asmi et al*., 2011; *Brito et al*., 2014
Asia	Physical and chemical and radiative properties	*Chen et al*., 2004; *Takami et al*., 2005; *Li et al*., 2007; *Nakajima et al*., 2007; *Lawrence and Lelieveld* , 2007; *Kondo et al*., 2007; *Stone et al*., 2013; *Ho et al*., 2015
Pacific ocean	Physical and chemical and radiative properties	*Quinn et al*., 2000; *Huebert et al.,* 2003; *Jacob et al.,* 2003; *Russo et al*., 2003
Atlantic ocean	Physical and chemical and radiative properties	*Fishman et al., 1992;O'Dowd and Smith, 1993; Bates et al.,* 2001; *Raes et al*., 2000b; *Russell et al.,* 1999; *Williams et al*., 2007

Chapter 2

Experimental Techniques and Data

2.1 Introduction

Chapter 1 presented an overview of the physical, chemical and optical/radiative characteristics of atmospheric aerosols along with their sources, sinks, production and removal mechanisms. The need for the studies on aerosol characteristics with a holistic approach also has been highlighted. To achieve this, systematic monitoring and measurements of aerosols with reasonable spatial and temporal resolutions using multi-instrumental methods are essential. This thesis is based on the in-situ measured, near-surface properties of aerosols as well as satellite-retrieved aerosol parameters. Measurement of near-surface aerosol number density-size distribution (NSD) has been carried out using a high resolution Aerosol Spectrometer and for the estimation of the aerosol mass concentration or loading a well-perceived sampling technique was used. The collected aerosol samples were analysed for the major chemical species by making use of state-of-the-art analytical techniques. The principle of operation of the aerosol spectrometer, sampler and the instruments used for chemical analysis along with their technical details are discussed in this chapter. The columnar aerosol data from the satellite-borne instrument, the MODerate resolution Imaging Spectrometer (MODIS) on board Aqua and Terra satellites were also utilized in this work. A brief account of the technical specifications and the retrieval methodologies of MODIS are also presented in this chapter. This is followed by short notes on the supplementary data namely the meteorological parameters, NCEP-NCAR reanalysis data and air mass back-trajectories used for the interpretation of the observed aerosol features in the present analysis.

2.2 Physical characterisation of aerosols

The major physical characteristics of the aerosol system examined in this work include the number density, size distribution and mass loading. Formed from a variety of sources, aerosols are polydisperse in nature existing in a wide spectrum of sizes with varying number densities. The aerosol number density and size distribution measurements form a crucial component in aerosol science. In the present study, the aerosol size distribution measurements are carried out by using an Aerosol Spectrometer and the mass loading measurements by gravimetric analysis of aerosol

samples, collected by a High Volume aerosol Sampler. The principle of operation, calibration and other technical details of these instruments are described in the following sections.

2.2.1 Aerosol spectrometer

The aerosol Number density -Size Distribution is measured by using an Aerosol spectrometer (Model 1.108 of GRIMM Aerosol Technik GmbH & Co. KG, Germany) which is basically an Optical Particle Counter(OPC).The aerosol spectrometer is a compact portable device which has been built for continuous measurement of airborne particles.This instrument operates at 15 size channels with cut-off diameters >0.3, >0.4, >0.5, >0.65, >0.8, >1, >1.6, >2, >3, >4, >5, >7.5, >10, >15 and >20µm to provide size-segregated number density in real time (http:/www.grimm-aerosol.com). It measures the aerosol number density at regular intervals of 5min and is capable of particle counts up to $2x10^6$particles l^{-1}.The instrument consists of (i) an aerosol inlet *(ii)* an optical bench with an integrated laser *(iii)* a sampling pump providing constant airflow *(iv)* particle sizing and characterizing circuit *(v)* a digital board for data conversion, processing storage and export *(vi)* a serial port. A photograph of the Aerosol spectrometer used in the present work is shown in Figure 2.1.The technical details of the instrument are listed in Table2.1.

Figure 2.1.*Aerosol Spectrometer model 1.108 of GRIMM.*

2.2.1.1 *Principle of operation of aerosol spectrometer*

The aerosol spectrometer works on the principle of scattering of light by single particle [*Grimm and Eatough*, 2009]. The schematic diagram in Figure2.2 illustrates the working principle of the instrument. This consists of a high-intensity light source, a controlled air flow and highly sensitive light gathering detector. Air sample is drawn into the unit through an air inlet (sampling head) using an internal volume-controlled pump operating at 1.2litre min^{-1}. The air sample enters perpendicular to the path of the focused light beam and the scattered signal is detected using a high-speed detector. An

internal flow controller maintains a constant airflow through the instrument. The sample air then passes through a particle filter after leaving the optical chamber which can be used for gravimetric or chemical analysis.

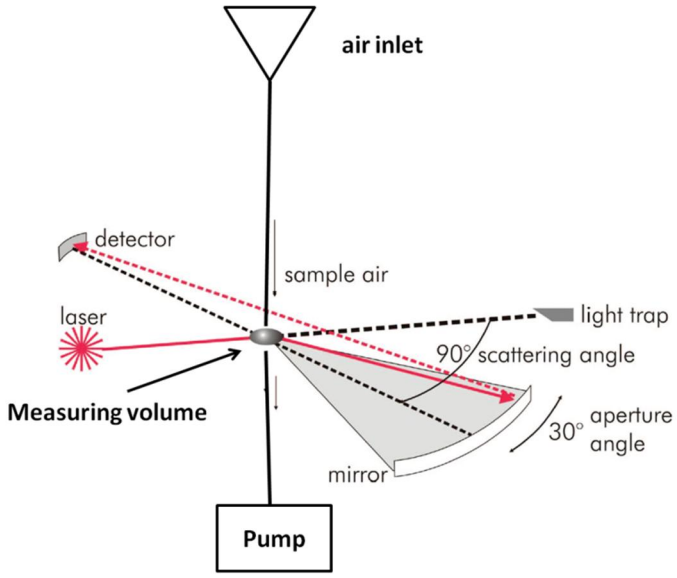

Figure 2.2. *Schematic diagram for measurement principle of the Aerosol Spectrometer.*

Figure 2.3 shows the assembly of the laser-based measuring chamber. The light source is a laser diode of wavelength 780nm and the beam then passes several collimator lenses, to get a wide, beam of light.

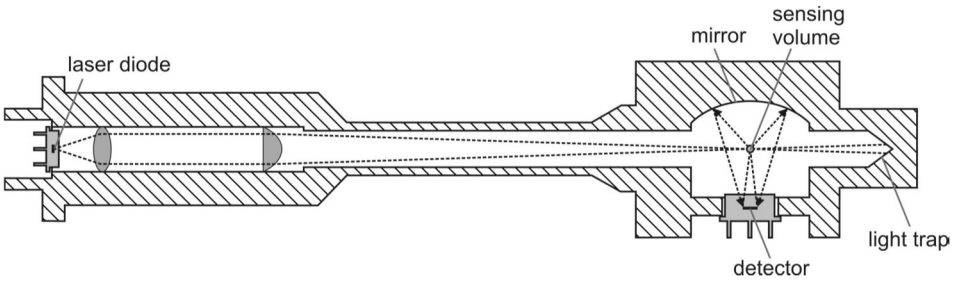

Figure 2.3.*Optical bench with integrated laser of the Aerosol Spectrometer.*

The sample air with particles of varying sizes is passed continuously through this laser beam and the scattered signal from each particle is detected. The detector is a high speed photo diode which is positioned right angle to the incident laser beam. This scattered light is collected by a mirror in a given angle and focused to the detector. This optical alignment increases the scattered light collected by the detector and optimizes the signal-to-noise ratio. Therefore even very small particles down to 0.3µm can be detected. In accordance with the Mie theory, each measured pulse height is directly proportional to the particle size. The pulses from the photo detector are sent to a Pulse

Height Analyzer (PHA). The PHA examines the magnitude of the pulse and places its value into an appropriate sizing channel, called the size bin and then counts it. The bins contain data about each pulse and this data is correlated to particle sizes. Each signal is amplified, counted and classified in 15 different size channels by an integrated pulse height analyzer. These counts are recorded at intervals of 6secs. The built-in software generates the aerosol number size spectrum averaged for a fixed time period (which is selected as 5mins for the present study). The particle counts can be displayed and are also stored in a data card and can be transferred to computer via the RS 232 for further analysis.

Parameter	Specifications
Size bins	15
Particle cutoff diameter (µm)	>0.3,>0.4,>0.5,>0.65,>0.8,>1.0,>1.5,>2,>3,>4 ,>5,>7.5,>10,>15 and >20µm
Particle count	1 to 2,000,000 particles litre^{-1}
Light source	Laser diode (780nm)
Sensitivity	1particles litre^{-1}
Flow rate	1.2litrem^{-1}
Operating temperature	4 to 45° C

Table 2.1. *Technical specifications of Aerosol spectrometer (model GRIMM1.108).*

At the beginning of each measurement, when the instrument is switched ON, it initiates a self-test, which last approximately 30 seconds. Here all optical, pneumatical, and electronic components are being checked. Afterwards the actual measurement starts and the LCD-display shows the measured aerosol number density continuously every six seconds. All actions of the instruments are activated and controlled through GRIMM's 1.174 software.

2.2.1.2 Calibration of OPC

The particle size detection and counting are calibrated with traceable NIST-certified (National Institute of Standards and Technology) mono disperse latex spheres (operation manual). In this procedure, the equivalent diameters of optical latex spheres are measured. The size channels are related to electronic thresholds. The scattered light from the single particle is collected by a mirror in a given angle and focused to the

detector (Figure 2.3). The photons collected by the detector will give a raw-signal which will be amplified and classified in a particle size channel. From this the number concentration and size of the particles are measured. Based on these measurements and the known characteristics of the calibration source, the instrument is calibrated. Instrument calibration is done periodically by the manufacturer.

2.2.2 High Volume aerosol Sampler

A High Volume aerosol Sampler (HVS) Model GH 2000 of Graseby Anderson, USA was used for aerosol mass loading measurements (Figure 2.4). It has the advantage of providing sufficient sample for both gravimetric and chemical analysis. Samples were collected on pre-conditioned quartz fibre filter (collection substrate) and analysed gravimetrically to estimate the aerosol mass loading.

Figure 2.4.*High Volume Sampler, model GH 2000 of Graseby Anderson.*

2.2.2.1 Principle of operation of HVS

The sampling is based on the principle of impaction of aerosols on substrates by aspiration, the process by which particles are drawn from ambient air through an opening called orifice by using a built-in vacuum pump. Air carrying particles passes through an orifice and air flow bypasses a solid object (i.e., a collection substrate) perpendicular to the orifice axis. While the air diverges to bypass the obstacle, the small particles will do the same. But large particles would tend to leave the streamlines and continue travel in the direction of their initial motion and get impacted and collected on the intervening collection media. The details of this mechanism are given in Chapter 1. The aspiration efficiency (EA) may be defined as [*Harrison and Van Grieken*, 1998],

$$EA = \frac{Concentration\ of\ particles\ in\ the\ air\ actually\ entering\ the\ orifice}{Concentration\ of\ particles\ in\ the\ undisturbed\ upstream\ air}$$

which determines the efficiency with which particles are drawn through the inlet.

2.2.2.2 Instrument Details

The aerosol sampler comprises of (1) a sampling head /inlet, (2) a transmission medium or collection substrate, (3) a calibrated flow control unit, and (4) a pump. The schematic diagram of a single stage HVS is given in Figure 2.5.

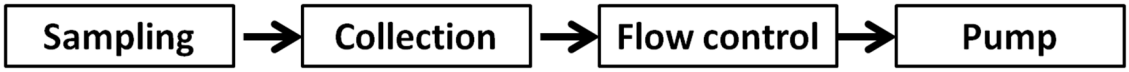

Figure 2.5. *Schematic block diagram of a High Volume aerosol Sampler.*

The HVS used for this study, has the inlet and the transmission medium built into a single sampling head in order to avoid particle losses to the internal walls of the transmission pipe. The sampling inlet is omni-directional and has performance independent of wind speed. The collection substrate used is quartz fiber filter. The fibrous filters have the advantage of providing in-depth particle collection and hence high load carrying capacity. Collection efficiency is close to 100% for particles of most size ranges and in the present study the sampler collects particles of size down to 0.01μm as estimated from the filter characteristics and air flow rate by the manufacturer.

In view of large variability in aerosol composition, aerosol sample need to be collected over short time span (i.e., 2-6 hours) and hence high flow rates are required to collect sufficient mass of particles. The pump employed in this sampler operates at a flow rate of 20 Cubic Feet per Minute which is continuously monitored by a flow monitor (rotameter) attached to the sampler. The sampler is periodically calibrated using the calibration equipment supplied along with the sampler as explained below.

2.2.2.3 Calibration of HVS

The calibration equipment of HVS (shown in Figure 2.6) provided along with the sampler by the manufacturer consists of a cylindrical hollow tube both ends having four orifices of equal diameter of ~1.5cm. This cylinder has a circular orifice plate having four identical orifices which moves on the top of the side, which is connected to HVS. By means of a knob fixed at the other end of the hollow cylinder, the orifices can be opened or closed and flow can be controlled. When the orifices of the plate overlap with orifices of cylinder, the calibrator is fully open. On one side of the calibrator, there

is a small vent acting as a pressure tap for the manometer used for measuring the pressure drop. The manometer is filled with water and water levels adjusted to read zero. A filter paper is mounted on HVS and the instrument is switched on. The flow rate reading is noted from the attached rotameter. Then, the filter holder of the HVS is removed and the calibrator in fully open position is attached. The pressure tap on one side of the manometer is connected to the calibrator and the other tap of the manometer is left open to the atmosphere.

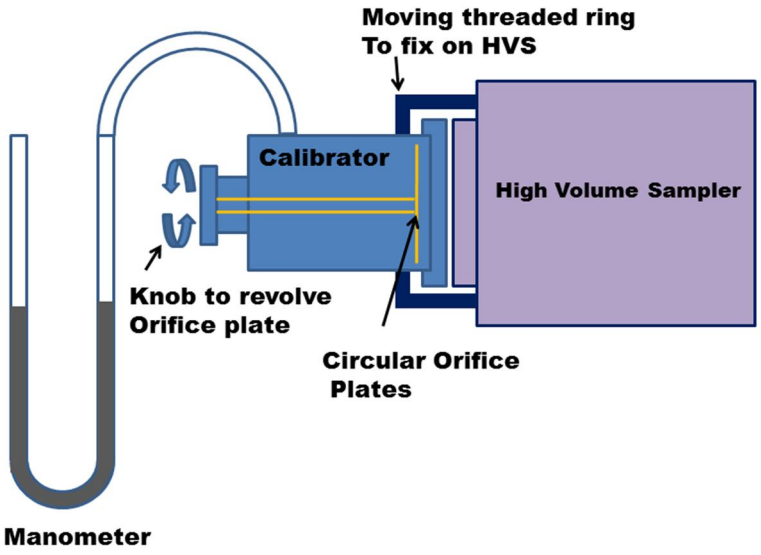

Figure2.6.*Schematic diagram of calibrator attached to HVS.*

The HVS is switched on again and the knob of the calibration equipment is adjusted till the rotameter shows the same reading as that with the filter mounted. The difference in water level in the manometer is noted as ΔH. The actual flow rate, Q_a is estimated as,

$$Q_a = \frac{\sqrt{\frac{\Delta H\, T}{P}}}{a'} - \frac{b'}{a'} \qquad 2.1$$

where T and P are the ambient temperature (in Kelvin) and pressure (mm Hg) and a' and b' are the slope and intercept obtained from the calibration curve of the equipment provided by the manufacturer as 0.99 and -0.017 respectively. Generally, ΔH is measured as ~1.27inch and the flow rate estimated as ~0.6m^3min^{-1}.

2.2.2.4 Sampling and estimation of aerosol mass concentration

Quartz fibre filters of 4" (110mm) diameter (Whatman QMA 4) were used as aerosol collection substrate/filter medium in the present study. These are pre-conditioned before sampling. First step in pre-conditioning is heating the substrates to 100° C in an electric oven for about three hours to remove moisture and any volatile

impurity and then desiccating for 24hours. Each filter is then tare-weighed using a microbalance (Model AT 20, Metler Toledo, Switzerland) having sensitivity of ±2µg and loaded into the sampling head of the HVS. The sampler is operated for a fixed duration of time, typically ranging from 2 to 6hours depending on the location of sampling (i.e. aerosol loading in the atmosphere). The sampling time is adjusted such that sufficient aerosols mass is collected for chemical analysis and also to avoid bounce off of particles. After operation/sample collection, the substrate is again desiccated and weighed under same laboratory conditions. The difference between the initial and final weights gives the mass of aerosols collected on the filter (m_a) during the sampling period (t). Product of flow rate and sampling time gives the total volume of air sampled. Hence the aerosol mass loading (M_L) in µg m^{-3} is estimated as,

$$M_L = \frac{m_a}{t \times Q_a} \qquad 2.2$$

Where Q_a is the flow rate of the sampler.

2.3 Chemical characterisation of aerosols

The aerosol samples collected using the HVS are subjected to chemical analysis to identify and quantify the various chemical species present in them. Distinctly different analytical techniques are used to quantify the chemical species. In the present study, the following techniques were employed:

(1) Ion Chromatography (IC) for water soluble anionic species SO_4^{2-}, NO_3^-, NO_2^-, Cl^-, PO_4^-, F^-, Br^-,and cationic species Na^+, K^+, Ca^{2+}, Mg^{2+} and NH_4^+

(2) Inductively Coupled Plasma - Atomic Emission Spectroscopy (ICP-AES) for the acid soluble species Fe, Al, Zn, Pb, Co, Ni, Cu, Cr, Mn, etc.

(3)Atomic Absorption Spectroscopy (AAS) for Na and K.

(4) Auto titrator for bicarbonate.

2.3.1 Sample handling and preparation

For all the four techniques mentioned above, the samples need to be in liquid form and hence they are digested in appropriate media/solvent. One quarter of the sample laden substrate is extracted in 50ml of de-ionized water (Milli-Q with18MΩ resistivity) using ultrasonic digestion for 30min for the analysis of water-soluble ionic species using IC. Another quarter of the substrate is digested in 25ml of de-ionized water by vigorous shaking for the analysis of the highly volatile NH_4^+. This sample is analysed immediately after preparation to avoid loss due to evaporation. Metallic

species which are not amenable to aqueous extraction are extracted with 3ml of Supra pure nitric acid (65%) and de-ionized water using microwave digestion. The aerosol sampling and preparation of samples for analysis were carried out with intense care to avoid contamination at all the stages. After collection, the sample-laden substrates were preserved in deep freezer till chemical analysis. Only teflon wares were used for storage and preparation of samples for analysis. The samples were prepared under a clean air laminar flow bench to ensure the clean environment and avoid contamination.

2.3.2 Ion Chromatography

Ion chromatography is an analytical technique of separating water-soluble ions (positively or negatively charged) from a solution in a relatively short time using a stationary phase. Generally, the stationary phase comprises of (a) the charged groups which are involved in the ion exchange process and (b) the matrix on which the charged groups are fixed. Ion exchangers are called cation exchangers if they have negatively charged functional groups and possess exchangeable cations. Based on this, there are two types of ion chromatography, namely, (1) anion exchange chromatography used to measure negatively charged ions and (2) cation exchange chromatography used to measure positively charged ions. The stationary phase for IC is usually in the form of a cylindrical column in which an ion-exchange material is uniformly packed and retained by means of porous frits located at each end of the column. Generally, the functional group used in anion chromatography is a quaternary ammonium group and for cation it is sulphonic acid groups.

In addition to the stationary phase, the ion-exchange chromatography essentially includes a mobile phase called eluent. Eluents are usually prepared by dissolving buffers, acids or bases in aqueous solvent or in an aqueous–organic solvent mixture. The mobile phase carries the analyte mixture through the stationary phase or column and the IC system. The analyte ions and similarly charged ions of the eluent compete to bind to the oppositely charged ionic functional group on the surface of the stationary phase. The stationary phase interacts more strongly with some components in the solution than others. This results in components passing through the stationary phase at different rates, effectively separating them. In short, in Ion Chromatography, the separation of ions is achieved based on differences in the extent to which they are partitioned between the column and the eluent.

2.3.2.1 Chromatographic System

The major components of an ion chromatograph are shown schematically in Figure 2.7. A pump delivers the mobile phase through the chromatographic system. The sample is injected into the system via a valve injector prior to the separator column. The sample injection hardware is designed to introduce a small volume (20µl) of sample into the ion chromatograph. Both manual and automated injection systems are available. The analytes (ions) are identified and quantified by a detection system. The most commonly employed detector in ion chromatography is the conductivity detector, which can be used with or without a suppressor system. The main function of the suppressor system as part of the detection unit is to chemically reduce the high background conductivity of the electrolytes in the eluent, and to convert the sample ions into a more conductive form.

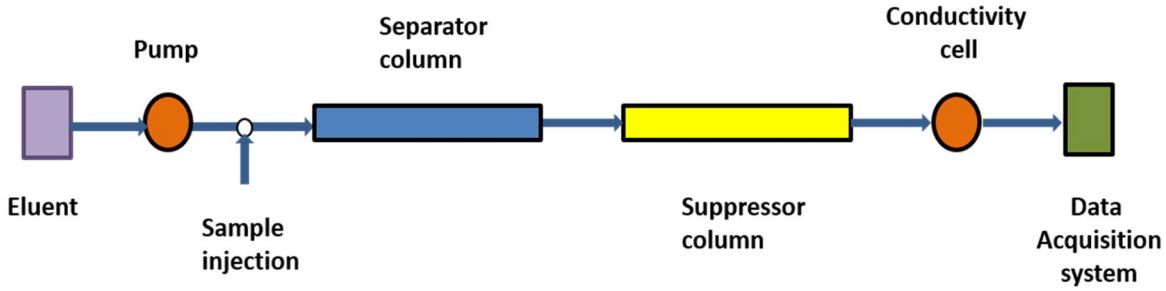

Figure 2.7. *Schematic showing the major components of an Ion Chromatograph.*

2.3.2.2 Theory of chromatography

As discussed earlier, the analyte ions and the ions of the eluent compete to bind to the oppositely charged ionic functional group on the surface of the stationary phase. Assuming that the exchanging ions are cations, the competition can be explained using the following equation [*Fritz and Gjerde*, 2009]:

$$R\text{-}X^{-}M^{+}+C^{+} \leftrightarrow R\text{-}X^{-}C^{+}+M^{+} \qquad 2.3$$

In this process the cation M^{+} of the eluent is replaced with the analyte cation C^{+} bound to the anion X^{-} which is fixed ion exchange resin (R). In anion exchange chromatography, the exchanging ions are anions and the equation is represented as,

$$R\text{-}X^{+}A^{-}+B^{-} \leftrightarrow R\text{-}X^{+}B^{-}+A^{-} \qquad 2.4$$

The anion B^{-} of the eluent replaced with the analyte anion A^{-} bound to the positively charged ion X^{+} on the surface of the stationary phase. The adsorption of the analyte to the stationary phase and desorption by the eluent ions is repeated during their journey in the column, resulting in the separation due to ion-exchange. Various ions in the sample migrate through the column at different rates, get separated from each other

and hence enter the detector at different times. This process of separation of two components A and B is illustrated schematically in Figure 2.8.

The equilibrium constant for the reaction 2.3 can be written as:

$$K_{eq}=\frac{[RX^{-}M^{+}][C^{+}]}{[RX^{-}C^{+}][M^{+}]} \qquad 2.5$$

where the name of species enclosed in square brackets denote their molar concentrations. Rearranging yields

$$\frac{[RX^{-}M^{+}]}{[M^{+}]}=K_{eq}\frac{[RX^{-}C^{+}]}{[C^{+}]} \qquad 2.6$$

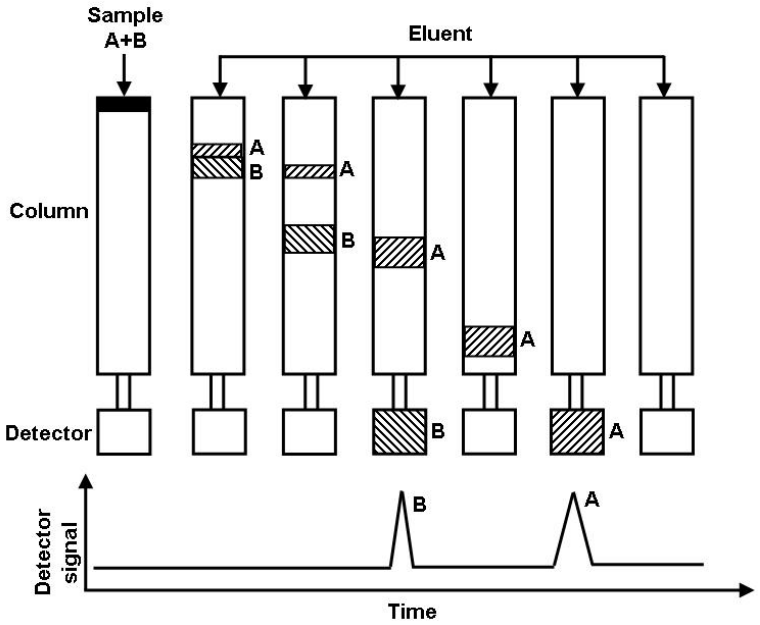

Figure 2.8.*Illustration of the chromatographic separation of two components A and B.*

During elution, the aqueous concentration of C^{+} is much larger than M^{+}. Also, the exchanger has large number of exchange sites with C^{+} ions relative to the number of M^{+} ions being retained. Thus the overall concentrations $[RX^{-}C^{+}]$ and $[C^{+}]$ are not affected significantly by shifts in the equilibrium. Therefore the right hand side of the Equation 2.6 is essentially constant and can be approximated as,

$$K=\frac{[RX^{-}M^{+}]}{[M^{+}]}=\frac{C_S}{C_M} \qquad 2.7$$

Where K is a constant known as the distribution or partition coefficient, C_S denotes the molar concentration of the sample solute ion in the stationary phase and C_M denotes its concentration in the mobile phase. When K is large, a strong tendency exists

for the solid phase to retain B^+, in which case the fraction of time spent by B^+ in the solid phase will be large thereby slowing down its movement through the column. When *K* is small, the opposite condition prevails causing fast movement of the ion through the column.

The results of this analytical technique are represented as plots of conductivity versus time referred as *chromatograms*. The presence of a particular species appears as a peak in the chromatogram. The area under the curve with this peak above the base line (which represents the conductivity of the eluent) is used for the estimation of the concentration of the particular species. The resolution (*R*) with which two sample components are separated in a column is expressed as the ratio between the two peak maxima to the mean value of the peak width at the baseline.

$$R = \frac{(t_A - t_B)}{(W_A + W_B)} \qquad 2.8$$

where t_A and t_B represents the retention times of components A and B respectively and W_A and W_B represents their base widths.

2.3.2.3 Instrument Details

For the present study, the water soluble anions F^-, Cl^-, Br^-, NO_2^-, NO_3^-, PO_4^{2-}, SO_4^{2-}, and cations Na^+, Mg^{2+}, Ca^{2+}, K^+ and NH_4^+ were analyzed using Ion chromatograph model DX-120 from Dionex, USA and Metrohm882 plus and 883 plus, Switzerland. The results obtained from these two instruments for same samples were compared and found to be in very good agreement (within 1% of deviation). DX-120 is equipped with two columns – one for the separation of anions (IonPac AS14) and the other for cations (IonPac CS12A). A 3.5mM solution of sodium carbonate (Na_2CO_3) along with a 1.0mM solution of sodium bicarbonate ($NaHCO_3$) is used as eluent for anions and a 20mM solution of Methane Sulphonic Acid (MSA, CH_3SO_3H) as eluent for cations. A high pressure pump forces the eluent through the column at a typical flow rate of about 1ml min^{-1}. The sulphonate functional groups ($SO_3^-H^+$) and the bicarbonate functional groups ($H^+CO_3^-$) attached to the polystyrene resins are used in DX-120, Dionex as the cation and anion exchangers respectively. The various cations elute out of the column in the order Na^+, NH_4^+, K^+, Mg^{2+} and Ca^{2+} and the various anions in the order F^-, Cl^-, NO_2^-, Br^-, NO_3^-, PO_4^{3-} and SO_4^{2-}.

Metrohm 882 Plus is equipped with MetroSep C2cation column and 883 Plus with Metrosep A Supp 5 anion column. The sulphonate functional groups and quarternary ammonium groups are used as ion exchangers for cation and anion columns

respectively. A 1.0mM solution of sodium carbonate (Na_2CO_3) along with a 1.0mM solution of sodium bicarbonate ($NaHCO_3$) and a 3mM solution of nitric acid (HNO_3) are used as the eluents for anions and cations respectively. A pump flow of 0.7ml min^{-1} is maintained for cation and 0.9ml min^{-1} for anion. A PC based data acquisition system with necessary software is used along with the IC (*PeakNet Chromatography Workstation* for Dionex and *MagIC Net* for Metrohm).

The photographs of the two ion chromatograph systems used in this study are shown in Figure 2.9. The analysis and calibration details are provided below pertain to Metrohm 882/883 Plus.

(a) (b)

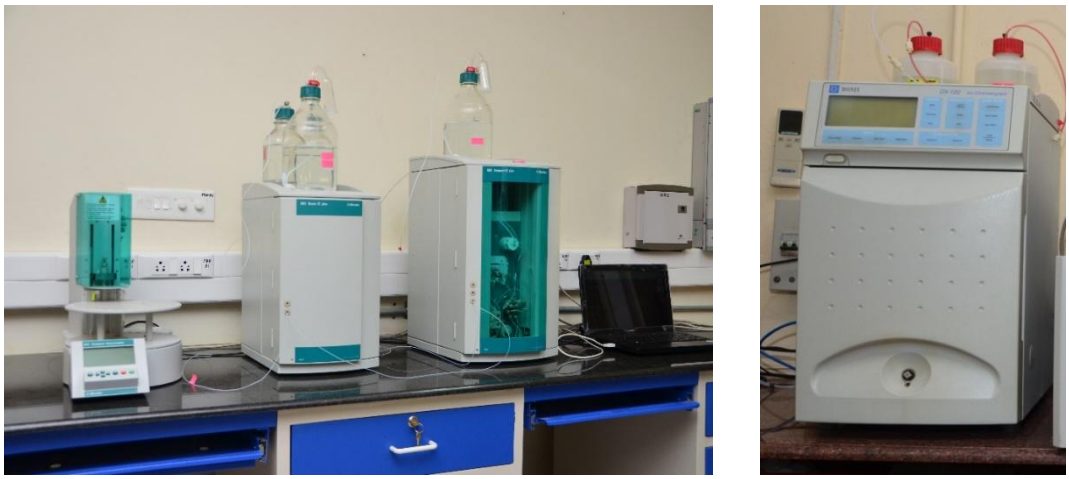

Figure 2.9. *(a) Ion Chromatograph model Metrohm 882 plus (Switzerland) for cation and 883 plus for anion with Auto Sampler (b) Ion Chromatograph Model DX 120, Dionex USA.*

2.3.2.4 Calibration and estimation of concentration

Prior to the analysis of each set of sample, the ion chromatograph is calibrated with appropriate standards. Three point calibrations are adopted in the present study. Multi element standards of 1000ppm concentration from M/s Merck containing Na, K, Ca, Mg, SO_4, F, Cl, NO_3, NO_2, Br, PO_4 are appropriately diluted to make cation and anion standards of known concentrations, typically 0.2ppm, 2ppm and 5ppm. The IC system is allowed to run until a stable base line (~890µS cm^{-1} for cation and ~15µS cm^{-1} for anion), corresponding to the suppressed conductivity of the eluent, is obtained. The standard solutions are then injected to the sample path one by one and the corresponding chromatogram is obtained. Figures 2.10a and b shows typical chromatograms obtained for an anion standard solution and cation standard solution respectively for 5ppm concentration. X axis is the retention time and Y axis represents

the measured conductivity in µS cm^{-1}. The first large peak (not shown fully) in the chromatogram for cation standard corresponds to all the anions present in the sample which elute first. The quantitative analysis of different ions is obtained based on the area under each peak for the respective ion. Knowing the order in which the ions elute out, the peaks are assigned to specific ions and the area of the peak is assigned to the concentration of the standard solution. The tables accompanying the chromatograms give the retention times, peak area and concentration of the different ions.

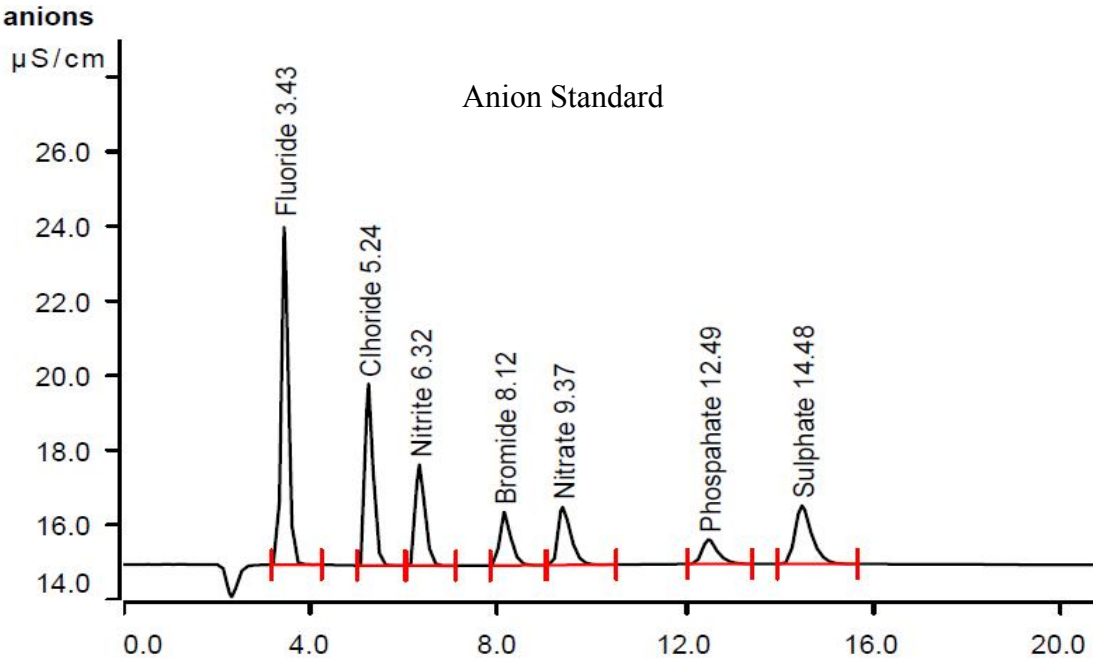

(a)

Peak number	Retention time(min)	Peak Area (µS/cm) x min)	Peak Height (µS/cm)	Concentration of standard(ppm)	Ion
1	3.4	1.49	9.0	5.000	Fluoride
2	5.2	0.93	4.86	5.000	Chloride
3	6.31	0.62	2.70	5.000	Nitrite
4	8.12	0.39	1.4	5.000	Bromide
5	9.4	0.49	1.6	5.000	Nitrate
6	12.48	0.25	0.66	5.000	Phosphate
7	14.47	0.64	1.56	5.000	Sulphate

Figure 2.10. (a) *Typical chromatogram along with the table of relevant parameters for quantification of anion standards. The name of ion and its time of elution are given above each peak.*

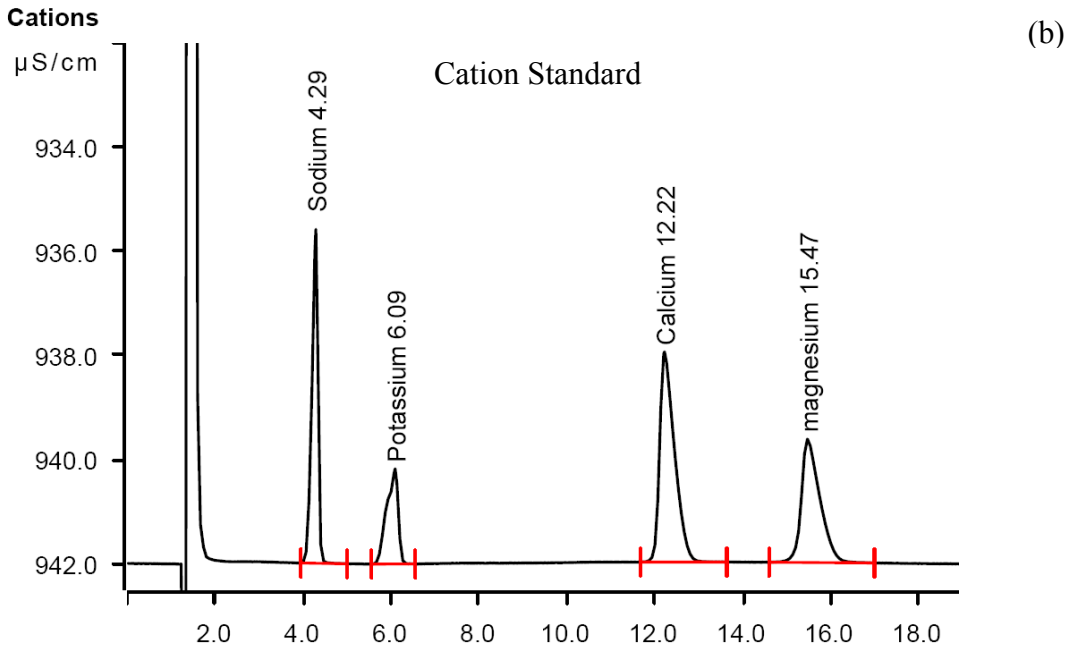

Peak number	Retention time(min)	Peak Area (µS/cm) x min)	Peak Height (µS/cm)	Concentration of standard(ppm)	Ion
1	4.29	2.0896	0.489	5.000	Sodium
2	6.09	1.1102	.549	5.000	Potassium
3	12.22	3.3982	3.857	5.000	Calcium
4	15.47	2.5090	2.443	5.000	magnesium

Figure 2.10. (b) *Typical chromatogram along with the table of relevant parameters for quantification of cation standards. The name of ion and its time of elution are given above each peak.*

Once the system has been calibrated, the sample solution (prepared as detailed in section 2.3.1) is injected into the IC in the same manner and the chromatograms are obtained. Ions in the samples are identified by comparing their retention time with that of the standards and the concentration of each ion is quantified by the respective peak area. Blank filters are also analysed following the same procedure and the concentration of each of the ions present in the blank filter is subtracted from the estimated mass concentrations in the sample solution. The details are discussed in section 2.3.4.4. Figure 2.10 c and d shows the chromatograms of anions and cations respectively in the sample and the tables below give the details of respective ions analysed.

Sample

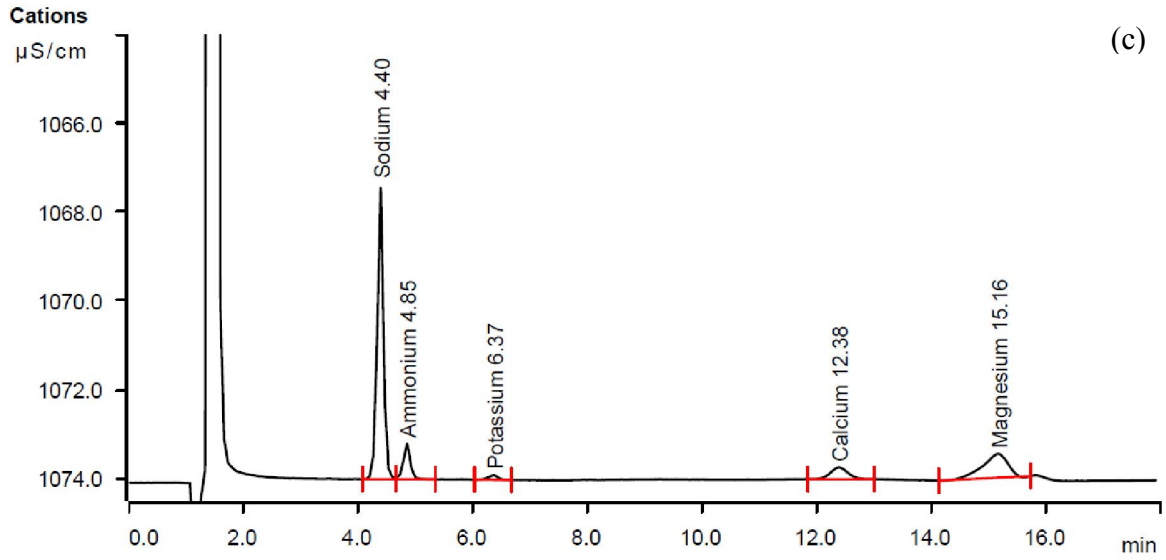

(c)

Peak number	Retention time (min)	Peak Area (µS/cm) x min)	Peak Height (µS/cm)	Concentration (ppm)	Ion
1	4.4	0.9198	4.216	2.197	Sodium
2	6.37	0.1029	0.237	0.465	Potassium
3	12.3	0.2704	0.336	0.395	Calcium
4	15.16	0.7491	0.581	1.467	magnesium

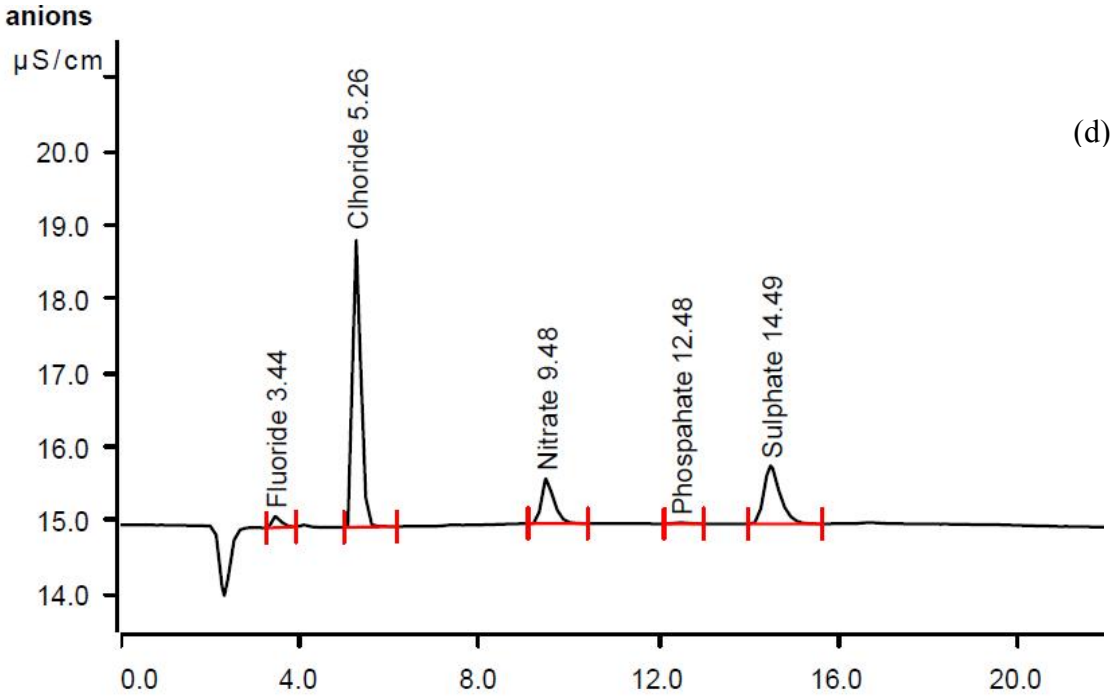

(d)

Peak number	Retention time (min)	Peak Area (µS/cm) x min)	Peak Height (µS/cm)	Concentration of standard (ppm)	Ion
	3.44	0.037	0.15	0.05	Fluoride
	5.25	0.75	3.88	4.1	Chloride
	9.48	0.19	0.6	1.9	Nitrate
	12.48	0.005	0.016	0.01	Phosphate
	14.48	0.32	0.78	2.44	Sulphate

***Figure 2.10**. (c)Ion chromatograms along with the table of relevant parameters obtained for cations and **(d)** ion chromatograms along with the table of relevant parameters obtained for anions, of a sample collected over Thiruvananthapuram.*

2.3.3 Inductively Coupled Plasma-Atomic Emission Spectroscopy (ICP-AES)

Inductively Coupled Plasma-Atomic Emission Spectroscopy (ICP-AES) is one of the most common analytical techniques used for elemental analysis. Its high sensitivity, specificity, multi-element capability and good detection limits favour the use of this technique in a variety of applications.

2.3.3.1 Principle of operation of ICP-AES

The atomic emission spectroscopy technique is based on the fact that excited atoms emit energy at a wavelength characteristic of the particular atom as they return to ground state. This process can be illustrated as follows:

$$M + energy \rightarrow M^* \rightarrow M + \Delta E \qquad 2.9$$

where, M and M^* represent the atom in the ground state and excited state respectively and ΔE the excitation energy (or the difference in energy between ground state and excited state of the atom) given as,

$$\Delta E = h\nu = hc/\lambda \qquad 2.10$$

where, his Planck's constant, and ν is the frequency of the radiation, c is the speed of light and λ is wavelength at which emission takes place.

Every element has its own characteristic set of energy levels and thus its own unique set of emission wavelengths. This property makes atomic emission spectrometry useful for element-specific analytical techniques. In addition to this transition, other transitions from higher to lower energy levels are also possible, resulting in more than one emission wavelength for an element. The most sensitive and interference free wavelength among the multiple wavelengths emitted by an element is used for the

estimation of concentration. The intensity of the radiation emitted at the chosen wavelength is proportional to the concentration of that element in the sample.

To produce strong atomic emission from atoms/elements it is necessary to attain considerably high excitation energy which is not available from simple flames. For the excitation, ICP-AES uses high temperature inert-gas plasma, in this case Argon plasma, with temperature in the range of 7,000K to 10,000K. It is a very effective medium for volatilization, atomization and excitation of atoms. The aerosol sample is introduced into the plasma as droplets.

2.3.3.2 ICP-AES: Instrument Details

ICP-AES, model Optima 4300V of Perkin Elmer, was used for the present study to quantify the metallic species in aerosols. The ICP-AES system is consist of five basic components, namely, (1) Plasma source (ICP torch), (2) Nebulizer, (3) Polychromator, (4) Detector, and (5) Data Acquisition System, as shown in the schematic diagram in Figure 2.11.

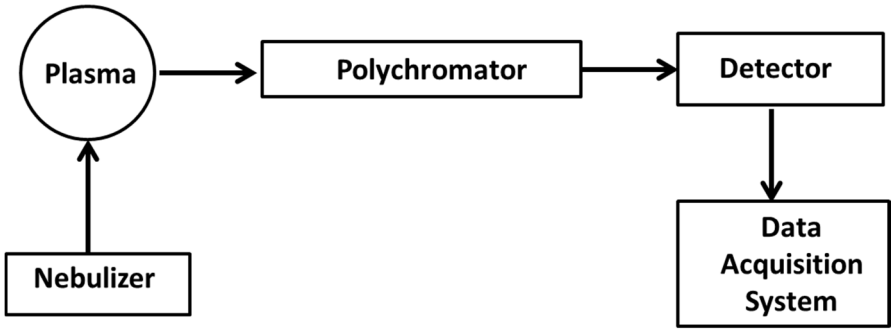

Figure 2.11. *Schematic of Inductively Coupled Plasma-Atomic Emission Spectrometer*

In ICP-AES, the excitation of atoms is provided by an inductively coupled plasma source, commonly known as the ICP torch, a schematic of which is shown in Figure 2.12.It consists of three concentric quartz tubes through which streams of argon flow at a rate of 15litre min^{-1}. Surrounding the top of this tube is a water-cooled induction coil that is powered by a radio-frequency (RF) generator, producing 1500W of energy at ~40MHz. Ionization of the flowing argon is initiated by a spark from a Tesla coil. The resulting ions, and their associated electrons, interact with the fluctuating magnetic field produced by the induction coil. This interaction causes the ions and electrons within the coil to flow in closed annular paths as depicted in the figure. The resistance in this movement results in Ohmic heating. The temperature of the plasma formed is so high that it requires thermal isolation from the outer quartz

cylinder, and this is achieved by flowing argon tangentially around the walls of the tube. This tangential flow cools the inside walls of the centre tube and confines the plasma radially.

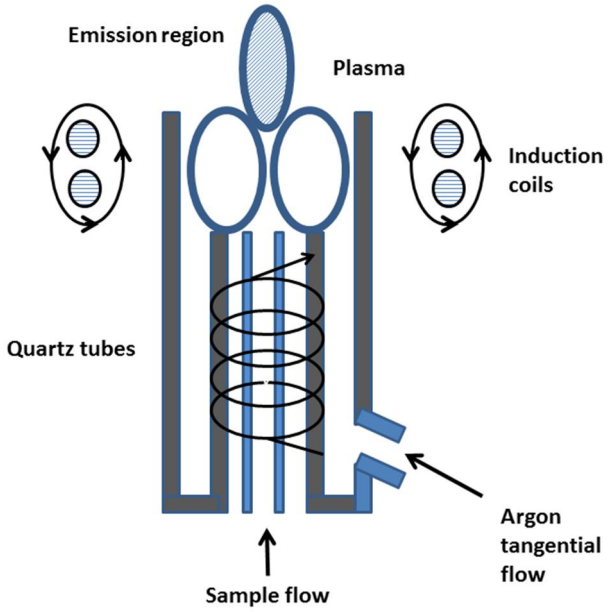

Figure 2.12. *Schematic of an ICP Torch*

Parameter	Specifications
Principle	Atomic emission
Excitation source	Plasma (Ar gas)
RF power	1500W
Temperature attained	6000 – 10000K
Sample flow rate	1.5mlmin^{-1}
Plasma flow rate	15litre min^{-1}
Plasma viewing	radial
Polychromator	Echelle grating
Detector	2D Charge Coupled Device (CCD)
Wavelength range	165 – 782nm
Sensitivity	0.02 – 10ppb
Resolution	0.006nm

Table 2.2. *System specifications of ICP-AES model Perkin Elmer Optima 4300V.*

In addition to this, the instrument is equipped with a spray chamber and a nebulizer. The ICP-AES has the capability of simultaneous measurement of ~72 elements with the emission wavelengths in the range of 165-782nm with a resolution of 0.006nm. The sample intake rate is kept at 1.5ml min^{-1}.The sample to be analyzed should be in liquid form and to be divided in to fine droplets and this is achieved through a nebulizer which uses pneumatic forces to break up the sample liquid into fine droplets. Method of preparation of liquid samples is discussed in section 2.3.1.

The temperature in the analytical zone of the plasma ranges from 6000 to 10000 K, and the samples reaching the zone are completely atomized. The plasma emits a continuum of background radiation, extending from ultraviolet to visible region, which excites the atoms. The characteristic radiation emitted by the excited atoms is isolated with the help of Echelle gratings used as a polychromator and detected by an advanced Segmented Charge Coupled Device (SCCD). Detailed technical specifications of the system are summarized in Table 2.2. In the present study ICP-AES is used for the quantitative analysis of the metallic species Al, Ca, Cr, Cu, Fe, Mg, Mn, Pb, Ti, and Zn. The sensitivity of the instrument depends on the species and ranges from 0.02ppb to 10 ppb.

2.3.3.3 Calibration of ICP-AES and estimation of concentration

For the quantitative analysis of the aerosol sample and determination of elemental concentration, the system is to be calibrated. Calibration is done before and after each set of analysis. The calibration standards used were prepared from ICP grade standard solution of Perkin Elmer make QC21,comprising of 21 elements which includes Fe, Cu, Mn, Cr, Ni, Pb, Ca, Mg, Zn, Ti and Aldrich make single element standard for Al and Si. Here also, multi-point calibration is adopted with standards having concentrations 0.1, 1.0 and 10ppm. Before giving samples these standards are analysed and the corresponding emission intensities at the characteristic wavelength are noted. Calibration curve is plotted with intensity against known concentrations (a typical calibration curve obtained for Fe is shown in Figure 2.13). Subsequently, the sample is aspirated, emission intensity is measured and the concentration corresponding to this intensity is determined based on the calibration curve.

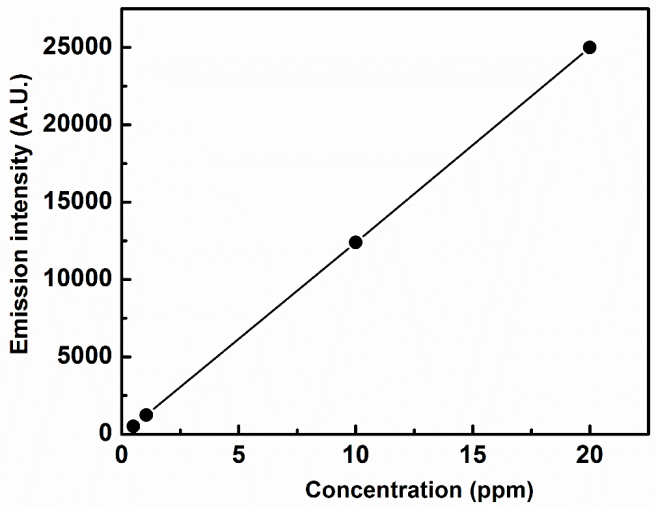

Figure 2.13. *Calibration curve obtained for Fe using ICP-AES.*

Figure 2.14. *ICP-AES model Perkin Elmer Optima 4300V.*

2.3.4 Atomic Absorption Spectroscopy (AAS)

Atomic Absorption Spectroscopy is a spectrometric technique based on the measurement of the wavelength-specific absorption of radiation by free non-ionized atoms in the gas phase. In the present study, the two major ions Na and K in the acid-digested samples are quantified using AAS since they get volatilized at the very high temperatures encountered in ICP-AES. It is to be noted that the water soluble ions Na^+ and K^+ are analysed using IC.

2.3.4.1 Principle of AAS

Atom in ground state absorbs light energy of a specific wavelength and gets into the excited state. In AAS, the probing beam of electromagnetic radiation of wavelength λ from a source passes through the observing volume where it is absorbed by the atoms. The energy (E) absorbed corresponds to the energy gap between the ground state (E_0) and the excited energy level (E_1) is given as

$$E = E_1 - E_0 = h\nu \qquad 2.11$$

The characteristic wavelength (λ) of absorption is given as

$$\lambda = hc/E \qquad 2.12$$

where c is the speed of light.

The absorption that takes place in an atomic absorption system follows Beer's law, given as,

$$I = I_0 e^{-A} \qquad 2.13$$

where

I= intensity of radiation after passing through the medium (aerosol sample in this case)

I_0 = intensity of incident radiation falling on the sample and *A is absorptance* which is proportional to the concentration of the absorbing species as depicted by the equation

$$A = \log \frac{I_0}{I} = \alpha l C \qquad 2.14$$

α is the absorption coefficient, l is the path length through the sample and C is the concentration of the species in the sample, which is quantified from the measured intensity I.

2.3.4.2 Instrument Details

Figure 2.15 shows the schematic of an Atomic Absorption Spectrometer. The Atomic absorption spectrometer essentially comprises of (1) Light/radiation source (2) Atomizer (Nebuliser-burner system) (3) Monochromator (4) Detector and (5) Data Acquisition System. The source of light is a hollow cathode lamp which contains a tungsten anode and a cylindrical hollow cathode emitting the characteristic line spectrum of the element to be analysed. To transfer the analyte to free atoms an atomizer consisting of a nebuliser-burner system is utilized.

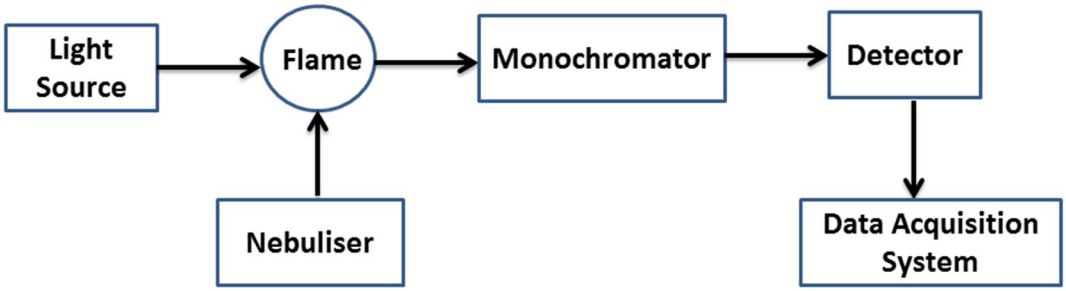

Figure 2.15. *Schematic of Atomic Absorption Spectrometer.*

This unit produces gaseous metal atoms by using a suitable combustion flame. The flame is produced by a fuel gas – oxidant gas mixture, in this case acetylene is used as the fuel, paired with air as the oxidant to attain temperatures in the range 2100°C to 2400°C. The atoms absorb their characteristic radiation emitted from the light source and get excited to higher energy levels. This absorption will cause a reduction in the intensity of radiation coming out of the chamber. By measuring the amount of radiation absorbed, a quantitative determination of the amount of analyte can be made as discussed above. The monochromator is used to select the specific wavelength of

radiation i.e. spectral line – which is absorbed by the sample, and exclude other wavelengths. The radiation selected by the monochromator is directed into a detector. A photomultiplier tube is used to detect the intensity of radiation from which the concentration of the atoms (Na and K in the present analysis) can be estimated.

Figure 2.16.*AAS model Varian Spectr AA 250 plus.*

A computer-based data acquisition system is used to generate the absorption intensity versus wavelength curve for each of the atomic species. In the present study, characteristic wavelength of 589nm for Na and 766.5nm for K were used for the quantification of Na and K. Figure 2.16 shows the photograph of AAS model Varian Spectr AA 250 plus used in the present study.

2.3.4.3 Calibration and estimation of concentration

Multi-point calibration of the instrument is carried out using solutions of known concentrations obtained by appropriate dilution of standard solutions (from Merck). For this, standard solutions of concentration 0.1, 1.0 and 1.5ppm of each element or atom to be quantified are injected into the instrument and a calibration curve is generated. The sample solution is fed into the instrument and the unknown concentration of the element is determined based on the calibration curve.

2.3.5 Estimation of blanks and error estimation

As the samples are collected on the filters, it is possible that filter artefacts are present in the form of species measured by the above mentioned techniques. In order to avoid this, blank substrates (kept in ambient conditions) are digested and analysed along with each set of sample following the same procedure as done for the sample. With each set of sample, minimum of 2 blanks were also analysed and the mean of the

estimated concentration of the respective atoms in the blank is subtracted from those obtained for the sample. This procedure also enables to nullify the errors in the estimation procedure. Table 2.3shows the mean blank values along with standard deviation obtained for different water-soluble and acid-soluble species using different techniques.

In addition to the errors arising due to the filter artefacts as discussed above, other experimental errors and uncertainties also arise in the estimation of total aerosol total mass concentration as well as mass concentration of individual chemical species. The mass measurements were done using microbalance with sensitivity of ±2μg. The mass of aerosols collected during the sampling is of order of few milligrams and the aerosol mass collected is estimated by subtracting the mass of blank substrate from that of the sample-laden one. The maximum uncertainty of 4μg can be attributed to each measurement. In this condition, for minimum aerosol mass of 1mg the maximum error is of the order of ~10^{-4}%.

Water-soluble species	Mean (ppm)	Stddev (ppm)	Acid-soluble species	Mean (ppm)	Standard deviation (ppm)
F^-	0.05	0.03	Al	0.2	0.03
Cl^-	0.4	0.03	Ca	0.5	0.1
Br^-	0.00	0.00	Cu	0.02	0.01
NO_3^-	0.05	0.02	Fe	0.1	0.02
PO_4^{3-}	0.1	0.01	K	0.08	0.04
SO_4^{2-}	0.3	0.05	Mg	0.09	0.04
Na^+	0.5	0.2	Mn	0.008	0.003
NH_4^+	0.3	0.03	Na	2.4	0.2
K^+	0.09	0.02	Pb	0.03	0.01
Mg^{2+}	0.01	0.0	Ti	0.003	0.001
Ca^{2+}	0.01	0.0	Zn	0.02	0.01

Table 2.3.*Mean and standard deviations of blank concentrations obtained for different water-soluble and acid-soluble species.*

Collection efficiency of 98% is given by the manufacturer for the type of filter used (quartz fibre, Whatman QMA4). Another artefact with chemical analyses arises due to the uneven distribution of samples on the collection medium. To confirm this, the sample-laden filter is cut into 4 quarters and analysed independently for various species and the results showed a variation of <1%. The errors in the chemical analysis depend basically on the sensitivity/lower detection limit of the instrument and the amount of various species present in the blank. To account for this, 2-3 blanks are analyzed along with each set, and subtracted from the total mass concentration of

respective species (sample + blank). The mean concentrations of individual species in the blanks are around 2 to 5% of the minimum concentration collected on substrates for all species except for those like SO_4^{2-}, NO_3^-, Mn, Pb, and Zn and also for Na, a major element in the blank. For these components the substrate blank at times exceeded 25% of the minimum concentration collected. The overall error estimated is ~9%.

2.3.6 Auto Titrator

In this work, bicarbonate measurements are made using an auto titrator. Titration is an analytical technique which allows the quantitative determination of a specific substance (analyte) dissolved in a sample. It is based on a complete chemical reaction between the analyte and a reagent (titrant) of known concentration which is added to the sample. Autotitrator is an instrument which allows the automation of all operations involved in titration, like titrant addition, monitoring of the reaction, recognition of the endpoint, data storage, calculation and results storage. Automated titrators follow a defined sequence of operations performed and repeated several times until the endpoint or the equivalence point of the titration reaction is reached. For the estimation of bicarbonate, the 848 Titrino plus of Metrohm, Switzerland designed for volumetric titration is used. Figure 2.17shows the photograph of the autotitrator used in this study.

Figure 2.17. *Autotitrator, model 848 Titrino plus of Metrohm.*

The instrument supports three different titration modes: Dynamic equivalence point titration, Monotonic equivalence point titration and Endpoint titration, in this analysis, End point titration mode is adopted. With this automatic titrator, the sample is titrated until a predefined measurement pH value is reached, here pH=4.3. In the Equivalence point titration mode the end point is identified where analyte and reagent

(0.005M HCl) are present in equivalent amounts. The product of concentration and the titrant consumption gives the amount of substance which has reacted with the sample.

2.3.7 Aethalometer

The real-time measurement of black carbon (BC) carried out at the site by another group is also used in this work for chemical closure. A multi-wavelength Aethalometer (AE-41, Magee Scientific USA) operating on the principle of filter based optical attenuation technique [*Hansen et al.,* 1984] is used for BC measurements. Aethalometer has an optical unit which consists of aerosol inlet, the optical source assembly, the light guides for the photo-detectors and the filter tape support. The light source is high intensity LED lamps operating at 370, 470, 520, 590, 660, 880, and 950nm.A mass-flow meter is used for monitoring the sample airflow.

An in-built pump sucks the ambient air at the flow rate of 5litre min^{-1} which passes through a fibrous filter tape on which aerosols get deposited. The instrument works on the principle of optical attenuation method, in which attenuation of a beam of light transmitted through the sample (BC) collected on the filter is measured. This attenuation is linearly proportional to the amount of BC deposited on the filter. If I_0 is the intensity of light transmitted through the blank portion of the filter and I is the intensity of light transmitted through the portion of the filter on which the BC is deposited. The optical attenuation denoted as ATN is defined as,

$$ATN = 100 * \ln (I_0 / I) \qquad 2.15$$

Since the absorption of light by a broad band absorber such as BC is inversely proportional to the wavelength of the light used, for a given mass of BC, the optical attenuation at a fixed wavelength can be written as,

$$ATN(\lambda) = \sigma(1/\lambda) * [BC] \qquad 2.16$$

where [BC] is the mass of BC, and $\sigma(1/\lambda)$ is the optical absorption cross-section that is wavelength dependent. Aethalometer measures the reference *ATN* values by passing the light through the blank filter (before sample collection).The change in attenuation (ΔATN) of incident radiation while passing through the BC deposited filter tape and reference measurement is converted to BC mass concentration (ng m^{-3}) using a specific absorption cross section (16.6m^2 g^{-1}) of BC. Sensitivity of the instrument for the current configuration was 50ng m^{-3}.

2.4 Satellite retrievals

Satellite remote sensing is recognized as a potential tool for measurement of columnar (in unit column of the atmosphere) properties of aerosols with reasonable spatio-temporal coverage. Several payloads are in orbit for aerosol studies which include Stratospheric Aerosol and Gas Experiment (SAGE), MODerate resolution Imaging Spectrometer (MODIS), Ozone Monitoring Instrument (OMI), etc. In the present study, the columnar aerosol data of aerosol optical depth, mass concentration, Angstrom exponent and effective radius retrieved by MODIS is used.

2.4.1 MODIS retrievals: an overview

MODIS is a key instrument aboard the Earth Observation System's (EOS)Terra and Aqua satellites (launched in December 1999 and May 2002, respectively). MODIS is a passive cross-track-scanning imaging radiometer making near-global daily observations of the earth in 36channels in the spectral range 0.41–14.235μm [*Salomonson et al*., 1989].The field of view (FOV) of the instrument is $\pm 55^{o}$ from the nadir. Both satellites are in a sun-synchronous orbit, at an altitude of 700km, with Terra on a descending orbit (southward) crossing the equator about 10:30 local time, and Aqua on an ascending orbit (northward) over the equator about 13:30 local time. MODIS views the earth with a swath of about 2330km, along scan by 10km (at nadir) along track, thereby observing the globe daily, and repeat orbits every 16 days. Both Terra and Aqua MODIS are able to provide near-global coverage in 2 days, enabling comprehensive short and long-term studies of the Earth's land, oceans, and atmosphere. Detailed specifications and information on components are available at http://modis.gsfc.nasa.gov which is referred in this study. A brief account of the principle of retrieval of aerosol parameters is given below.

Band/Channel	Wavelength Band (μm)	Spatial Resolution (m)
1	0.620-0.670	250
2	0.841-0.876	250
3	0.459-0.479	500
4	0.545-0.565	500
5	1.230-1.250	500
6	1.628-1.652	500
7	2.105-2.155	500

Table 2.4.*Wavelength bands used in MODIS along with their spatial resolution.*

The aerosol retrieval by MODIS makes use of seven wavelength bands in visible and near IR and bands in thermal IR are intended for getting information on cloud and other interfering parameters which need to be screened out [*Li et. al.,* 2003]. Table 2.4 gives the list of these seven wavelength bands along with their spatial resolution. The spectral stability for each instrument is better than 2nm (0.002μm).

The MODIS algorithm uses the spectral reflectanceρ_λ, defined as a function of the satellite measured spectral radiance, L_λ, the solar zenith angle (θ_0), and the solar irradiance $F_{0\lambda}$in the wavelength band λ given by [*Remer et al*., 2005],

$$\rho_\lambda = L_\lambda \frac{\pi}{F_{0\lambda}\cos(\theta_0)} \qquad 2.17$$

The surface reflectance is highly heterogeneous over the land and but it is more or less uniform over the ocean [*Remer, et al.,* 2005]. Hence MODIS uses different algorithms over the land and the ocean. In this study, the aerosol parameters over the oceanic environment of Bay of Bengal (BoB) are used.

The radiance measured by satellite comprises of solar radiation reflected from the earth's surface as well as radiation scattered by the atmosphere in the direction of the sensor. For retrieving atmospheric/aerosol parameters, surface contribution in the total radiance is eliminated. This process is very complex over land than that over ocean. After carrying out corrections for the effects of water vapour, ozone and carbon dioxide, the reflectance in all the six channels are organized into nominal 10km boxes corresponding to 20 by 20, or 400pixels for each box. If all pixels in the 10km box are identified as water pixels based on the reflectance, then ocean algorithm is used the details of which are given by *Tanré et al*.,[1997] and *Remer et al.,*[2005].

2.4.2 Aerosol Retrievals

The raw file obtained from MODIS contains counts from sensor detectors which form the Level 1A data. Level 1B provides calibrated geolocated radiances or reflectances which along with cloud mask product and NCEP meteorological data go as input to the aerosol retrieval algorithm [*Remer, et al.,* 2005]. The resulting geophysical products are designated as Level 2 data. The Level 3 data is the daily and monthly average products organized in 1°×1° latitude x longitude grids. MODIS aerosol algorithm consists of three sets of algorithms with separate assumptions about the earth's surface and aerosol types observed. One is the Dark Target (DT) algorithm developed for vegetated land surfaces [*Kaufman, et al*., 1997] and second for remote oceans [*Tanre, et al.,* 1997]. The third algorithm is known as Deep Blue (DB)

Algorithm [*Hsu, et al*., 2004; *Hsu, et al*., 2006] which was designed for the application over bright desert surfaces. Ocean and Land algorithms are totally separate but use similar techniques to derive aerosol properties. The algorithm takes a set of observed values at the Top of the Atmosphere (TOA) and tries to match with the values of Look Up Tables (LUT) which represents the atmospheric optical properties for a set of aerosol conditions.

The primary MODIS retrieved aerosol products include, columnar spectral aerosol optical depth (AOD) at 550nm (τ_{550}), the effective radius of the aerosol (R_{eff}), and the fine (small) mode fraction of the total optical depth [*Tanre´ et al*., 1997; *Remer et al*., 2002; *Ignatov et al*., 2005]. The derived parameters include Angstrom exponent (α) and columnar aerosol mass concentration (M_c) in $\mu g\ cm^{-2}$ [*King et al*., 1997; *Remer et al*., 2005]. In this study, we have used the MODIS Aqua Daily Level-2 data (MYD04_L2) of Collection 6 (C006) for AOD at 550nm (τ_{550}), M_c, α, R_{eff} and the small mode and large mode AOD retrieved over BoB during the study period as obtained from LAADS web page https://ladsweb.nascom.nasa.gov/data/search.html. The data has a spatial resolution of 10km × 10km. The estimation of these parameters are detailed in *Levy et al*. [2007].The error in AOD is estimated as $\Delta\tau=0.03\pm0.05\tau$ over ocean [*Remer et al*., 2008].

2.5 Supplementary data

The source characteristics, removal mechanisms as well as transport processes of aerosols depend on the prevailing meteorological conditions and air-mass type. In this context, the real time concurrent measurements of meteorological parameters become essential. Knowledge on the prevailing air-mass type can be obtained by examining the air-mass back trajectories for the respective period and geographical location. In addition, the meteorological fields provided by reanalysis data also have been used in this study. A brief account of the measurement of the meteorological data and method of retrieval of air-mass back trajectories are given in the following subsections. A short note of the NCEP/NCAR reanalysis data used in this analysis is also given below.

2.5.1 Meteorological data

The meteorological data obtained from an Automatic Weather Station (AWS) of M/s Dynalab, Pune has been used in this work. It is an integrated system of meteorological sensors and data logger installed at the experimental site. The

meteorological sensors in the AWS include that of temperature, pressure, wind velocity, wind direction, humidity, radiation and rainfall. These sensors are mounted at~3m above the ground on a mini tower. The rainfall measurement is carried out using tipping bucket mechanism. The technical details of the sensors are summarized in Table 2.5.

Sensor	Parameter	Specifications
Wind Speed	Sensor	3-cup anemometer
	Starting threshold	$0.25ms^{-1}$
	Range	$0\ ms^{-1}$ to $65ms^{-1}$
	Accuracy	Better than $0.5ms^{-1}$
Wind Direction	Sensor	Wind vane
	Resolution	1°
	Range	0° to 357°
	Accuracy	±3°
Air Temperature	Sensor	Platinum resistance temperature detector
	Resolution	0.1° C
	Range	-40° C to +60° C
	Accuracy	0.2° C
Relative Humidity	Sensor	Solid state capacitive sensor
	Resolution	0.1%
	Accuracy	±3% of full scale reading
Pressure	Sensor	Stainless steel bellows coupled to a strain guage
	Range	600 to 1100 millibars
	Accuracy	0.25% of full-scale reading
Rainfall	Sensor	Tipping bucket
	Resolution	0.5mm
	Range	1mm
	Accuracy	unlimited

Table 2.5.*The technical details of meteorological sensors on AWS.*

2.5.2 NCEP/NCAR Reanalysis data

In order to investigate the effects of wind field and other meteorological parameters on aerosols, the NCEP/NCAR Reanalysis data is used. NCEP/NCAR provides several meteorological fields like pressure, temperature, Relative Humidity and wind components (u, v and w) at 2.5° × 2.5° resolution for 17 atmospheric pressure levels from 1000hPa to10hPa [*Kistler et al.,* 2001; *Kanlay et. al*., 1996]. NCEP/NCAR

reanalysis uses a long term data base of several parameters including wind components by using a frozen state-of-the-art global assimilation system and a data base built from many sources including ground- based, ship-borne, balloon-based, aircraft-based and satellite-borne measurements from different countries and organizations [*Kalnay et. al*., 1996]. The data collected from different sources are quality controlled and then assimilated using a data assimilation system, which is kept unchanged over the period of reanalysis. The data from NCEP/NCAR reanalysis are provided by NOAA through the websitehttp://www.esrl.noaa.gov/psd/data/ gridded/data.ncep.reanalysis. pressure.html. Since the present study focuses on near-surface aerosols or those confined within the lower troposphere, the reanalysis data of the lower level (at 925hPa, within boundary layer) is mostly used in the present analysis. The reanalysis data from NCEP used for the present study are uwind, vwind, temperature and Relative Humidity.

2.5.3 Air-mass back trajectories

Air mass back-trajectory analysis is a widely used tool for identifying the source regions of aerosols and trace gases [*Hondula et al*., 2010]. The HYbrid Single-Particle Lagrangian Integrated Trajectory (HYSPLIT) model is the most accepted one in this context. The model consists of a modular library structure with main programs for each primary application namely trajectories and air concentrations. For evolving the air-mass back trajectories, gridded meteorological data, on a latitude-longitude grid or on one of three conformal (Polar, Lambert, Mercator) map projections, are required at regular time intervals. A Lagrangian model can compute air concentrations making use of two different assumptions namely puff model and particle model [*Hurley,* 1994]. In puff model, the source is simulated by releasing pollutant puffs at regular intervals. Each puff contains the appropriate fraction of the pollutant mass. The puff is advected according to the trajectory of its center position while the size of the puff (both horizontally and vertically) expands in time to account for the dispersive nature of a turbulent atmosphere. In addition to the advective motion of each particle, a random component to the motion is added at each step according to the atmospheric turbulence at that time. In this way, a cluster of particles released at the same point will expand in space and time simulating the dispersive nature of the atmosphere. In a homogeneous environment, the size of the puff (in terms of its standard deviation) at any particular time should correspond to the moment of the particle positions. The present hybrid approach, developed by *Hurley,* [1994], incorporates particle dispersion in the vertical

direction and puff dispersion in the horizontal. Regardless of which approach is used, stability and mixing coefficients need to be computed from the meteorological data. Once the basic meteorological data (velocity vectors u,v,w) have been processed and interpolated to the internal model grid, trajectories (the integrated advection term of a particle) can be computed.

The advection of a particle or puff is computed from the average of the three-dimensional velocity vectors for the initial-position P(t) and the first-guess position P'(t+Δt). The velocity vectors are linearly interpolated in both space and time. The first guess position is

$$P'(t+\Delta t) = P(t) + V(P,t)\,\Delta t \qquad 2.18$$

and the final position is

$$P(t+\Delta t) = P(t) + 0.5\,[\,V(P,t) + V(P',t+\Delta t)\,]\,\Delta t \qquad 2.19$$

The integration method given by *Kreyszig*, [1968] is used for trajectory analysis [*Draxler*, 1996].The model can be run interactively through the website or with the code executable with meteorological data downloaded to a computer. In this study, the air-mass back trajectory for a particular location is obtained online from the model run with location specific inputs like latitude, longitude, pressure level (altitude), time etc. These trajectories essentially trace back the path (during a given period) of the air-mass reaching the particular location and at a pressure level (height). Since the aerosol residence time is nearly one week in troposphere, the model is run for 7 days back-trajectories (or for appropriate temporal scales) which helps in locating the source regions effectively.

2.6 Optical Properties of Aerosols and Clouds (OPAC) model

This work also addresses the radiative characteristics of the aerosols at the tropical coastal site Thiruvananthapuram and the surrounding oceanic regions based on the measured physico-chemical characteristics for the first time. This involves the estimation of the aerosol scattering coefficient, absorption coefficient, extinction coefficient, single scattering albedo and the phase function using the OPAC model. OPAC is a software package which provides the optical or radiative properties of atmospheric aerosols in the solar and terrestrial spectral range from 0.25 to 40μm and for modelled aerosol types.

In OPAC, the properties of the clouds and aerosol components are given together with a FORTRAN program, which allows the calculation of optical parameters for any mixture of clouds and aerosol components. OPAC consists of two parts, first a

dataset which gives the microphysical and optical properties of 10 internally mixed aerosol components (and also for water/ice clouds, which are not discussed here since it is not used in this work) at 61 discrete wavelengths in the range 0.25 to 40μm and for 8 values of relative humidity stored in ASCII files. The other part is a FORTRAN program which extracts data from this dataset and calculates the optical properties of mixtures of already stored aerosol components. Since aerosols originate from diverse sources, they are modelled as components with different compositions [*Deepak and Gerber*, 1983], each of them representing certain origin, that is, an internal mixture of all chemical substances that have a similar origin [*Hess et al*., 1998]. These components are externally mixed to form aerosol types.

The major components described in OPAC are: (a) Water insoluble consisting mostly of soil and insoluble part of organic material, (b) Other Water soluble part consisting of sulphates, nitrates and organics, (c) the component Soot represents the absorbing black carbon particles characterized by high imaginary part of the refractive index, (d) Sea-salt particles are described with two components differing in size (accumulation mode and coarse mode), (e) Mineral aerosols produced from arid regions are described by four components (Nucleation mode, accumulation mode, coarse mode and mineral transported),Mineral transported is used to describe aerosol transported over long distances, and (f) Sulphates describe the stratospheric aerosols and those found in the Antarctic aerosols (not applicable in this study).

Each component is characterized with lognormal distributions, number density N and density ρ. For aerosol size distributions, lognormal distributions defined by equation [*Deepak and Gerber* 1983] are applied for each aerosol component i

$$n_i(r) = \frac{1}{\sqrt{2\pi}\sigma_{mi}\, r_{mi}} \exp\left[\frac{-\left(\ln r - \ln r_{mi}\right)^2}{2\sigma_{mi}^2}\right] \qquad 2.20$$

with r_{mi} and σ_{mi} denoting the mode radius and standard deviation respectively.

The software estimates the mass concentration integrated over the size distribution and normalized to 1 particle per cc of air. 10 aerosol mixtures are defined within the software by the mixing of various aerosol types. OPAC uses the aerosol mixtures as presented in the Global Aerosol Data Set GADS [*Koepke et al*., 1997], with respect to global distribution. Along with this, the user can also define new aerosol component by mixing various aerosol types relevant to the study region. This capability of the model is made use in this study. More details on the estimation of aerosol radiative characteristics are discussed in Chapter 3.

2.7 Principle Component Analysis

To identify the sources of aerosols using the measured chemical composition data the technique of Principle Component Analysis (PCA) was utilized in this study. PCA involves a mathematical procedure that transforms a large number of (possibly) correlated variables into a smaller number of uncorrelated variables called principal components [*Kline, 1994*].

The mathematical technique used in PCA is called eigen analysis, which includes the solution for the eigen values and eigenvectors of a square symmetric matrix. In PCA, from a set of p variables a reduced set of m components or underlying factors are extracted that accounts for most of the variance in the p variables. These underlying factors are inferred from the correlations among the p variables. For making the interpretation of the factors that are considered relevant, different methods of rotation of the factors is employed. In the present analysis the orthogonal transformation method with Varimax rotation [*Kaiser*, 1958; *Afifi and Clark,* 1984] was made use. After varimax rotation each variable tends to be associated with one of the factors, and each factor represents only a small number of variables. The first principal component or factor accounts for as much of the variability in the data as possible, and each succeeding component accounts for the remaining variability.

Chapter 3

Temporal changes in physical, chemical and radiative properties of near-surface aerosols at the coastal site Thiruvananthapuram: Changing sources and meteorology

3.1 Introduction

The optical and radiative properties of aerosols depend on their size distribution, chemical composition and the wavelength of interacting radiation. The vast diversity in the aerosol sources, sinks, transport and chemical transformations brings in large heterogeneity in the above properties demanding region-specific studies. Above all these, meteorology also plays crucial role in deciding the physical and chemical properties of aerosols at any location. Studies done world-wide have strengthened the database of aerosol characteristics and brought out important scientific results on their radiative, environmental and climatic impacts [*Ramanathan et al*., 2001; *Lee et al*., 2003; *Salcedo et al*., 2006; *Ramanathan and Carmicheal*, 2008; *Poschl et al*., 2010]. Most of the regional studies focussed on the physical, chemical or radiative aspects of aerosols. Knowledge on chemical composition of aerosols is highly limited on regional scales and an integrated picture on their physical and chemical characteristics are scarce, particularly over Indian region. The present work is an attempt to bring out a comprehensive account of the physical, chemical and radiative properties of aerosols at the tropical coastal site Thiruvananthapuram based on simultaneous and collocated measurements. Earlier studies on aerosols at this location were based on ground-based multi-wavelength radiometry [*Moorthy et al*., 1991; *Nair*, 1993], in-situ measurements of near-surface mass concentration using quartz crystal microbalance [*Parameswaran et al*., 2004; *Pillai and Moorthy*, 2001], and aethalometer-based black carbon measurements [*Babu*, 2005]. Later, *George et al*., [2008] made a study on the inorganic chemical components in atmospheric aerosols at this location as measured during day time when sea-breeze (wind from sea to land) prevailed over the site. The present work is an extension of earlier studies, focussing on the physico-chemical properties of aerosols along with their radiative characteristics at this coastal environment. This study is based on the simultaneous measurement of (1) aerosol number density (2) number size distribution (3) mass concentration/loading and (4) chemical composition for a period of 2 years from 2011-2013 and the detailed analysis. Moreover, in this

work, the measurements carried out during day time (sea breeze regime) and night time (land breeze regime) were used to understand the role of mesoscale meteorology.

The major studies carried out include (1) diurnal variation in the aerosol number density, size distribution and mass loading of aerosols and effect of mesoscale meteorology (2) role of synoptic meteorology in the seasonal characteristics of aerosol total number density, size distribution, mass loading and chemical composition (3) source characterisation using Principal Component Analysis (PCA) (4) association between size-resolved number density and chemical species in aerosols (5) estimation of radiative/optical characteristics of aerosols using the Optical Properties of Aerosols and Clouds (OPAC) model making use of the measured aerosol properties (6) approximate estimation of mean aerosol density and (7) decadal changes in aerosol characteristics at the location.

3.2 Experimental Site and Meteorology

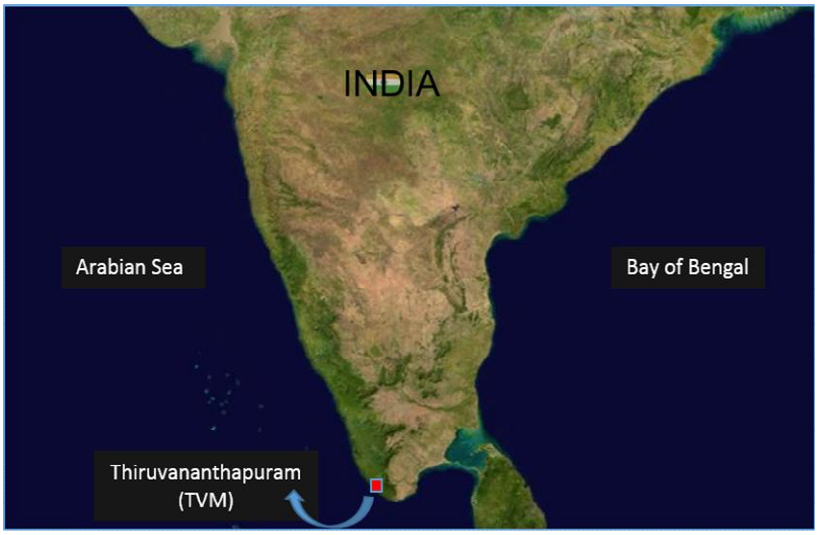

Figure 3.1. *Geographic location of the experimental site Thiruvananthapuram (TVM).*

Observational site Thiruvananthapuram (8.55ºN, 77ºE, 3m amsl), referred as TVM hereafter, is located on the west coast of India, ~500m away from the coastline of Arabian Sea and on the southern tip of Indian mainland. The terrain is fairly flat, sandy and mostly free from thick vegetation, large scale agricultural and industrial activities. The city of Thiruvananthapuram is located ~10km due southeast of the experimental site whose north-northeast part is surrounded by moderately populated region. The population of the city is 3,307,284 [*Census*, 2011]. The location of the experimental site TVM in India is given in Figure 3.1.

TVM, being a tropical coastal location, experiences typical hot and humid (wet) tropical climate with moderate changes in the meteorological conditions. The most important synoptic meteorological phenomena acting at this region is the strong southerly/ south westerly winds and the extensive rainfall associated with the Asiatic monsoon, which sets in by the beginning of June and lasts till September [*Asnani,* 1993; http://www.imd.gov.in].

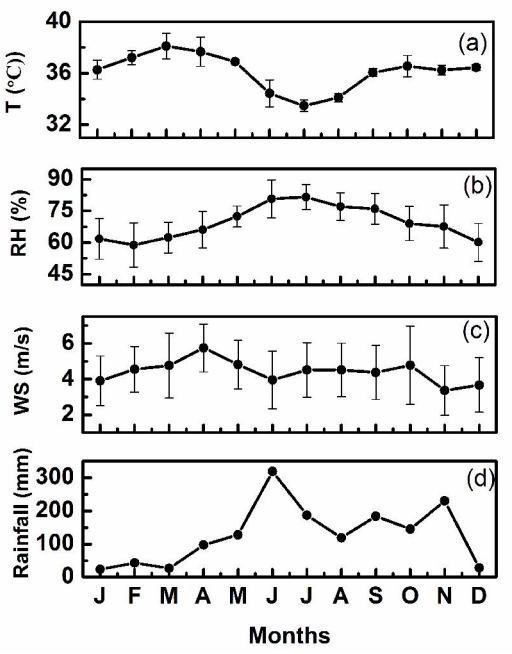

Figure 3.2*. Variation of monthly mean (a) temperature (b) Relative Humidity (RH) (c) Wind speed (WS) and (d) Rainfall recorded at 11:30hrs over the period 2011-2013 at the tropical coastal station of TVM.*

Figure 3.2a to c shows the mean monthly variation of the surface level meteorological parameters: temperature (T), Relative humidity (RH) and wind speed (WS) recorded at 1130 IST (close to noon) at the experimental location for the study period from 2011-2013. In Figure 3.2d is shown the mean variation of monthly total rainfall (RF) for the same period. The temperature varied in the range of 33°C to 38°C with maximum during March to May and minimum during June to September. RH ranges from 55% to 85% with minimum in months of December, January and February and maximum during June to September. The mean wind speed varied between 3ms^{-1} and 8ms^{-1} over a year. In general, the months of December, January and February along with the month of March are characterized by weak rainfall which is less than 100mm. Monsoon rain onsets on Kerala coast generally by first week of June and extends till September with heavy rainfall and strong south-westerly winds with speeds often exceeding 10ms^{-1}. Rainfall starts increasing from April onwards reaching peak in June-

September (with year-to-year variation). About 70% of annual rainfall at this location is received during this period.

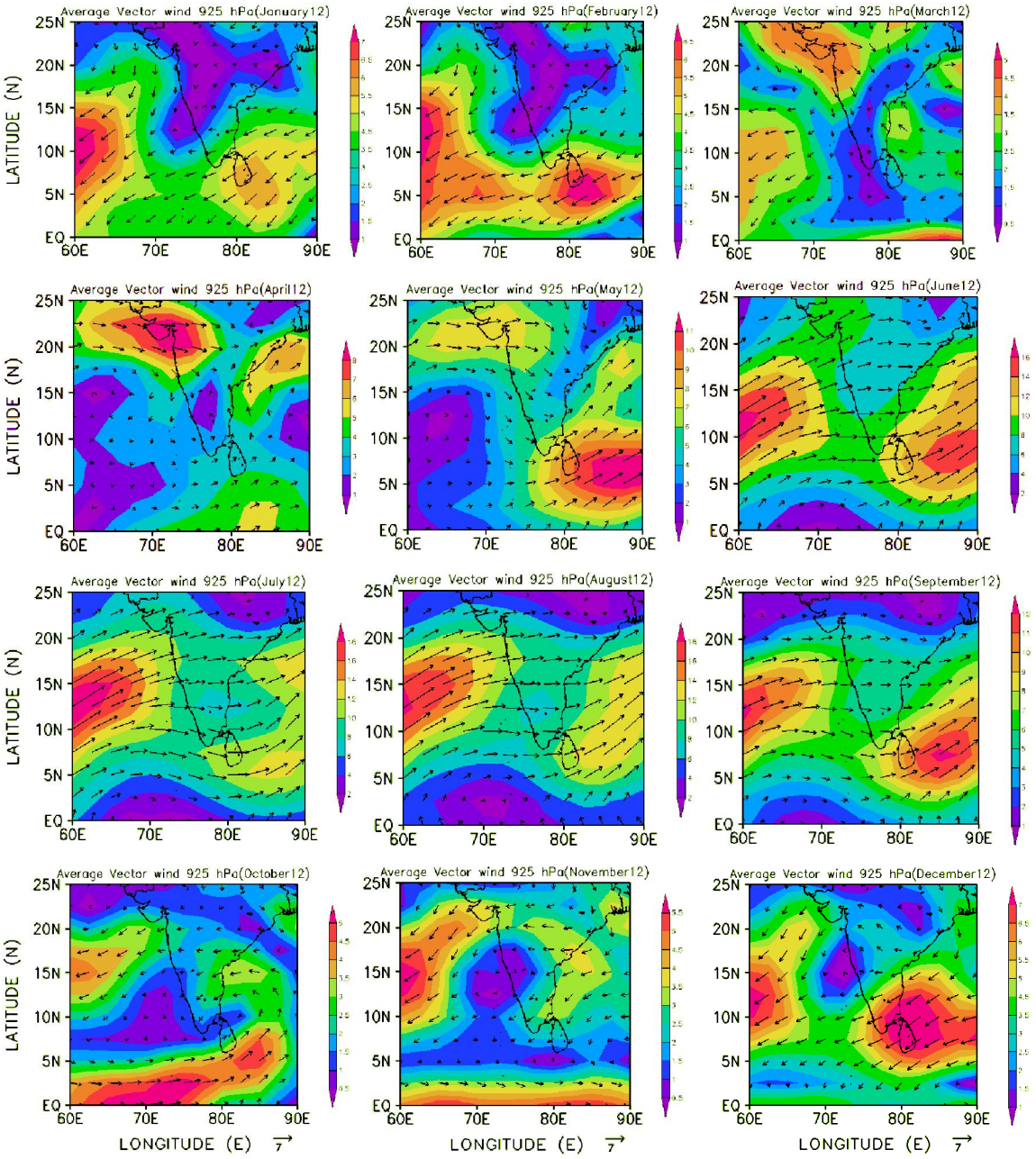

***Figure 3.3**. Monthly average air flow patterns at 925hPa over the Indian subcontinent and the adjoining oceans during 2012 obtained from NCEP/NCAR Reanalysis.*

The typical monthly mean wind (airflow) pattern over the Indian subcontinent and adjoining oceans in the 0°N-25°N latitude and 60°E-90°E longitude sector at 925hPa level derived from NCEP/NCAR reanalysis1 data (http://www.esrl.noaa.gov/psd/data/ gridded/data.ncep. reanalysis. pressure.html.) as observed for the year 2012 is presented in Figure 3.3. During December, January, February and March months the winds are weak north-easterlies. The prevailing winds

start strengthening and shifting direction during May and become south westerlies by June-July. The wind speed starts decreasing by October and reverses to northerly/north-easterly which lasts till March/April. Based on the prevailing meteorological conditions of the location, a year is divided into four seasons. Months of December, January and February characterized by low temperature, dry atmosphere (low RH), low wind speed and little or no rainfall, constitute the Winter season. March to May is the Pre-monsoon/ Summer season with high temperature and wind speed ranging from 2-6m s^{-1} and direction changing from north-easterly to south-westerly. This season is also characterized with pre-monsoon showers. Months of June, July, August and September is characterized as Monsoon season with heavy rainfall and strong south westerly winds. The months of October and November are the Post-monsoon season with moderate rain (return monsoon) and moderate north-easterly winds.

Being a coastal site, TVM is also influenced by strong mesoscale phenomena like sea breeze (SB) and land breeze (LB) circulations. The most significant feature of this coastal site is the development of the thermal internal boundary layer (TIBL) [*Stull*, 1988; *Kunhikrishnan et al*., 1993]. The coast line lies along 145°-325° azimuth. The wind blowing between 145° and 325° (towards land) is considered to be the SB, while the seaward wind blowing between 325° and 360° and 0°-145° represents the LB. In general SB prevails during daytime and LB during night time. This geographical setting of the location makes the boundary layer aerosols a mixture of marine and continental components.

3.3 Physical characteristics of aerosols at TVM

The physical characteristics such as total number density, number density-size distribution and mass concentration of aerosols along with their temporal variations were investigated and detailed in this section.

3.3.1 Aerosol number density

The number density/concentration of aerosols is measured by the Aerosol Spectrometer (model 1.108, GRIMM, Germany), in 15 discrete channels of aerosol sizes (aerodynamic diameter) ranging from 0.3µm to 20µm. The size channels correspond to the aerodynamic diameter of aerosols >0.3, >0.4, >0.5, >0.65, >0.8, >1, >1.6, >2, >3, >4, >5, >7.5, >10, >15 and >20µm. Technical details and theory of operation of the instrument are given in Chapter 2. Instrument is operated round the clock inside the laboratory by drawing ambient air through an inlet placed 3m above

the ground level. The aerosol number density data in 15 size channels, averaged at 5minutes interval are recorded. During the study period of 28 months from September 2011 to December 2013, about 220 days of number density-size distribution data have been collected (10 to 15 days per month except during monsoon) and used in the present study. The measurements during monsoon are limited (7 to 8 days per month) due to adverse weather conditions. The heterogeneity in aerosol sources and sinks, the wide size spectrum, short life times along with prevailing meteorology result in significant variation of aerosol properties diurnally, monthly and seasonally.

3.3.1.1 Diurnal variation of total number density

The aerosol number density measured at the first channel of the Aerosol spectrometer corresponds to the total aerosol number density (N) in this study and represents the aerosols of aerodynamic diameter>0.3μm. The total aerosol number density N shows strong and consistent diurnal variation throughout the year.

Irrespective of the year, the diurnal patterns are characterized by day time low and night time high. A sharp peak is often seen ~0700-0800hrs, superposed on this diurnal pattern. The prevailing boundary layer characteristics, proximity to major sources and sink processes play key role in controlling the diurnal patterns of aerosol loading at any location [*Moorthy et al*., 2003; *Tripati et al*., 2005; *Hussein et al.*, 2006]. Figure 3.4a show the annual mean diurnal pattern of N as measured for the entire study period.

The observed diurnal changes at the present study region are found to be closely linked with the mesoscale meteorological conditions of this location. To illustrate this, a typical diurnal variation of aerosol number density as measured on 29 Jan 2013 is shown in Figure 3.4b along with the corresponding meteorological parameters, wind speed (WS), wind direction (WD), Temperature (T) and relative humidity (RH). The aerosol number density which remains high during night till morning drops by ~09:00-10:00AM, remains low till ~1900hrs and then increases.

With sun rise (~06:43hrs, marked in Figure 3.4b), temperature starts increasing and humidity decreases. As time advances, the land becomes hotter and the land-sea contrast in temperature results in the onset of the landward blowing SB at ~0950hrs as seen from the change in WD and increased WS in Figure 3.4b. Associated with this, the TIBL develops [*Stull*, 1988] and grows in height. As the day progresses convective activity gains strength, lower atmosphere becomes turbulent, causing thorough mixing of air. The aerosols (also other trace gases) get lifted to higher altitudes, mixed up in a

large volume, thus reducing the concentrations at surface level. The SB prevails till night when land sea contrast reduces and reverses (sea become warmer than land) and the LB sets in by ~19-20hrs [*Prakash et al.*, 1993]. The SB and LB regimes (dotted line) during a day are marked in Figure 3.4b.

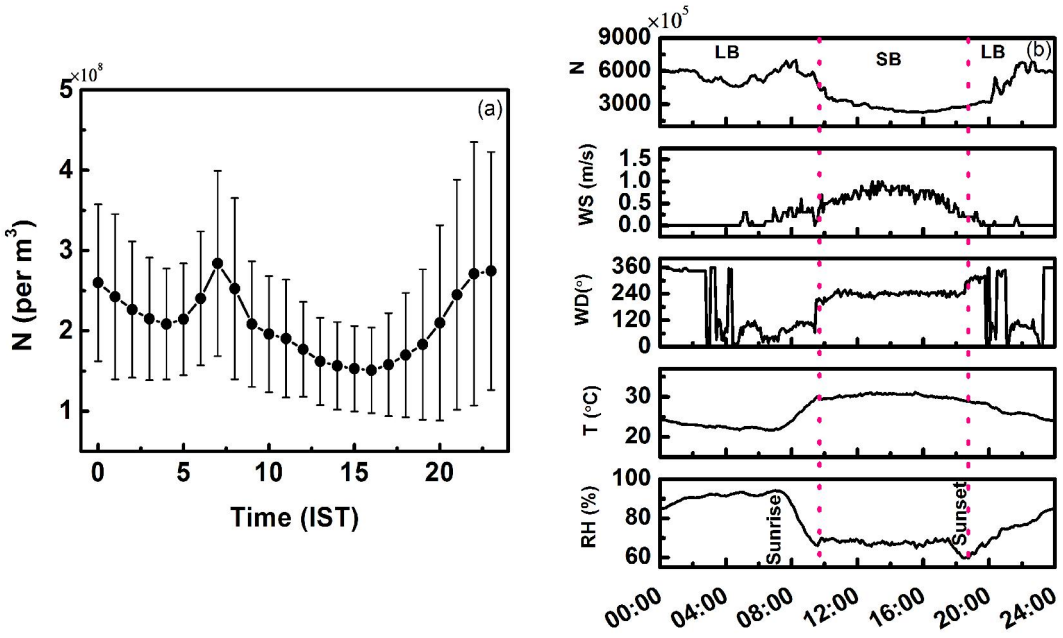

Figure 3.4. *(a) Mean diurnal pattern of total number density (N per m^3) for 2011-2013 at TVM along with standard deviation (b) Typical diurnal pattern of N along with meteorological parameters (dotted line indicates the land/sea breeze transition time)recorded on 29 Jan 2013.*

With sun set, earth's surface starts cooling faster due to radiative cooling, there by changing the nature and structure of the atmospheric boundary layer. A shallow stable nocturnal boundary layer develops at night which confines aerosols to surface levels, thereby increasing the aerosol concentration. During the evolution of night time stable boundary layer, a part of the aerosols, which got lifted up during daytime, remain above this nocturnal boundary layer (i.e. in the residual layer). Next morning, as the sun rises, the nocturnal boundary layer breaks and the aerosols trapped in the residual layer intrudes down. This causes a sudden short-living enhancement in the surface level aerosol number density which is manifested as a sharp peak in the diurnal pattern of aerosols number density ~0700hrs as observed in Figure 3.4a and b. This is known as the fumigation effect. As the boundary layer develops these particles get mixed up and the peak disappears. Morning increase in traffic and other anthropogenic activities may also contribute to the morning enhancement. Similar diurnal variation in aerosol mass

concentration and black carbon have been observed at this station associated with SB/LB [*Pillai*, 2003; *Babu*, 2005]

3.3.1.2 Monthly /seasonal variation of total aerosol number density

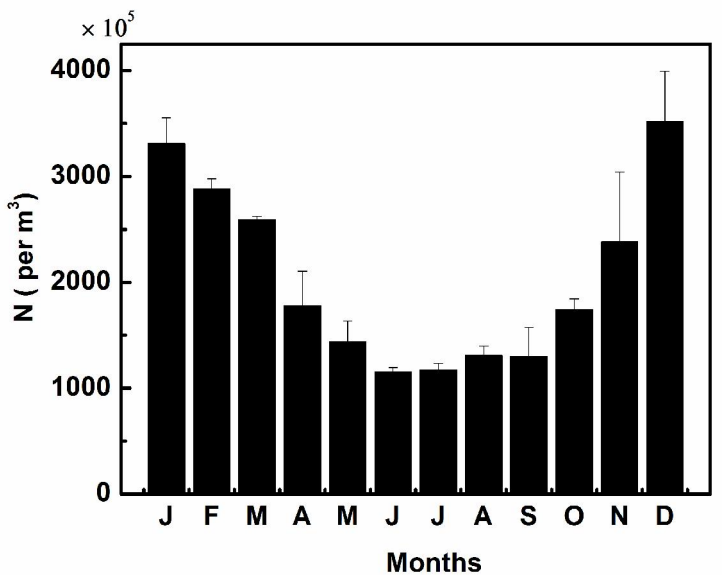

Figure 3.5. *Mean monthly variation of total aerosol number density (N) along with the standard error.*

The mean monthly variation of total number density observed during the study period as obtained from daily data is shown in Figure 3.5. The vertical bars indicate the standard deviation. Aerosol number density peaks during the winter months of December-February (DJF) with values reaching $>3.5\times10^{8}m^{-3}$. The number density decreases through the month of March to May (pre-monsoon) with a mean value of $(2.1\pm1.1)\times10^{8}\ m^{-3}$. During the monsoon months of June-September (JJAS), N reduces drastically with the minimum of $1.2\times10^{8}\ m^{-3}$ occurring in June.

3.3.2 Number density- size distribution

The aerosol Number density-Size Distribution (NSD) is a critical parameter in deciding their radiative impacts. It also decides the relative strength of different source and sink mechanisms active at the location [*Jaenicke*, 1993; *Tunved et al*., 2004]. The aerosol number density measurements at the 15 size channels were utilized to estimate the aerosol NSD function given as,

$$n(r)= dN(r)/dr \qquad 3.1$$

where the differential number density $dN(r)=N_1-N_2$ and $dr = r_1-r_2$, with N_1 and N_2 representing the aerosol number density of aerosols at radii r_1 and r_2 respectively (or

the lower and upper limit of the respective size bin). The estimated n(r) is plotted against the radius $r = (r_1 + r_2)/2$ on log scales to depict the nature of the NSD.

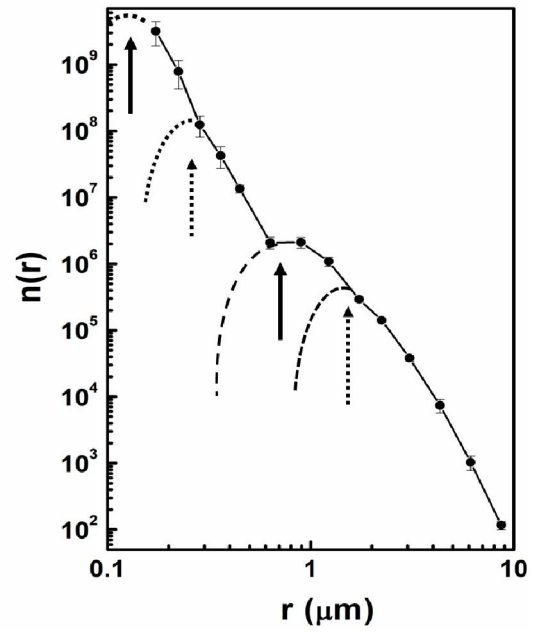

Figure 3.6. *Mean NSD observed during the study period, the different modes are also indicated with arrows. The solid arrows point to the prominent modes and the dotted arrows point to the indicative modes.*

Figure 3.6 shows the nature of the mean NSD observed during the study period. The vertical bars denote the standard deviation. The size distribution is of multi-modal nature with two prominent modes/peaks, one in the fine particle range ≤0.1μm and the other in the accumulation size range (~1μm) both marked by solid arrows. The NSD also indicates presence of less pronounced modes in the radii range, ~ 0.3-0.5μm and ~5-8μm (marked by the dotted arrows). An examination of the individual NSDs revealed that they exhibit significant day-to-day variability in terms of their number density in each size channel.

3.3.2.1 Monthly/seasonal variation of NSD

In spite of the day-to-day variability, the NSDs exhibit, obvious seasonal features. To get an insight into this, the estimated aerosol size distributions on daily basis were grouped and averaged month-wise for the period 2012 and 2013 separately to obtain the monthly mean NSDs (Figure 3.7a and b respectively). These monthly size distributions (Figure 3.7a) reveal systematic annual variation. For more clarity, these size distributions are zoomed in for the size range 0.15μm up to 0.5μm (small/fine

particles) and >0.5µm radius (large/coarse particles) as can be seen in Figure 3.7c and e for the year 2012 and d and f for 2013.

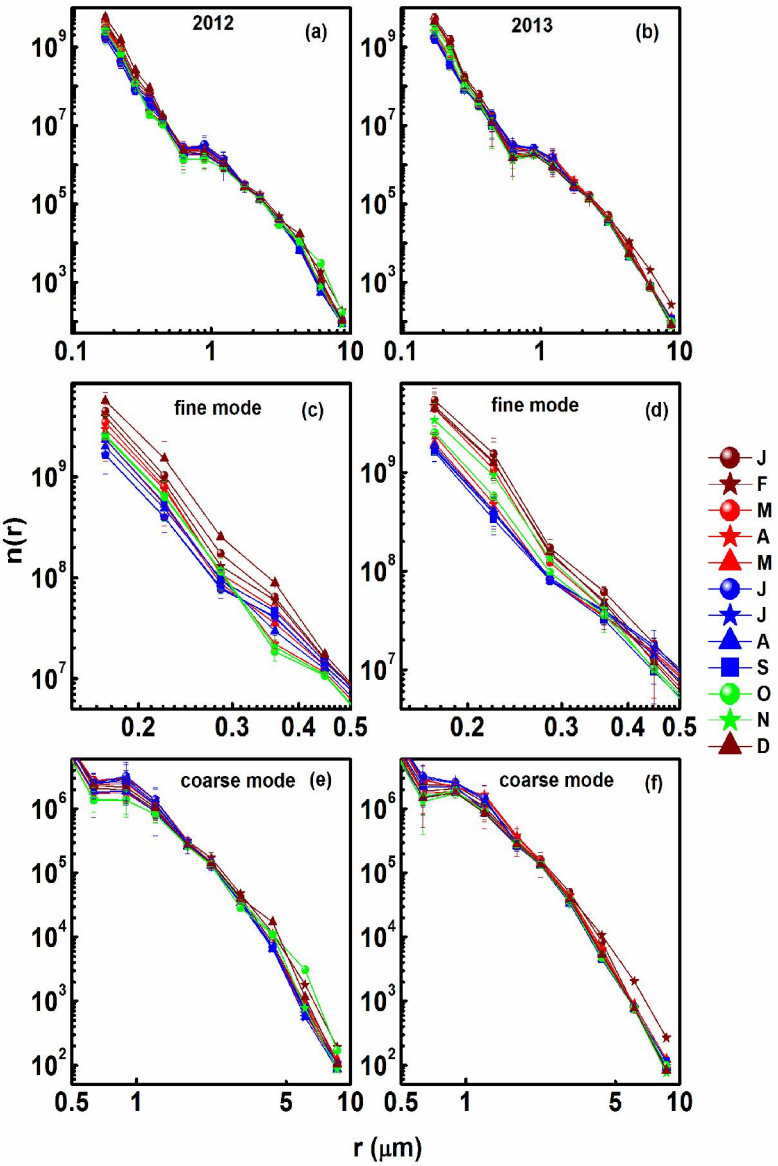

Figure 3.7. *Monthly mean NSDs for (a) 2012 and (b) 2013 along with the zoomed distributions for the radii range 0.15 µm to 0.5µm (fine particles) and >0.5µm (large/coarse particles), (c) and (e) for the year 2012 and (d) and (f) for 2013.*

All the monthly distributions are also multi-modal in nature with two prominent modes and two less pronounced modes, (as discussed in Section 3.3.2) during most of the months. The fine particle concentration peaks in winter months of DJF (shown in brown colour) and decrease by MAM (red colour) reaching minimum in monsoon (blue colour). On the other hand, number density of the large particles of radius ~1-3µm peaks in monsoon. Particles of radius >3µm remain high during all the seasons except monsoon (Figure 3.7e and f).

By grouping the NSDs corresponding to various months into respective seasons and averaging, the seasonal mean NSDs have been obtained (Figure 3.8). It can be seen that the fine particle mode is more pronounced during winter (Figure 3.8) compared to the other seasons with lowest values observed during monsoon season. On the other hand, the accumulation mode which is observed around 0.9-1.0μm becomes prominent during the monsoon period. Another feature is that this large particle mode is of comparable amplitude during monsoon, pre-monsoon and winter. In fact the seasonal changes in NSD are more pronounced for the fine particles.

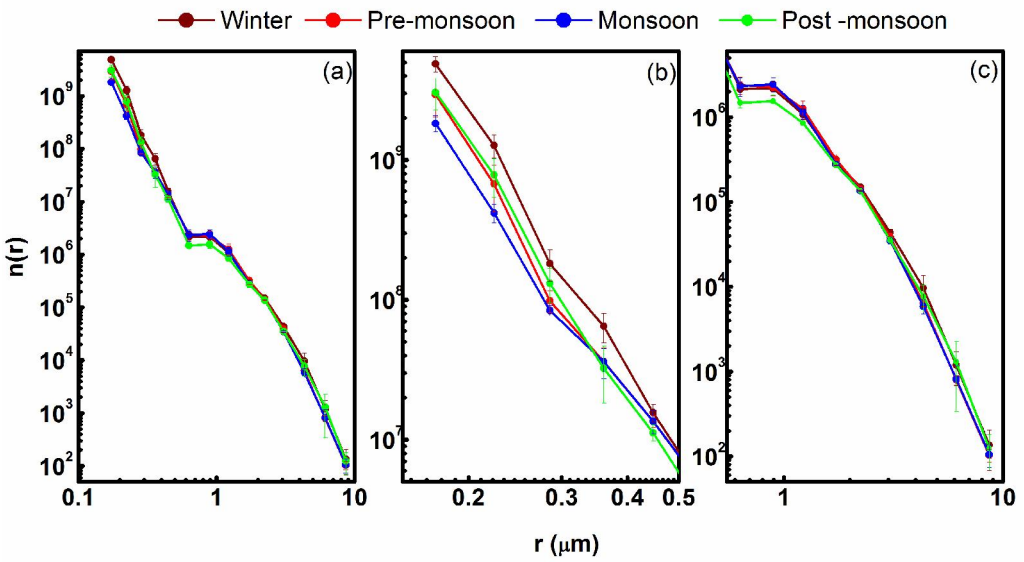

Figure 3.8. *(a) Seasonal mean NSD at TVM along with the zoomed NSD(b) for fine particles and (c) for coarse particles.*

The fine mode aerosols are generally formed from gas-to-particle (GPC) mechanisms and are mostly of anthropogenic origin. The coarse mode originates from bulk-to-particle (BPC) and contributed by sea-salt, mineral dust etc. Earlier studies done at the study region have reported a trimodal mass size distribution [*Pillai et al.,* 2001]. The columnar NSDs derived by the numerical inversion of spectral optical depth measurements at this location are of four types of distributions namely power law, monomodal, bimodal and combination of power law and monomodal [*Nair*, 1993; *Beegum et al*., 2010].

In order to have a quantitative assessment, the retrieved seasonal mean NSDs were fitted with appropriate analytical distribution functions. In the fine mode extending from 0.175μm to 0.5μm the aerosol number density (n(r)) shows decrease with increase in r. This part of NSD is fitted with the widely accepted inverse power law distribution also called Junge distribution [*Junge*, 1982] of the form

$$n(r) = n_0 r^{-\nu} \qquad 3.2$$

where n_0 is a constant and ν is called the size index. The size index ν (explained in Chapter 1) is an indicator of relative dominance of small particles and large particles. ν and n_0 are obtained as the slope and y-intercept respectively of the linear regression fit for the scatter plot between log n(r) and log (r).

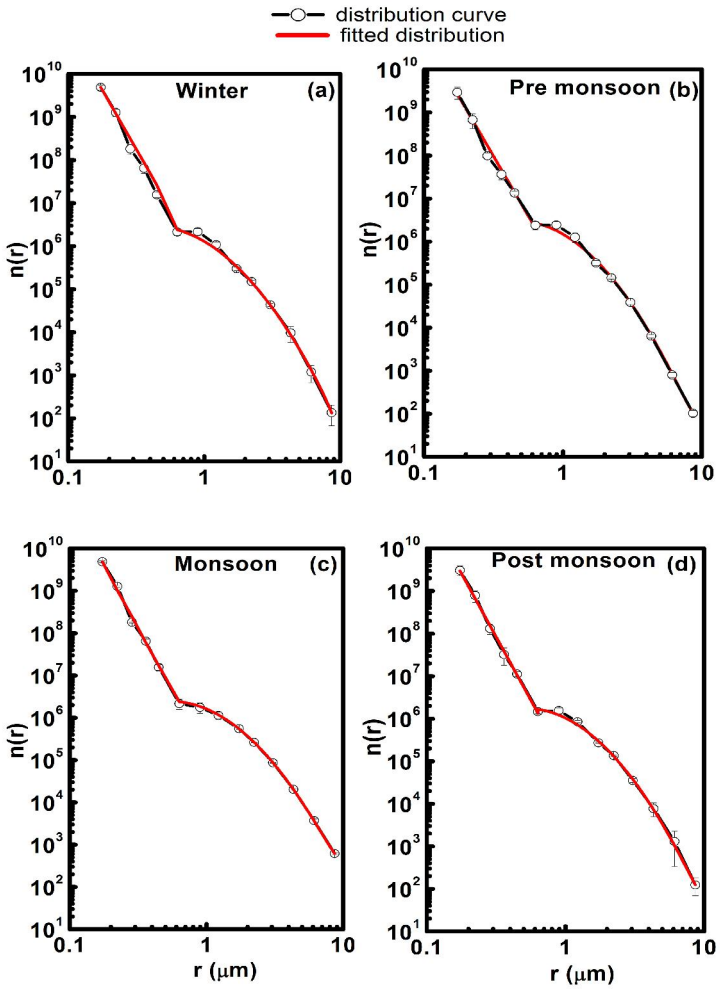

Figure 3.9. *Seasonal mean NSDs fitted with inverse power law (for small particle mode) and log normal distribution for the large particle mode for (a) winter (b) pre-monsoon (c) monsoon (d) post-monsoon.*

The large particle mode was fitted with log-normal distribution (LND) which is of the form

$$n(r) = \frac{1}{\sqrt{2\pi}\sigma_m r}\exp\left[\frac{-(\ln r - \ln r_m)^2}{2\sigma_m^2}\right] \qquad 3.3$$

where r_m is the mode radius and σ_m the standard deviation. LND is fitted by using OriginPro 8.5 software.

The observed seasonal NSDs shown in Figure 3.8 are fitted with the inverse power law and LND as discussed above (Figure 3.9) and the estimated constants n_0, ν, r_m, σ_m are given in Table.3.1.

Season	Power law		Log normal distribution	
	n_0	ν	r_m	σ_m
Pre-monsoon	162468.8	5.5	0.70	0.70
Monsoon	129529.4	6.0	0.85	0.66
Post-monsoon	89133.2	5.9	0.78	0.64
Winter	317804.8	5.5	0.67	0.68

Table 3.1. *Fitted parameters (n_0, ν, r_m, σ_m) for seasonal NSDs.*

The ν values corresponding to the aerosol radii range from 0.175 to 0.5μm lies between 5.5 and 6 at this location. These values are slightly higher than the previously reported values [*Nair*, 1993; *Beegum*, 2010] and indicative of higher concentration of small particles. The large particle mode ranges from 0.67 to 0.85μm with the width of the distribution (σ_m) lying between 0.64 and 0.70. The mode radius r_m peaks in monsoon (0.85μm) with minimum in winter. The chemical characteristics of the aerosols presented in Section 3.4 and the Principal Component Analysis (PCA) in section 3.4.2 throw more light into the different species which constitute these modes.

3.3.2.2 *Seasonal variation of particles of different size ranges (PM1, PM1-3, PM3-5 and PM>5)*

Along with the optical/radiative and climatic impacts of aerosols, their effects on human health and the living environment are also of great concern [for e.g. *Pope et al*., 2011]. The respiratory system is the most frequently affected organ system by Particulate Matter (PM) or aerosols. Aerosols with aerodynamic diameter up to 1μm, 2.5μm and10μm (PM1, PM2.5, PM10) are of biological importance in this context. Even though the measurements done as part of the present study is not directly of PM1/PM2.5/PM10, the size resolved measurements of aerosol number density at more finer size bins were made use to make inferences on particulate matter of different sizes. Primarily the present study focuses on aerosols of the following major classes given below:

1. Particles with size (aerodynamic dia) between 0.3 to 1μm diameter (referred as PM_1 or fine particles in this study).

2. Particles with size >1μm denoted as PM>1 and referred as the coarse particles.

In addition, to examine the finer details, the coarse particle range is subdivided into

(a) Particles between size range 1-3μm represented as PM1-3 which can represent PM2.5.

(b) Particles of size greater than 3μm and ≤ 5μm represented as PM3-5.

(c) Particles of size greater than 5μm represented as PM>5.

The seasonal pattern of the number density of aerosols in the two major classes namely PM1 (fine) and coarse particles (PM>1) are shown in Figure 3.10a and b.

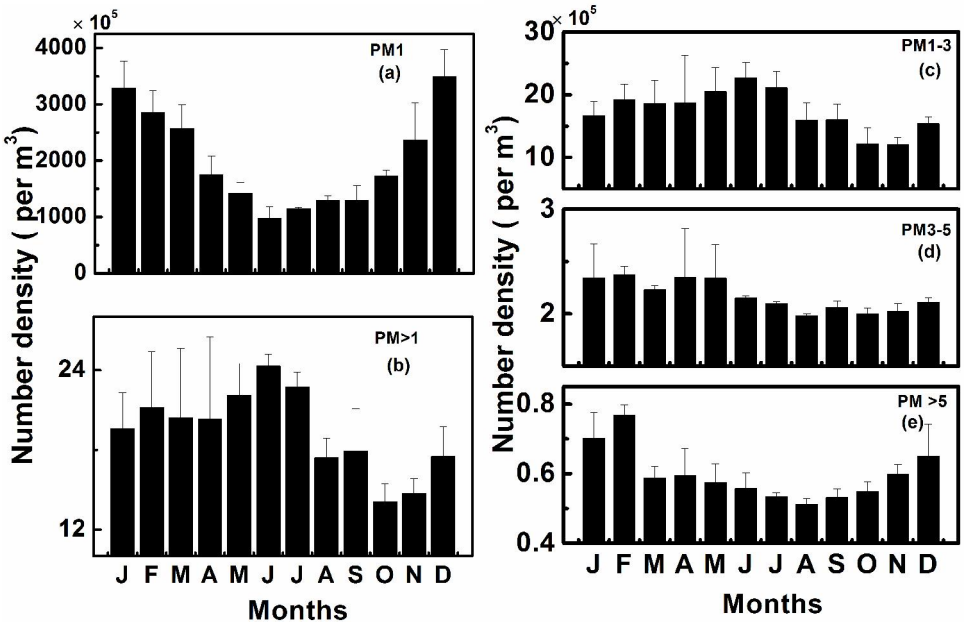

Figure 3.10. *Monthly variation of (a) PM1 (b) PM>1 (c) PM1-3 (d) PM3-5 and (e) PM>5 for the study period.*

PM1 particles showed a pattern similar to that of total aerosol number density (Figure 3.6) since N is dominated by PM1 particles (or the fine mode particles). These particles show an increase towards the winter months with value reaching ~$3.5\times10^{8}m^{-3}$. This increase is attributed to the enhancement of anthropogenic aerosols transported from continental regions over to the site under favourable wind direction (north/north-easterlies (Figure 3.5)) and the prevailing dry conditions characteristic of the season. Moreover, the low temperature and weak convective activities results in shallow boundary layer which in turn confines the aerosols close to ground thereby increase their near-surface concentration. The number density of PM1 reaches minimum in monsoon (~ $1\times10^{8}m^{-3}$) with an intermediate value in pre-monsoon (~ $2\times10^{8}m^{-3}$). On the other hand, the coarse particles (PM>1) show a different pattern with peak values in pre-monsoon/monsoon period and minimum in post-monsoon. Coarse particles are

often produced through bulk-to-particle-conversion mechanisms and include soil dust, sea-salt, and those of vegetative origin, like pollens, spores, etc. This analysis shows the seasonally changing aerosol sources acting at this location.

To get more insight into the size-resolved number density, the seasonal patterns of PM1-3, PM3-5 and PM>5 are also examined (Figure 3.10c to e). The pattern of PM1-3 is more or less similar to that of the coarse particles (PM>1) with peak in monsoon months (JJA) and minimum in post-monsoon (ON). PM3-5 is characterized by an extended peak from winter to pre-monsoon (DJF and MAM). Particles with size >5μm (PM>5) peaks in winter season and remains more or less steady in other seasons. Peaking of aerosol number density in different size ranges in different seasons confirm the highly varying seasonal sources. Here it is to be noted that large sized particles contribute more to the aerosol mass. The percentage contribution of fine particles to the total number density ranged from 96-98% with monsoon season showing minimum.

3.3.3 Monthly variation of aerosol mass loading

Along with the number density-size distribution of near-surface aerosols, measurements of the aerosol mass loading (M_L in μg m^{-3}) were also carried out by operating the High Volume Sampler (GH 2000, Graseby Anderson, USA) at the same level (3m above ground) from where air is drawn for number density measurements. The technical details, sampling procedure, protocol and estimation of mass concentration are described in Chapter 2. *George et al.*, [2008] have reported a mean value of M_L as 52.4±16μg m^{-3} during sea-breeze regime (day time). In the present study, aerosol samples were collected during SB and LB regimes. Sampling duration was 3hours centred on noon, for the SB regime and midnight for LB, confirmed by monitoring the wind direction. A total of 110 samples collected during the study period have been used in the present study. Among this, 32 samples fall in winter season, 38 samples in pre-monsoon and 20 samples in monsoon and 20 during post-monsoon. Rainy days restricted the sampling during the monsoon months.

Aerosol mass concentration showed day-to-day variation with values ranging from ~30 to ~100μg m^{-3}. The mean monthly variation of M_L for the period of September 2011 to December 2013 is shown in Figure 3.11.

The mean value of M_L is obtained as 67±30μg m^{-3} for the entire study period of two years. There exist two peaks in M_L, one for the winter season (DJF) and other in monsoon season (JJAS). M_L decreases during the summer months of MAM. The minimum M_L is observed during SON after which it increases.

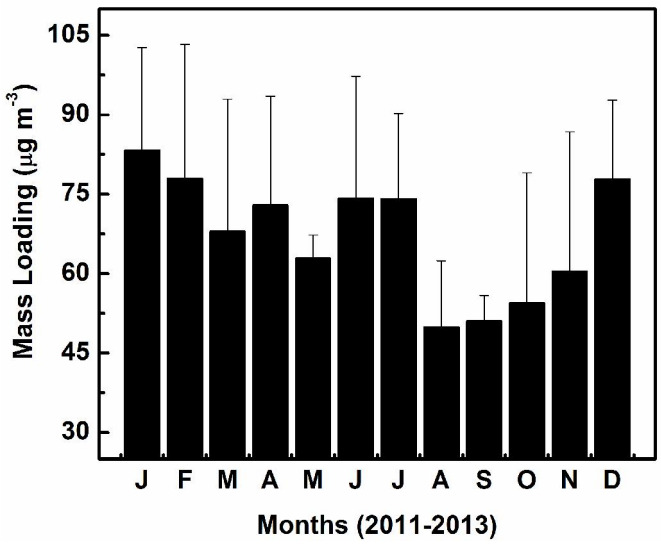

Figure 3.11. *Monthly mean aerosol mass loading (M_L) for the study period at TVM.*

It is to be noted that the seasonal variation of N (shown in Figure 3.6) and M_L (Figure 3.11) are not exactly matching even though both of them exhibit peak during winter months (DJF). While the number density dips during monsoon, M_L shows enhancement during monsoon months (JJ). Here, it is to be noted that, large sized particles contribute more to the total aerosol mass. The increased loading of large/coarse particles PM1-3 and above (Figure 3.10) could be partially responsible for the increase in M_L during monsoon.

3.3.4 Change in M_L and N during SB & LB (day to night changes)

In this work, measurements of N, NSD and M_L were carried out during SB and LB regimes for the first time. As observed over this site, the SB sets in by 0900 to 1000hrs and prevails till 1900-2000hrs when LB sets in [*Prakash*, 1993]. In view of the large day-to-day variability, to characterize the aerosol properties, the measurements done on the same day during SB and LB periods only are considered in this analysis. In Figure 3.12a and b are shown the monthly mean N and M_L measured during SB and LB regimes.

Aerosol number density N remained invariably high during LB regime (night time) in all months. This is because the LB brings aerosols from inland where anthropogenic activities take place, to this coastal site. Moreover, the shallow and stable boundary layer during night time confines the aerosols to surface level. SB favours influx of sea-salt aerosols which are less in number. The mass loading also remains high during LB regime in most of the months. But, from the pre-monsoon

months of April, M_L during SB starts exceeding that during LB and remains high till July, after which M_L during LB overrides that of SB.

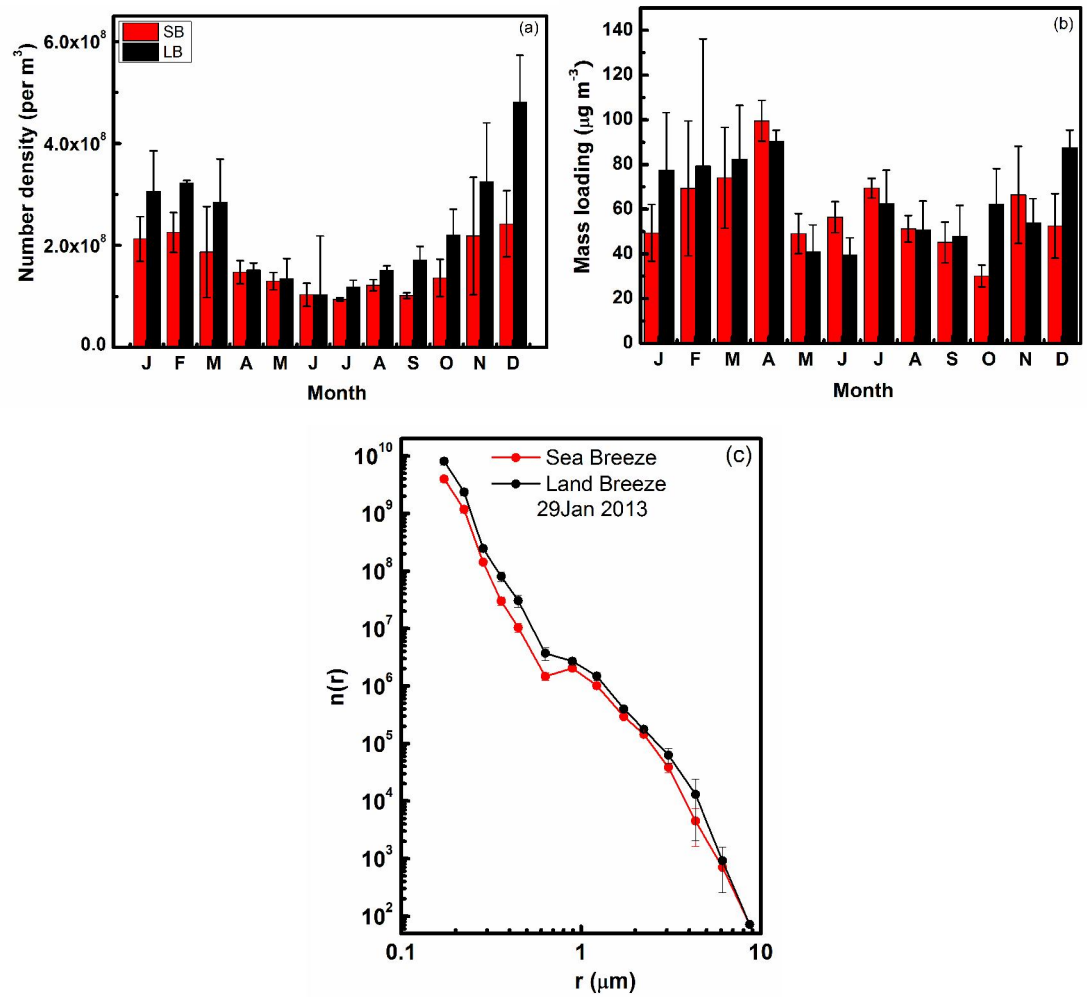

Figure 3.12. *Monthly variation of (a) Total number density (b) Mass loading and (c) NSDs during SB and LB regimes.*

The SB-LB contrast is largest in the winter months of DJF when the synoptic scale flow is from inland. M_L in LB and SB become comparable during summer months of April/May and M_L during SB exceeds than that during LB in monsoon. The influx of sea-salt aerosols contribute to high M_L during monsoon, since they are of larger size. In this context, it is worth noting that large sized particles contribute more to the mass and increase in M_L is indicative of presence of large/coarse particles. In Figure 3.12c is shown the typical aerosol NSDs for SB and LB regimes. These NSDs clearly reveal the presence of more fine particles during LB period. Particles in the size range 1-3μm (radii from 0.5 to 1.5μm) are also dominant during LB due to influx of continental species like soil dust from inland.

3.3.5 The seasonal patterns and synoptic scale meteorology

Synoptic scale meteorology plays key role in controlling the seasonal behavior of aerosol characteristics at the study region [*Moorthy et al.,1991*; *Pillai et al*., 2001; *Babu et al*., 2004; *David et al*., 2011]. Air mass back trajectory analysis pertaining to the location is a potential tool in identifying the source regions of aerosols. In view of the short lifetime of near-surface aerosols, which is less than a week, the 7-day air mass back trajectories arriving at the observation site at 925hPa (within the boundary layer) for the mean sampling time are simulated by running the Hybrid Single Particle Lagrangian Integrated Trajectory (HYSPLIT) model [*Draxler et al*., 2003] (www.arl.noaa.gov/ready/HYSPLIT.php), details of which are discussed in Chapter 2, and shown in Figure 3.13 for different seasons.

The systematically changing pattern of air mass over the study location representing the four seasons can be clearly visualized in Figure 3.13. During monsoon, the air mass is from the marine environments of Indian Ocean (IO) or Arabian Sea (AS) from where strong westerlies/south westerlies originate. This will bring in sea-salt aerosols over to the site. Air mass prevailing at the site in winter is obviously from north-east or east. But in pre-monsoon and post-monsoon the air mass trajectories are of mixed origin. While in pre-monsoon, most of the trajectories are of marine origin, in post-monsoon, air mass of mixed origin-oceanic as well as continental- arrive at the site. It is observed that the seasonal behaviour of aerosol number density, NSD and mass loading are closely linked with those of meteorological parameters.

As mentioned in Section 3.2 the winter season (DJF) is characterised by low temperature and minimum RH. The removal processes (rainfall) are also weak during this period and thus increases the lifetime of aerosols. The wind pattern (Figure 3.3) as well as air mass back trajectories indicate northerly/north-easterly flow (from inland) bringing in continental air mass. Since the continental air mass is more loaded with aerosols, this condition can lead to an increase in aerosol loading both in terms of number density and mass loading as seen in Figures 3.5 and 3.11. The fine particles (PM1 in Figure 3.10) as well as coarse particles (PM>1) clearly show their peak during winter months. Thus aerosols of mixed sources arrive at the study location during winter. South west monsoon (JJA) starting in June at this location and extending till Aug/Sep, is manifested with heavy rainfall and strong south/south-westerly winds bring in marine air mass (Figure 3.4). Consequently, the aerosol total number density shows a decrease of ~36% from that of winter. In fact, from March onwards, the number density starts decreasing and reaches minimum by JJ. This decrease is notable in fine particle

number density (PM1, see Figure 3.11a).The PM1-3 particles peaks in monsoon when the air mass of oceanic origin prevails over the experimental site, bringing in sea-salt aerosols.

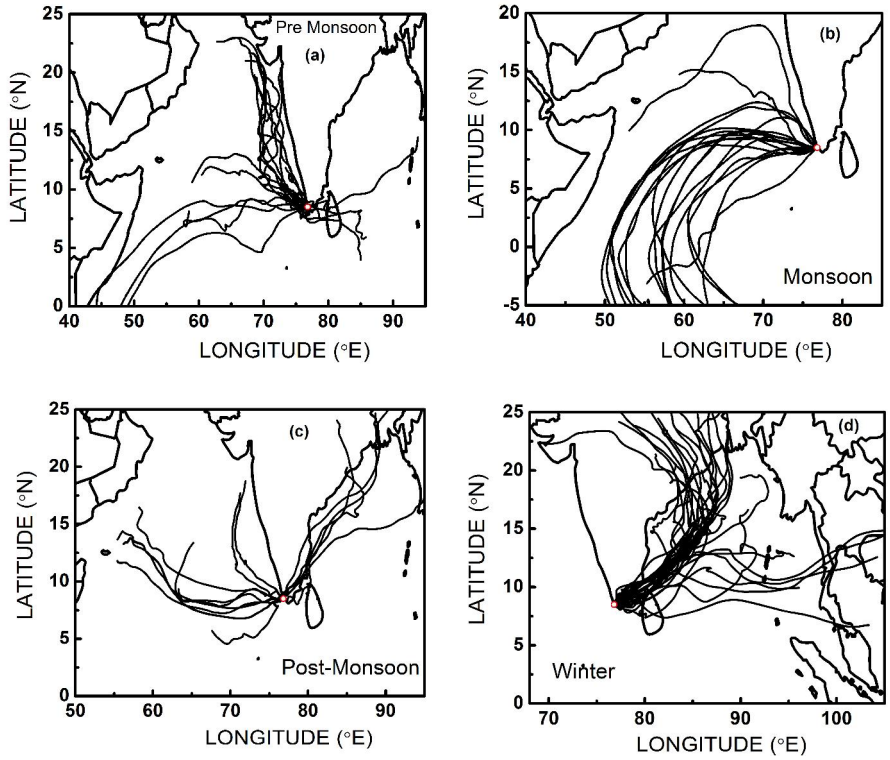

Figure 3.13. *7-day air mass back trajectories reaching TVM at 925hPa for (a) pre-monsoon (b) monsoon (c) post-monsoon and (d) winter.*

The pre-monsoon months (MAM) are generally dry and hot and also the season in which the transition of air mass from continental to the marine occurs (Figure 3.4). The air mass back trajectories originates mostly from marine environment of AS and traverses the coastal regions. However, few trajectories originating over eastern side and passing through land mass also reaches the site. So it is possible that both fine and coarse particles of marine and continental sources reaches the site. Since the temperature attains peak values during pre-monsoon, the convective activities get strengthened, mixing the air vertically to higher altitudes and thus reduces the near-surface aerosol loading. The post-monsoon months ON also represent transition period for wind, from south-westerly to northerly/north-easterly (return monsoon). The air mass is mostly of oceanic origin from both AS and BoB. In this case also, it traverses the landmass on the eastern side of the site.

3.4 Chemical characteristics of aerosols

The collected aerosol samples were subjected to chemical analysis using various analytical techniques as described in Chapter 2. The mass concentrations of major water soluble anions SO_4^-, NO_3^-, Cl^- and cations of Na^+, Ca^{2+}, Mg^+, K^+, NH_4^+ were estimated by using Ion Chromatograph (DX-120 of Dionex USA and Metrohm 882 plus, Switzerland). Bicarbonate in aerosols was measured using the autotitrator (model 848/877 Titrino Plus) for the first time. Acid soluble metallic species Fe, Al, Mn, Zn, Ca, etc are measured with ICP-AES (Optima 4300V of Perkin Elmer), and Na and K with AAS (Varian Spectr AA 250 plus). In addition to this, the in-situ-measured Black Carbon (BC) using aethalometer (model AE-41, Magee Scientific USA) operated during the same period is also used in this study.

3.4.1 Seasonality in chemical composition

The measured mass concentrations of the various species exhibited large day-to-day variability and also seasonality. The most dominant species in aerosols over this region include the marine species Na^+ and Cl^- and the anthropogenic component SO_4^- ,the mean concentrations being 5.1±3.0, 6.1±4.1 and 7.3±4.2μg m^{-3} respectively. In spite of the significant day-to-day variability, chemical composition exhibit systematic seasonal behaviour which is species dependent. In Figure 3.14a is shown the seasonal behaviour of the oceanic species Na^+, Cl^- and Mg; crustal species Fe, Ca, HCO_3 and Al; the anthropogenic components SO_4^-, NO_3^- , NH_4^+ and BC along with K^+. Species K^+, Ca, Mg and SO_4^- have both sea-salt (ss) and non-sea-salt (nss) contribution over the site [*George et al*., 2008]. The ss component of each of these species (X) were estimated using Na as the reference species and given as [*Duce et al*., 1983]

$$M_{Xss} = \left(\frac{X}{Na}\right)_{sw} \times M_{Na} \qquad 3.4$$

where , M_{Xss} and M_{Na} are the mass concentrations of , ss-component of X and Na respectively and $(X/Na)_{sw}$ is the mass ratio of species X to Na in sea water the typical - values being 0.25, 0.037, 0.038 and 0.12 for SO_4^{2-}, K, Ca and Mg respectively [*Berg and Winchester,* 1978]. The nss component is estimated by subtracting M_{Xss} from the total mass concentration of the respective species (m_X). The seasonal patterns of ss and nss components are shown in Figure 3.14b and c. Source of nss-Ca is mostly crustal, nss-K of biomass origin and nss-Mg has soil origin. Major oceanic species Na^+ and Cl^- and the ss components peaked in monsoon (JJAS) and decreased during post-monsoon

(ON). The mass concentrations of oceanic species are comparable in pre-monsoon and post-monsoon, but significantly low in winter. The monsoon high is due to the increased production of sea-salt by strong south-westerly winds which blow during monsoon period as explained in section 3.2. During pre-monsoon and post-monsoon also presence of marine air mass can be noted in the pattern of back trajectories shown in Figure 3.7. But in winter the air mass is of continental origin (Figure 3.7a) and winds are calm with minimal sea-salt production. This results in less or absence of marine species at the site.

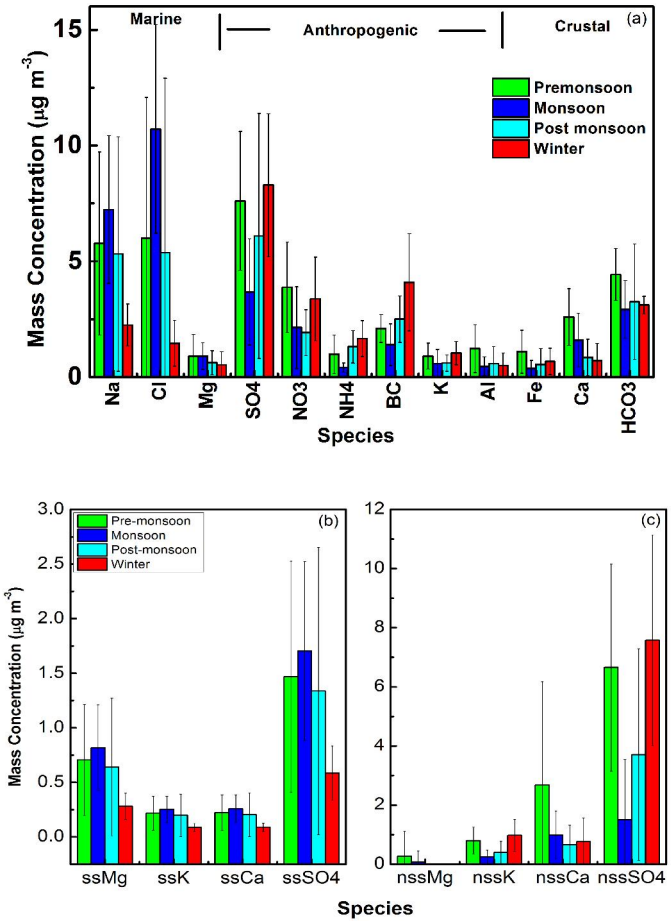

Figure 3.14. *Seasonal variation of (a) various chemical species in aerosols at TVM (b) ss components and (c) nss components*

Species of anthropogenic origin like SO_4^-, NH_4, BC and the nss components of K, Ca, and SO_4^{2-} peak in winter season and decreases through the post-monsoon and pre-monsoon seasons reaching minimum in monsoon. The winter peak in anthropogenic species can be attributed to (1) influence of continental air mass (2) low boundary layer height (3) low temperature and calm winds leading to less ventilation and inefficient removal processes resulting in longer residence time of aerosols. The source of SO_4^{2-} is mainly fossil fuel combustion and hence is a tracer for anthropogenic

activities. Black carbon also originates mainly from the exhaust from automobiles. NO_3^- is mainly formed from the oxidation of NO_x produced from fossil fuel combustion, emissions from soil and lightning discharges. Though nitrates mostly originate from anthropogenic sources, the highest values were observed during the pre-monsoon season indicating other sources of nitrates at the site.

The crustal species including Fe, Al, nss-Mg and nss-Ca shows a predominant high for pre-monsoon period. This is attributed to long range transport from arid regions on west/northwest of the site. From Lidar based measurements *Rajeev et al*., [2010] have inferred that during pre-monsoon/monsoon long range transport from north and north-western regions is active bringing mineral/soil dust to troposphere. *Mishra et al*., [2013] also observed that the study region lies within the mineral dust plumes that occur over the arid regions. Thus the enhanced presence of crustal species during monsoon and pre-monsoon period provides evidence for the long range transport of mineral dust during these periods.

Bicarbonates were also found in significant quantities at this location with values in the range 3.1-4.9μg m^{-3} with peak concentration in pre-monsoon. Carbonates and bicarbonates have crustal and marine sources. Soil containing dolomite form the crustal source and sea-salt in the form of calcium carbonates/bicarbonates constitute the marine source [*Chow et al.*, 2004]. The high bicarbonate in pre-monsoon along with Fe and Al also support the long-range transport of mineral dust.

3.4.2 Source identification by Principle Component Analysis

To identify the possible sources that determine the aerosols over the study region, the Principle Component Analysis (PCA) details of which are given in Chapter 2 was utilized. In the present study, PCA was applied to aerosol chemical composition data by using Statistical Package for Social Sciences (SPSS) version 12 and quantitative inferences are made on the sources based on the factor loadings. Factor loading determines the most representative species in each factor and a loading > 0.7 is typically regarded as excellent and shows greater association of that species to the source, whereas a loading <0.3 is considered non-significant [Stevens, 1996]. The higher the factor loading greater will be the association of that species to the source. PCA has been used effectively for identifying aerosol source from various locations over Indian region [*Srivastava et al.,* 2008; *Chakraborthy and Gupta,* 2009*; Kulshrestra* et al., *2014*; *Hegde and Kawamura, 2012*].

The PCA was carried out by grouping the chemical composition data (mass concentration of each species) of aerosols on seasonal basis for the four seasons discussed above. For each season the major factors along with the loading were obtained using SPSS and given in Table 3.2. The eigen values, % variance and the cumulative percentages of the obtained factors are also listed in the table. Most of the loadings were ≥0.7, suggesting that the extraction of all the factors is reasonable to make interpretations for this study.

Species/variables	Pre-monsoon Factors			Winter Factors			Monsoon Factors			Post-monsoon Factors		
	F1	F2	F3	F1	F2	F3	F1	F2	F3	F1	F2	F3
Cl	0.0	0.0	0.6	0.5	-0.2	-0.6	0.9	0.1	0.3	0.9	0.1	0.0
NO3	0.4	0.5	0.2	0.8	0.3	0.0	0.1	0.9	0.0	-0.1	0.9	0.0
SO4	-0.1	0.9	0.0	0.1	0.8	0.0	0.4	0.5	0.5	0.0	0.9	0.0
Na	-0.1	0.1	0.9	0.0	-0.5	-0.6	0.8	0.1	0.4	0.9	-0.1	-0.1
K	0.2	0.5	0.6	0.8	0.3	-0.1	0.9	0.3	-0.1	0.1	0.7	0.4
Mg	0.9	-0.1	0.2	0.1	0.0	0.8	0.0	0.3	0.9	0.9	-0.4	0.1
Ca	0.9	-0.1	0.1	0.9	-0.2	-0.1	0.8	0.6	-0.1	0.8	0.3	0.4
NH4	-0.5	0.5	0.2	0.1	0.9	0.1	0.0	0.6	0.6	-0.1	0.8	0.0
Al	0.9	0.0	-0.1	0.7	-0.1	0.6	0.4	0.8	0.2	0.1	0.0	0.9
Fe	0.9	0.1	-0.2	0.9	0.1	0.4	0.3	0.6	0.3	0.1	0.2	0.9
Eigen values	3.8	1.7	1.6	3.6	1.8	1.7	3.6	3.0	2.1	3.3	3.1	2.3
%Variance	34.9	15.1	14.9	33.1	16.9	15.7	32.7	27.1	18.9	33.1	31.3	22.8
Cumulative %	34.9	49.9	64.9	33.1	50.0	65.8	32.7	59.8	78.6	33.1	64.4	87.2

Table 3.2. *The extracted factors in aerosol species (factor matrix) along with % of variance and cumulative % for different seasons as revealed from PCA (the blue, red, green and yellow represents the crustal, anthropogenic, marine and mixed type of aerosols respectively).*

For pre-monsoon season the first factor showed loadings of 0.9 with Al, Fe, Mg and Ca which have crustal origin. This factor represents crustal or soil re-suspension and accounts for 34.9% of variance. The second factor correlates with NH_4^+, SO_4^{2-}, K^+ and NO_3^{-}. Both NO_3^- and SO_4^{2-} are largely produced as secondary aerosols during the process of coal combustion, biomass burning and vehicular emissions [*Seinfeld and Pandis*, 2006]. Thus Factor 2 represents for anthropogenic source for the pre-monsoon

season. Factor 3 which shows high loadings for Cl^-, Na^+ and K^+ is identified as marine sources mixed with biomass burning contribution.

During winter, the first factor comprises of 33.2% of the total variance having high loadings of NO_3^-, Cl^-, K^+, Ca, Fe and Al all having significant contribution form soil/continental source. The second factor is contributed by the anthropogenic species SO_4^{2-} and NH_4 existing as probably $(NH_4)_2SO_4$ or NH_4HSO_4. Factor 3 has Mg and Al which possess crustal sources. The study location TVM and nearby region has laterite soil which is rich in Al and Mg (www.keralasoils.gov.in).

In monsoon season, the first factor (32.7% of variance) comprises of the marine species Na and Cl along with K and Ca, which are also having strong oceanic contribution. The anthropogenic species NO_3^- , NH_4^+, SO_4^{2-} along with mineral species Al and Fe contribute to the second factor with 27.1% of the total variance, which represents a mixed composition of aerosols which would have formed due to the processing of aerosols. Factor 3 presents the Mg, NH_4^+ and SO_4^{2-} as main constituents. During this season, both NH_4^+ and SO_4^{2-}, seems to have two distinct sources (marine and anthropogenic), as the components are equally, distributed among factor 2 and 3.

Post-monsoon season also called the return monsoon shows the first factor is highly loaded with marine species Na, Cl along Mg and Ca having both marine and crustal component. Second factor is contributed by anthropogenic components SO_4^2, NH_4^+, and NO_3^- along with biomass burning species K^+ accounts for 31.3% of the total variance. The third factor has Al and Fe and as prominent components which is having crustal origin. This analysis has brought out a quantitative information of the various aerosol sources acting at TVM in different seasons. This along with airflow and back-trajectory analysis (Section 3.3.4) revealed a comprehensive picture on the source characteristics of aerosols at this location.

3.4.3 Dependence of size resolved aerosol number density on chemical composition

The main uncertainty in predicting the radiative forcing effects of aerosols arise due to the poor representation of their size-resolved chemical composition in the radiative transfer models. Even though in the present study, size-resolved chemistry could not be included, simultaneous and concurrent measurements of NSD, total aerosol mass concentration and mass concentration of different chemical species were done. In this context, a correlation analysis between mass concentration of different chemical species and number density of aerosols in two size regimes viz. the fine

particle mode (diameter <1μm) and coarse particle mode (diameter >1μm) were carried out using the linear regression technique in order to understand their mutual dependence. This analysis was carried out on seasonal basis and the regression coefficients are listed in Table 3.3. The correlation coefficients with significance level p>0.001 are presented in bold letters. Since the analysis for post-monsoon season did not reveal any significant results, it is not presented.

	Correlation coefficient (R)					
	Winter		**Premonsoon**		**Monsoon**	
Species	Fine mode	Coarse mode	Fine mode	Coarse mode	Fine mode	Coarse mode
Na	-0.42	-0.5	-0.45	**0.44**	0.18	**0.50**
Cl	0.34	0.34	-0.54	**0.65**	0.10	**0.58**
Mg	0.02	**0.57**	-0.45	**0.61**	**0.46**	**0.43**
NO3	**0.48**	**0.47**	-0.04	**0.44**	**0.53**	-0.40
K	**0.82**	**0.67**	0.31	0.34	**0.41**	-0.10
SO4	**0.55**	0.29	**0.57**	-0.13	**0.68**	-0.10
Ca	**0.40**	0.25	-0.46	**0.56**	**0.43**	0.15
Al	0.14	**0.59**	-0.50	**0.72**	**0.85**	**0.54**
Fe	**0.64**	**0.66**	-0.13	**0.59**	**0.75**	**0.68**
NH4	**0.50**	0.22	**0.85**	-0.14	**0.59**	0.07

Table 3.3. *Correlation coefficient (R) obtained through linear regression analysis between mass concentrations of various chemical species and fine mode and coarse mode aerosol number density.*

The major results of this analysis include:

(1) Oceanic species Na^+ and Cl^- show positive correlation (R value 0.45 with the significance level of p<0.001) with coarse mode number density during pre-monsoon and monsoon. This ascertains that majority of the sea-salt particles are in coarse mode (diameter >1μm). But their correlation is negative or insignificant with fine mode number density in any season.

(2) In winter, Na shows negative correlation with both fine mode and coarse mode, but Cl^- shows positive correlation with both the modes. This has the implication that sources other than oceanic exists for Cl^- in winter. PCA also showed that Cl is one component in factor 1 in winter, but Na^+ is not.

(3) The mass concentration of anthropogenic species SO_4^- and NH_4^+ are positively correlated with fine mode (R>0.5). This again confirms their formation mechanism as GPC.

(4) Another component of anthropogenic origin, NO_3^- depicts a different picture. Its correlation is positive with both the modes in winter, coarse mode in pre-monsoon and

fine mode in monsoon. This analysis also indicates different sources for this species or it undergoes season dependent processing. The significant correlation observed for NO_3^- in coarse mode suggests that their production is not through GPC, but they originate from sources like suspension from soil dust or processed with dust or other salts [*Clarke et al.*, 1999; *Moore and Blough* 2002, *Dahl et al*., 2005]. The PCA as explained in Section 3.4.2 also points towards this argument where NO_3^- was found in the factor 2 in monsoon and post-monsoon along with crustal/continental species. Ca behaves in a manner similar to NO_3^- indicating different sources.

(5) K^+ a strong tracer of biomass burning shows strong positive correlation in both the modes in winter indicating that it has sources from biomass burning as well as marine origin. Studies done over the same site by *George et al*., [2008] had shown that the nss component of K^+ is 80% to total K^+ during the pre-monsoon season which could be due to biomass burning.

(6) Fe and Al are positively correlated with coarse mode in all seasons. But during monsoon it shows positive association with fine mode also. It is observed that the transported mineral dust is often in accumulation mode (0.1 to 1μm) [*Kandler et al*. (2009); *Denjean et al*., 2016]. This analysis again supports the view that long-range transport of mineral dust from arid Arabian regions is active during monsoon.

3.5 Mean density of aerosols

The density (ρ) of an aerosol particle is of great importance for the prediction of particle mechanics, life cycles, both in the atmosphere and in the human respiratory system [*Seinfeld and Pandis*, 2006]. The density depends on chemical composition which in turn decides the refractive index and the radiative characteristics of the medium.

In this work, it is attempted to estimate the mean density of aerosols at this location based on the mass loading and NSD measurements.

The mass loading (M_L) in μg m^{-3} is related to the number size distribution through the relation,

$$M_L = (4/3)\pi\rho\sum_{i=1}^{14}[r_i^2 n_i(r_i)] \qquad 3.7$$

where r_i and n_i are the mean radius and number density of aerosols in the size channel i. The mean density (ρ) is estimated as

$$\rho = (M_L)/[4/3\pi\sum_{i=1}^{15} r_i^2\{r_i^3 n_i(r_i)\}] \qquad 3.8$$

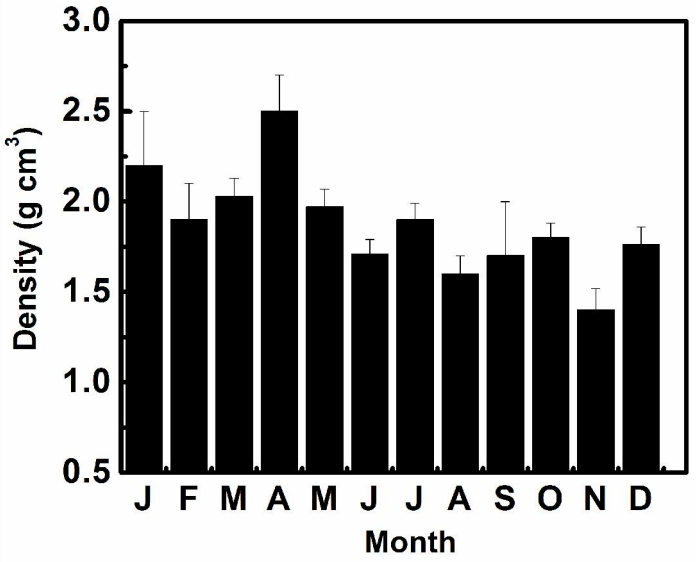

Figure 3.15*. Variation of monthly mean density of aerosols at TVM.*

The density is estimated on monthly basis using the monthly mean number density n_i in size channel i with mean radius r_i and presented in Figure 3.15. ρ varies in the range 1.4 to 2.6g cm^{-3} annually probably due to mixed nature of aerosols. It is higher during the pre-monsoon and winter compared to monsoon and post-monsoon probably due to the influence of mineral dust/continental aerosols, as revealed by the chemical composition analysis (Section 3.4.1).

Density of the basic materials of aerosols range from ~2.0g cm^{-3} for soot, 2.25g cm^{-3} for sea spray to >2.6g cm^{-3} for minerals *Hand and Kreidenweis*, [2002]. *Mc Murry et al*. [2002] determined the density of spherical liquid particles as 1.5g cm^{-3} by selecting particles of specific diameter using an electrostatic classifier and subsequently measuring mass using an aerosol particle mass analyzer. *Hand and Kreidenweis*, [2002] calculated the effective density using a differential mobility analyzer to measure mass and an aerodynamic particle sizer to measure aerodynamic diameter as 1.85±0.14g cm^{-3} for PM2.5 aerosols at Mexico. The aerosol density determined for different aerosol types like dust, water soluble, soot, sea-salt volcanic dust etc show a wide range of densities from 1.6 to 5.2g cm^{-3} [*d' Almeida ,* 1991].

3.6 Major aerosol components and first-cut chemical models

Based on the chemical composition and their radiative effects, the atmospheric aerosols are broadly classified into 5 major components (1) Sea-salt (SS) (2) Other Water soluble Non-sea-salt components (WSN) (3) Mineral dust (MD) (4) Particulate Organic Matter (POM) and (5) Black Carbon (BC). The mass concentration of sea-salt

aerosols (SS) is estimated from the mass concentrations of Cl and Na as [*Duce et al*., 1983]

$$SS = M_{Cl} + 1.47 * M_{Na} \quad (3.9)$$

where 1.47 is the seawater ratio of $(Na^+ + K^+ + Mg^{2+} + Ca^{2+} + SO_4^{2-} + HCO_3^-) / Na^+$. In this approach the non-sea-salt K^+, Mg^{2+}, Ca^{2+}, SO_4^{2-} and HCO_3^- in the sea-salt mass is eliminated and also allows for the loss of Cl^- through depletion process.

Mineral dust (MD) in the sample is estimated as [*Malm et al*., 1994]

$$MD = 2.2M_{Al} + 2.49M_{Si} + 1.63M_{Ca} + 2.42M_{Fe} + 1.94M_{Ti}, \quad (3.10)$$

M_{Si} is estimated by making use of the mass ratio of Si/Al as 3.84 and since Ti was not detected it is not included in this estimation.

The POM is the least known and least studied component in aerosols at this location and also over Indian region. No direct measurements are available at the study region. An approximate estimate of POM can be made based on the organic carbon (OC) concentration as [*Turpin and Lim*, 2001]

$$POM = 1.6 * M_{oc} \quad (3.11)$$

where 1.6 is a factor which represents the average organic molecular weight per carbon for the organic aerosol. *Hegde et al*., [2015] has given OC mass concentration (M_{OC}) at this location as 17±4.7µg m^{-3} for pre-monsoon, 16±4.9µg m^{-3} for monsoon and 17±4.2µg m^{-3} for winter and these values are used in this study for the estimation of POM.

The water soluble component WS is given by,

$$WS = M_{Cl} + M_{NO3} + M_{SO4} + M_{Na} + M_{Mg} + M_{NH4} + M_{Ca} \quad (3.12)$$

The other water soluble species comprising mostly of non-sea-salt particles of continental origin is given as

$$WSN = WS - SS \quad (3.13)$$

The BC concentration used in this analysis is that measured using aethalometer at the experimental location during the study period [*Kompalli et al*., 2013]. The unanalysed mass or residual part if any, is termed as the Residual Fraction (RF). The concentrations of different aerosol components thus estimated on daily basis were grouped and averaged seasonally to obtain a first-cut chemical model for each season and are shown as pie charts in the Figure 3.16.

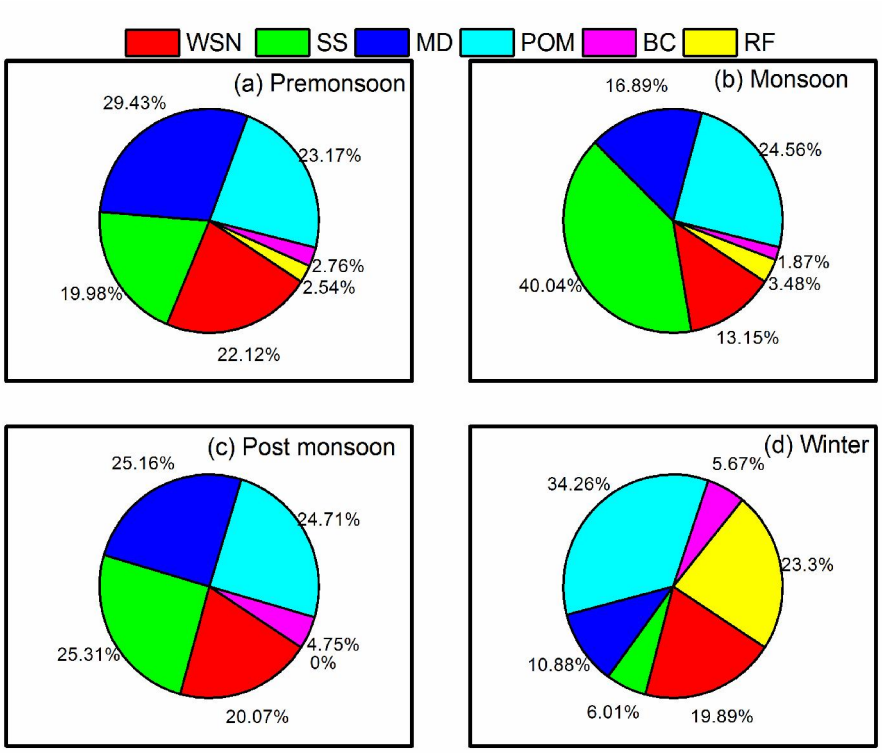

Figure 3.16. *First-cut models for aerosol chemical composition at TVM for different seasons.*

The component SS shows higher percentage (40%) for the monsoon season and least in winter (6%) and remained 20% and 25% in pre-monsoon and post-monsoon seasons. WSN contributes 20-22% in pre-monsoon, post-monsoon and winter with minimum in monsoon (13%). MD peaks in pre-monsoon (29%) and showed least for winter (10%) with monsoon and post-monsoon values being 25% and 17% respectively. BC and POM were highest in winter (~5% and 34 % respectively). POM remained more or less same (~23-24%) in all other seasons. On the other hand, BC attained minimum in monsoon (2%) and remained 3-5% in pre monsoon and post monsoon. The RF remained high (23%) for the winter season and was found to be negligible in post-monsoon. This mass concentrations of various aerosol components form input for the model-based estimation of the radiative characteristics as discussed in the following section.

3.7 Estimation of Radiative characteristics

The aerosol radiative characteristics like aerosol scattering coefficient (β_{sc}) absorption coefficient (β_{ab}), extinction coefficient (β_{ex}), single scattering albedo (ω) and the phase function $P(\theta)$, optical depth (τ) etc. depend on both number density-size distribution (NSD) and chemical composition of aerosols [*Mc Cartney*, 1976; *Kokhanovsky*, 2008]. For any realistic estimation of these parameters, experimentally

measured aerosol characteristics like mass concentration and/or NSD and chemical composition are essential. In this work it is attempted to estimate the aerosol radiative properties incorporating the measured data on aerosol mass loading, size distribution and chemical composition making use of the software package OPAC (Optical Properties of Aerosols and Clouds) model [*Hess et al*., 1998] the details of which are given in Chapter 2. In this study the major aerosol optical parameters were estimated using OPAC, giving the measured aerosol parameters as input. The seasonal changes in the radiative properties are also investigated in this study.

OPAC is capable of providing aerosol optical/radiative properties of aerosols such as β_{sc}, β_{ab}, β_{ex}, ω and $P(\theta)$ for a user-defined set of aerosol components. The estimated parameters β_{sc}, β_{ab}, and β_{ex}, are given as,

$$\beta_{sc} = \int_{r1}^{r2} \pi r^2 Q_{sc}(m,\lambda,r) n(r) dr \qquad 3.14(a)$$

$$\beta_{ab} = \int_{r1}^{r2} \pi r^2 Q_{ab}(m,\lambda,r) n(r) dr \qquad 3.14(b)$$

$$\beta_{ex} = \int_{r1}^{r2} \pi r^2 Q_{ex}(m,\lambda,r) n(r) dr \qquad 3.14(c)$$

where, Q_{sc} Q_{ab} Q_{ex} represent the scattering, absorption and the extinction efficiency, m is the refractive index of the particle, λ is the wavelength of the radiation and r is the radius of the particle having a number size distribution n(r).

$$Q_{sc} = \frac{2}{\alpha^2} \sum_{n=1}^{\infty} (2n+1)(|a_n|^2 + |b_n|^2) \qquad 3.15$$

where $\alpha=2\pi r/k$ is the size parameter a_n and b_n are the Mie coefficients The values of these complex funtions are found from Ricatti-Bessel functions [*McCartney*, 1976].

$$Q_{ex} = \frac{2}{\alpha^2} \sum_{n=1}^{\infty} (2n+1)[\mathrm{Re}(a_n + b_n)] \qquad 3.16$$

The Single Scattering Albedo (ω) defined as the ratio of scattering coefficient to extinction coefficient is given by,

$$\omega = \beta_{sc}/\beta_{ex} \qquad 3.17$$

The scattering phase function $P(\theta)$ describes the angular distribution of scattered radiation with respect to the incident radiation. It is defined as the ratio of the energy scattered per unit solid angle in a given direction (θ) with respect to the incident direction, to the average energy scattered per solid angle in all directions.

$$P(\theta) = \frac{\beta_{sc}(\theta)}{\frac{1}{4\pi}\int_0^{4\pi} \beta_{sc}(\theta) d\psi} \quad 3.18$$

where $\beta_{sc}(\theta)$ is the angular scattering coefficient.

In the present analysis, OPAC is configured for 5 inputs entered in an ASCII text file which include:

(1) Aerosol components: A new mixture is defined based on the mass concentrations of 5 aerosol components (a) sea-salt (SS), (b) other water soluble components including organics (c) BC, (d) mineral dust (MD) and (e) water insoluble organic component (The seasonal mean mass concentration of water soluble and insoluble organics given by *Hegde et al.,* [2015] are included).

(2) Wavelength range: Ten wavelengths 0.45, 0.5, 0.55, 0.6, 0.65, 0.7, 0.75, 0.8, 0.9, 1.0μm are selected for which optical/radiative parameters are estimated.

(3) Relative humidity (RH): The measured RH values pertaining to respective seasons were selected as input.

(4) The optical/radiative parameters: The parameters estimated include β_{sc}, β_{ab}, β_{ex}, ω and $P(\theta)$ in the present study.

(5) Height profile of aerosols: This is not included in this study since columnar aerosol optical depth is not estimated.

The output of the computations of optical/radiative parameters is written to an ASCII output file.

3.7.1 Seasonal variation in estimated radiative properties

The estimated parameters β_{sc}, β_{ab}, β_{ex}, ω and $P(\theta)$ for the 10 wavelengths and for the four seasons are shown in Figure 3.17a to e. Scattering coefficient varied from 0.07 to 0.11km^{-1} with maximum values during pre-monsoon and winter for shorter wavelengths ≤0.5μm. At higher wavelengths, pre-monsoon values are higher than that of winter season implying the abundance of anthropogenic species of scattering nature during the period. Absorption coefficient varied in between 0.01 and 0.055km^{-1} with maximum values for the winter season (0.025-0.055km^{-1}) indicating the presence of more absorbing aerosols.

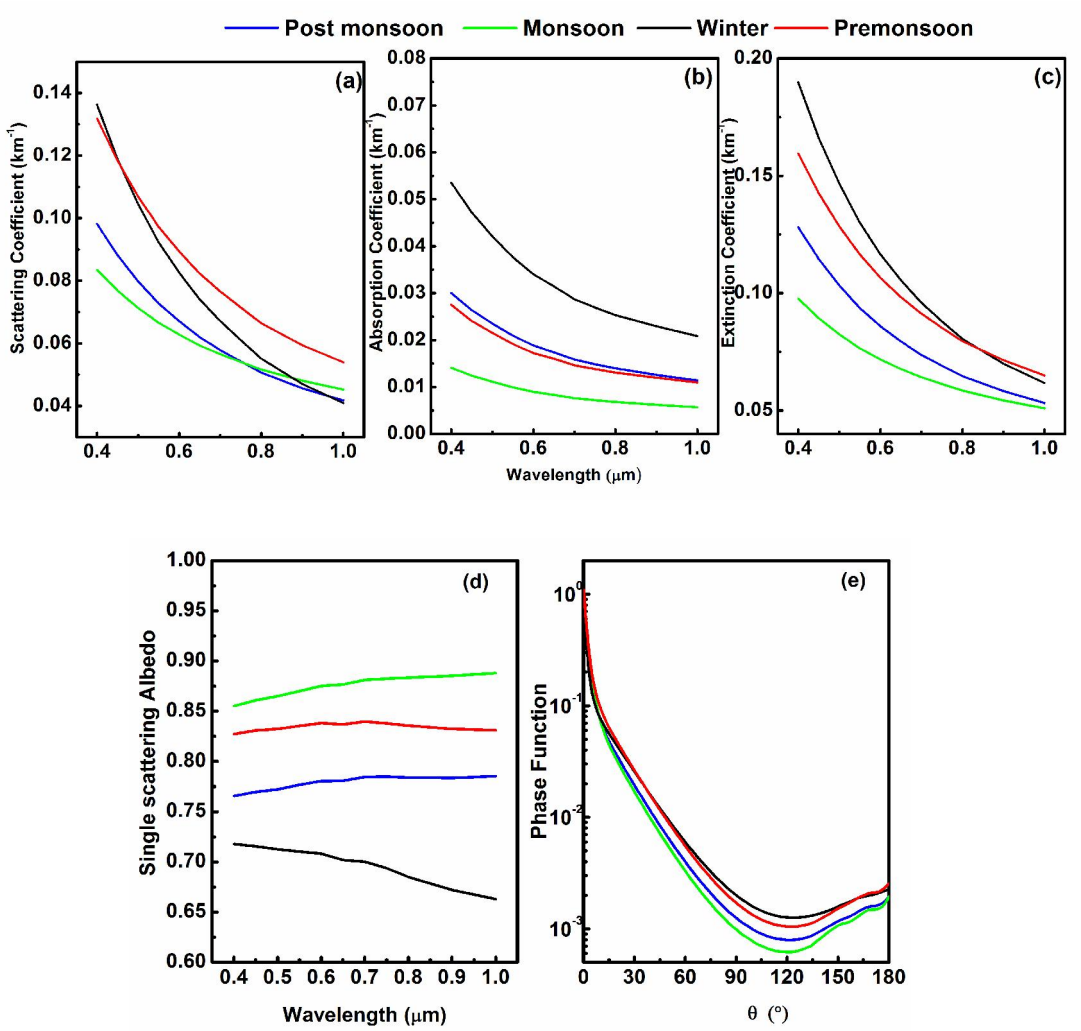

Figure 3.17. *Spectral dependence of the estimated β_{sc}, β_{ab}, β_{ex}, ω and $P(\theta)$ for the four seasons.*

The seasonal pattern of extinction coefficient is also different and wavelength dependent. β_{ex} attains highest values in winter and minimum in monsoon through pre-monsoon and post-monsoon. However, the seasonal differences decrease with increase in wavelength. In short, the influence of absorbing species at the study region is clearly seen in this analysis. The estimated β_{sc}, β_{ab} and β_{ex} values at 0.5μm are comparable to those estimated for continental aerosols and polluted maritime aerosols (*d' Almeida, et al.*, 1991). Lidar based measurement of extinction coefficient at TVM showed values in the range 0.07-0.14km^{-1} at 550nm [*Parameswaran et al.*, 1998] and over Gadanki (13.5°N, 79.2°E) it was found to be ~0.01km^{-1} at altitudes >3km [*Radhakrishnan et al.,* 2009)].

The single scattering albedo (ω) (Figure 3.17) is relatively low (~ 0.71-0.67) for the winter season showing the presence of significant amount of absorbing species like BC. The chemical model (Figure 3.16) also shows the presence of BC fraction 6%

during winter. During other seasons ω is >0.77 with the highest value being 0.89 for the monsoon season, due to presence of more scattering species like sea-salt. The phase function also exhibits seasonal differences, particularly at θ>60º.

3.8 Decadal changes in aerosol properties from 2003 to 2013

The measurements of aerosols number density, size distribution, mass concentration and chemical composition started by the beginning of 2003 at this study location. This section presents the results of an analysis of the decadal change in near-surface aerosol number density N, NSD and mass concentration M_L at this location based on the studies carried out during 2003-2005 [*George et al*., 2008] and 2011-2013 (present study) using same type of instruments.

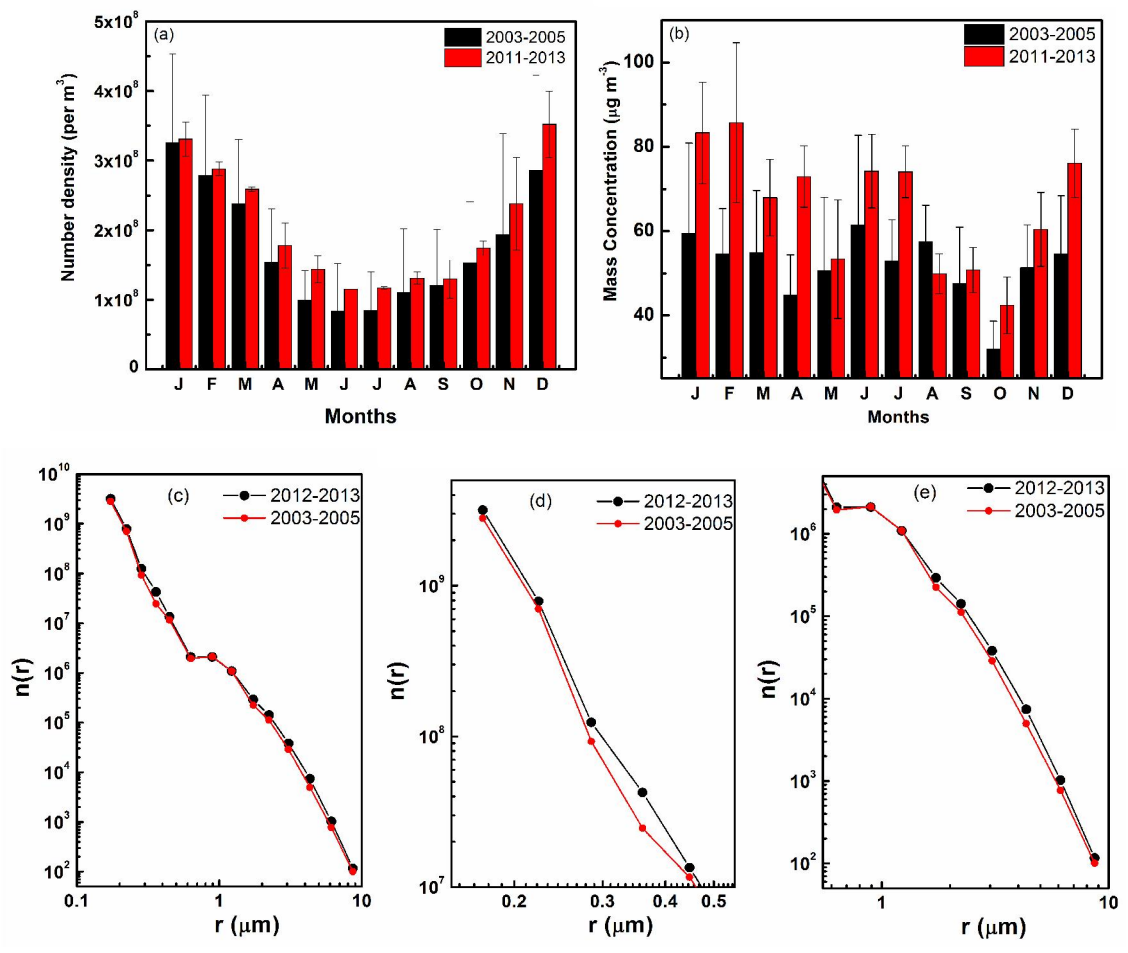

Figure 3.18. *Decadal change in the mean monthly pattern of (a) Number density (b) Mass loading and (c) NSD from 2003-2005 to 2011-2013 (d) NSDs zoomed for small particle regime upto 0.5μm (fine mode) and (e) NSDs zoomed for large particle regime >0.5μm (coarse mode) respectively.*

Figure 3.18a to e shows the mean monthly pattern of N, M_L and NSD respectively for the two periods viz 2003-2005 and 2011-2013 along with the number densities zoomed for the small particle regime (<0.5μm) and large particle regime (>0.5μm). Both N and M_L show increase from 2003 to 2013. The NSD shows an overall shift to higher number density during 2011-2013 in all size ranges. But the increase is more prominent for fine mode (19%) compared to that of coarse mode (5%). The total number density (N) showed an increase of ~9% to 23% monthly basis with the mean decadal increase of 19%. But increase in mass concentration is much higher ranging from 13% to 45% in different months with mean decadal increase being 29%. This can be attributed to increase in large particles which are mostly sea-salt aerosols or transported mineral dust since large particle contributes to more mass. Apart from the over all increase, the decadal changes in aerosol parameters also show seasonal dependence.

Parameter	Pre-monsoon		Monsoon		Winter	
	2003-2005	2012-2013	2003-2005	2012-2013	2003-2005	2012-2013
M_L	50.1±2.8	64.7±5 (29%)	54.9±5.0	62.2±10.1 (13%)	56.2±5.9	81.7±13.7 (45%)
N	1.63E+08	1.94E+08 (19%)	9.98E+07	1.23E+08 (23%)	2.97E+08	3.24E+08 (9%)

Table 3.4. *Decadal change in aerosol number density (N) and mass loading (M_L) from 2003-2005 to 2011-2013 along with the percentage changes.*

Table 3.4 lists the mean decadal changes in M_L and N on seasonal basis. Highest % increase in M_L is seen during winter (45%) followed by pre-monsoon and monsoon (29% and 13% respectively). Percentage increase in N is largest in pre-monsoon followed by monsoon and winter. In this context, it is worth noting that the winter time aerosol loading at the location is dominated by the anthropogenic/continental species from inland and during pre-monsoon and monsoon, sea-salt aerosols or transported mineral dust show dominance. The decadal increase in aerosol number density and total aerosol mass loading has implications on large scale changes in synoptic scale meteorology and source flux which needs further investigations.

3.9 Summary

a) Simultaneous and collocated measurement of total aerosol number density (N), number density size distribution (NSD), mass loading (M_L) and chemical composition was carried out at TVM for the first time. Here it is to be noted that the results related to number density and size distribution is limited to aerodynamic diameter >0.3μm at the lower size and doesn't convey information on smaller particles. The physical properties such as N, SD, M_L showed diurnal changes associated with mesoscale meteorological features like sea-breeze (SB) and land-breeze (LB) and monthly/seasonal changes associated with synoptic scale meteorology and transport. While N is higher during LB regime throughout the year (except in June when it is comparable), M_L during SB exceeded that during LB in monsoon months.

b) The source identification based on Principal Component Analysis showed three prominent sources over the region namely anthropogenic, crustal and marine which varied seasonally. Strong mixing of aerosols from these sources is also observed in different seasons, in particular during winter season.

c) The NSDs are of multi-modal in nature with two prominent modes at radius ≤ 0.175μm and other ~0.7-0.8μm. Presence of other modes both in fine particle and coarse particle regimes are also indicated. While the small particle mode becomes prominent in winter due to advection of inland aerosols loaded with anthropogenic species, the coarse mode gets strengthened in monsoon due to wind-induced sea salt production.

d) Correlation analysis between the mass concentrations of various chemical species and size-resolved number density indicated that the anthropogenic species like NH_4, SO_4 are mostly in fine mode (diameter<1μm) for all the seasons while Na, Cl, Fe and Al in coarse mode (diameter>1μm). Species Ca, NO_3, K and Mg, Fe are present in both the modes showing multiple sources for these species.

e) First-cut chemical models of aerosols were evolved on seasonal basis including components of sea salt (SS), Water-soluble non-sea-salt (WSN), Mineral dust (MD), Particulate Organic Matter (POM) and Black Carbon (BC). SS contributes maximum in monsoon (~40%) minimum in winter (with 6%) with 20% and 25% in pre-monsoon and post-monsoon respectively. WSN contributes 20-22% in pre-monsoon, post-monsoon and winter with minimum in monsoon (13%). MD peaks in pre-monsoon (29%) and showed least for winter (10%) with monsoon and post-monsoon values being 25% and 17% respectively. BC and POM were highest in winter (~5% and 34% respectively). While POM remained more or less same (~23-24%) in all other seasons.

BC attained minimum in monsoon (2%) and remained 3-5% in pre monsoon and post monsoon.

f) Estimates of the aerosol radiative characteristics over TVM based on the measured aerosol properties showed that the scattering coefficient varied from 0.04 to 0.14km^{-1} and absorption coefficient between 0.01 and 0.05km^{-1}. Single scattering albedo was 0.71 for winter and 0.89 for monsoon season indicating the presence of more absorbing aerosols in winter.

g) An approximate estimate of the density of aerosols over the location varied in the range of 1.4 to 2.6g cm^{-3} annually.

h) Over a span of ~10 years from 2004 to 2015, the aerosol number density over TVM showed an increase of 19% and aerosol mass loading increased by 29%.

Chapter 4

Spatial characteristics of aerosol size distribution, chemical composition and radiative properties over Arabian Sea and Bay of Bengal during pre-monsoon

4.1 Introduction

Oceans covering more than 70% of earth's surface constitute the largest source of natural aerosols by mass in the atmosphere [*Prospero et al*., 1983; *Yoon et al*., 2007, *Vignati et al*., 2010, *Crippa et al.,* 2013]. There are several studies suggesting that ocean-derived aerosols play key roles in controlling the Earth's radiation balance, cloud formation, cloud properties, and chemistry of the atmosphere [*Charlson et al*., 1987; *O'Dowd et al*., 1997; *Keene et al*., 1998; *Quinn et al.*, 1998; *Orellana et al*., 2011]. Aerosols in the marine environment consist generally of two types of aerosols (1) aerosols of oceanic origin comprising primarily of sea-salt particles produced by the action of wind over the sea surface and those produced through marine biological activities comprising of organics and sulphates from the oxidation of biogenic Dimethyl sulphide (DMS) [*Fitzgerald*, 1991; *O'Dowd et al*., 1997; *Andreae*, 2007; *O'Dowd and de Leeuw*, 2007] and (2) aerosols transported from the nearby continents. Marine aerosols also have a significant influence on the coastal urban air quality by their ability to interact chemically as well as physically with other aerosol species and gases [*O'Dowd et al*., 2002; *Athanasopoulou et al*., 2008; *Fuzzi et al.,* 2015].

The marine aerosols depict a wide size spectrum with their radii ranging from submicron's to >10μm and represent the optically active aerosols to incoming solar radiation as well as outgoing terrestrial radiation [*Kleefeld et al*., 2002; *Bates et al*., 2006; *Mulcahy et al*., 2008] and thus playing a vital role in radiative forcing and hence climate. Several cruise-based, campaign mode studies have been conducted over the oceanic environments all over the globe to investigate the physical, chemical and radiative properties of aerosols and to understand the long-range transport active over these regions [*Arimoto et al*., 1996; *Russel et al*., 1999; *Johansen et al*., 2000; *Raes et al*., 2000; *Verver et al*., 2001; *Ramanathan et al*., 2001; *Huebert et al*., 2003; *Bates et al*., 2004; *Sakerin et al*., 2015). In spite of all these efforts, quantitative information is limited over the marine environments, particularly over AS, IO and BoB.

The landmass surrounding the Arabian Sea (AS) and Bay of Bengal (BoB) comprise of highly industrialized, thickly populated and arid, semi-arid regions which are rich sources for natural and continental/anthropogenic aerosols such as mineral dust, sulphates, nitrates, trace metals, black carbon and organics. The knowledge of the size distribution and chemical composition of these highly heterogeneous aerosols is essential to estimate their radiative characteristics like the scattering and absorption properties. The Integrated Campaign for Aerosols, gases and Radiation Budget (ICARB), a multi-platform and a multi-institutional campaign, was conducted with the aim to capture the regional and temporal variability of aerosol sources and sinks, their natural and anthropogenic hot spots over the marine environments of AS and BoB and the Indian landmass and to assess the regional scale radiative forcing [*Moorthy et al*., 2008]. Few papers have been published with details and results from the cruise-based measurements of physical, chemical, and radiative characteristics of aerosols made during this campaign [*Nair et al*., 2008, 2014; *George et al.,* 2008; *Kedia et al*., 2010].

In this chapter, the results of a detailed analysis of the aerosol number density-size distribution along with the simultaneously measured mass loading and chemical composition over the marine environment of AS and BoB are presented, which are not addressed in the earlier studies. In addition, the dependence of mass concentration of various aerosol species on the size resolved number density and the wind dependence of aerosols were investigated. The radiative/optical parameters of aerosols namely scattering coefficient (β_{sc}), absorption coefficient (β_{ab}), extinction coefficient (β_{ex}), single scattering albedo SSA (ω) and the phase function P(θ) were also estimated for AS and BoB based on the realistic measurements of mass concentration of different chemical components in aerosols and using the OPAC model (explained in Chapter 2 and 3).

4.2 Cruise track

The results presented in this chapter pertain to the ICARB conducted during the pre-monsoon months of March-May 2006 over the oceanic environment of BoB and AS. Measurements were carried out on-board the Oceanic Research Vessel (ORV) Sagar Kanya (cruise no: SK233). The cruise had mainly two legs; SK223A covering the BoB from 17 March 2006 to 13 April 2006, and SK223B covering the Arabian Sea from 18 April 2006 to 10 May 2006. Figure 4.1 shows the cruise track during the two legs with the arrows showing the direction of movement of the ship and the solid circles representing the mean position of the ship when aerosol sample was collected

with the numbers denoting the date of sampling. The ship took several latitudinal and longitudinal transits over the entire oceanic region covering a track of >25,000km length in 56 days.

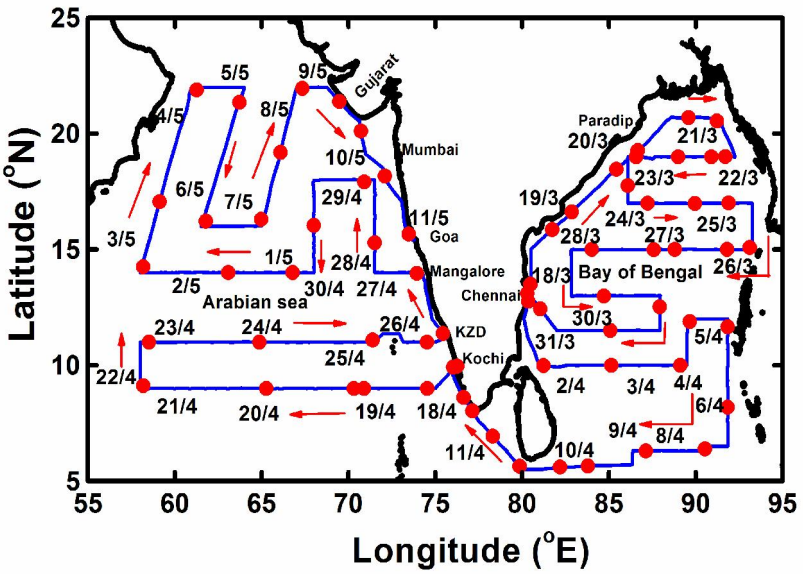

Figure 4.1. *Cruise track of ORV Sagar Kanya over BoB (cruise No: SK 223A) and AS (SK 223B) during ICARB with the arrows denoting the direction of movement of the ship. The red solid circles represent the mean position of the ship when aerosol sampling was done with the corresponding date written near to each sampling location.*

SK233A started on 17 March 2006 from Chennai (13°N, 80.3°E) and moved northward parallel to the coast reaching 20.7°N by 20 March 2006. After this, the ship took several latitudinal tracks (along 20.7°N, 19°N, 17°N, 15°N, 13°N, 11.5°N and 6°N) and longitudinal tracks (along 82.8°E, 86°E, 88°E and 93.2°E) covering the entire BoB from 6˚N to 21°N and 80°E to 93°E ending the journey on 13 April 2006 at Kochi. The second leg (SK223B) of the campaign started off from Kochi (marked as A) on 18 April 2006. The ship moved west along 9°N latitude reaching 58°E longitude and then turned to north, making several latitudinal and longitudinal scans subsequently as shown in Figure 4.1. The latitudinal transits were along 9°N, 11°N, 14°N, 16°N, 18°N, and 22°N. The ship also sailed parallel to the Indian coast near Kozhikode (KZD), Mangalore, Gujarat, etc and close to the Arabian coast (150-200 km off the coast). The cruise ended at Goa (15.4°N, 73.8°E) on 11 May 2006. Aerosol sampling was carried out over the entire oceanic environments, including the coastal regions adjacent to major urban centres such as Chennai, Bhubaneswar, Kolkata, Thiruvananthapuram, Goa, Mangalore, Kochi, Mumbai, etc. and the dust laden areas close to the arid Arab regions.

4.3 Meteorology

The meteorological conditions of the region play a major role in dispersing aerosols and modifying their physical and chemical properties. The prevailing meteorology during the ICARB was predominantly of calm synoptic conditions with weak winds and clear skies. The mean synoptic wind patterns over AS and BoB at 925hPa (derived from the NCEP reanalysis2 data) during the cruise period is shown in Figure 4.2a and b respectively. Over north-BoB the winds were weak and coming from northwest, that is, from Indo Gangetic Plains (IGP) while over the south-BoB it is southerly or south-westerly. A weak anti-cyclonic flow is seen between 8°N to 15°N latitude and 85°E to 90°E longitude.

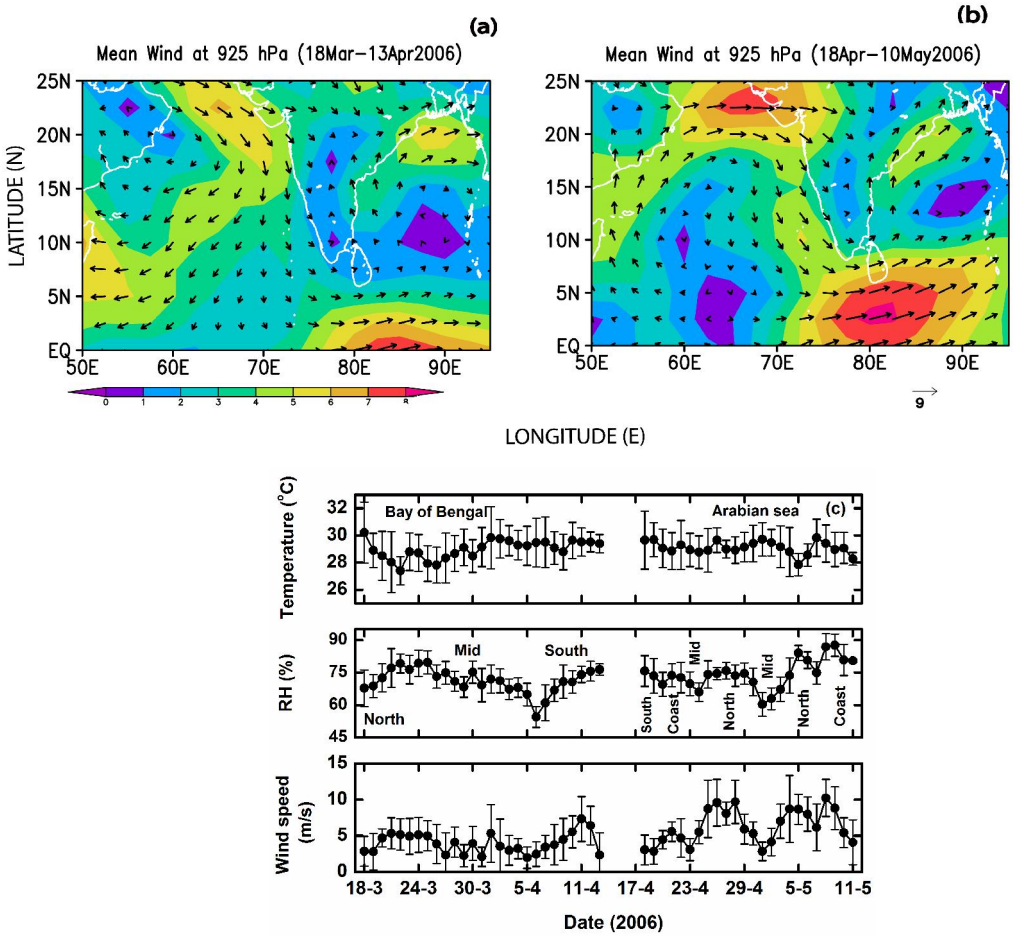

Figure 4.2. *(a) Mean airflow pattern over BoB and (b) Mean airflow pattern over AS during cruise period and (c) Day to day variation of Temperature, RH and Wind speed recorded on board the ship during the cruise.*

Wind pattern over the AS showed strong northerlies/north westerlies over south-eastern AS with increasing speed towards the Indian Ocean (IO) and low winds over the south-western AS. Over northern AS (above 20°N) high north westerly winds were observed blowing from Arab regions towards Indian peninsula. During the second half of April when the ship was traversing AS, a strong anti-cyclone existed at 13°N;

60°E (Figure 4.2b) which made the strong westerlies in the north to turn sharply to northerlies close to the peninsula. For the continuous measurements of meteorological parameters, two Automatic Weather Stations (AWS) were installed on the port side and starboard side of the ship deck at 10m level. Hourly values of the apparent Wind Speed (WS), Wind Direction (WD), Relative Humidity (RH) and Temperature (T) have been measured using these instruments. All the measurements were synchronized with the time information available through a GPS receiver on-board the ship, which recorded the latitude, longitude, time, ship course and ship speed at every 1 second. The apparent wind speed and direction was corrected for the ship's motion to deduce the true wind speed and direction, following the method discussed by *Smith et al*., [1999]. Figure 4.2c shows the daily mean temperature, RH and the true wind speed measured on-board the ship during the entire cruise (while travelling over AS and BoB). The regions travelled by the ship during these days are also marked in the figure. The mean temperature varied in the range 27°C-30°C for both BoB and AS while the RH varied in the range 55%-80% over the BoB and 60% to 88% over the AS. High RH values were observed in the northern part of AS. The mean wind speed showed variation from 2 to 12ms^{-1}.

4.4 Instrumentation and Database

During the campaign, the aerosol measurements were made from a customized laboratory on the top deck of the ship. The number density-size distribution (NSD), mass loading (M_L) and chemical composition of aerosols measured on-board the ship form the main database for this study. The NSD measurements were carried out using the Aerosol Spectrometer (model Grimm 1.107 Aerosol Tech, Germany) by drawing air into the instrument through a sampling inlet projecting over the ocean at 10m above the sea level. Continuous measurement of total aerosol number density (representing aerosols of aerodynamic diameter>0.3μm) as well as size resolved number density at 15 size channels have been carried out using the Aerosol spectrometer at the time interval of 5min, along the cruise track over the AS and BoB. The technical details and operation procedures are discussed in Chapter 2. Aerosol samples were also collected by operating the High Volume Sampler (model GH2000 of Graseby Anderson, USA) installed at the front deck of the ship when it was in motion. Extreme care was taken to avoid the effect of any exhaust from the chimney of the ship by constantly monitoring the wind direction. The sampler was calibrated for flow rate before, during and after cruise using the calibration equipment provided along with the sampler. The aerosol sampling and mass loading measurements were carried out enroute. About 38 samples

were collected from the BoB region and 32 samples from the AS. Duration of aerosol sampling using HVS varied from 3-5hr and during this period the ship covered a distance of 50 to 80km. The date of sampling is also marked in Figure 4.1 close to the circles which represent the mean position of aerosol sampling. The aerosol mass loading (μg m^{-3}) was estimated by gravimetric analysis as discussed earlier in Chapter 2. The collected samples were subjected to chemical analysis following the procedures and techniques described in Chapter 2 and 3. The major ions and metallic species quantified include Cl^-, SO_4^{2-}, NO_3^-, Na^+, Mg^+, Ca^{2+}, K^+, NH_4^+, Fe, Al, Pb, Cr, Co, Ni and Mn. The meteorological parameters Temperature, RH, WS, WD recorded on-board the ship by the AWS and shown in Figure 4.3 are also utilized in this study.

4.5 Aerosol characteristics over the marine environment

The observational results of the study on the aerosol number density (N), size characteristics, number density-size distribution (NSD), mass loading and chemical composition of aerosols over the two marine environments namely AS and BoB are presented in Part I and II respectively.

4.5.1 Part I. Arabian Sea

4.5.1.1 Aerosol number density and mass loading over Arabian Sea

Figure 4.3a shows the spatial distribution of total aerosol number density (N) in m^{-3}, measured along the cruise track over AS. The colour bar shown on right hand side shows the magnitude of N. N showed a distinct spatial pattern over the AS with values ranging from ~1.7E+07m^{-3} to ~4.0E+08m^{-3}. The southern AS (<10ºN latitude) showed high number density around 62ºE -75ºE longitude where the values remained greater than 8E+07m^{-3}. Several hotspots were observed as the ship moved along the coastal regions of Gujarat (GUJ), Mumbai (MUM), Goa, Mangalore (MGL), Kozhikode (KZD), and Kochi (KOC) being about 1E+08m^{-3}, 1.1E+08m^{-3}, 2.03E+08m^{-3}, 1.7E+08m^{-3}, 9.6E+07m^{-3} and 4E+08m^{-3} respectively. This increased aerosol loading close to coastal regions suggests the influence of polluted air being transported from anthropogenically active continental sites to the marine environment. Except for the high number density over southern AS and north east AS, it remained low throughout this marine environment. The mid AS showed minimum number density (mean value ~1.7E+07m^{-3}). This region of low corresponds to that of the anti-cyclonic flow seen in Figure 4.2b.

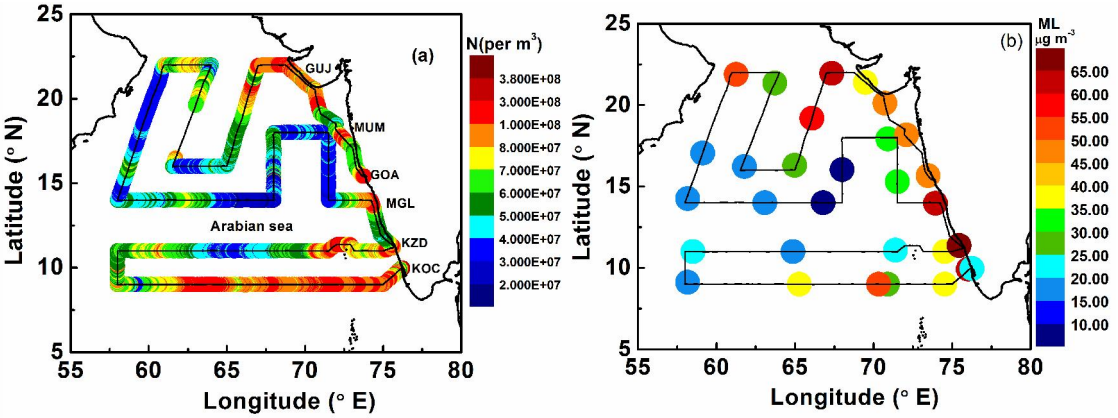

Figure 4.3. *Spatial variation of (a) total aerosol number density (N) and (b) mass loading (M_L) along the track over the marine environment of AS.*

Along with aerosol number density, the total mass loading of aerosols (M_L) is crucial in the assessment of radiative and environmental impacts of aerosols. Figure 4.3b shows the variation of M_L along the cruise track, with colour bar showing the magnitude. M_L varied from 5 to 66μg m^{-3} over AS with high loading close to the Indian coastal regions and also southern AS, as in the case of N. M_L and N showed more or less similar spatial features over this marine environment. The measurements done at various coastal sites like Mangalore (MGL) [*Moorthy et al.,* 2005], Mumbai (MUM) [*Venkataraman et al*., 2002], etc have also revealed high levels of aerosol pollution. An average mass loading of 187μg m^{-3} was observed over MUM by *Venkataraman et al*., [2002], the sources being vehicular emissions, power plants, industrial oil burning and refuse burning [*Larssen et al*.,1997]. Mass loading of 56±20μg m^{-3} was reported over the coastal site of TVM [*George et al*., 2008]. The steady expansion of Rann of Kutch leads to desertification of more areas in Gujarat (GUJ) which in turn produce more dust aerosols which can intrude into AS. The hotspots close to coastal areas of GUJ could be partly due to the transport of these aerosols over to AS.

The aerosol number density measured over the AS region is comparable to those measured at other oceanic regions over the globe. The typical number density observed over Pacific as described by *Hoppel and Frick* [1990] were 1.5 to 3E8m^{-3} and by *Tomilson et al*., [2007] is ~3.9E8m^{-3} for south-eastern Pacific. During the Aerosols99 experiment over the Atlantic Ocean, total number concentration ranging between 1.9E08 to 5.8E08m^{-3} was measured with varying air mass types [*Bates et al*., 2001]. Higher aerosol number concentrations were observed over the Mediterranean Sea (5.3E09m^{-3}) [*Eleftheriadis et al*., 2006] and south-eastern Baltic Sea (1.5 to 4.5E08m^{-3}) [*Steigvile et al*., 2013]. All these studies suggest that the marine environments are getting polluted by the nearby continental areas.

4.5.1.2 Air mass type over AS: Back trajectory analysis

The sources of aerosols influencing the marine environment of AS are examined by analysing the 7-day air mass back trajectories reaching the cruise track and 100m above sea level at 0600UT and 1800UT, retrieved by running HYSPLIT model [*Draxler et al*., 2003] (www.arl.noaa.gov/ready/HYSPLIT.php).

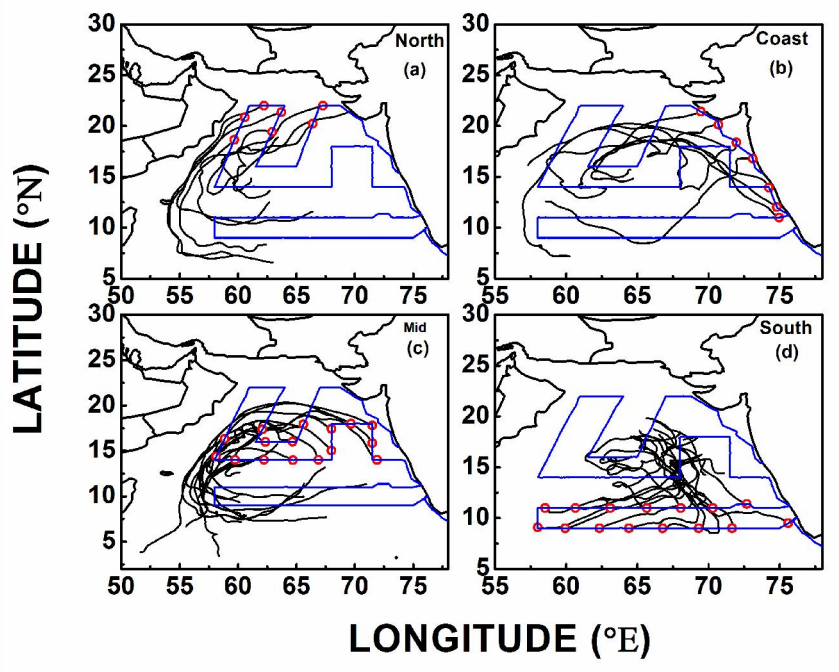

Figure 4.4. *The 7-day air mass back trajectories (obtained by running HYSPLIT model) arriving at the sampling locations for the four regions namely (a) north-AS, (b) coast, (c) mid-AS, and (d) south-AS.*

The back trajectories reaching the four regions namely north (18°-22° N ; 60° to 70° E), mid (18°-14°N; 58°-68°E), south (<14°N; 58°- 72°E) and coastal side of India (where aerosol characteristics showed variations) during sampling time are shown in (Figure 4.4). It can be seen that all these back trajectories originate and traverse the oceanic environment only. Trajectories reaching the north of AS start from the southern AS, travel close to the Arabian coast and reach north AS. Those reaching the south AS and the coastal region originate from the north or mid AS. This reveals that basically the marine air mass prevails over AS during the cruise period, but it passes close to coastal regions also. However, the aerosol physical properties as described in the earlier sections and the chemical composition discussed in section 4.5.1.5 suggests the presence of significant amount of continental aerosols over AS. This can be due to the intrusion of anthropogenic/continental aerosols into the sea due to local or mesoscale circulations and there by getting dispersed through the coastal belt and later mixed up

with the entire marine environment [*Leon et al*., 2001; *Verma et al*., 2006; *Zhu et al*., 2011]. This type of mixing can occur when mesoscale circulations like land breeze move dust and other continental aerosols off-shore and over to sea, and from where it is carried to remote oceanic regions. *Tindale and Pease* [1999] observed that local, regional-scale land-sea breeze active over the coast of Oman play role in moving dust offshore. Studies conducted during INDOEX also revealed penetration of continental air mass deep into the oceanic environment of BoB [*Lelieveld et al*., 2001]. Another study over AS showed the existence of SB/LB effects from 80-130km off-shore [*Subramanyam et al*., 2001]. In this context, the high loading of anthropogenic species over the Indian coastal regions can also be attributed to the influence of mesoscale circulation, in the absence of any synoptic scale circulation, favouring transport of aerosols to AS. However, upper level long range transport from arid Arabian landmass has been reported during pre-monsoon and monsoon seasons [*Aloysius et al*., 2008].

4.5.1.3 Number density size distribution over AS

For the first time, the size-resolved number density measurements were carried out over the entire AS region during this cruise. Based on the aerosol number density measurements at the 15 channels, the aerosol NSD was retrieved for each set of measurements as discussed in Chapter 3. The mean size distributions for the four different regions of AS north, mid, south and coast were estimated by averaging all the NSDs of the respective regions and presented in Figure 4.5a. The patterns of the size distributions are more or less similar in shape throughout AS. All the size distributions depict a multimodal structure, with two prominent modes/peaks one ≤0.175µm and the other ~0.9µm. Other less pronounced modes centred on 0.3µm and 3µm are also seen in the NSD in Figure 4.5.

In Figure 4.5b and c are illustrated the NSDs split and zoomed for $r \leq 0.5\mu m$ and $r > 0.5\mu m$ (fine particles and coarse particles respectively). The small particle concentration showed regional differences being highest over south AS followed by coastal and north AS. There is a drastic reduction in aerosol number density of both fine and coarse particles over mid-AS, where the anti-cyclonic flow existed. Also mid AS being far away from all the landmasses, is less affected by the direct influence of the surrounding continent. The coarse particle concentration (Figure 4.5c) shows minor differences over regions except mid AS where it also reaches minimum.

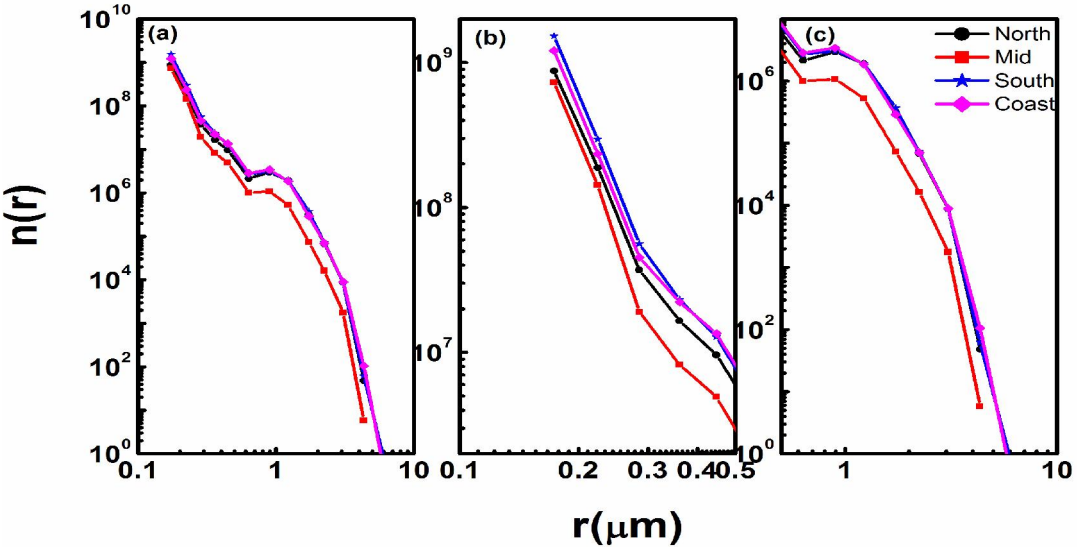

Figure 4.5. *(a) Number Size Distribution (NSD) of aerosols over the marine environment of Arabian Sea (b) the zoomed NSD for fine mode and (c) the zoomed NSD for coarse mode regimes.*

The aerosol NSD's reported for the marine boundary layer of various oceans are mostly bimodal in nature [*Hoppel et al*., 1986, 1990; *Clarke and Porter*, 1993; *Quinn et al*., 1995; *Heintzenberg et al*., 2000]. However, the presence of less prominent modes is also reported. Measurements over the Atlantic Ocean by *Williams et al*., [2007] for size ranges between 0.03μm and 25μm had shown a similar type of multi-modal distribution with 4 modes; first one in sub-micrometer range <0.15μm radius. The two other modes were observed between 0.1 and 1μm (fine mode) and the fourth mode in super micron range or coarse mode (>1μm). The presence of a mode at ≤0.17μm [*Williams et al*., 2007; *Fitzgerald,* 1991; *O'Dowd,* 1997] and another in the super micrometre range with mode diameter ranging from 1μm to 7μm also has been observed [*Exton,* 1985; *O'Dowd,* 1997].

4.5.1.4 Spatial pattern of fine and coarse particles

In order to have a broad understanding of the aerosol sources over AS, the spatial distribution of fine and coarse mode aerosols (PM1 and PM>1 respectively) were examined by segregating the measured number density at the 15 channels into these two modes (Figure 4.6a and b).

It is clearly seen that both the modes show distinct spatial features, but with similarities also. The fine mode number density varies in the range 1.6E+07 to ~3.8E+08m^{-3} with minimum observed over the mid AS and the western AS close to the Arabian coastal regions. The southern part of AS and the coastal regions of Indian subcontinent showed relatively high values with hot spots close to urban areas. The

coarse mode aerosol number density also showed least values over the mid AS where the values reached as low as 1.9E+05m^{-3}. But, it reaches values as high as 9.8E+06m^{-3} towards south and north AS and close to Gujarat coast. In general, the coarse mode is prominent over north AS and fine mode over south-AS. But, significant amount of coarse particles are present over south AS also.

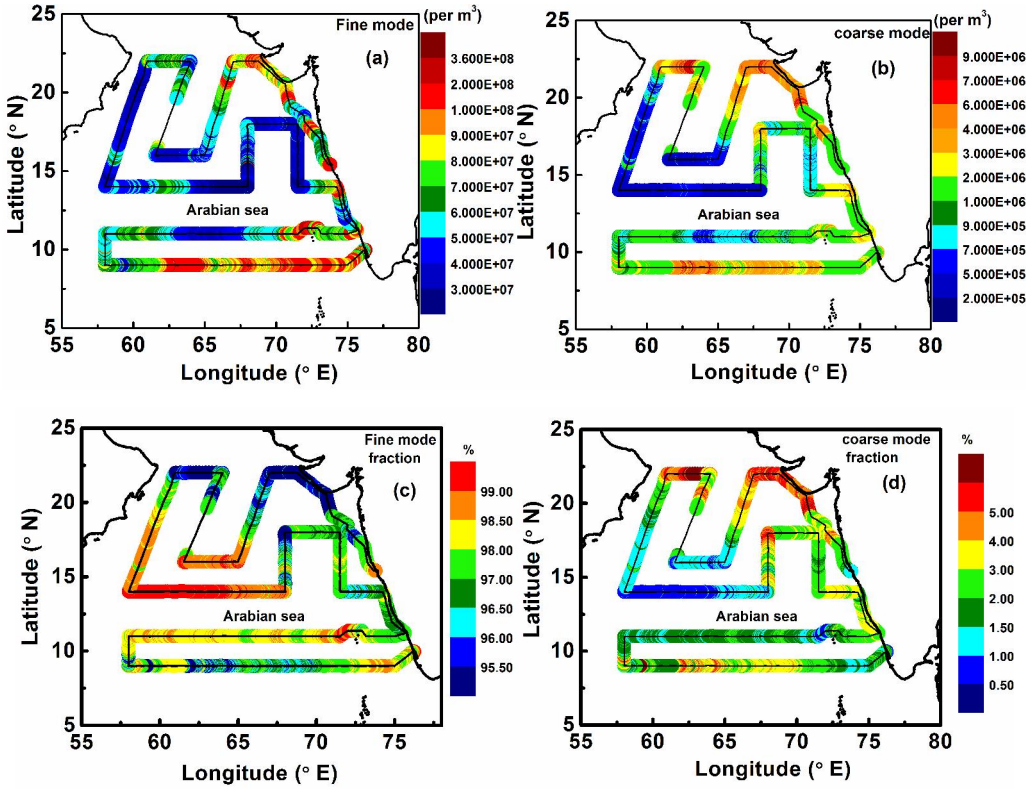

Figure 4.6. *Spatial pattern of (a) fine mode number density of aerosols over AS (b) coarse mode number density of aerosols over AS (c) fine mode fraction in % over AS and (d) coarse mode fraction in % over AS.*

In addition to total number density, the fractional loading of the fine and coarse particles, defined as the ratio of number density of the respective mode to total number density (expressed in %), over the region is also important in assessing the strength of aerosol sources and radiative properties. In Figure 4.6c and d are shown the spatial patterns of the percentage contribution of fine mode and coarse mode particles. The fine mode contributes >95% of the total number density and depicts a pattern opposite in nature to that of the corresponding number density, with maximum over mid AS and minimum over north and north-east AS. This indicated that the mid AS region is loaded with more fine particles even though total number density is minimum. Perhaps, the existing anti-cyclonic circulation removes the larger particles away (which are less in number). Or, some biological activity (like phytoplankton boom) over the region

inducts more fine particles into the marine atmosphere. The south AS where the fine mode number density peaked, the fraction is less. The spatial variation of coarse mode fraction is different from that of fine mode. Both number density and fractional loading of coarse mode particles are similar (Figure 4.6b and d). It can also be seen that over north and south AS coarse mode contribution is high reaching up to 5% compared to mid AS (where it is only 1%).

Aerosols in marine environment mostly consist of the in-situ generated sea-salt aerosols, those generated through biogenic activities and the transported component from the near-by continents. The transported component comprises of fine mode aerosols as well as the large sized/coarse particles like soil/mineral dust from the arid/semi-arid regions surrounding the oceans. Aerosols of biogenic origin primarily comprise of sulphates and organics and are mostly in fine mode. Studies also suggest that the fraction of the wind generated sea-salt aerosols contributes significantly to the sub-micrometer size range [*O'Dowd and Smith*, 1993; *O'Dowd et al*., 1997]. The dominance of coarse mode particles over north AS and close to coast of Gujarat is attributed to (a) sea-salt particles produced by strong winds (speed> $7ms^{-1}$ as seen from Figure 4.2 and (b) dust transport from Kutch region and long-range transport from Arab regions along the coastal belt. Chemical characterization and the fractional contribution of different species can throw more light into the main sources of these particles which is discussed in section 4.5.1.5.

4.5.1.5 Chemical composition of aerosols over AS: mass concentration and mass fractions

The analysis of the aerosol samples (as discussed in Chapter 2) from the marine environment has yielded the mass concentrations of various chemical species mentioned in Section 4.4. The estimated mass concentrations are plotted in Figure 4.7 along the cruise track. The X-axis shows the date of sampling. The oceanic region of sampling also is marked in the figure (top panel). Different aerosol species show varying spatial distributions.

Oceanic species like Cl, Na and Mg shows similar pattern with a prominent high over north and towards coast and low values over the south western AS, indicating their common source (sea salt origin). Similarly, the major anthropogenic species SO_4^{2-}, NH_4^+ and NO_3^- show more or less similar pattern. These species are abundant over the south AS and close to the Indian coast and are relatively low over the northern/mid AS.

The mass concentration of crustal components Al, Fe and Ca showed features similar to that of the anthropogenic species, indicating that they are also continental origin.

Spatial variability in aerosol chemical species and thereby their sources can be parameterized more precisely in terms of their mass fractions (m_f) which is estimated as m_x/M_L where m_x denote the mass concentration of the species X and M_L is the total aerosol loading corresponding to each sample. The mass fractions of different chemical species have implications in the radiative forcing due to aerosols [*Satheesh et al*., 2006; *Kedia et al*., 2010].

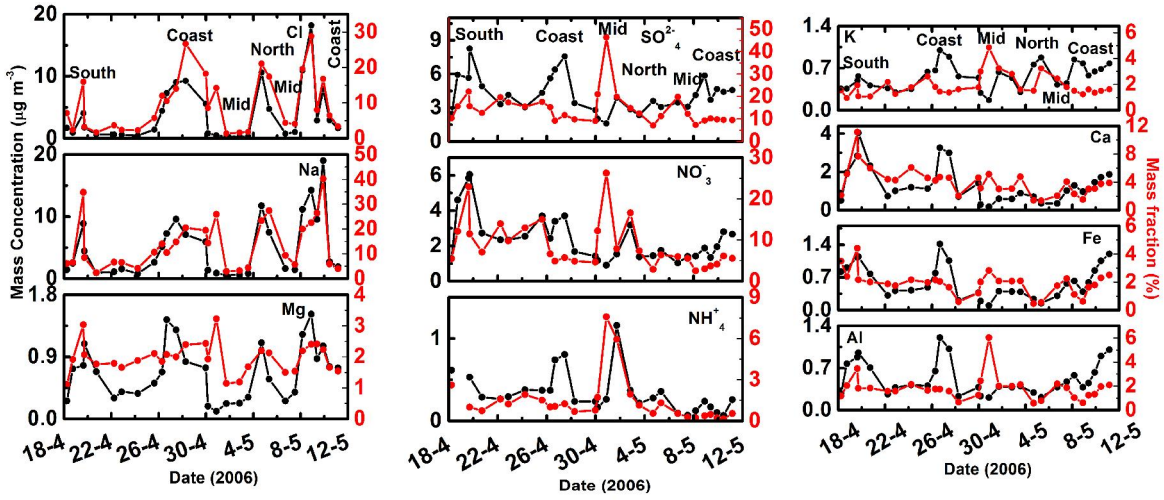

Figure 4.7. *Variation of aerosol mass concentration (m_x) of various chemical species along the cruise track over AS in black colour along with their mass fraction (m_f) in red colour. The oceanic regions, where these measurements were done are marked on the top panel.*

Along with the mass concentration, Figure 4.7 also shows the variation of m_f for each of the species. It is to be noted that the spatial patterns of m_f of marine species like Cl^-, Na^+ and Mg^+ have one-to-one correspondence with respective m_x over the entire region. The anthropogenic species like SO_4^{2-} and NH_4^+ along with soil components Al, Fe and Ca exhibits high mass fractions over mid AS. This is probably because the total mass loading over these regions were low and the continental species contribute significantly to the total loading. Here, it is worth noting that the fine mode fraction of number density also showed high over mid AS. The concentrations of oceanic species were very low over mid AS were the wind speed was $<3 ms^{-1}$ (Figure 4.2). But over other regions, m_x and m_f showed more or less similar variation.

4.5.1.6 Correlation of chemical species with fine and coarse number density over AS

As discussed in Chapter 3, knowledge on the size-resolved chemical composition is desirable for the estimation of radiative parameters of aerosols. Since size-resolved chemical composition is not available in this study, a correlation analysis has been carried out to make indirect inferences on this aspect as done for the coastal site TVM in Chapter 3. The results of this analysis is given in Figure 4.8 as the scatter plots between the fine mode or coarse mode number density and mass concentration of different chemical species. The regression fitted line and the respective correlation coefficients are also shown in figure. Correlation coefficient >0.50 is significant with p-value >0.0001 and those >0.40 is significant to the level of p=0.007. The regression fitted lines with correlation coeffficient <0.40 are not shown in the scatter plots.

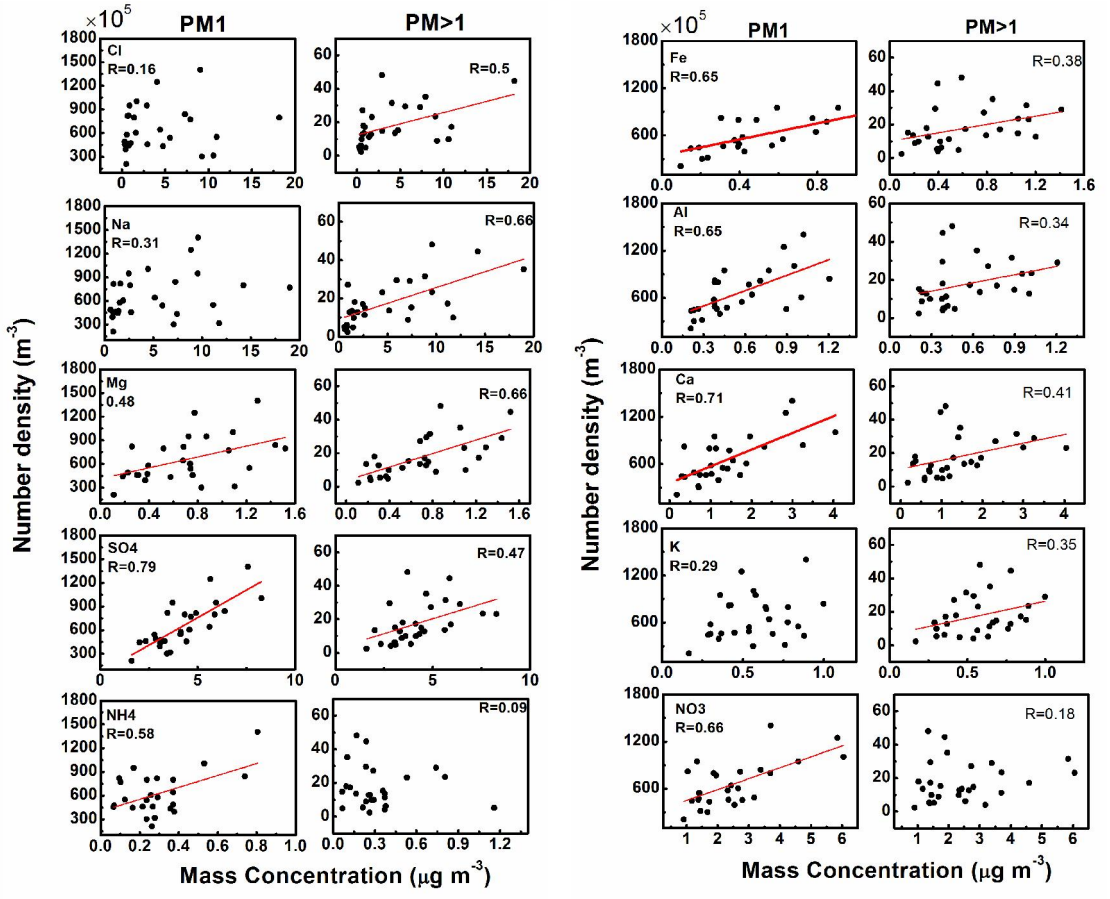

Figure 4.8. *Scatter plots between the fine mode or coarse mode number density and mass concentration of different chemical species over AS along with the regression fitted line and correlation coefficients (R).*

From Figure 4.8 it is clear that the mass concentration of species like SO_4^{2-}, NH_4^+ and NO_3^- are positively correlated with the fine mode number density. These are mostly of anthropogenic origin and formed through the gas-to-particle conversion

mechanism (or secondary aerosols). It was also observed that, on an average ~80% of SO_4^{2-} over this region is of non-sea-salt origin and the remaining 20% is from sea salt [*George and Nair*, 2008]. In this analysis, SO_4^{2-} shows relatively good correlation of 0.47 in coarse mode too, indicating their source as sea-salt or mineral dust [*Zhang et al*., 1999]. On the other hand, oceanic species Na^+, Cl^- and Mg^+ showed positive correlation (>0.5) with coarse mode number density supporting the view that they are produced from wind induced seaspray and are large particles. Mg which has both sea-salt and mineral dust origin showed a significant correlation with fine mode (0.48) also. In general, species like Al, Fe and Ca which have crustal/soil origin are mostly in coarse mode [*Kulshrestha et al.*, 1998; *Heintzenberg*, 2009]. But the present analysis showed strong positive correlation of these species with fine mode number density (coefficient ~0.65 to 0.71) with reasonable correlation with that of coarse mode (coefficient ~0.34 to 0.41).

This observation supports the view that the long-range transported mineral dust (crustal species) occurs in fine particle mode also [*Koulouri et al*., 2008, *Stone et al*., 2011]. Potassium (K) have both sea-salt and non-sea-salt contribution (mainly from biomass burning) is not well correlated with either fine or coarse mode, indicating mixed sources. The dominence of fine mode fraction over AS can be partly attributed to the presence of species like Fe, Al etc in fine mode. At the coastal site TVM also there are evidences that these crustal species occur in the fine mode, as presented in Chapter3.

4.5.1.7 Wind dependence of aerosol concentration over Arabian Sea

In the study region, the wind speed measured using the AWS on-board the ship ranged from 2 to 14ms^{-1}. Making use of the size-resolved number density and the surface wind speed, the dependence of number density of aerosols in different size ranges on wind speed was carried out. The number density measurements were segregated into five size bins viz. PM1, PM1-3, PM3-5 and PM5. These number density values in each size bin were further grouped in terms of the wind speed and averaged for wind speed bins of 1ms^{-1}. The scatter plots in Figure 4.9a to c show the variation of aerosol number density with wind speed for different size bins. PM1 particles did not show any notable dependence on wind speed and hence not shown here. In all other size ranges, aerosol number density (N_s) showed an exponential increase with wind speed (U) of the form $N_s=N_0e^{bU}$ where U is the wind speed and N_0 is the background number density.

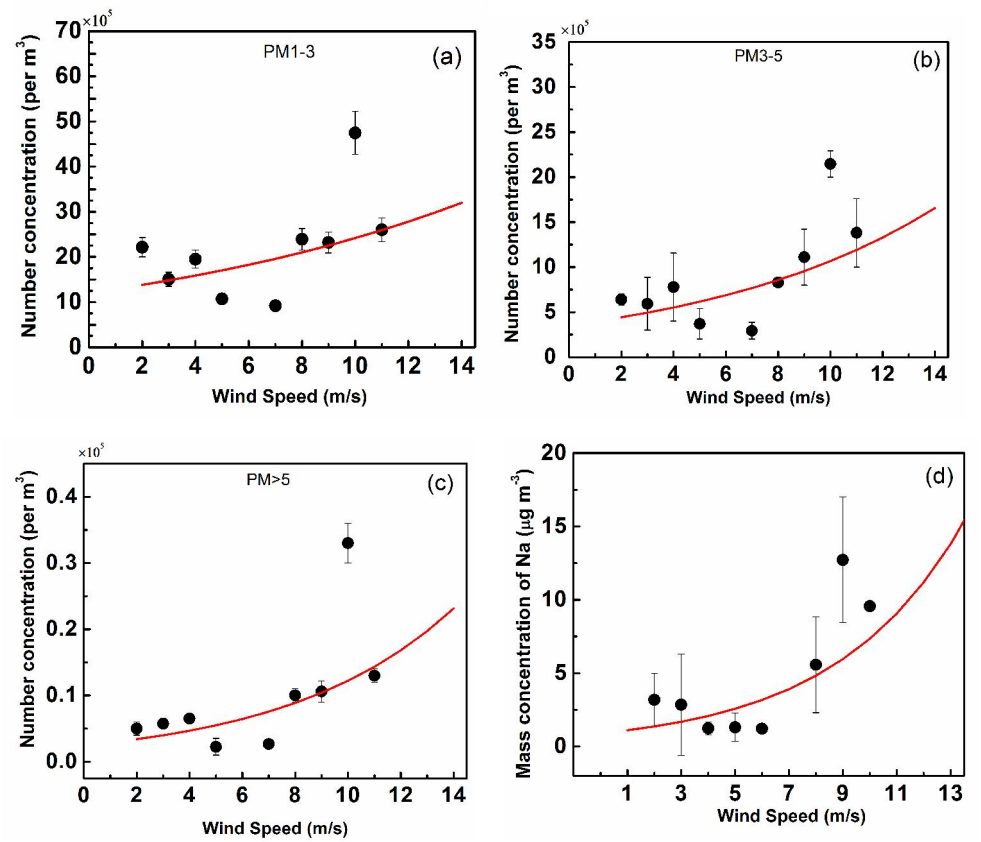

Figure 4.9. *Variation of aerosol number density with wind speed for each size range (a-c) and (d) variation of mass concentration of Na with wind speed, along with the exponential fit.*

The exponential fit is also shown in Figure 4.9. Since Na is the tracer for sea-salt aerosols, the wind dependence of mass concentration of Na, denoted as M_{Na} was also examined as in the case of number density and presented in Figure 4.9d which also follows an exponential relation of the form $M_{Na}=M_o e^{b0U}$ with U. The positive correlation of Na with U is attributed to the wind induced production of Na over the marine boundary layer.

Size range	b or b_0	N_0 (m^{-3}) or M_0 (μg m^{-3})	Correlation coefficient (R)
PM1-3	0.07	1.2E6	0.47
PM3-5	0.11	3.5E5	0.60
PM>5	0.16	2.5E3	0.63
Na	0.16	1.2 (M_0)	0.66

Table 4.1. *Wind dependence of aerosol number density in different size ranges (of the form $N=N_0e^{bU}$) and Mass concentration of Na (of the form $M_{Na}=M_oe^{b0U}$) given by the fitted parameters b, N_0 (M_0 for Na) along with the correlation coefficient (R).*

The fitted parameters, correlation coefficient, N_0 or M_0 and b or b_0 are listed in Table 4.1 for each of the above cases. An increase in b is observed with increase in size revealing that the number density of large sized particles increase faster with wind speed in this marine environment. The correlation coefficient also increased with increasing size range (Table 4.1). From this analysis it is inferred that the sea-salt particles produced during this period is mostly of sizes >1μm.

In the past several decades a number of efforts have been made to understand the relation between ocean surface wind and marine aerosol characteristics like number density, mass concentration and aerosol optical depth. Diverse relationships such as linear [*Huang et al.,* 2009, *Lehahn et al.,* 2010], exponential [*Moorthy et al*., 1997; *Moorthy and Satheesh*, 2000] and power law [*Mulcahy et al*., 2008; *Glantz et al*., 2009; *O'Dowd et al*., 2010] have been put forth. Most of these studies report the wind speed dependence of number density or mass concentration of aerosols typically adhering to an exponential relation discussed above or a power law of the form $M_{ss} = mU^b$. A typical b value of ~0.16 was reported over Pacific Ocean [*Woodcock*, 1953] and Atlantic Ocean [*Lovett*, 1978] where the wind speeds ranged from 0 to 35m s^{-1} as compared to the present study which is 0 to 14ms^{-1}. Measurements by *Quinn et al*. [2000] over the Pacific and South Sea showed a similar wind dependence with sea salt concentration with b value of 0.12. *Nair et al*. [2005] reported a power law dependence over the Indian Ocean during INDOEX campaign. An exponential increase of satellite retrieved aerosol optical depth (AOD) with wind speed is reported by *Kedia and Ramachandran*, [2008] over AS, with b value of 0.03. *Moorthy and Satheesh,* [2000] brought out an exponential dependence of AOD on wind speed with b value ranging from 0.05-0.11 for the spectral range 0.38 to 1.025μm over Minicoy Island, Arabian Sea.

4.5.2 Part II. Bay of Bengal

The BoB is well known for its peculiar geographic setting, being surrounded by densely populated land mass with diverse geographical features on three sides (north, west and east) and as a region of frequently active weather systems like cyclones [*Das*, 1986; *Kedia et al*., 2012]. It lies between the longitude sector of 80˚E and 100˚E and latitude sector of 5˚N to 22˚N sharing coast line of ~2000km with India. The outflow of pollutants from the densely populated and industrialized Indo-Gangetic Plains (IGP), aided by the prevailing westerly winds through the natural channel created by the orography of the Himalayas in the north and the Vindhya-Satpura ranges to the south,

results in significant loading of natural and anthropogenic aerosols in the northern BoB [*Girolamo et al*., 2004; *Nair et al.,* 2007; *Niranjan et al.,* 2007; *Nair et al.,* 2009). Significant outflow from the East Asian regions over to BoB is also observed favouring pollution of this oceanic environment [*Girach et al*., 2010; *Lawrence and Lelieveld*, 2010]. The regional radiative forcing due to aerosols over the BoB plays role in altering Asian monsoons and the precipitation pattern over India even though the exact effects are still being debated [*Konwar et al*., 2012; *Verma et al*., 2011; *Das et al*., 2014]. Thus quantifying the aerosol properties over this oceanic region is important in environmental as well as climatic viewpoint.

The entire analysis done for AS (section 4.5.1) was repeated for BoB and the observational results presented below. Due to technical issues with the instrument, number density measurements could not be done over a part of north BoB and mid BoB. However, mass loading and chemical composition data are available for the entire BoB region.

4.5.2.1 Spatial variation of total aerosol number density and mass loading over BoB

The spatial variation of N over BoB shown in Figure 4.10a reveals that the marine environment of BoB is more polluted than AS in terms of aerosol loading. Also, the spatial heterogeneity in aerosol number density is less over BoB and in general, N is higher compared to the AS. Aerosol number density ranged from ~3E+07 to 4E+08m^{-3} with maximum (2.9E+08±1.2E+08m^{-3}) over north BoB and minimum (~3.9E+07m^{-3}) towards the Southeast BoB. Relatively high aerosol number density (7.7E+07 to 4E+08m^{-3}) was recorded close to the Srilankan coast when the ship travelled along the international ship route (along ~ 6°N). South-BoB showed values varying from 3.6E+07 to 1.2E+08m^{-3}.

The spatial pattern of M_L over BoB (Figure 4.10b) also shows highest loading over north BoB. M_L varied from 60-90μg m^{-3} over the northern parts of BoB to 10–20μg m^{-3}over southern parts (an exceptionally large value of 150μg m^{-3} was measured near the Chennai port which is not included in this analysis). It may also be noted that there are hot spots of M_L near south of Kolkata, Bangladesh and north of Andaman Islands (shown by brown and red colored circles in Figure 4.10b) depicting the influence of anthropogenic activities. Continental outflow from highly polluted IGP and East Asian countries surrounding the ocean contribute to the aerosol loading over BoB.

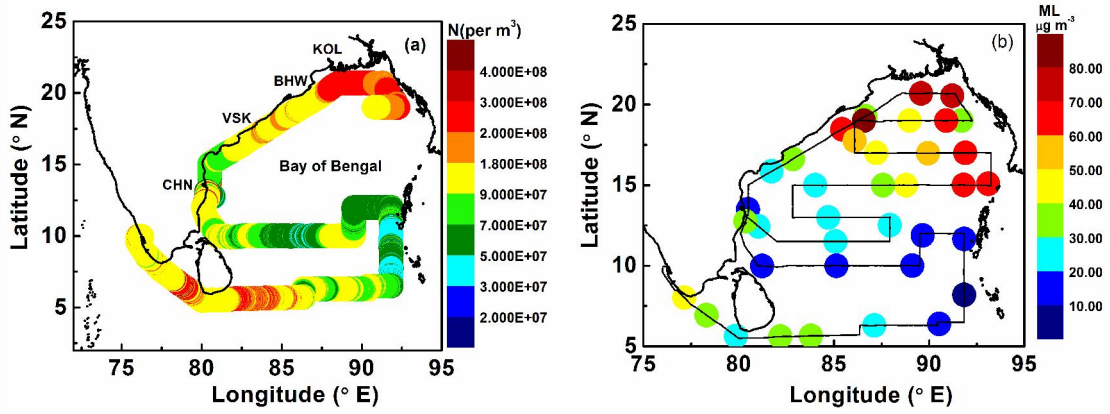

Figure 4.10. *Spatial variation of (a) total aerosol number density (N) and (b) mass loading (M_L) along the cruise track over the marine environment of BoB.*

The winds over northern BoB are mostly north westerly (Figure 4.2b) directed from the Indian landmass, bringing in aerosols from the IGP region. The high aerosol loading along the coastal side is due to the presence of many industrialized urban sites and busy seaports including Chennai (CHN), Vishakhapatnam (VSK) and Bhubaneswar (BHW), Kolkata (KOL), etc. Studies conducted over these sites independently support the elevated aerosol loading existing there [*Das et al*., 2009; *Pavulari et al*., 2011; *Ram et al*., 2012]. Over south BoB, winds are strong and directed from south or south west (Figure 4.2b).

4.5.2.2 Air mass back trajectories reaching BoB

For more quantitative analysis, the marine environment of BoB is divided into four regions; Coast (covering the west coast regions of Indian subcontinent), North BoB(>15°N apart from the coastal region), Mid BoB (no NSD data available), and South BoB(4-10°N) and air mass type reaching each of these regions were examined. The 7-day air mass back trajectories reaching cruise track during sampling as obtained from HYSPLIT model are presented in Figure 4.11a to d for the above 4 regions.

Over N-BoB and close to coastal regions, the air mass originating from Indian landmass persists. On the other hand, the air mass back trajectories reaching the mid and southern BoB originate from relatively pristine oceanic environments (Figures 4.11c and d). However, many of these trajectories pass near by western and southern coastal regions of India. Also the airflow patterns during this period (Figures 4.2a and b) indicate strong flow from western side of Indian landmass towards southern AS to northern Indian Ocean and then to BoB which can bring in continental species. The high aerosol loading over south AS and southwest BoB can be due to this peculiar flow from AS to BoB.

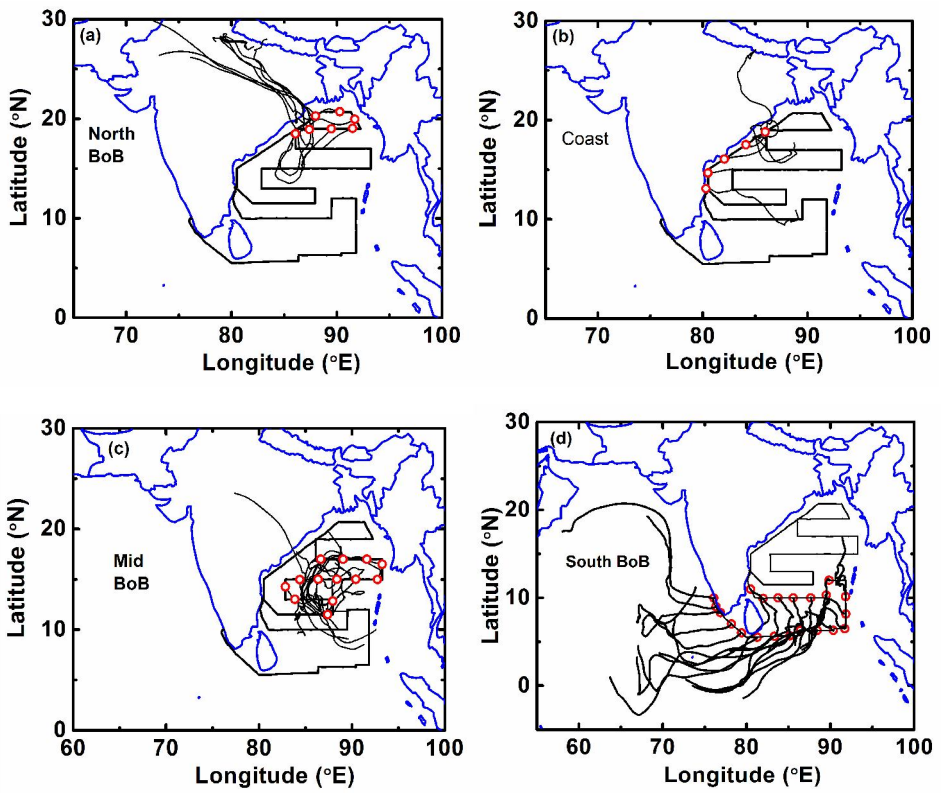

Figure 4.11. *The 7-day air mass back trajectories reaching the sampling locations over different parts of BoB (a) North-BoB (b) Coast (C) mid- BoB (D) South- BoB including northern Indian Ocean.*

4.5.2.3 Aerosol number size distribution over BoB

From the size-resolved number density measurements, the aerosol NSDs were derived and averaged for each of the regions viz. north BoB, south BoB and Coast (for mid BoB, no NSD data is available) and shown in Figure 4.12a along with the zoomed NSD for fine mode and coarse mode in Figure 4.12b and c.

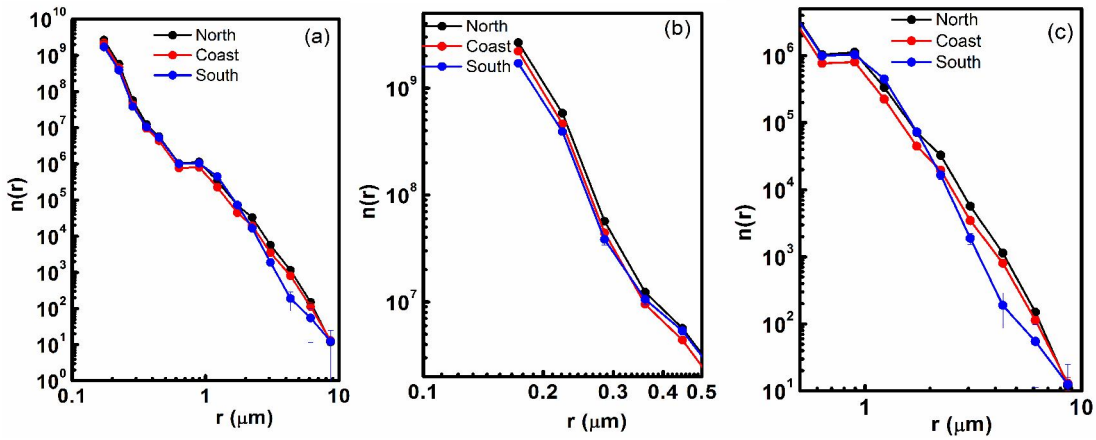

Figure 4.12. *(a) NSDs of aerosols over the marine environment of BoB (b) the zoomed NSD for fine mode and (c) the zoomed NSD for coarse mode regimes.*

The NSDs clearly show a multi-modal distribution, with two prominent modes one at radius <0.1μm and the other ~0-8 to 0.9μm as in the case of the NSDs over AS (Figure 4.5) and the coastal station TVM (Chapter 3). The second mode is broader than that over the AS. The fine mode particle number density is higher for north BoB and also over coastal region. The coarse mode number density was comparable over north BoB and south BoB up to r≤1.2μm as can be seen from Figure 4.12c.

4.5.2.4 Number density of fine and coarse mode aerosols

As done for AS, the number density was segregated into fine and coarse modes and their fractional loading estimated for the cruise track and plotted in Figures 4.13a to d. Spatial variation of the number density of fine particles over the BoB (Figure 4.13a) follows the same pattern as the total number density (Figure 4.11b) with high values over north BoB (>2.0E+08m^{-3}), Indian coast and south/south western regions.

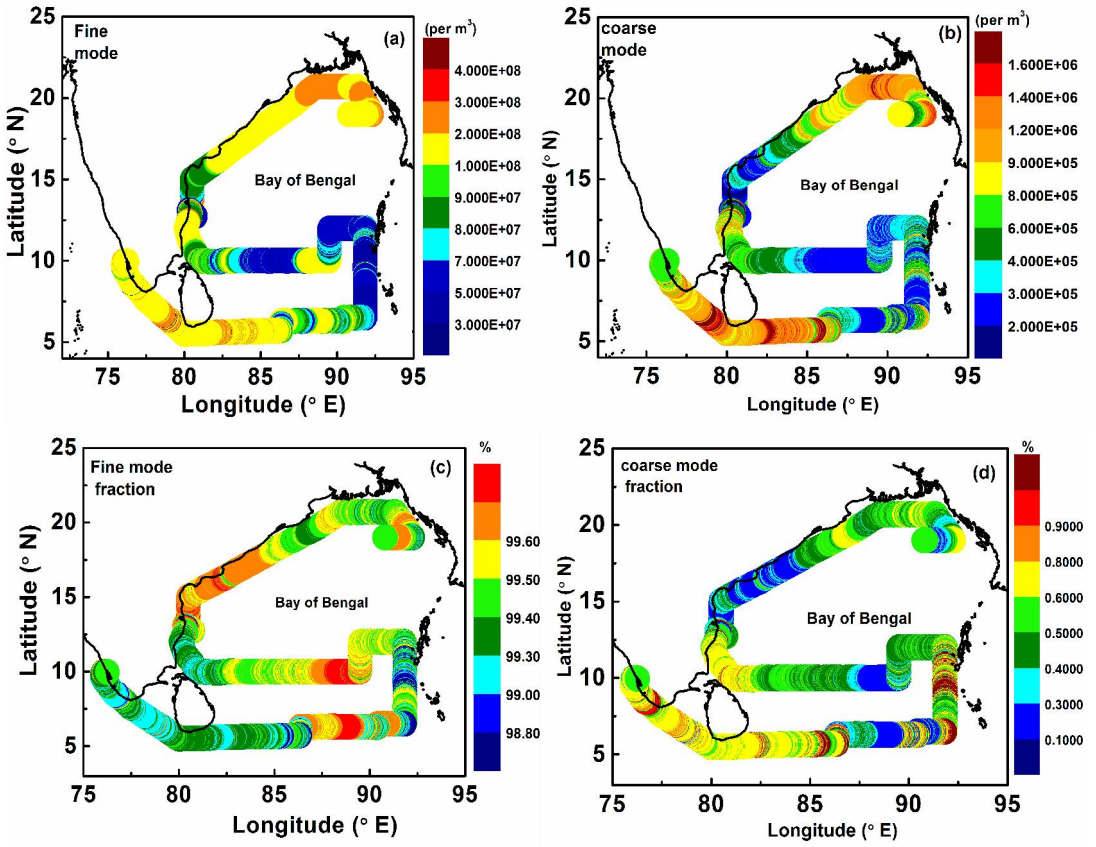

Figure 4.13*. Spatial pattern of (a) fine mode number density of aerosols over BoB (b) coarse mode number density of aerosols over BoB (c) fine mode fraction in % over BoB and (d) coarse mode fraction in % over BoB.*

Highest value of ~4E+08 was observed for fine mode towards the Srilankan coast. Lowest value was obtained over the south-east region of BoB (4.1E+07m^{-3}). In fact, the entire marine environment of BoB was dominated by fine particles (except

over SW BoB) rather than the coarse mode particles as revealed by the respective fractions presented in Figure 4.13c and d. The fine mode fraction of aerosols over the study region contributed upto ~99%. This is possible since the BoB region is more prone to continental outflow from anthropogenically active areas due to favourable winds during the study period.

The coarse mode number density ranged from 5E+05 to 1.6E+06m^{-3} with peak values over north BoB and south BoB and near to Srilankan coast. The fine mode fraction is high along the coastal regions also. The spatial patterns of coarse and fine mode number densities are more or less similar, but those of the fractional loading differ (Figure 4.13c and d). While the fine mode fraction shows minimum over SW BoB, coarse mode fraction maximizes in this region. However, significant amount of both fine and coarse particles exists over north BoB.

4.5.2.5 Chemical composition of aerosols over BoB: mass concentration and mass fractions

The aerosol mass concentration (m_x) of various chemical species over BoB along the cruise track and the corresponding mass fractions (m_f) are shown in Figure 4.14a to c. The oceanic regions are also shown on top panel.

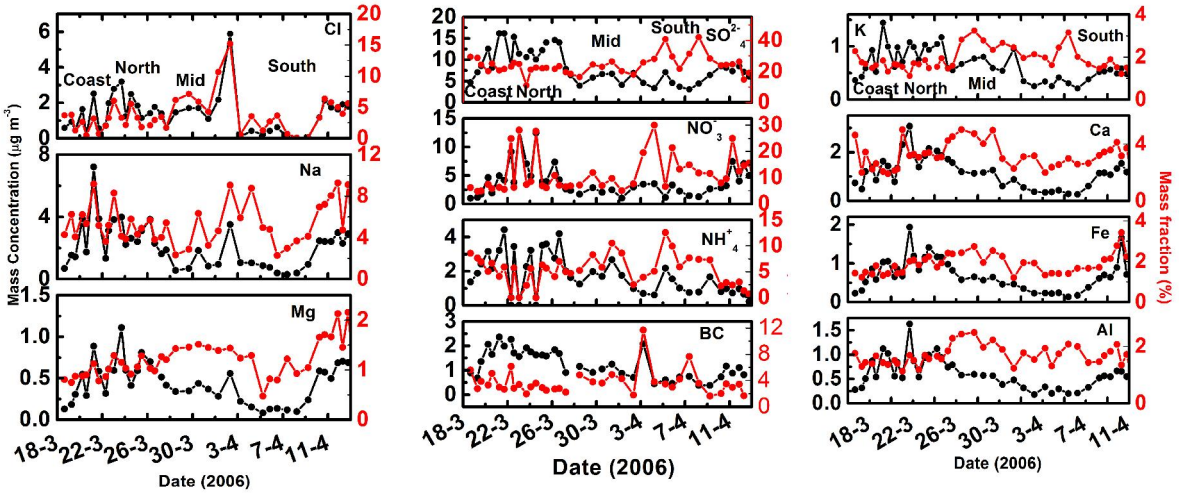

Figure 4.14. *Variation of aerosol mass concentration (m_x) for various species along the cruise track over BoB along with their mass fraction (m_f) (The oceanic regions are marked on the top panel).*

It is to be noted that for most of the species m_x and m_f exhibit one to one correspondence over BoB unlike AS. While mass concentrations of most of the continental species (SO_4^{2-}, NH_4^+, Al, Ca, BC and K^+) showed prominent high over north BoB their mass fractions are high over mid and southern parts of BoB. This implies that the continental species contribute more to the total loading over these

regions. Despite the fact that north BoB was more loaded with anthropogenic aerosols, the anthropogenic radiative forcing over BoB during this period remained more or less constant, ranging from -3.3 to -3.6W m^{-2} [*Nair et al*., 2010], probably due to this. More information on the anthropogenic contribution and radiative properties over BoB are given in sections 4.5.3 and 4.5.6 respectively.

4.5.2.6 Correlation of chemical species with fine and coarse number density over BoB

As in the case of AS, a correlation analysis was carried out between mass concentrations of various chemical species and the fine mode and coarse mode number densities, the results of which are shown in Figure 4.15 along with the respective correlation coefficients. Almost all species including crustal species showed positive correlation with the fine mode number density over BoB unlike over AS. But with coarse mode, only the sea-salt and crustal species showed positive association. This indicates highly varying sources of aerosols over BoB. Here it is to be noted that the mineral dust over AS has fine mode contribution also, which could be due to aging of aerosols transported from the far off arid Arabian region. On the other hand, the mineral dust reaching BoB is mostly from nearby IGP region.

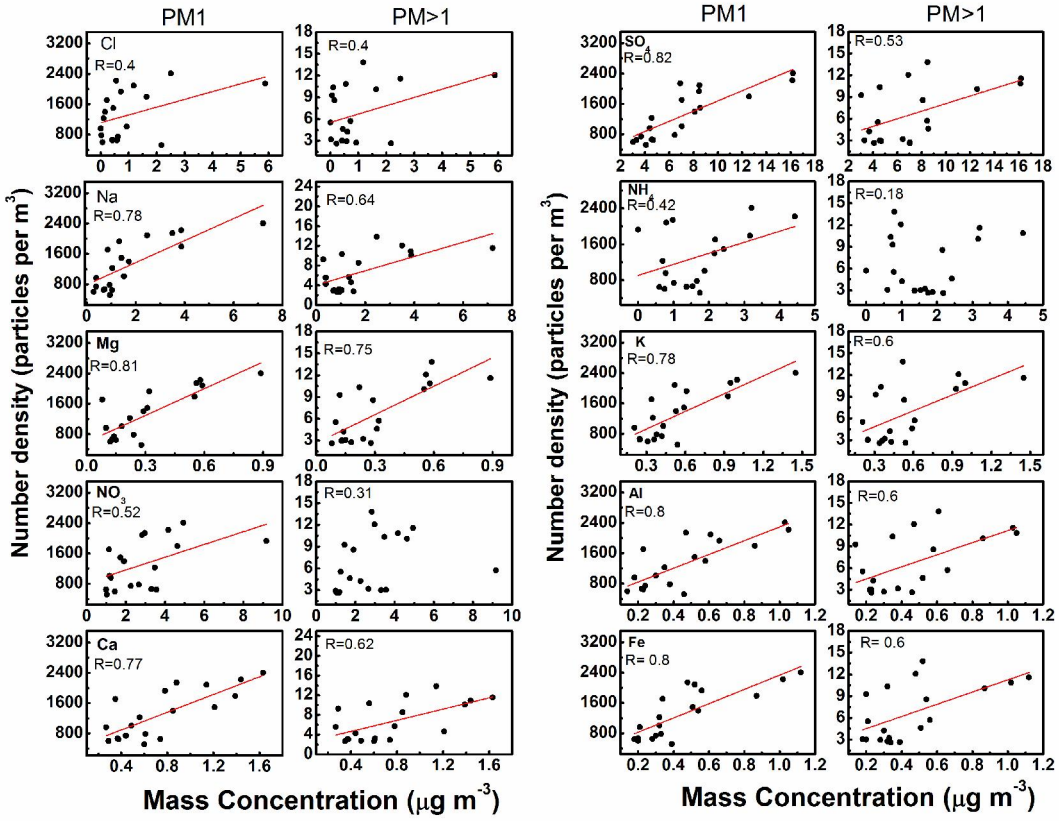

Figure 4.15. *Scatter plots between the fine mode (PM1) and coarse mode(PM>1) number density and mass concentration of different chemical species over BoB along with the regression fitted line and correlation coefficients (R) written in each panel.*

4.5.3 Anthropogenic and natural components of aerosols over BoB and AS

The anthropogenic aerosols, advected across the Indo-Gangetic Plain (IGP) and East Asia, make the BoB one of the highest aerosol laden oceanic regions of the world [*Satheesh et al*., 2002; *Moorthy et al.,* 2003; 2008; *Vinoj et al., 2004*, *Girolamo et al*., 2004, *Jethva et al.,* 2005; *Satheesh et al*., 2006]. In this section, it is attempted to quantify the anthropogenic and natural components in the marine environments of AS and BoB by grouping the estimated chemical components according to their sources. The total anthropogenic component in aerosols is estimated as the sum of nss-$SO4^{2-}$, NH_4^+, BC, nss-K, NO_3^-, the trace species and a fraction of Particulate Organic Matter (POM) which is of anthropogenic origin. The non-sea-salt component of SO_4^{2-} (nss $SO4^2$) and nss-K^+ value estimated by making use of sea water mass ratio of the respective species to Na as discussed in section 3.4 of Chapter 3. Since the measurement of POM was not done in this cruise, an approximate estimate of POM was made based on the measurements of EC, OC and BC by other groups [*Sudheer and Sarin,* 2008; *Kumar et al.*, 2008; *Nair et al.,* 2009] during the same cruise. The estimate of the total POM is made as POM=1.6*OC the details of which are discussed in Chapter 3 [*Turpin and Lim*, 2000, 2001].

The natural component of the aerosol system includes sea-salt (SS) and mineral dust (MD) (estimated through equations 3.6 and 3.7 respectively in Chapter 3) along with the natural fraction of POM. The POM over the marine environment is of either natural or anthropogenic component, produced in situ and/or transported. Over pristine oceanic environments, biological activity is a major natural source for organics and during low activity period (as the case of the study period) the organic fraction is 10-15% [*O'Dowd and Leeuw*, 2007]. However, it is very difficult to delineate the natural and anthropogenic portions in POM. In view of the continental influence over AS and BoB (as revealed by high concentrations of other tracers of anthropogenic aerosols like SO_4) 90% of POM is considered to be of anthropogenic origin. Although largely uncertain, these estimates may provide order of magnitude levels of natural and anthropogenic aerosols over the marine environment of AS and BoB.

In Figure 4.16a and b is shown the mass concentrations and % contributions of the estimated natural and anthropogenic aerosols to the total aerosol mass over BoB along the cruise track (presented as a function of date). The anthropogenic component outweighs the natural one over the entire BoB. The mean contribution of anthropogenic aerosols is estimated as 58±16%. Over mid-BoB, contribution of natural aerosols is

sometimes comparable to their anthropogenic counterpart (~40-60%). However, the anthropogenic contribution is more over south-BoB (varying in the range of 70-90%).

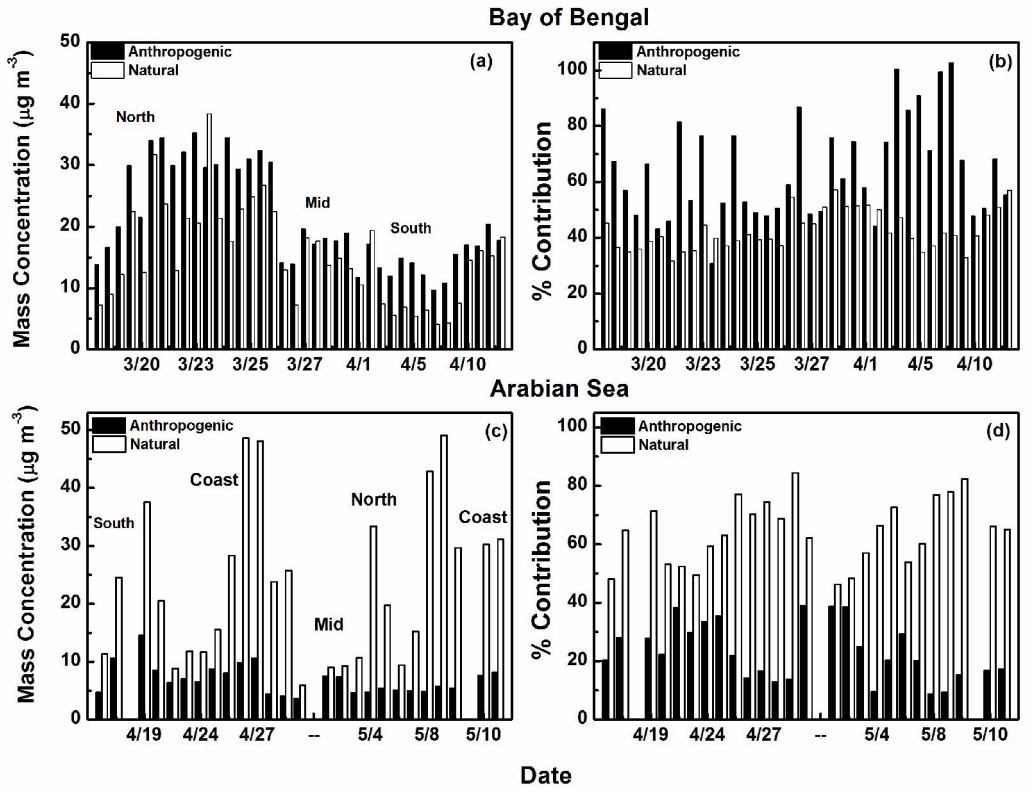

***Figure 4.16**. Spatial variations in the mass concentrations and percentage contributions of natural and anthropogenic aerosols over AS (a and b) and BoB (c and d).*

In Figure 4.16c and d is shown the variations in the mass concentrations and percentage contributions of natural and anthropogenic aerosols over AS estimated as in the case of BoB. Unlike BoB, AS shows dominance of natural aerosols during this period. Mean percentage contribution of natural aerosols over AS is estimated as 67±12% while that for anthropogenic is 21.7±9%.

4.5.4 High mass concentration of trace species: Signature of anthropogenic activities

The presence of trace species like Ni, Cr, Ti, Pb, Mn, Co, etc over BoB again confirms the continental/anthropogenic influence over this marine region. It may be noted that Pb is a marker of vehicular exhaust, Ni of oil combustion and Cu of smelting, Mn from ore processing and other metallurgical activities [*Pacyna et al., 2007*; *Galloway et al., 1982*]. In addition to industrial sources, Pb, Mn and Ti have

crustal components too. According to global emission estimates Zn and Cu are the highest emitted elements from non-ferrous metal production. Cu and Zn may also have minor oceanic sources, associated with marine colloids or from soil re-suspension [*Pacyna and Pacyna* 2001]. Spatial variations of the mass concentration of Ni, Cr, Ti, Pb, Mn and Co along with their mass fractions are shown in Figure 4.17a to f and g to l respectively. The mass concentrations of these species over BoB ranged from 0.0003 to 0.3µg m^{-3} which is well above the detection limit of the instrument. Significant concentrations of all the trace species are measured in the north-BoB region. Over other regions, their concentrations are very low and below detection limit of the instrument. Their mass fractions also exhibit spatial patterns similar to mass concentrations.

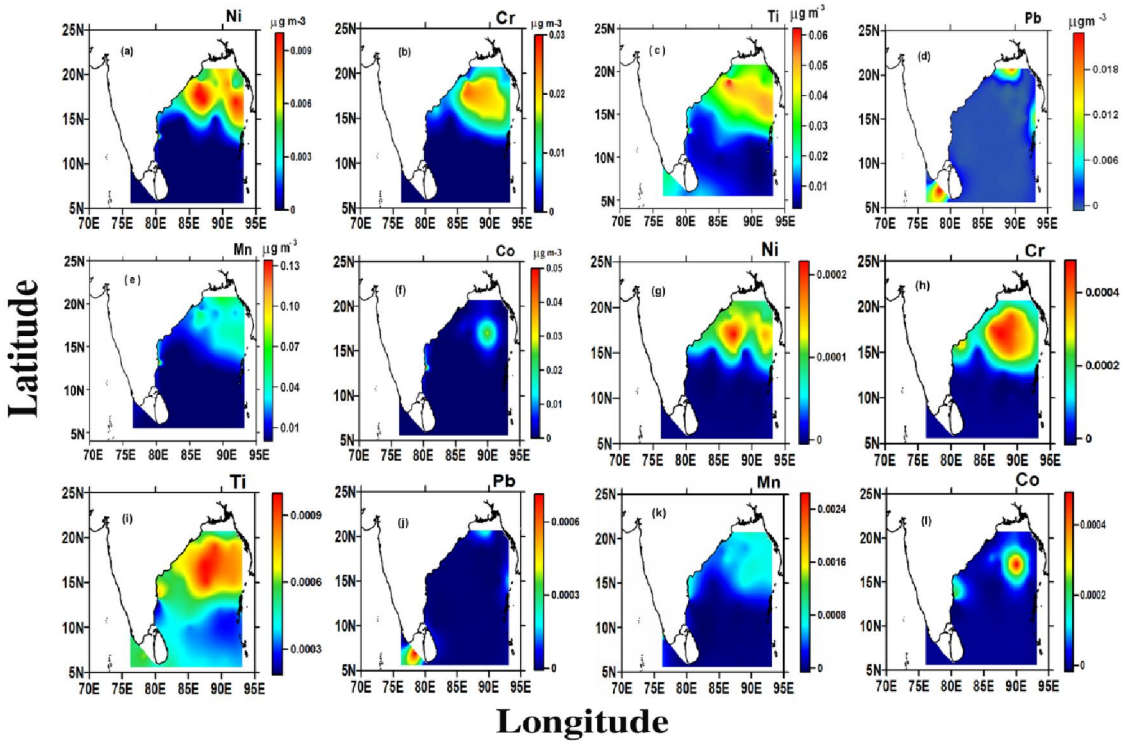

Figure 4.17. *(a) to (f):Spatial distribution of mass concentration of various trace species over BoB and (g) to (l): Spatial distribution of mass fraction of the various trace species.*

Trace metal species were detected and reported from different oceanic regions. *Witt et al*. [2006] reported mean concentrations for Cu, Ni, and Zn as 0.7ng m^{-3}, 0.18ng m^{-3} and 2.56ng m^{-3} respectively for remote southern Atlantic Ocean. High metal concentrations were observed for Zn (3.23ng m^{-3}), Cu (0.81ng m^{-3}), Sr (2.63ng m^{-3}), and Cr (0.53ng m^{-3}), over Cape Verde Atmospheric Observatory, North Atlantic [*Fomba et al*., 2013].

It is also to be noted that the oceanic environment of AS is devoid of these trace species (their concentrations were too low and below the detection limit of the instrument) hence anthropogenically less influenced.

4.5.5 Region-specific aerosol chemical model for AS and BoB

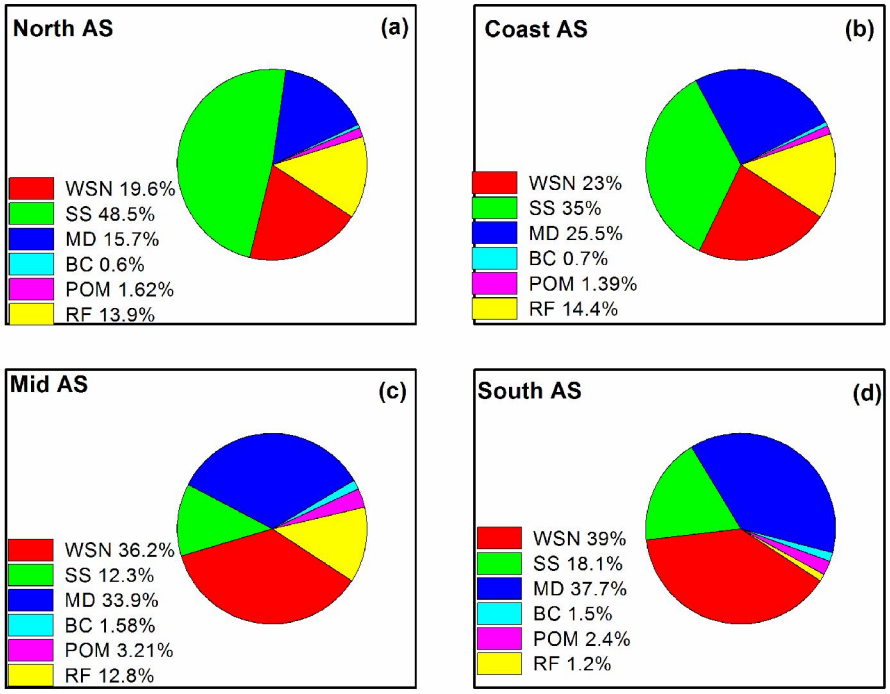

Figure 4.18. *The percentage contribution of various aerosol components over different regions of AS (a) north AS (b) Coast (c) mid AS (d) South AS*

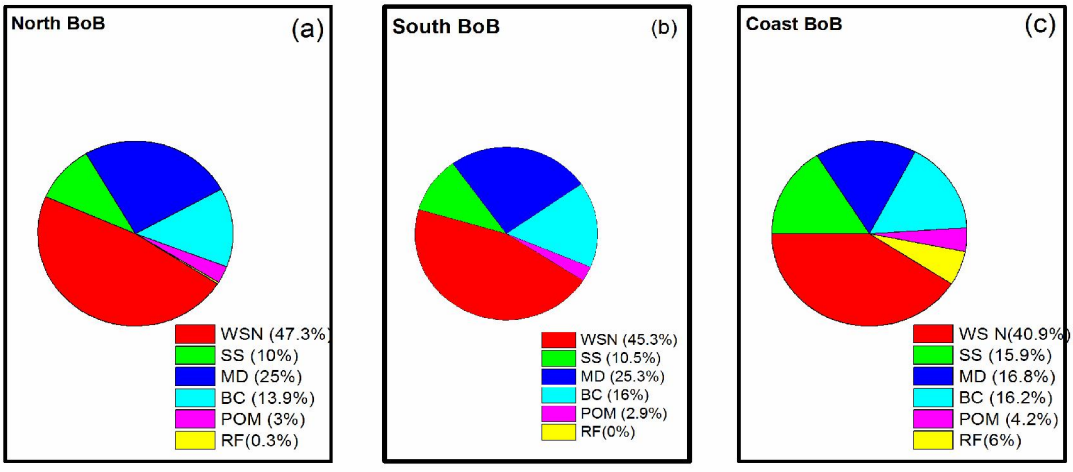

Figure 4.19. *The percentage contribution of various aerosol components over different regions of BoB (a) north BoB (b) South BoB (c) Coast.*

Based on the chemical composition of aerosols, the mean mass concentration of the 5 major components (1) Sea-salt (SS) (2) Other Water Soluble Non-sea-salts (WSN) (3) Mineral dust (MD) (4) POM (Particulate Organic Matter) and (5) Black

Carbon (BC) have been estimated as discussed in Chapter 3 section 3.7. The pie charts in Figure 4.18a to d show the mean percentage contribution of each of these components over the different regions of AS and Figure 4.19a to c gives the same for BoB as pie diagrams. The unaccounted residual fraction of the total aerosol mass concentration RF is also shown in the pie charts.

While sea salt particles contributed more to the total loading of aerosols over north AS (48%) and coast (35%), WSN was high over south (39%) and mid AS (36%). The contributions from BC and POM were low throughout AS. MD contributed to 37% of total aerosols over the south AS. Considerable dust loading can be seen over the marine environment of AS (varying from 15% to 37%). About ~13% of aerosol mass remained unanalyzed over the north, coast and mid AS, whereas over south AS the unanalysed components is ~ 1.2% only.

The contribution of WSN was found >40% throughout BoB revealing the strong anthropogenic influence. The SS contribution was between 10-16% which was low as compared to AS (12-49%). Considerable amount of BC (~16%) was found over this marine region while POM remained <4% throughout. Contribution of MD is ~25% indicating the transport from nearby landmass. Here it needs to be noted that the contribution of MD over south AS is also high and a circulation originating from Arab regions, passing through western AS and the western cost of India reached south BoB (see the air flow pattern in Figure 4.2). While for the north and south BoB, the unanalyzed fraction (RF) was negligible/nearly zero; near to Indian coast 6% of aerosol mass remained unanalyzed.

4.5.6 Radiative characteristics of aerosols over AS and BoB

Based on the measured aerosol characteristics over the two oceanic regions AS and BoB, the radiative/optical characteristics were estimated by using OPAC model, the details of which are given in Chapter 2 and 3. The aerosol scattering coefficient (β_{sc}) absorption coefficient (β_{ab}), extinction coefficient (β_{ex}), Single Scattering Albedo (SSA) and the phase function P (θ) estimated as a function of wavelength for each region of AS are shown in Figure 4.20a to d. Similarly, the wavelength dependence of these parameters for north-BoB, south BoB and coastal region are illustrated in Figure 4.21a to c. The radiative parameters show regional variations over AS, with maximum scattering and extinction coefficient close to coastal region (~0.075km^{-1}) and minimum over mid-AS.

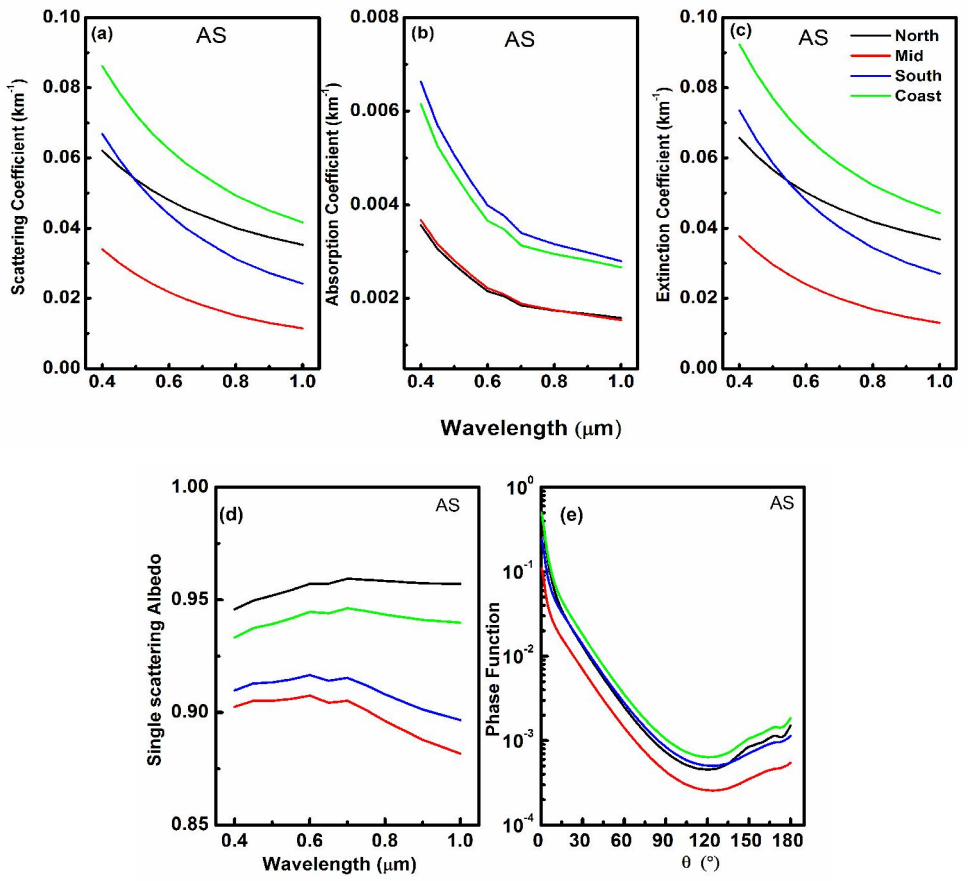

Figure 4.20. *Estimated Spectral variation of (a) aerosol scattering coefficient (β_{sc}) (b) absorption coefficient (β_{ab}) (c) extinction coefficient (β_{ex}) (d) Single Scattering Albedo (ω) and the (e) phase function P(θ) for different regions of AS.*

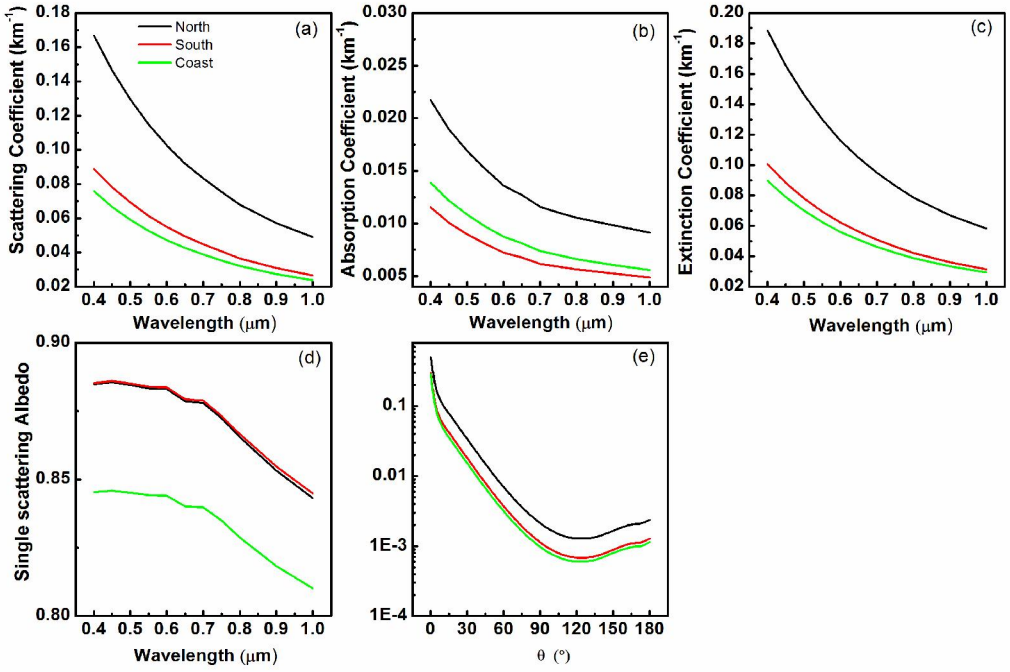

Figure 4.21. *Estimated Spectral variation of (a) aerosol scattering coefficient (β_{sc}) (b) absorption coefficient (β_{ab}) (c) extinction coefficient (β_{ex}) (d) Single Scattering Albedo and the (e) phase function P(θ) for different regions of BoB.*

The SSA varied in the range 0.9 to 0.96 over AS. It is low and strongly dependent on wavelength over mid and south AS. Compared to AS the scattering, absorption and extinction coefficient are higher over BoB (extinction coefficient reaching up to 0.14km^{-1}) and highest over north-BoB. The mean scattering coefficient for south-BoB was 0.062km^{-1} and over north-BoB is 0.12km^{-1}. In general, SSA is lower over BoB being 0.84 to 0.885 indicating the abundance of absorbing aerosols there. But SSA remained more or less same over north and south-BoB, but showed less values ~0.84 close to coastal region.

Phase function also exhibited regional differences. Estimates of SSA over AS and BoB made during various campaigns are available in literature. The SSA estimated over BoB based on the measurements using nephelometer and aethalometer varied from 0.96 to 0.84 over BoB and the nephelometer based measurements showed the scattering coefficient in the range 0.025 to 0.2km^{-1} with high values over north and least over south east BoB [*Nair et al*., 2008].

During INDOEX the mean SSA over AS and BoB were 0.93 and 0.83 respectively [*Ramachandran*, 2005]. At the KCO observatory SSA was found to be ~0.92 [*Satheesh et al*., 2004]. *Vinoj et al*., [2001] estimated SSA value of 0.90 over AS and 0.86 over BoB based on the columnar AOD measurements by MODIS.

4.6 Summary

This chapter deals with the spatial features of aerosol number density (N), number density size distribution (NSD), mass loading (M_L) and mass concentrations of various chemical species measured over the marine environment of Arabian Sea (AS) and Bay of Bengal (BoB) during pre-monsoon. Based on the measurements of chemical composition of aerosols, region specific first-cut chemical models were evolved for AS and BoB which were used for the estimation of the radiative characteristics of aerosols namely scattering coefficient (β_{sc}) absorption coefficient (β_{ab}), extinction coefficient (β_{ex}), SSA (ω) and the phase function P(θ).

Table 4.2 gives a comparison of the major aerosols characteristics over AS and BoB as revealed from this study.

Parameter	Arabian sea	Bay of Bengal
Mean aerosol number density (N)	6.8E7±3.56E7	1.24E8±6.0E8
PM1	6.6E7±3.6E7	1.20E8±6.0E8
PM>1	1.8E6±1.4E6	6.8E5±4.2E6
M_L	35.1±16.7	38.3±21.8
SO_4	4.6±1.8	8.5±3.9
NO_3	2.9±1.7	3.8±2.8
NH_4	0.4±0.2	1.9±1.1
Na	4.6±4.5	2.0±1.4
Cl	3.6±4.1	1.3±1.1
Mg	0.7±0.3	0.4±0.2
K	0.5±0.1	0.7±0.3
Ca	1.3±0.8	1.2±0.6
Fe	0.6±0.3	0.7±0.4
Al	0.5±0.2	0.6±0.3
Natural component (%)	81±1	37±16
Anthropogenic component (%)	21.7±9	64±17
Scattering coefficient at 0.5μm	0.05±0.02	0.08±0.04
Absorption coefficient at 0.5μm	0.003±0.001	0.01±0.004
SSA	0.93±0.02	0.87±0.02

Table 4.2. *Comparison of the major aerosol characteristics over AS and BoB.*

The results can be summarised as given below.

1) As compared to AS, BoB was found to be anthropogenically more affected in view of aerosols number density, mass loading and mass concentrations of anthropogenic species like SO_4^{2-}, NO_3^-, NH_4^+ etc. Considerable amount of trace species like Ni, Cr, Ti, Pb, Mn, Co, etc was found over BoB. Both fine mode and coarse mode number density of aerosols over BoB are one order higher than those over AS. The high aerosols loading over BoB is reflected in the scattering and extinction coefficients also.

2) Associated with an anti-cyclonic flow, both N and M_L showed low values over AS as well as BoB.

3) While aerosols of natural origin like sea-salt, mineral dust etc dominate over AS, continental species contribute more over BoB. The mean % contribution of anthropogenic aerosols over AS is estimated as ~21%, whereas that over BoB is ~64%.

4) Considerable amount of mineral dust was observed in both the oceanic regions (15-37% over AS and ~25% over BoB) revealing long range transport form arid/semi-arid regions and near-by land mass.

5) Aerosols of size >1μm (PM>1) showed an exponential increase with wind speed over AS. The number density of large sized particles increased faster with wind speed.

6) Correlation analysis of size-resolved number density with mass concentration of various species showed that the anthropogenic species exists mostly in fine mode and marine species in coarse mode. Mineral dust (Fe and Al) was found to be in both fine and coarse mode over AS. Almost all species including crustal species showed positive correlation with the fine mode number density over BoB. The dominence of fine mode fraction over AS is partly due to the presence of crustal species like Fe, Al etc in fine mode.

7) The SSA varied in the range 0.9 to 0.95 over AS and 0.84 to 0.885 over BoB indicating the presence of more absorbing aerosols over BoB.

Chapter 5

Winter-time aerosol characteristics over the Bay of Bengal: Transport pathways and continental influence

5.1 Introduction

Continental outflow over to oceanic regions has been a topic of interest in view of pollution transport and their localized radiative forcing impacts [*Ramanathan et al*., 2001; *Satheesh et al*., 2006]. Bay of Bengal (BoB) has its peculiar geographic surroundings with inhabited landmass on three sides and acting as an outflow region for pollution from Indo Gangetic Plains (IGP) which is one of the largest river basins in the world with >40% of Indian population residing over there. Being downwind to highly aerosol laden IGP and East Asian (EA) regions, the BoB is known to experience contrasting influence of the outflows from these two regions [*Nair et al*., 2009; *Moorthy et al*., 2009; *Lawrence and Lelieveld*, 2010]. The winter season with its characteristic north/north easterly air flow, is the most conducive period for transport of aerosols and trace gases over to BoB.

In Chapter 4 of this thesis is presented the results of the cruise-based study on the aerosol number density- size distribution, mass loading and chemical nature of aerosols as observed by simultaneous and collocated measurements over BoB during pre-monsoon. This chapter focuses on the spatial variation of total aerosol mass loading and mass concentration of various chemical species in aerosols over BoB during the winter season with a view to identify the major sources of aerosols over this wide oceanic environment, the transport pathways/mechanisms and to delineate the natural and anthropogenic contributions, based on the ship-borne measurements. These measurements form part of the second phase of ICARB conducted during winter (called W-ICARB). In this campaign, measurements were carried out over SE-BoB for the first time. A case study of wind induced production of marine aerosols and rain deposition of various species during a rain event occurred during the cruise is also addressed here. It is also attempted to evolve a first-cut chemical model of aerosols for the BoB region for this particular season and to estimate the radiative properties based on this model.

The following sections present the details of cruise track, the prevailing meteorology, instruments and data followed by the observational results.

5.2 Cruise track

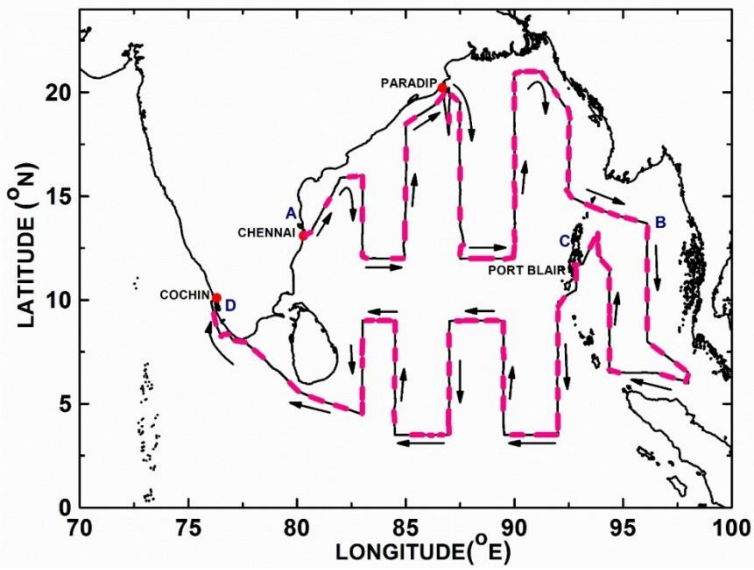

Figure 5.1. *Cruise track of ORV SagarKanya (Cruise No: SK 254) during the W-ICARB campaign with the arrows denoting the direction of movement of the ship and the pink lines denoting the distance travelled when aerosol sampling was done.*

W-ICARB was conducted during the period 27 December 2008 to 30 January 2009. Figure 5.1 shows the cruise track of Oceanic Research Vessel (ORV) Sagar Kanya *(Cruise No: SK 254)* during the campaign. The cruise started on 27 December 2008 from Chennai port (13.09°N; 80.29 °E marked as A in Figure 5.1). From there, the ship travelled north upto 16°N and then moved southward along 83°E latitude. By making several longitudinal (85°E, 87°E, 90°E) and latitudinal transits (along 9°N and 12°N) it covered most of the northern part and mid-BoB (21°to 12°N). On 9 January 2009 the ship entered the eastern side of BoB (marked as B) and after sailing close to Myanmar and Thailand coast, it reached Port Blair (11°N, 93°E) on 16 Jan 2009 (C), from there it travelled further south and made few more longitudinal and latitudinal scans over south-BoB. For the first time, in-situ measurements were carried out over the south east BoB. The cruise ended at Cochin on 30 January 2009 (D) after moving close to Sri Lanka. The orange lines through the tracks show the distance travelled by the ship when the aerosol sampling was going on. The sampling time varied from 2-6 hours, depending on the oceanic region (remote and pristine regions need more

duration). During this cruise, the ship travelled a total distance of ~13900km, in 34 days, within the latitude-longitude sector 3.4°N - 21°N and 76°E - 98° E, on an average covering a distance of ~408 km per day.

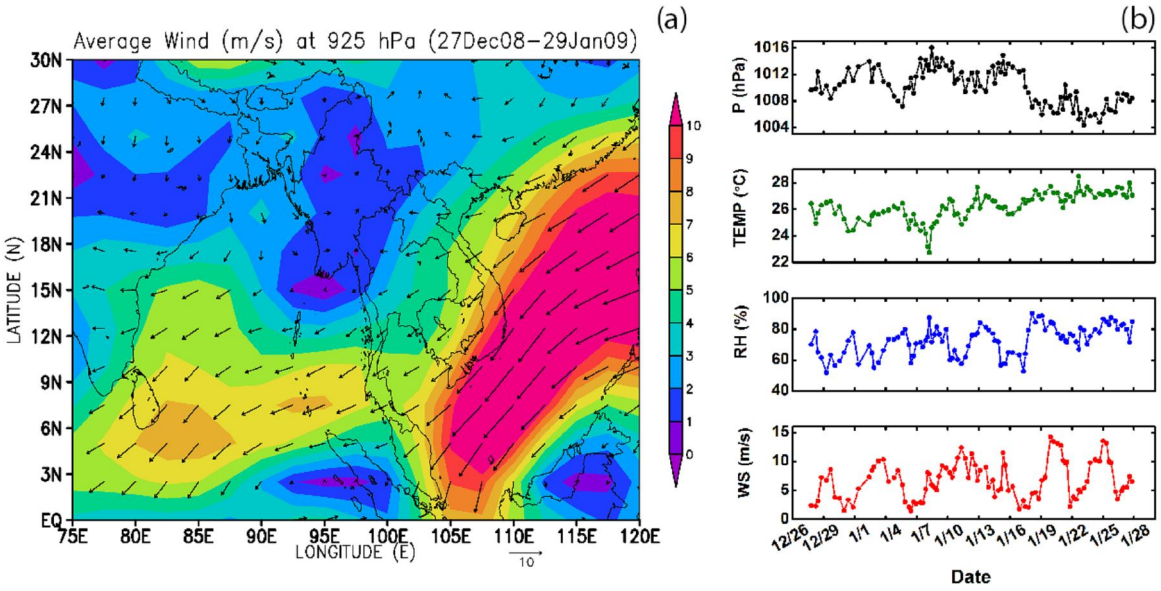

Figure 5.2. *Meteorological conditions prevailing over the cruise period (a) Average wind pattern at 925 hPa obtained using NCEP/NCAR Reanalysis data (b) Meteorological parameters corresponding to the sampling time as obtained from AWS onboard ship.*

5.3 Meteorology

During the cruise, the prevailing air flow over Indian subcontinent is predominantly north-easterly/ northerly as seen from the mean air flow pattern (Figure 5.2a) at 925 hPa obtained using the NCEP/NCAR Reanalysis data (http://www.noaa.gov/ready-bin/fnl.pl). This favours advection of air mass and hence the pollutants over to this oceanic environment. Also different parts of BoB receives air masses from distinctly different continental locations (as seen from the wind direction) implying the possibility of finding chemical species originating from different regions to be present over BoB. Northern part of BoB receives weak northwesterly winds from highly polluted IGP while the southern and south-eastern region was mainly affected by strong winds of speed 6-10m s^{-1} from south-east Asia. In mid-BoB the winds were mostly easterly and weak. An automatic weather station (AWS) on board the ship continuously recorded the meteorological parameters pressure, temperature, relative humidity (RH) and wind speed along the cruise track. Figure5.2b shows the mean values of these parameters corresponding to the sampling time and along the cruise

track presented as a function of date. The temperature and pressure ranged from 23°C to 27°C and 1004hPa to 1012hPa respectively. RH, which is an important parameter whose variation readily influences the growth of hygroscopic particles, varied from 55%-90% during the campaign, being high towards south-BoB. Correspondingly, temperature showed high and pressure dropped. The wind speed (corrected for ship speed and direction) was between 5ms^{-1} and 10ms^{-1} throughout the cruise period except for few days when the sea was extremely calm (with wind speed was 2ms^{-1} to 3ms^{-1}) when the ship cruised through north-BoB and wind speed increased up to 14ms^{-1} when the ship was traversing through south-BoB. During the cruise, except for the rain event occurred on January 18, the weather was calm and clear. All these parameters directly or indirectly affect the physical, chemical as well as the thermo dynamical properties of aerosols.

5.4 Instrumentation and Database

The High Volume aerosol Sampler, model GH2000 of Graseby Anderson, USA was operated at the front deck of the ship for collecting the aerosol samples. Sampling technique, calibration and gravimetric calculation of mass loading is explained in Chapter 2 and 3. During the W-ICARB cruise, about 101 samples were collected from the marine environment of BoB, uniformly spread over the track. Quantitative estimate of the major inorganic species in each sample has been made by carrying out the chemical analysis of the collected aerosol samples using Ion Chromatograph, Inductively Coupled Plasma-Atomic Emission Spectroscopy and Atomic Absorption Spectroscopy. Apart from this, the Black Carbon data collected along the track, using the Aethalometer (model AE 31 of Magee Scientific, USA) was also used in the present study. The details on the aerosol sampler, analytical techniques and calibration of the instruments and the uncertainties are discussed in Chapter 2.

5.5 Aerosol spatial characteristics over BoB during winter

5.5.1 *Aerosol mass loading*

The variation of total aerosol mass loading M_L along the cruise track, on day-to-day basis and the spatial map of mass loading generated with Surfer software is shown in Figure 5.3a and b respectively.

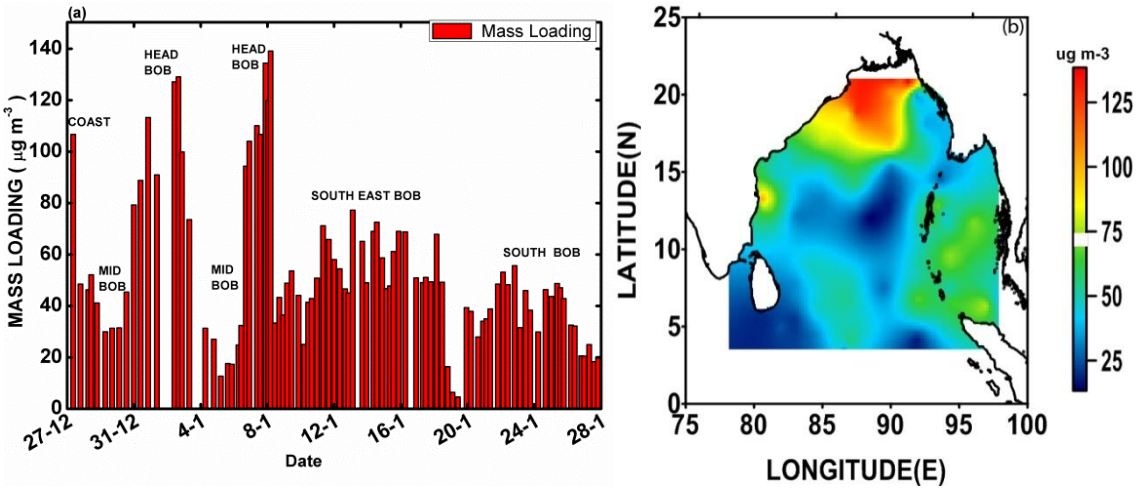

Figure 5.3. *(a) Variation of M_L along the cruise track (on day to day basis). Regions where ship cruised while sampling was done are also marked in the figure (b) Spatial pattern of M_L (in μg m^{-3}) over BoB.*

The respective region of BoB where the M_L measurements were done is also marked in Figure 5.3a. The M_L values during the cruise period (winter season) ranged from a maximum of 139μg m^{-3} to a minimum of 12μg m^{-3} with a mean value of 53± 29μg m^{-3}. Mean values are significantly higher than the oceanic background levels [*Prospero et al*., 1989; *Savoie et al.,* 1994; *Johansen et al.,* 2000; *Bates et al.,* 2002; *Eleftheriadis et al*., 2006].

Two extremely low values of 4 and 6μg m^{-3} were observed over south-BoB consequent to the rain event and this aspect is discussed separately in Section 5.10. In general, high aerosol mass loading was observed throughout BoB with highest values over north-BoB with an average of 88 ± 26μg m^{-3} indicating high levels of pollution. Comparitively less loading of about 45 ± 21μg m^{-3} was measured over mid-BoB where an anticyclonic flow prevailed (Figure 5.2a). An interesting feature observed during this campaign was the relatively high aerosol mass loading (55 ± 9μg m^{-3}) over southeast-BoB, a region unexplored earlier. The spread of aerosol loading far into ocean (red and yellow colour in Figure 5.3b) clearly reveals the signature of continental outflow from nearby landmass to the ocean, extending to several kilometres. The wind pattern discussed in Section 5.3 also indicates the transport from IGP to north-BoB and East-Asia to southeast-BoB. Moreover, the high aerosol loading over this marine region during winter can be partly due to the peculiar meteorological conditions with shallow boundary layer and less ventilation, characteristic of the season, confining the pollutants to lower altitudes [*Subramanyam et al*., 2011].

Based on the observed spatial features of aerosols, the study region is divided into 5: the north-BoB (16 ℃N to21°N;86 ℃E to 93°E), the coastal side of west BoB from Chennai (13.18°N, 80.30°E) to Paradip (20.30 ℃N, 86.55 ℃E), the mid-BoB (12ºN-16°N and 83ºE-90°E), the southeast-BoB(3ºN-14°N and 93ºE-98° E) and the south-BoB (3ºN-9°N and 78ºE-92°E).

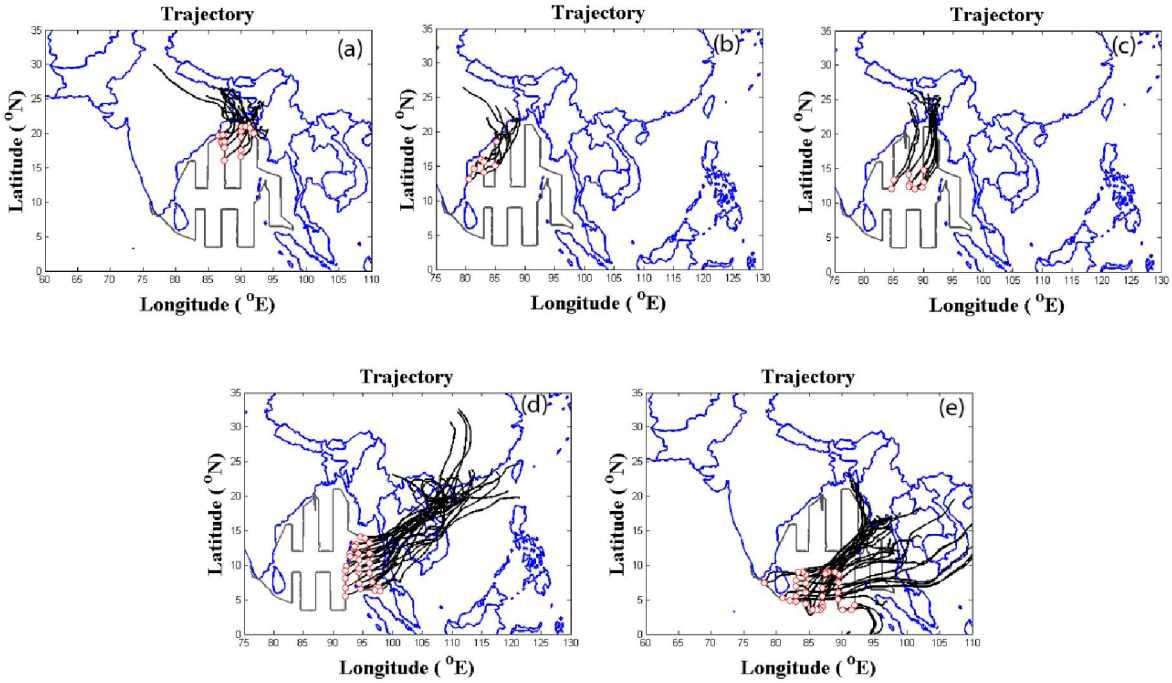

Figure 5.4. *7-day back trajectories of air mass reaching at 100m above surface at aerosol sampling points (marked as red) for the five regions (a) North (b) Coast (c) Mid (d) South-East and (e) South selected over BoB.*

Figure 5.4 shows the 7-day back trajectory of air masses reaching different regions of BoB, at an altitude of 100m above the sea surface (within marine boundary layer), during the cruise period. The air mass back trajectories were obtained by running HYSPLIT (Hybrid Single Particle Lagrangian Integrated Trajectory) model [*Draxler and Rolph,* 2003], for the respective mean position of the ship during the sampling period of each sample.

Northwest and north-BoB receive air masses from the IGP and Central India which will bring highly polluted air containing anthropogenic and crustal species (Figure 5.4 a,b). Air mass reaching the mid-BoB was long range transported from the northern side of India (Figure 5.4c).The southeast-BoB receives air mass from the East Asia (Figure 5.4d), the high loading observed over this region could be from this region having specific sources of biomass burning and anthropogenic activities like combustion burning and industrial emission [*Russo et al*., 2003; *Sahu and Sheel*, 2013].

The air mass reaching south-BoB originates from the coastal sites of East Asia (Figure 5.4e) including Myanmar and travels long distance through the oceanic regions and hence both marine as well as continental species can be present. Strong winds (Figure 5.2) results in the production of sea-salt species leading to more aerosol mass loading over this region. The wind induced sea-salt production is discussed in Section 5.8. The spatial patterns of various chemical species, discussed in following sections, throw more light on the sources of aerosols reaching different regions of BoB.

5.5.2 Mass concentration of various chemical species over BoB

Species	Coast	North-BoB	Mid-BoB	Southeast-BoB	South-BoB
M_L	80.7±31	88±26	45±21	55±9	36.9±10
Na	1.4±.7	4.1±3.3	3.1±3.2	3.9±2.3	4.1±2.2
K	1.1±.4	1.9±0.6	0.7±0.29	0.4±0.2	0.3±0.1
Mg	0.2±0.06	0.4±0.2	0.3±0.29	0.3±0.2	0.3±0.2
Ca	1.5±0.4	1.7±0.5	0.9±0.29	0.6±0.2	0.5±0.2
NH_4	7.2±1.3	6.2±1.9	1.6±1.55	1.5±0.8	0.9±0.3
Cl	0.7±0.6	2.6±3.5	1.7±3.1	3.2±2.5	4.6±3.4
NO_3	5.2±3.1	7.3±3.5	1.7±0.4	2.3±1.4	2.1±0.9
SO4	16.7±3.7	19.4±5.1	6.9±2.5	6.7±4.4	4.8±0.3
Fe	1.0±.4	0.9±0.4	0.5±0.3	0.2±0.1	0.3±0.4
Al	0.7±0.2	0.6±0.5	0.5±0.2	0.2±0.08	0.1±0.1
nss-SO4	16.45±3.6(98%)	18.55±5(96%)	6.13±2.5(89%)	5.61±4.2(84%)	3.6±1.02(75%)
nss-K	1.04±0.4(97%)	1.77±0.6(93%)	0.60±0.2(84%)	0.27±0.1(63%)	0.12±0.07(45%)
nss-Ca	1.42±0.4(97%)	1.59±0.5(92%)	0.77±0.2(87%)	0.45±0.2(74%)	0.3±0.1(65%)
ss-SO4	0.26±0.2(2%)	0.87±0.8(4%)	0.77±0.8(11%)	0.97±0.5(14%)	1.04±0.5(22%)
ss-K	0.04±0.2(4%)	0.13±0.12(7%)	0.11±0.1(16%)	0.14±0.08(34%)	0.15±0.08(55%)
ssCa	0.04±0.3(3%)	0.13±0.1(8%)	0.12±0.1(13%)	0.15±0.08(25%)	0.16±0.08(35%)

Table 5.1. *Mean mass concentration (in μg m^{-3}) of various chemical species along with that of the sea-salt and non-sea-salt components of SO4, K and, Ca over the five regions of BoB. The % contribution of ss and nss components are shown in parenthesis.*

The chemical analysis of the 101 aerosol samples collected during the cruise has provided the quantitative estimate of 7 anions namely F^-, Cl^-, Br^-, NO_2^-, NO_3^-, PO_4^{2-}, SO_4^{2-} and 5 cations Na^+, Mg^+, Ca^{2+}, NH_4^+ and K^+ along with the metallic species Fe and Al. As discussed and explained in earlier chapters, Cl^- and Na^+ are mostly of oceanic origin, Fe and Al of crustal, K^+ is from biomass burning and SO_4^{2-} and BC are tracers of anthropogenic activities. Table 5.1 lists the mass concentration of various chemical species measured over the marine environment of BoB during winter. The spatial variation of mass concentration of all species are presented and discussed in the following sections. These spatial patterns along with the airflow pattern/ air mass back

trajectories help in identifying the potential source regions of aerosols over this marine environment.

5.5.2.1 Spatial pattern of oceanic species

Spatial pattern of the ocean-derived chemical species like Na^+, Cl^-, Mg^+ (Figure 5.5a,b,c) show similar spatial pattern, with high over the mid, south and south-west BoB. But this pattern is different from the distribution of total aerosol mass loading M_L (Figure 5.3b) indicating that the aerosol distribution is species dependent.

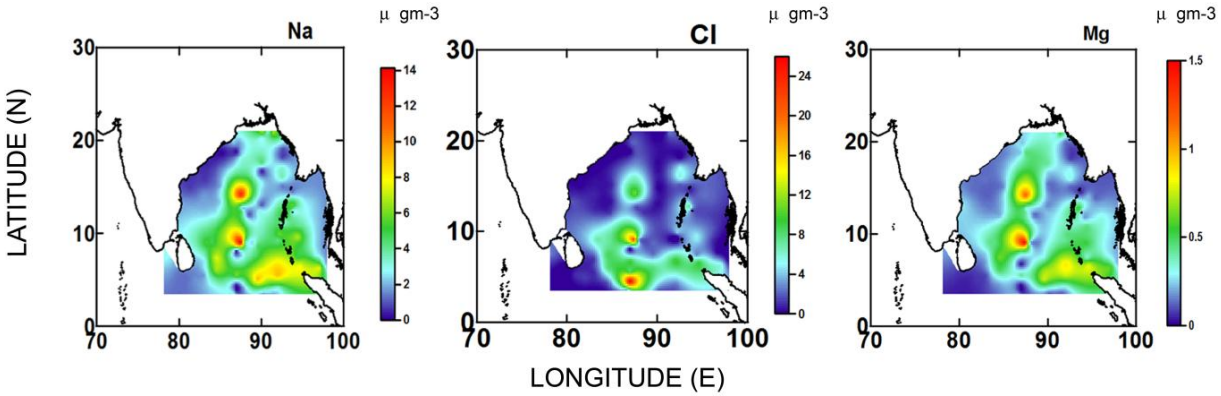

Figure 5.5. *Spatial distribution of mass concentration of oceanic species Na, Cl and Mg in μg m^{-3}.*

These oceanic species showed very low values towards the north-BoB and western coastal regions, where overall aerosol loading was high but wind speeds were very low (Figure 5.3b and 5.2). Moreover, these patterns differ from those of anthropogenic species (shown in Figure 5.6). Mass concentration of Cl^- ranged from 0.1 to 25μg m^{-3} with a mean value of 3 ± 2μg m^{-3} and Na^+ ranged between 0.1 to 13μg m^{-3} and Mg^+ 0.2 to 1.4μg m^{-3}. High mass concentrations of these oceanic species over south-BoB are attributed to the high wind (speed >10m s^{-1}) blowing over this region (Figure 5.2b) and this aspect is discussed in detail in section 5.8.

5.5.2.2 Anthropogenic species over BoB

The mean mass concentration of anthropogenic species SO_4^{2-}, NO_3^-, NH_4^+ and BC observed over BoB were 8.8±6.3μg m^{-3}, 3.1±2.6μg m^{-3}, 2.40±2.3μg m^{-3} and 2.41±1.7μg m^{-3} respectively. The spatial maps of these anthropogenic components are shown in Figure 5.6. The abundance and the seaward extent of the loading of these species (shown in red and yellow colours) clearly show their intrusion from the anthropogenically active landmass and the coastal regions to a fairly long distance of oceanic environment (few hundred kilometres). Peak concentrations of anthropogenic

species are observed over the north-BoB, the mean concentration being 19.5μg m^{-3} for SO_4^{2-}, 6.5μg m^{-3} for NH_4^+,7.7μg m^{-3} for NO_3^- and 5.5μg $m^3$for BC. This is attributed to the transport from the highly polluted IGP regions as revealed from the wind pattern in Figure 5.2a and the air mass back trajectories reaching north-BoB (Figure 5.4). A hot spot is seen for SO_4^{2-} near the port of Chennai (marked as A in Figure 5.1), a metropolitan city and a major port.

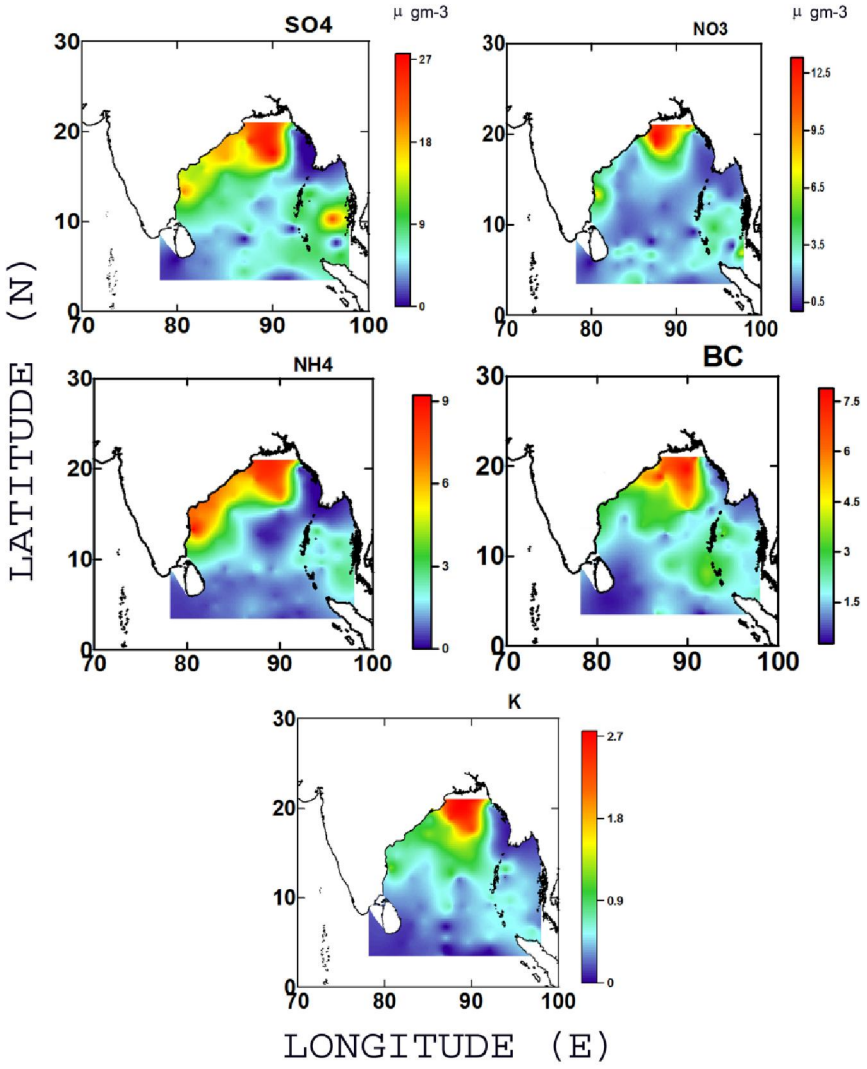

Figure 5.6. *Spatial distribution of mass concentration of anthropogenic species SO_4^{2-}, NO_3^-, NH_4^+ and BC (in μg m^{-3}) along with K (tracer for biomass burning) over BoB.*

Another notable feature is that these species show dominance over southeast-BoB also, even though their mass concentrations (8.5μg m^{-3} for SO_4^{2-}, 1.6μg m^{-3} for NH_4^+, 2.5μg m^{-3} for NO_3^- and 2.9μg m^{-3} for BC) are less than those over north-BoB. The air mass reaching this region is of different type since their origin is Southeast Asia, as seen from trajectories shown in Figure 5.4. The spatial distribution of NO_3^- is more or less similar to the other components but it shows more spread towards

southwest-BoB (coast) probably due to diverse sources of this species, which include biomass burning, fossil fuel combustion, industrial processes, soil re-suspension etc. Moreover high levels of NO_2 emissions are observed along the international ship route along ~6º N latitude. Also, NH_4^+ is observed high close to coastal regions and very low over southern and mid BoB, probably due to the short life time of this species.

The major source of K^+ is biomass burning, with soil dust, sea-salt, coal fire and industrial activity as secondary sources [*Zhang et al*., 2013; *Zong et al*., 2016]. The mean concentration of K^+ over BoB is observed as 0.65±0.5µg m^{-3}. It peaked over north BoB and extends a fairly large distance to the oceanic environment. Southeast-BoB lying in the downwind region of Southeast Asia also shows relatively high values of K^+ (0.35 to 0.75µg m^{-3}).

As K^+ has sources other than biomass burning, a ratio of K^+ to BC is a better measure than the concentration of K^+ alone to identify the source [*Andreae and Merlett*, 2001]. K^+/BC values between 0.1 and 0.6 are suggested to identify biomass burning [*Andreae and Merlett*, 2001]. K^+/BC ratio of ~0.5 and 0.3 are observed over north and south-BoB respectively, indicating dominant contribution of biomass burning emissions transported to these regions. This analysis again highlights the intense pollution of north-BoB and moderate pollution over southeast-BoB by aerosols from near-by continents. While the trace gases like O_3 and CO showed comparable mixing ratios over north BoB and southeast-BoB [*David et al*., 2011; *Girach and Nair*, 2014] aerosol loading over southeast-BoB was lower than that over north-BoB.

5.5.2.3 Crustal species over BoB: Fe enrichment in soil dust

Significant amount of Al and Fe source of which is soil dust were detected in the samples collected over BoB region with maximum values close to the eastern coast of India as seen from Figure 5.7. Unlike the anthropogenic species, concentrations for Fe and Al are less prominent over north-BoB. And the noticeable hotspots in crustal species were away from the Indian coast (centered on 16° N, 85° E) and protruding to the mid-BoB. These hot spots are not due to direct advection from the near-by land mass. Such isolated high can occur when long range transport of air mass from arid/semi-arid regions becomes strong and subsequent subsidence occurs at isolated regions. Analytical studies done earlier have shown that long range transport of air mass from IGP over to BoB and localised downdrafts and convergence leading to piling up of aerosols, away from coast which has resulted in high aerosol optical depths [*Aloysius et al*., 2008; *Prijith et al*., 2012]. During the present study, the airflow pattern

also reveals presence of transport over to BoB (Figure 5.2). The isolated high in crustal species Fe and Al is an evidence of long-range transport of mineral/soil dust to this oceanic region. Over south-BoB notable levels of Fe and Ca are observed but Al is not observed, suggesting different types of soil dust present over here.

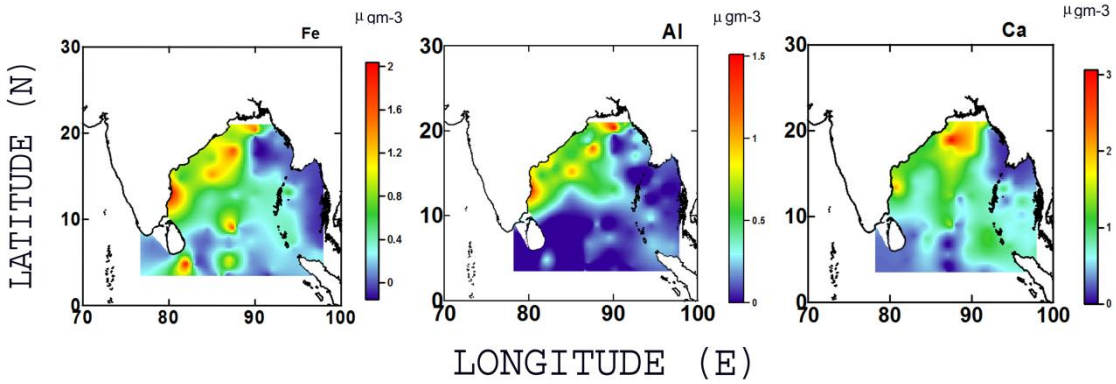

Figure 5.7. *Spatial variation of mass concentration of crustal species Fe, Al and Ca in μg m^{-3}over BoB.*

Figure 5.8a shows the scatter plot between Fe and Al along with the straight line representing the best fit obtained by linear regression analysis. It is clear that Fe and Al are well correlated (with correlation coefficient of 0.88 as shown in the figure) indicating that both species have same or similar sources, which is soil in this case. The slope of the best-fit line yields the Fe/Al mass ratio as 1.15 which is well above the mean crustal ratio 0.44 [*Taylor and McLennan*, 1995]. These high ratios indicate enrichment of Fe in the soil over Indian region. Earlier studies over the land also have revealed this feature with 1.4±0.4 over coastal site Thiruvananthapuram and 1.7±0.2 over Kharagpur [*George et al*., 2008, 2011].

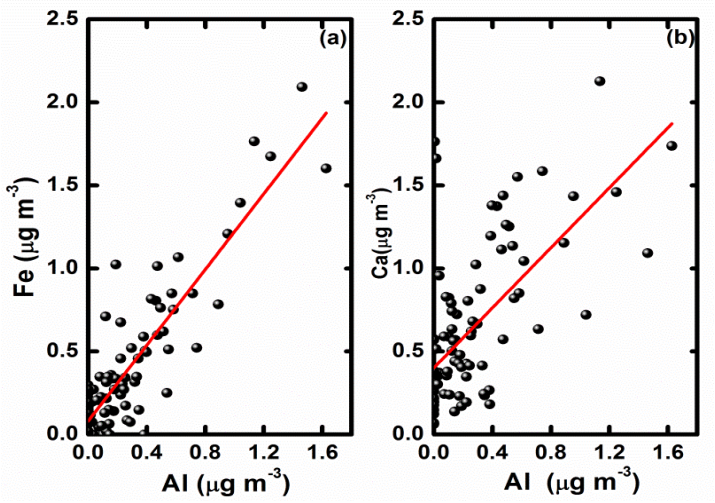

Figure 5.8. *Scatter plot of (a) Al against Fe and (b) Al against Ca.*

A scatter plot of Ca, which is mostly of soil origin, against Al is shown in Figure 5.8b along with the best fit line.

The slope of the best fit line in Figure 5.8b gives the Ca/Al ratio as 0.87 with a correlation coefficient of 0.68, suggesting soil dust as a major source of Ca. The ratio is also higher than the global mean upper crustal ratio (which is 0.38). The study conducted over BoB during pre-monsoon season also gives a Fe/Al ratio of 1.1±0.2 which is comparable to the present study while the Ca/Al ratio 1.7±0.4was higher.

Region	Period of study	Fe/Al	Ca/Al	Reference
Thiruvananthapuram	2003-2005	1.4±0.4	1.7±0.5	George et al., 2011
Bay of Bengal	March-April 2006	1.1±0.2	1.8±0.5	Nair et al., 2014
Arabian Sea	April-May 2006	0.51±0.05	0.89±0.27	Kumar et al., 2008
Mt Abu	Jan07-Feb07	0.6±0.14	1.1±0.3	Kumar and Sarin 2009
Bombay	March-May2001	0.57±0.3	1.2±0.3	Venkataraman et al., 2002
Ahmedabad	Dec2006-Jan2007	0.53	1.15	Sudheer and Rangarajan 2012
Kharagpur (IGP)	Dec 2004	1.7±0.2	1.7±0.3	George et al .,2011
BoB	Jan2009	1.15	0.87	Present study

Table 5.2. *Fe/Al ratio measured over Indian landmass and the adjoining marine environment.*

Table 5.2 presents the Fe/Al and Ca/Al ratio measured over Indian landmass and the adjoining marine environments. The high Fe/Al ratios reveal that aerosols over these regions are enriched with Fe.

5.5.2.4 Carbonaceous aerosols

The carbonaceous aerosols comprising of EC or BC and organic species form major contributor to the total aerosol content in all geographical areas and measurement of these species in the tropical oceanic regions is sparingly done. In the absence of measurements of organic species, the organic fraction of aerosols is often estimated by making use of empirical relations involving BC or EC and OC as discussed in Chapter3 and 4. BC data from aethalometer operated in this cruise [*Babu et al*., 2012] along with OC and EC data collected during the same cruise by *Srinivas et al.* [2011] is used in the present study. The total Particulate Organic Matter or POM is estimated as POM =k * OC [*Turpin and Lim* 2001; *Xing et al.,* 2013], where k is the average organic molecular weight per carbon weight which have values from 1.2 to 2.6 depending on sources. *Turpin and Lim,* [2001] suggested that aerosol heavily impacted by biomass burning

can have a higher organic matter to organic carbon ratio (2.2–2.6). In this analysis, in view of the fact that BoB is highly impacted by biomass burning as revealed by the high mass concentration of K and the K/BC ratio (Section5.5.2.2), k value of 2.4 is used to estimate POM. This is higher than that used for TVM in Chapter 3 and for BoB in pre-monsoon (Chapter 4).

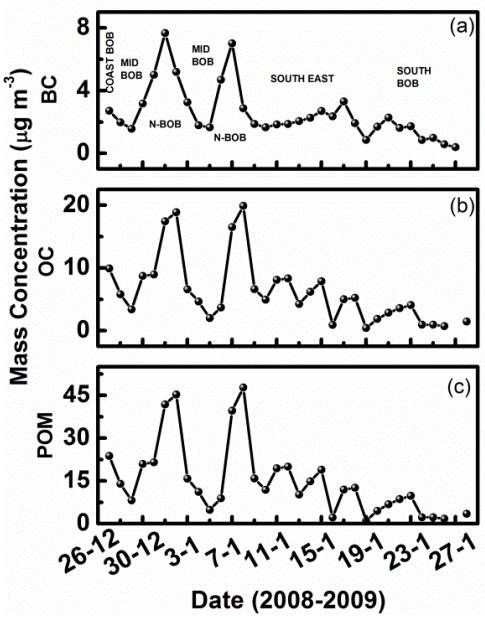

Figure 5.9. *Variation of BC, OC and POM along the cruise track (day to day basis).*

In Figure 5.9 is plotted the day-to-day variation of BC, OC and POM, along the cruise track with different regions marked in the top panel. It is seen that all the carbon containing species also peaked over north-BoB (peaks corresponding to Jan 01 to 03 and 06 to 07) with maximum values of ~8μg m^{-3} and 20μg m^{-3} for BC and OC respectively, POM showed maximum upto 46μg m^{-3} over north-BoB. The spatial pattern of BC is also shown in the figure. The prominent peak in BC appears over north-BoB. It also shows secondary high over southeast-BoB, where the arrival of air mass is from southeast Asian region (where regions of biomass burning/frequent forest fire exists). The BC measured over BoB is extremely high reaching 8μg m^{-3} over north-BoB with the mean value being 2.5±1.2μg m^{-3}. This is comparable to those over polluted urban locations like Ahmedadad (0.21-10.02μg m^{-3}) [*Ramachandran and Rajesh,* 2007], Hyderabad (0.5-16μg m^{-3}), Mumbai (12.4±5.6μg m^{-3}), Beijing (8.7-10.1μg m^{-3}) and Seoul (4.86-9.86μg m^{-3}), again revealing the continental pollution of marine environment.

5.6 Chlorine depletion

From the spatial pattern of Cl^- (Figure 5.5) an important feature observed is the extremely low values at several locations particularly close to coastal areas and north-BoB. This chloride deficit was found to be correlated with the proximity to continental landmasses and the concentrations of acidic pollutants such as SO_4^{2-} and NO_3^- [*Sturges and Shaw*, 1993]. Recent studies have shown that Na^+ in aerosols may contain a minute fraction of crustal component given as 0.1 M_{Al} where M_{Al} denote the mass concentration of Al in aerosol sample [*Chiapello et al.,* 1999]. This crustal fraction was estimated and subtracted from the mass concentration of Na^+ to get the sea-salt Na^+. A scatter plot of sea-salt Na^+ and Cl^- is shown in Figure 5.10 along with the best-fit line which has a slope of 1.10±0.07 with correlation coefficient of 0.85. The low Cl^-/Na^+ ratio presented by the slope implies that considerable chloride depletion has occurred. Depletion arises due to the reaction of Cl^- with the acidic species SO_4^{2-} and NO_3^- liberating HCl thereby producing halogen radicals [*Clegg and Brimblecombe*, 1985].

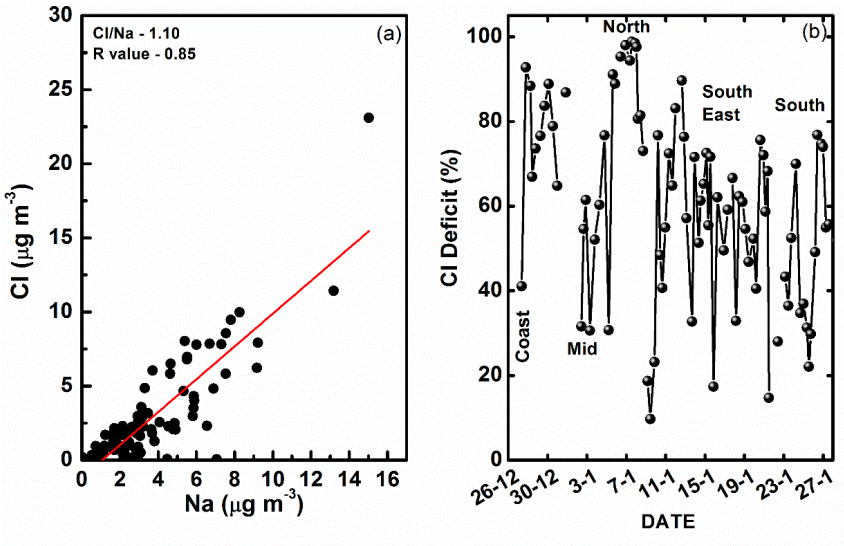

Figure 5.10. *(a) Scatter plot of Na Versus Cl (b) Percentage Cl deficit (%) along the cruise track, with the regions marked.*

The reaction sequence is envisaged as reaction of H_2SO_4 or HNO_3 with sea-salt particles releasing HCl in gaseous form, for example,

$$H_2SO_4(g) + 2NaCl\ (p) = 2HCl\ (g) + Na_2SO_4(p)$$

$$HNO_3 + NaCl = HCl + NaNO_3 \qquad 5.1$$

where g and p denote gaseous and particulate (solid) phase.

The chloride deficit in aerosol samples (compared to seawater) is estimated from the measured concentrations of Na^+ and Cl^- as [*Quinn et al*., 2000],

$$\%Cl^{-}\ depletion = \frac{1.8[Na^{+}]_{meas} - [Cl^{-}]_{meas}}{1.8[Na^{+}]_{meas}} \times 100\% \qquad 5.2$$

where 1.8 is the ratio of concentrations of Na^+ and Cl^- in sea water.

The estimated Cl^- deficit for each sample is shown in Figure 5.10b. The values ranged in between 10% to 98% with highest deficit observed over the north-BoB which is strongly influenced by the outflow from IGP region (Section5.3) where the anthropogenic species SO_4^{2-} also showed highest values (Section 5.5.2.2). For few samples, the Cl^- deficit percentage is less than 40% which mostly correspond to the south-BoB, where the winds were strong resulting in production of sea-salt aerosols. Over the southeast-BoB substantially influenced by the polluted air mass from South East Asia, ~70% of chlorine depletion was observed. Such depletion has been reported from many other polluted environments also [*Johansen et al*., 2000; *Quinn et al*., 2000; *Eleftheriadis et al*., 2006]. Most of the oceanic environments show percentage Cl^- depletion > 50% with seasonal dependence attributed to various causes. *Johansen et al*., [1999] observed Cl^- deficit of 15±9% for inter monsoon over the northern Indian Ocean. Observations over South China Sea showed a size dependent chlorine depletion with finer particles (86%) getting depleted more than coarse mode (29%). Studies over Arctic, Mediterranean and Arabian Sea showed a seasonal dependence of chlorine depletion decided by the pollution level of the environment. The mean percentage depletion over BoB also showed seasonal variation with comparatively higher depletion for winter season (present study) than the pre-monsoon period which is 65.7 ±23.3% [*Nair et al.,* 2014]. This seasonal difference arises due to the difference in concentration of acidic species like SO_4^{2-}, of both natural and anthropogenic origin.

5.7 Sea-salt (ss) and non-sea-salt (nss) components

Even though sea-salt (ss) is a major constituent of oceanic aerosols, the intrusion of continentally influenced species to the oceanic environment due to transport demands the delineation of sea-salt (ss) and non-sea-salt (nss) component in the specific oceanic environment. It is also known that the chemical species like SO_4^{2-}, Ca^{2+}, Mg^+ and K^+, have both ss and nss fractions. The ss and nss fractions of each of these species are estimated based on equation 3.4 in Chapter 3.The spatial variations of the mass concentrations of both ss and nss components are shown in Figure 5.11. The mass concentrations of nss components are 3-5 times that of ss counterpart as can be seen from Figure 5.11, thus revealing the dominance of nss components throughout

BoB. The nss-SO_4^{2-} is the major tracer for anthropogenic activity and nss-K^+ is that of biomass burning. The spatial patterns of the nss components of all these species (Figure 5.11) are more or less similar to that of anthropogenic or crustal species (Section 5.5.2.2 and, Figure 5.6 and 5.7). The percentage contribution of the nss components (M_{nss}/m_x) of all the major species are also listed in Table 5.1. The contribution of nss-SO_4^{2-} ranges from 95-98% over north-BoB and coastal regions, reduces to 88% over mid BoB and 74-83% over south and southeast-BoB.

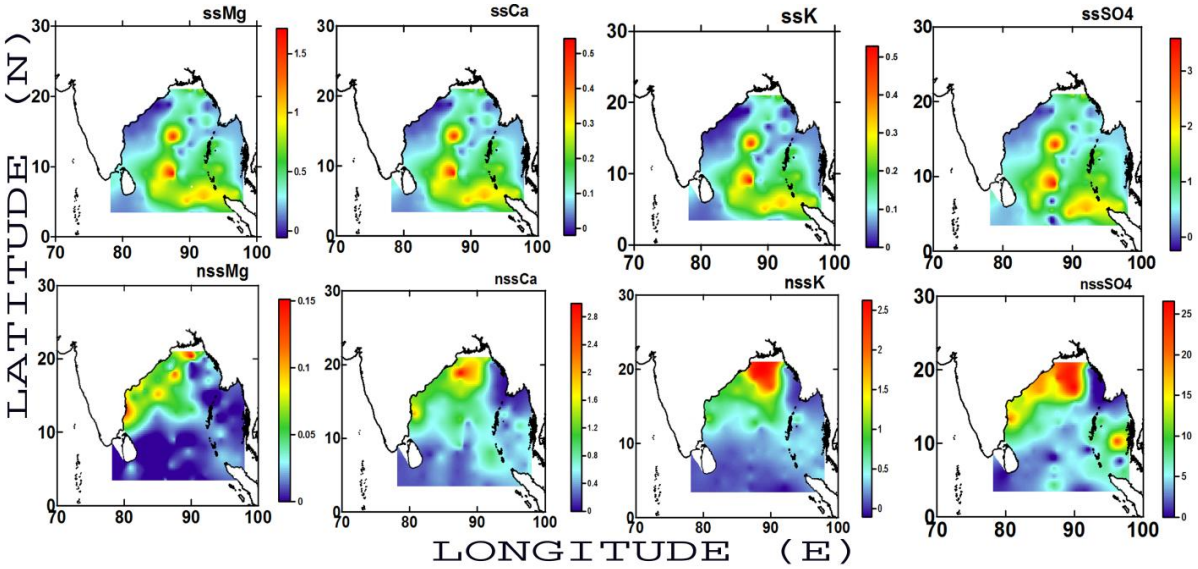

Figure 5.11. *Spatial variation of mass concentration of sea-salt and non-sea-salt components of various species over the marine environment of BoB in µg* m^{-3}.

Another striking feature is that the spatial patterns of all the ss components of Ca^{2+}, K^+, Mg^+ and SO_4^{2-} estimated show patterns similar to that of Na^+, Cl^- and Mg^+ (as seen in Figure 5.5) with highest levels over south-BoB and minimum over coastal regions and north-BoB. Apart from the individual species, an approximate estimate of total sea-salt component (M_{ss}) in the marine environment has also been made by using Na^+ as the reference species for sea-salt as [*Quinn et al.,*2002],

$$M_{ss} = M_{Cl} + 1.47 \times M_{Na} \qquad 5.3$$

where 1.47 is the sea water ratio of $(Na^+ + Mg^+ + Ca^{2+} + K^+ + SO_4^{2-} + HCO_3^-)/Na^+$ and the non-sea-salt component M_{nss} is estimated as,

$$M_{nss} = M_L - M_{ss} \qquad 5.4$$

In Figure 5.12a is given the variation of M_{nss} and M_{ss} along the cruise track (date wise) and Figure 5.12b depicts the percentage contribution of M_{nss} and M_{ss} over the cruise region. The dominance of nss aerosols over the marine environment of BoB, in particular the northern parts is clear, with the highest values of about 120µg m^{-3}

which contributed upto ~99% of total mass loading. Southeast part of BoB (where the ship was cruising from Jan11 - 18), anthropogenically influenced from the potential source regions of East Asia, was observed with an average of 80% nss component. As the cruise proceeded to southern part of BoB, away from the source regions, the nss contribution started decreasing with percentage values lying between 70 and 40% and the ss contribution started increasing.

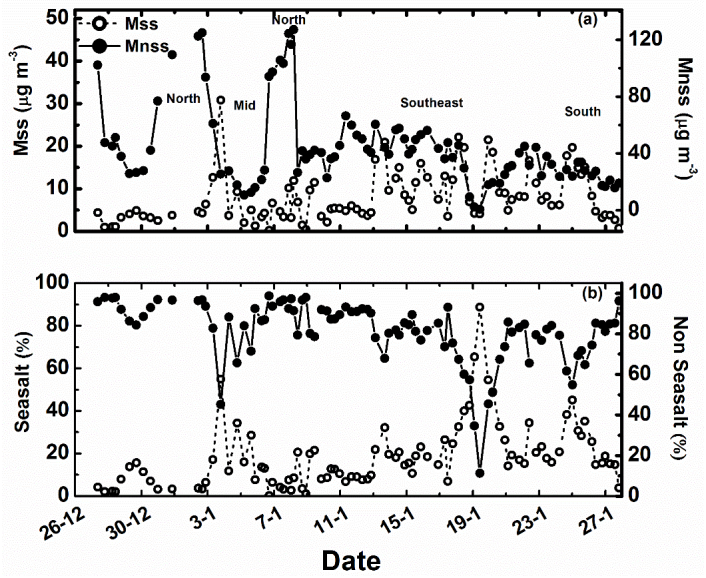

Figure 5.12. *(a) Variation of total sea-salt (dotted lines) and non-sea-salt (solid line) component and (b) Percentage contribution of total sea-salt and non-sea-salt over the cruise region.*

Throughout BoB, the nss component of aerosol mass varied from 40-99% apart from the very low values seen on 19 January which is due to a rain event. In pre-monsoon season also, BoB is dominated by nss component, varying from 41 to 95% [*Nair et al.*, 2014].

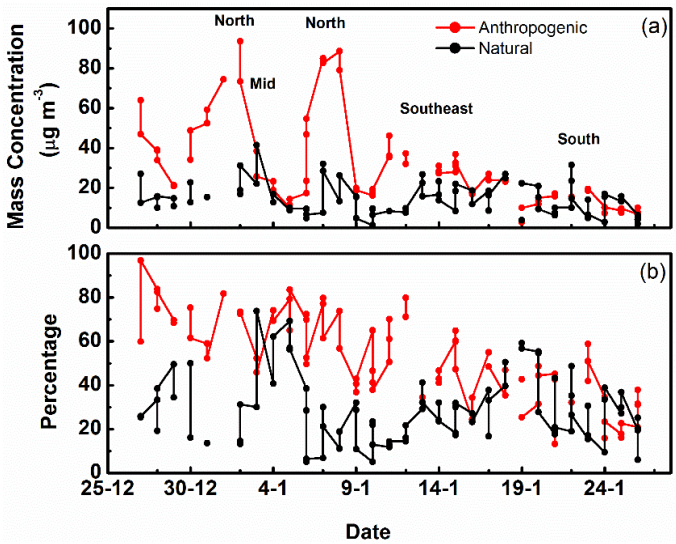

Figure 5.13. *(a) Variation of natural and anthropogenic component in aerosols over BoB and the (b) Percentage contributions of natural and anthropogenic components.*

The mass concentrations of the natural and anthropogenic components in aerosols and their percentage contributions in winter season over BoB were estimated as discussed in Section 4.5.3 of Chapter 4 and presented in Figure 5.13. Dominance of anthropogenic component is seen throughout BoB with highest values over north-BoB. The percentage contribution of anthropogenic aerosols decreases, from north to south, while its natural counterpart increases over the south-BoB.

5.8 Role of wind

An examination of the spatial pattern of aerosol mass loading in Figure 5.3b and the air flow pattern in Figure 5.2a reveals that the winds are strong over southern BoB and the observed high aerosol mass loading has some bearing on the wind speed. The high concentration of sea-salt species (Na, Cl, etc.) over this region (south-BoB) also supports this. On the contrary, the chemical composition of aerosols over north-BoB and southeast-BoB indicates the dominance of the soil dust/crustal and anthropogenic species. In this context, role of wind in sea-salt production was investigated by considering only the southern part of BoB.

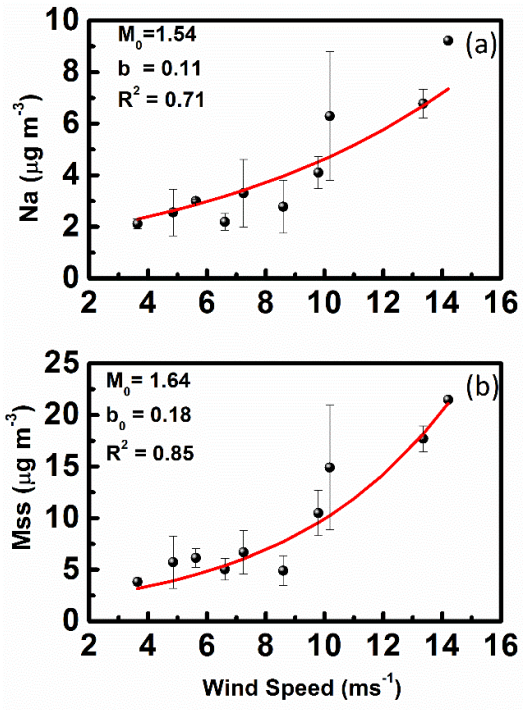

Figure 5.14. *(a) Scatter plot of mass concentration of Na against wind speed along with the fitted curve (b) Scatter plot of mass concentration of Mss against wind speed along with the fitted curve.*

The estimated mass concentrations of Na (tracer for sea-salt) has been grouped in terms of wind speed bins of 2ms^{-1}and averaged. The maximum wind speed observed over this region during sampling was 14ms^{-1}. In Figure 5.14a is shown a scatter plot of

mean mass concentration of Na (M_{Na}) against wind speed. The figure obviously shows increase in the mass concentration of Na with wind speed, in an exponential fashion. This data has been fitted with an exponential function of the form $M_{Na}=M_{01}\ e^{b1U}$ where U is the wind speed, and M_{01} and b_1 are constants. The solid lines in Figure 5.13a represents the fitted curve with b=0.11 and M_{01} =1.54. A similar scatter plot was obtained between U and M_{ss} (total mass loading of sea-salt aerosols discussed in Section 5.6) and shown in Figure 5.14b. This also follows an exponential dependence $M_{ss}= M_{02}\ e^{b2U}$ between U and M_{ss} with b_2=0.18 and M_{02}= 1.64. M_{02} is the measure of background sea-salt aerosol loading.

Several studies on the dependence of aerosol properties like mass loading, number density, optical depth, etc. on wind speed are available in literature. Table 5.3 summarizes the studies conducted over the major oceanic regions during different periods and the major results on the wind dependence of aerosol characteristics for a comparison.

Region	**Parameter**	**Relationship with Wind speed**	**b**	**M_0 or N_0**	**Reference**
Pacific	Mass concentration	Exponential ($Mss=M_oe^{bU}$)	0.16	2.57	Woodcock(1953)
Pacific	Mass concentration	Exponential ($Mss=M_oe^{bU}$)	0.1	Not given	Quinn et al. (2000)
Atlantic	Mass concentration	Exponential ($Mss=M_oe^{bU}$)	0.16	1.61	Lovett(1978)
Atlantic	Number concentration	Exponential ($N_{ss} = N_oe^{bU}$)	0.16	-4.8	Smith et al., (1989)
Indian ocean	Mass concentration	Power law ($M_{ss} = M_0U^b$)	0.64	2.2	Nair et al., (2005)
N-E Atlantic	Number concentration	Exponential ($N_{ss} = N_oe^{bU}$)	0.10	1.46	O'Dowd (1993)
N-E Atlantic	Number concentration	Exponential ($N_{ss} = N_oe^{bU}$)	0.16	Not given	De Leeuw (1986)
Arabian Sea coast	Number concentration	Exponential ($N_{ss} = N_oe^{bU}$)	0.10	Not given	Parameswaran et al., (1995)
Indian Ocean	AOD	Exponential $\tau =\tau_0 e^{bU}$	0.08	0.04	Parameswaran et al.,(2008)
Minicoy	AOD	Exponential $\tau =\tau_0 e^{bU}$	(0.05-0.11)	1.19	Moorthy and Satheesh, (2002)
S- Bay of Bengal	Mass concentration	Exponential ($Mss=M_oe^{bU}$)	0.18	1.64	(Present study)

Table 5.3. *Studies conducted on wind dependence of aerosol characteristics over the major oceanic regions during different periods with their respective observed relationships and b, M_0/N_0values.*

5.9 Spatial variation of mass fractions of ionic species

The mass fraction of each chemical species as explained in Chapter 4 Section 4.5.1.5is an effective parameter in understanding the impact of specific sources and their radiative forcing implications. The spatial patterns of the mass fractions of the various species are depicted in Figure 5.15.

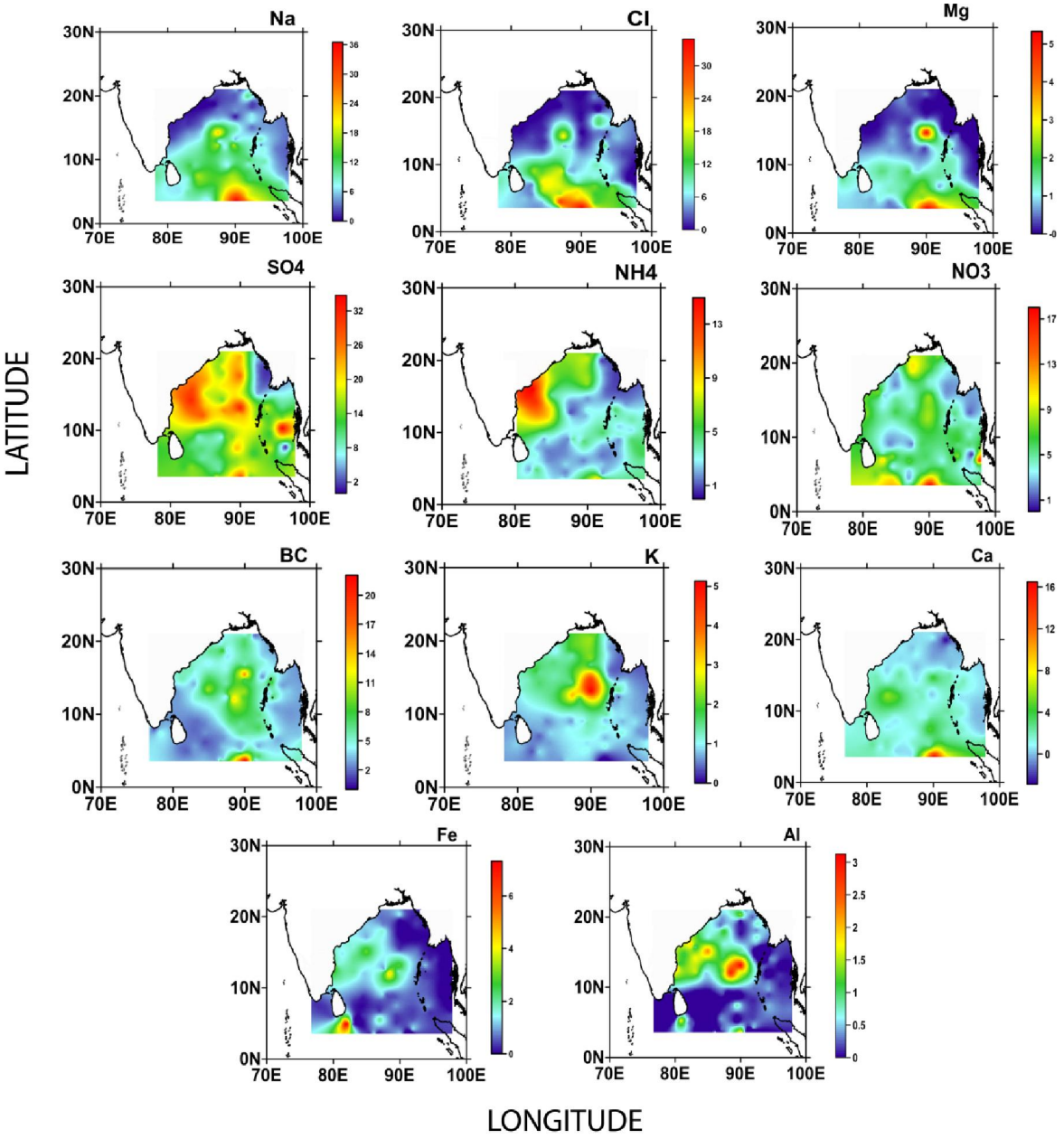

Figure 5.15. *Spatial variation of mass fractions (in %) of various chemical species over BoB during winter.*

The mass concentration (shown in Figure 5.11) as well as mass fractions of all sea-salt ions (Na^+, Cl^- and Mg^+) show similar spatial pattern with high over south-BoB. While the mass concentration of anthropogenic species like SO_4^{2-}, NH_4^+, and NO_3^- peaks over north-BoB, the mass fraction peaks close to coast of India (west-BoB) and

over southeast-BoB. NO_3^- fraction was found high towards the south-BoB and regions close to the landmass. Compared to other components SO_4^{2-} has significant contribution over the entire BoB.

The crustal components (Al and Fe) also show distinct spatial patterns for mass concentration and fraction. While mass concentration of Al and Fe peaked over east coast of India, mass fraction showed a hotspot over mid/southeast-BoB in addition to the coastal high. BC and K^+ showed similar spatial patterns with mass concentration showing high over north-BoB and mass fraction peaking over mid-BoB and towards southeast-BoB. The similar pattern of these species implies that biomass burning is a major source of these species. Since the cumulative radiative effect of aerosols depends on the relative contribution of absorbing and scattering aerosol species, mass fractions of individual species has significance in radiative forcing estimations.

5.10 Effect of rain: a case study

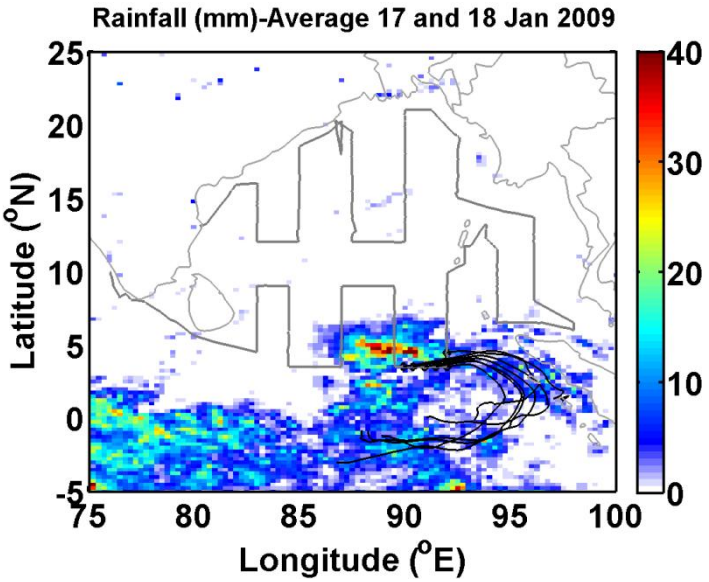

Figure 5.16. *Daily accumulated rain on January 17 and 18, 2009 from TRMM with cruise track and air mass back trajectories over the region.*

Rain events form the most important removal process of aerosols through rain out or wash out mechanism. During the cruise period one such rain event occurred on January 18.The spatial record of the rainfall on January 17 and 18 by The Tropical Rainfall Measuring Mission (TRMM) is shown in Figure 5.16. The daily rainfall is derived from the 3-hourly product using 3B42 algorithm, with 0.25°×0.25°spatial resolution (disc.sci.gsfc.nasa.gov). About 15mm of accumulated rain was recorded near

and along the cruise track. Back trajectories reaching the cruise track on January 18 show that the air parcels are originating from the ocean (Figure 5.16).

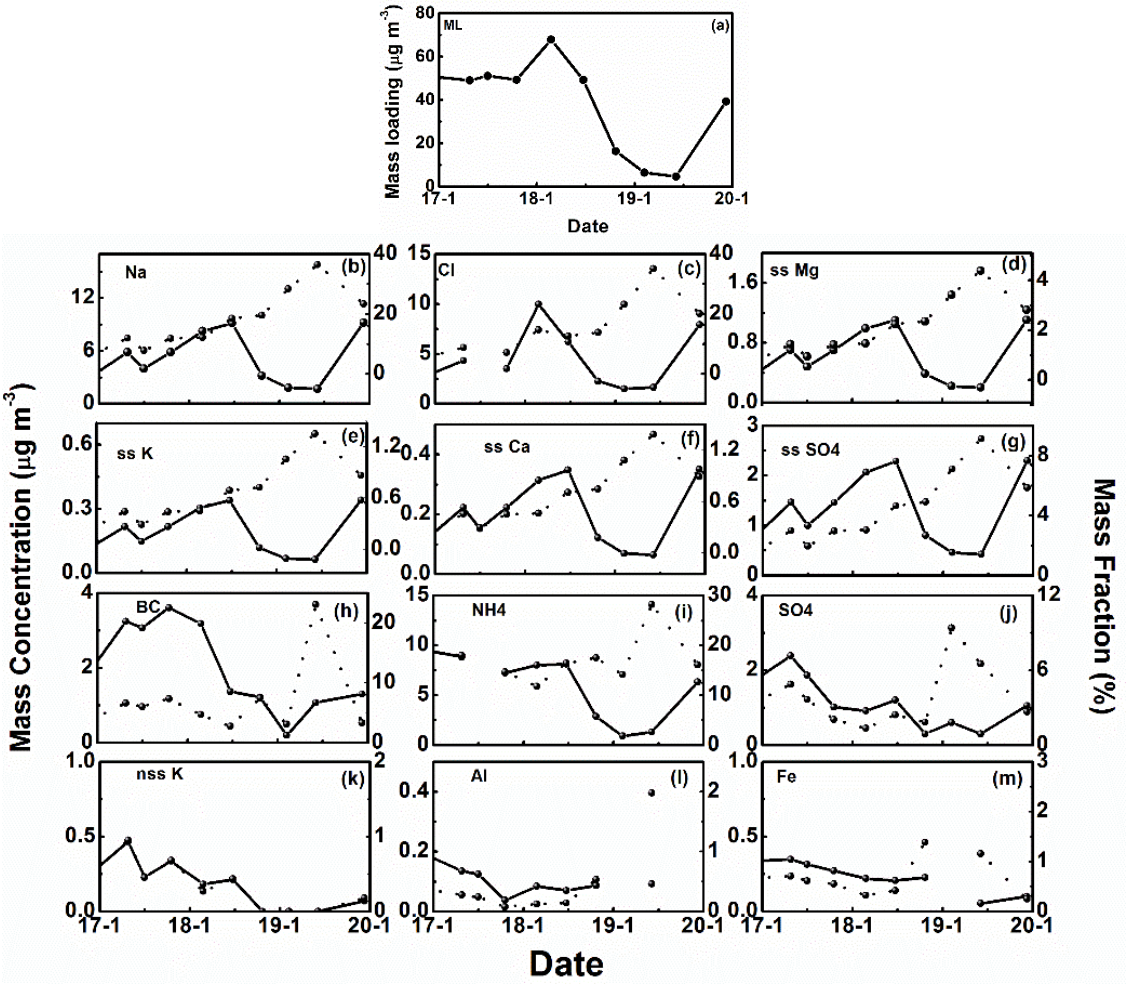

Figure 5.17. *(a) Effect of rainfall on the aerosol mass loading, (b to m) effect of rainfall on the mass concentrations (solid line) and mass fractions (dotted line) of various species.*

In Figure 5.17a is shown the temporal changes in aerosol mass loading from Jan 17 to 20.This figure obviously depicts the depletion of aerosol mass immediately after the rain which occurred on January 18. The mass loading decreased from 40μg m^{-3} to 6μg m^{-3}depicting 85% reduction. In order to examine whether the wash out process has any bearing on different species, the mass concentrations as well as the mass fractions of individual species were examined. The mass concentrations of most of the species showed depletion after rain. But the changes observed in the mass fraction of various species showed difference. This indicates that rain induced removal of aerosols need not be uniform for all chemical species; instead, it can be species dependent. In Figure 5.17b to g are shown the changes in the mass concentration of oceanic species Na^+, Cl^- and the ss components of SO_4^{2-}, K, Ca, and Mg along with that of their respective mass

fractions prior to and after the rain event. While the mass concentration of these species decreased after rain, the mass fraction increased. The increase in mass fraction is due to decrease in total loading (M_L) while the mass concentration of individual species remaining same or high. In this case, it is possible that associated with rain, strong winds also prevailed over the region which produced sea-salt aerosols. On the other hand, for anthropogenic/crustal species BC, SO_4^{2-}, NH_4^+, nss-K, Al, and Fe (Figure 5.17h to n), both mass concentration and mass fraction show similar variations. The percentage reduction in the mass concentration of species like SO_4^{2-}, NH_4, NO_3 and K were found to be 78%, 72%, 68% and 76% respectively and for Al and Fe it was <25% while marine species like Cl^- and Na showed ~70% depletion indicating that rain removal is species dependent. The concentration of Al and Fe were very low prior to rain and hence their changes are not very prominent. As the study area was away from the continental source regions, the anthropogenic species present over the region was transported from adjoining continents. And these species were directly washed out by rain resulting in decreased mass concentration and thereby the mass fraction. Another important inference is that, over the oceanic environment, even though rain depletes aerosols, wind induced sea spray production can cause increase in total aerosol mass loading and sea-salt aerosols.

5.11 Region specific composition of aerosols over BoB

The estimated aerosol chemical species are grouped as (1) Sea-salt (SS), (2) Water Soluble Non-sea-salt(WSN) (3) Mineral dust (MD) (4) POM (Particulate Organic Matter) and (5) Black Carbon (BC)as discussed in section 3.7 in Chapter 3.These aerosol components were grouped and averaged for each of the five regions mentioned in Section 5.5. The pie charts in Figure 5.18 show the region wise distribution of these aerosol components over BoB.

Water soluble non-sea-salt component (WSN) showed significant contributions over BoB (39% for coast, 33% for north, 31% for southeast and 36% for mid) except for south-BoB (19%). SS contribution over this marine region was relatively low being 10-16% over north, mid and southeast-BoB with a minimum of 3.6% over coastal regions. Largest SS contribution is observed over south BoB (~29%). Mid and coast-BoB showed MD contributions as ~18% and 14% respectively as these regions are influenced by long range transport from IGP.

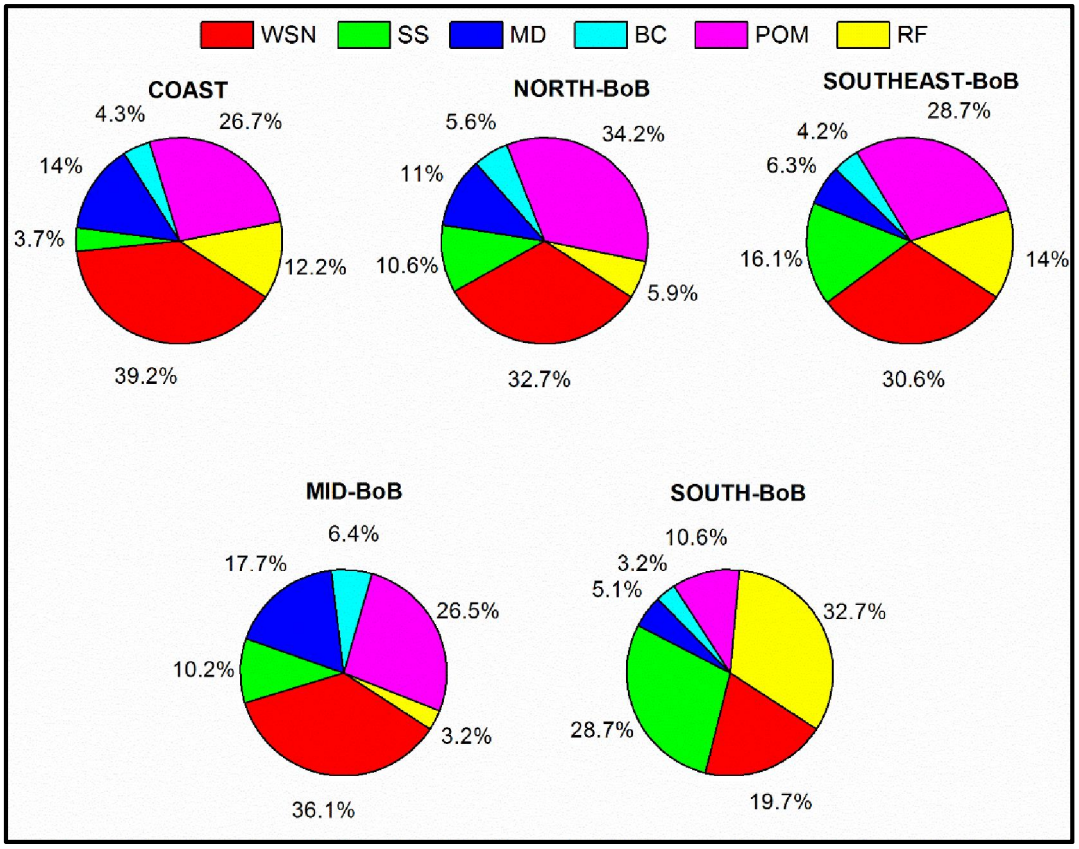

Figure 5.18*.Contributions of SS, WSN, MD, POM and BC components over different regions over BoB.*

The contributions of MD (5%), BC (3%) and POM (10%) were very less over South BoB compared to other regions. Interestingly the residual fraction is highest (28%) over this region (whereas it remained 5-14% over other regions). This could be probably due to the under-estimation of POM over South BoB.

5.12 Radiative properties

Based on the mass concentration of different aerosol components discussed above and using OPAC model, the major optical/radiative properties of aerosols were estimated for the wavelength regime 0.4 to 1.0μm for the five regions. The scattering and absorption coefficients were highest over the north BoB (0.22km^{-1} and 0.045km^{-1} respectively) followed by the coast (0.15km^{-1} and 0.025km^{-1} respectively) at 0.5μm wavelength, indicating the abundance of both scattering and absorbing aerosols over these regions. These values are higher than those observed during pre-monsoon over BoB (Chapter 4). The minimum in scattering, absorption and extinction coefficient is seen over south BoB. Measurements done for scattering and absorption coefficients

with nephelometer and aethalometer onboard the ship also depicted very high values (>0.20 and >0.015 km^{-1}) over the north-western BoB [*Babu et al.,* 2012]. Lower values of β_{sc} *and* β_{ab} were observed over mid (0.1km^{-1} and 0.012km^{-1}), south (0.065km^{-1} and 0.01km^{-1}) and southeast-BoB(0.09km^{-1} and 0.018km^{-1}) [*Babu et al*., 2012].

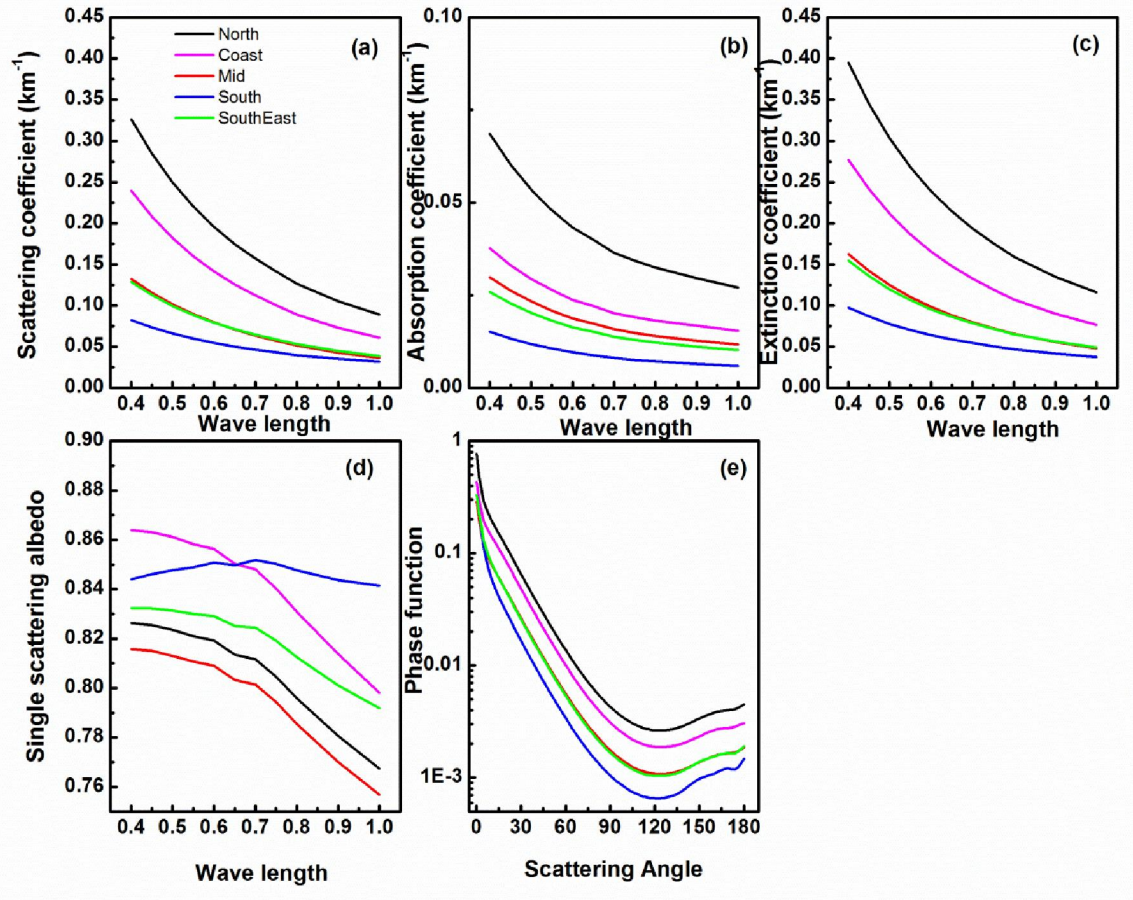

Figure 5.19. *Spectral variation of scattering coefficient, absorption coefficient, extinction coefficient, SSA and Phase Function over the five different regions over BoB.*

Single scattering albedo, an important parameter in the calculation of radiative forcing was found to be in range of 0.83-0.86over SE and south BoB. Over mid-BoB and north-BoB it was <0.82 with minimum over mid BoB (0.760to 0.815). Phase function attain minimum at ~120˚ with regional differences. *Babu et al.,*[2012]observed very low values (<0.8) over the mid-BoB and moderately low values over the south-BoB (0.85–0.9)based on measurements using nephelometer and aethalometer. This low value over mid-BoB is due to the increased mass fraction of absorbing species (BC and Mineral Dust) contributing more to absorption than scattering.

5.13 Summary

The ship-based measurement of total aerosol mass loading and the mass concentration of various chemical species over the entire marine environment of BoB covering South east part during winter for the first time revealed the following features.

(1) Spatial distribution of total aerosol mass loading showed two prominent high regions one over north BoB and other over SE-BoB.

(2) The aerosol mass loading was minimum over the mid BoB region where an anticyclonic circulation existed. While the high over north BoB is caused by transport from the populated and industrialized IGP, that over SE BoB is due to transport from the anthropogenically active SE Asian region.

(3) The oceanic species (Na, Cl, Mg, etc), crustal species (Al and Fe) and anthropogenic species (SO_4^{2-}, NH_4^+, BC, etc) showed distinctly different spatial patterns.

(4) Sea-salt aerosol dominated over south-west part of BoB due to the action of strong winds. Wind induced sea-salt production showed an exponential relation between the mass concentration of sea-salt aerosols and wind speed.

(5) For the species like Ca, K and SO_4^{2-} having both sea-salt (ss) and non-sea-salt (nss) fractions, the ss and nss components showed distinctly different patterns, with ss component peaking over SW-BoB and nss component exhibiting maximum over north-BoB.

(6) The anthropogenic species (SO_4^{2-}, NO_3^-, NH_4^+, BC, etc) peaked over north-BoB and the crustal components were high near to the eastern coastal regions of India with isolated hotspots away from the coast. Strong anthropogenic influence is observed throughout BoB. The mass of nss aerosols contribute upto 98% over north-BoB.

(7) Over regions were acidic species like $SO_4^{2-}$and NO_3^- are dominant, strong chloride deficit was also noticed. Significant loading of anthropogenic aerosols was estimated over entire BoB.

(8) The accumulated rainfall of 15mm occurred close to cruise track produced 85% reduction in total aerosol mass loading. The rain induced depletion of aerosols was species dependent. Strong winds associated with rain replenish the sea-salt species.

(9) The percentage contributions of the major aerosol components sea-salt(SS), water soluble non-sea-salt (WSN) component, mineral dust(MD), particulate organic matter (POM) and BC over different regions of BoB were estimated and found to be region dependent.The scattering and absorption coefficients were highest over north BoB ($0.22km^{-1}$ and $0.045km^{-1}$respectively) followed by the coast ($0.15km^{-1}$ and $0.025km^{-1}$

respectively) at 0.55µm wavelength, indicating the presence of more scattering and absorbing aerosols over these regions. Single scattering albedo was found to be in the range of 0.83-0.86 over SE and south BoB, and it was <0.82 over mid-BoB and north-BoB. In spite of the low aerosol loading, the minimum values of single scattering albedo were estimated over mid-BoB.

These results points to the pollution of a near pristine marine atmosphere due to aerosol transport from near-by landmass with anthropogenic activities, which can have serious environmental and climatic impacts.

Chapter 6

Seasonal changes in the near-surface aerosol characteristics and their columnar properties over Bay of Bengal: a multi-campaign analysis

6.1 Introduction

With the high density of population and increasing industrialization, the south Asian landmass surrounding Bay of Bengal (BoB) is an important source region of many chemically and radiatively active trace gases and aerosols present over this oceanic environment as discussed in Chapter 4 and 5. Along with this, the contrasting meteorological processes, strong solar radiation and the humid tropical conditions make this oceanic region dynamically and chemically very active [*Bhat,* 2001*; Wang* 2006*; Lawrence and Lelieveld,* 2010*; Lau and Kim,* 2006*; Rao,* 1976]. Hence the aerosol characteristics over this marine environment can be attributed to emission capacity of near-by continent and meteorology. The outflow of the continental pollutants over to BoB is of serious environmental concern in view of the fact that this region plays crucial role in Asian monsoon and is frequently affected by extreme weather systems like cyclones [*Flierl and Robinson*, 1972; *Mohanty*, 1994; *Alam et al*., 2003]. Various cruise-based measurements, namely, BOBMEX (Bay of Bengal Monsoon Experiment), ICARB (Integrated Campaign on Aerosols, gases and Radiation Budget) and CTCZ (Continental Tropical Convergence Zone) campaign conducted over BoB in different seasons had brought out several results on the chemical, physical and optical properties of aerosols and gases over this region [*Bhat et al*., 2001; *Ramanathan et al*., 2001; *George et al*., 2008; *Moorthy et al*., 2008, 2010; *Nair et al*., 2008; *Sudheer and Sarin* 2008; *Babu et al*., 2012; *Nair et al*., 2014; *Aryasree et al.,* 2015]. Still the comprehensive information on aerosol characteristics available from this oceanic region is limited. Chapter 4 and 5 mainly addressed the near-surface aerosol characteristics during pre-monsoon and winter and the outflow from nearby landmass.

This chapter presents the results of a comprehensive study on the spatial and seasonal changes in the aerosol characteristics over BoB. It is based on (1) the ship-based in situ measured spatio-temporal properties of near-surface aerosols carried out as part of three major field campaigns namely: ICARB during the pre-monsoon season (March–April 2006), CTCZ in the monsoon season (July–August 2009), and second phase of ICARB conducted in winter (December 2008–January 2009) called WICARB

and (2) the columnar characteristics of aerosols namely columnar aerosol optical depth (AOD), fine-/small-mode AOD, large mode AOD, fine-mode fraction, Angstrom exponent (α), effective radius (R_{eff}), and column mass concentration (M_c) retrieved from satellite based MODIS on-board Aqua, for the same period. Most importantly, apart from the spatial and seasonal behaviour of near-surface aerosol characteristics and the columnar properties of aerosols, their mutual dependence is also investigated and results are presented.

6.2 Cruise tracks

As mentioned above, the results presented in this paper are the outcome of the ship-based measurements conducted over BoB during three seasons: pre-monsoon 2006, winter 2009 and monsoon 2009 in campaign mode as discussed above. A brief account of the cruise tracks during these campaigns is given below.

6.2.1 Pre-monsoon cruise

The first among the three campaigns was the ICARB conducted during the pre-monsoon period of March-April 2006. The details of cruise track are given in Chapter 4 section 4.2. The cruise started on 18 March 2006 from Chennai (13°N, 80.3°E) and ended on 13 April, 2006 reaching at Cochin completing its 25 days of journey over BoB.

6.2.2 Monsoon cruise

Another campaign referred as the CTCZ campaign was conducted during the monsoon period of 16 July to 17 August 2009 under the Indian Climate Research Programme (ICRP), Government of India to understand the monsoon meteorology. One of the objectives of this campaign was to explore the role of aerosols in the variability of monsoon. During this campaign also, aerosol sampling and chemical composition studies were carried out. Ship started sailing from Chennai (13.1°N, 80.3°E) on 16 July, 2009 moving towards south-east, covered latitude sector 11.0 to 21.1°N and longitude sector 80.3 to 90.1°E taking several tracks. The ship was stationary at 89° E, 19° N for fifteen days (July 22 to August 06, 2009) of time series measurements. The cruise ended on 17 August 2009 at Chennai completing 32 days of journey. The spatial coverage of this cruise was less compared to the other two.

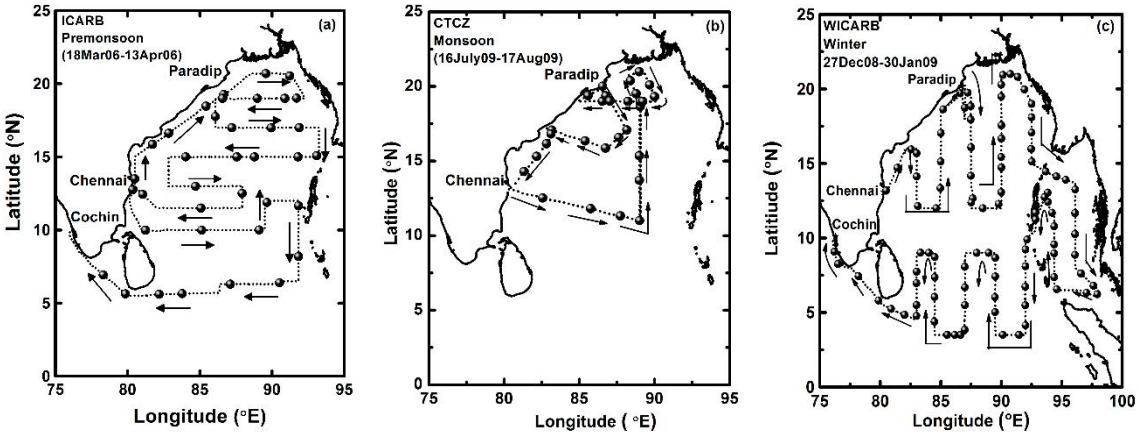

Figure 6.1. *Cruise tracks for the ship-campaigns conducted in (a) pre-monsoon (ICARB) (b) monsoon (CTCZ) and (c) winter (WICARB). Black dots represent the mean positions of aerosol sampling and the arrows indicate the direction of movement of the ship.*

6.2.3 Winter cruise

The cruise track and other details of this cruise (WICARB) is given in section 5.2 of Chapter 5. This cruise was conducted during the winter period of December 2008 to January 2009. For a comparison the cruise tracks for the three campaigns are shown in Figure 6.1a to c. In pre-monsoon, 38 samples were collected in 25 days, in winter 101 samples collected in 34 days and in monsoon 41 samples in 32 days. The mean sampling positions are also marked in the figures which show excellent spatial resolution in in situ sampling.

6.3 Meteorological background

Based on the annual pattern of meteorological parameters over Indian region, the months are grouped into four seasons namely winter (December to February), summer/pre-monsoon (March to May), monsoon (June to September) and post-monsoon (October and November) as discussed in Chapter 3. The seasonal features of aerosol characteristics examined in this study pertain to seasons of two different years, 2006 and 2009. It is noted that the broad meteorological features like airflow pattern, temperature, relative humidity (RH) etc. repeat systematically in all the years, over the Indian region [*Asnani*, 1993]. The spatial patterns of temperature, RH and airflow at 925hPa, for the months of January (representing winter), March (representing pre-monsoon) and July (typical monsoon month) for 2006 and 2009, obtained from NCEP-NCAR reanalysis are shown in Figure 6.2a to f, g to l and Figure 6.3a to f respectively.

These figures reveal the seasonal similarities in meteorological conditions irrespective of the year.

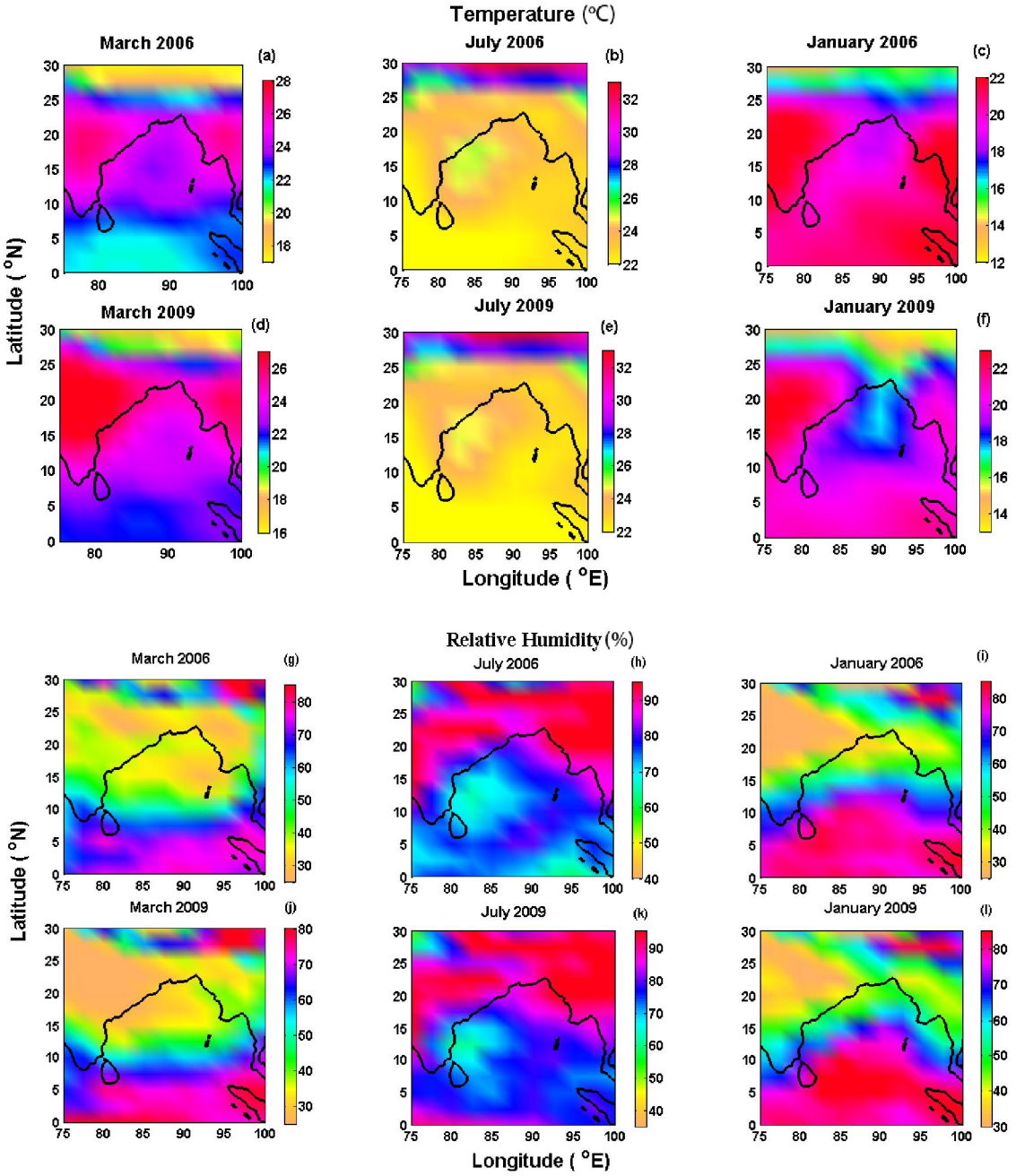

Figure 6.2. *The seasonal patterns of meteorological parameters, temperature in °C (a to f) and Relative Humidity(%) (g to l) at 925hPa over BoB for the months of March (pre-monsoon), July (monsoon) and January (winter) of 2006 and 2009 as obtained from NCEP/NCAR reanalysis data.*

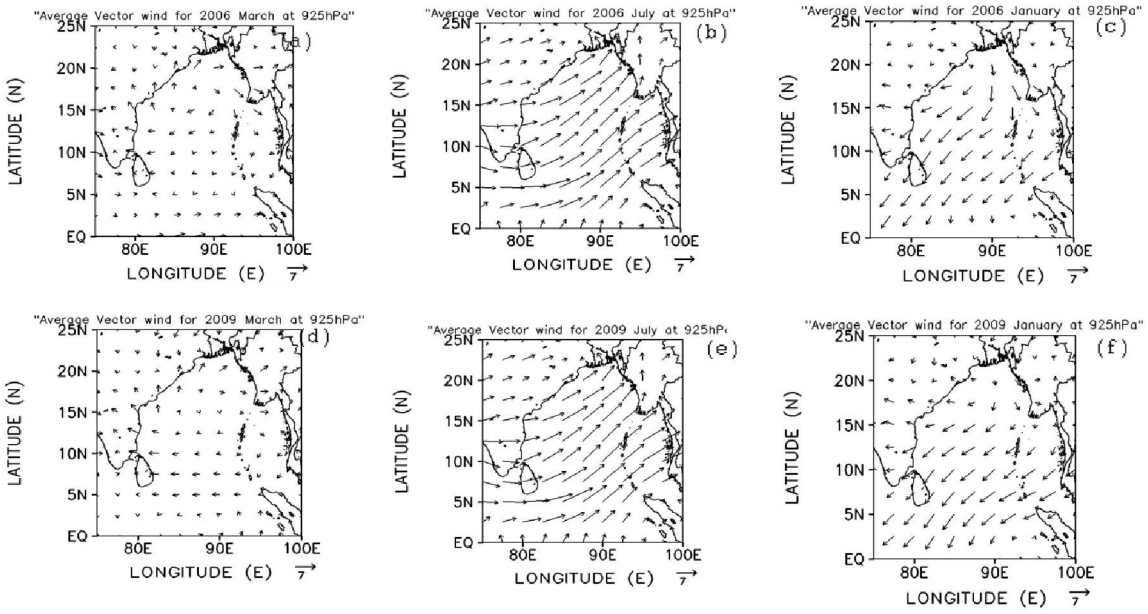

Figure 6.3. *(a to f) The seasonal patterns of mean wind pattern at 925 hPa over BoB for the months of March, July and January of 2006 and 2009 as obtained from NCEP/NCAR reanalysis data.*

While the temperature during January ranged between 17°-22°C for both the years with an increase towards the south-BoB, it increased to 23°-24°C for the pre-monsoon month of March and monsoon month of July. Winter and pre-monsoon season were characterised with RH varying from 40% - 80%. RH showed a consistent increase from winter (40% over north BoB) to monsoon reaching ~ 95%, in both the years with similar spatial pattern. The monthly pattern of wind (Figure 6.3) also remains more or less same in both the years, with strong north easterly winds in January, shifting to westerlies/south westerlies in the monsoon month of July. March is the transition period with weak winds, an anti-cyclonic flow was observed towards the middle of BoB for both the years with relatively low wind speed. As the broad meteorological features remain same for both the years (as observed in Figure 6.2 and 6.3), the seasonal features of aerosols observed during different years can be treated as representative of that season.

6.4 Experimental Techniques and data

6.4.1 Instrumentation

In all the three campaigns, the same High Volume aerosol Sampler (model GH2000 of Graseby Anderson, USA) was operated and samples collected following the sampling strategy discussed in Chapter 2. From the mass collected and the volume of

air sampled, the aerosol mass loading (M_L) in μg m^{-3} was estimated gravimetrically. The aerosol samples collected were analysed in the laboratory (as detailed in chapter 2) for quantification of various chemical species F^-, Cl^-, Br^-, NO_2^-, NO_3^-, PO_4^{2-}, SO_4^{2-}, Na^+, Mg^{2+}, Ca^{2+}, K^+, Al, Fe, Ca, and NH_4^+. Apart from this, the Black Carbon (BC) measurements carried out using Aethalometer (Model AE 31, Magee Scientific, USA) during the cruises were also used in this study [*Nair et al*., 2008; *Babu et al*., 2012; *Kompalli et al*., 2013].

6.4.2 Satellite data

In addition to the near-surface (boundary layer) data, the columnar aerosol data available from MODerate resolution Imaging Spectrometer (MODIS) instrument on-board Aqua satellite was also used in this study. Detailed discussions of MODIS retrieval of aerosol parameters are given in Chapter 2. In this chapter, the primary products from MODIS namely columnar AOD, effective Radius (R_{eff}) and the fine (small) mode fraction of AOD [*Tanre´ et al*., 1997; *Remer et al*., 2002; *Ignatov et al*., 2005; *Levy et al*. 2007] and the derived parameters namely Angstrom exponent (α), large mode AOD, and columnar aerosol mass concentration (M_c) in μg cm^{-2} [*King et al*., 1997; *Remer et al*., 2005] were made use.

In this study, the Angstrom Exponent (α) estimated based on the measured AODs at the wavelengths 550 and 870nm [*Remer et al*., 2008] is used. It is given as,

$$\alpha = \frac{\ln\left(\tau_{550} / \tau_{870}\right)}{\ln\left(550/870\right)} \qquad 6.1$$

Where τ_{550} and τ_{870} are the aerosol optical depths at 550nm and 870nm respectively.

The effective radius R_{eff} is defined as

$$R_{eff} = \frac{\int_{r_1}^{r_2} r^3 n(r) dr}{\int_{r_1}^{r_2} r^2 n(r) dr} \qquad 6.2$$

where n(r) is the number density of aerosol particle with mean radius r, r_1 and r_2 being the lower and upper radii limit of aerosols considered. For MODIS retrievals it is defined in terms of aerosol number densities at the small and large size regimes as [*Remer et al*., 2005],

$$R_{eff} = (N_{small}\, M^3_{small} + N_{large}\, M^3_{large}) / (N_{small}\, M^2_{small} + N_{large}\, M^2_{large}) \quad 6.3$$

And the mass concentration M_c is given by,

$$M_c = N_{small}\, M^3_{small} + N_{large}\, M^3_{large} \quad 6.4$$

with

$$M^k = \int_0^\infty r^k n(r) dr \quad 6.5$$

where N_{small} and N_{large} denote the number density of fine mode particles (<1μm) and coarse mode particles (>1μm) respectively, and M^k denotes the k^{th} moment of size distribution function n(r) of aerosols.

The MODIS Terra and Aqua Daily Level-2 data (MYD04_ L2) of Collection 6 (C006) retrieved over BoB for the cruise period as obtained from LAADS web page https://ladsweb.nascom.nasa.gov/data/search.html_has been used in this analysis. In case of C006 data, since improved cloud mask (MxD35_L2) algorithm produce input for the aerosol algorithm, it is considered as the best available uncontaminated data [*Levy et al*., 2013]. The downloaded Level 2 data was gridded for the respective study area (0:25°N; 80:95°E excluding landmass) by picking the values for each grid and averaged for a month using the MATLAB tool. The error in AOD is estimated as $\Delta\tau = 0.03 \pm 0.05\tau$ over ocean [*Remer et al*., 2008]. Validation of MODIS retrieved AOD with data collected from collocated sun photometer measurements including those from Aerosol Robotic NETwork (AERONET) stations by *Levy et al.,* [2013] have estimated an asymmetric expected error of ±(0.04 + 10%), ±(0.02 + 10%) for AOD and of ±0.41 for α. The uncertainty in R_{eff} is ±0.1μm in the non-dust regimes over ocean [*Remer et al. 2002*]. Uncertainty in fine mode AOD fraction is ~30% with greatest uncertainties occurring at low aerosol concentrations [*Remer et al 2005*]. The largest uncertainty is associated with M_c contributed by assumptions on several parameters like aerosol density, type of aerosols, fine and coarse mode fractions, etc. and can vary from 30% upto 100%.

6.5 Near-surface aerosol mass loading – seasonal patterns

The near-surface aerosol mass loading (M_L) over BoB shows varying range from 10 to 100μg m^{-3}, 41 to 117μg m^{-3} and 12 to 139μg m^{-3} with distinct spatial features for the three seasons, pre-monsoon, monsoon and winter (Figure 6.4a to c) respectively. Irrespective of the season northern part of BoB showed highest aerosol

loading with peak loading in winter. Continental influence is clearly discernible in the winter and pre-monsoon, which is explained in Chapter 4 and 5 as an outflow from the Indo Gangetic Plains (IGP) over to north-BoB, which gets spread out to the remote oceanic regions due south. Apart from the north-BoB, the western BoB (close to eastern coast of India) is also influenced by continental advection. Unlike winter season, monsoon and pre-monsoon period showed isolated hotspots of high aerosol loading (orange colouerd in Figure 6.4a and b) far from the coast.

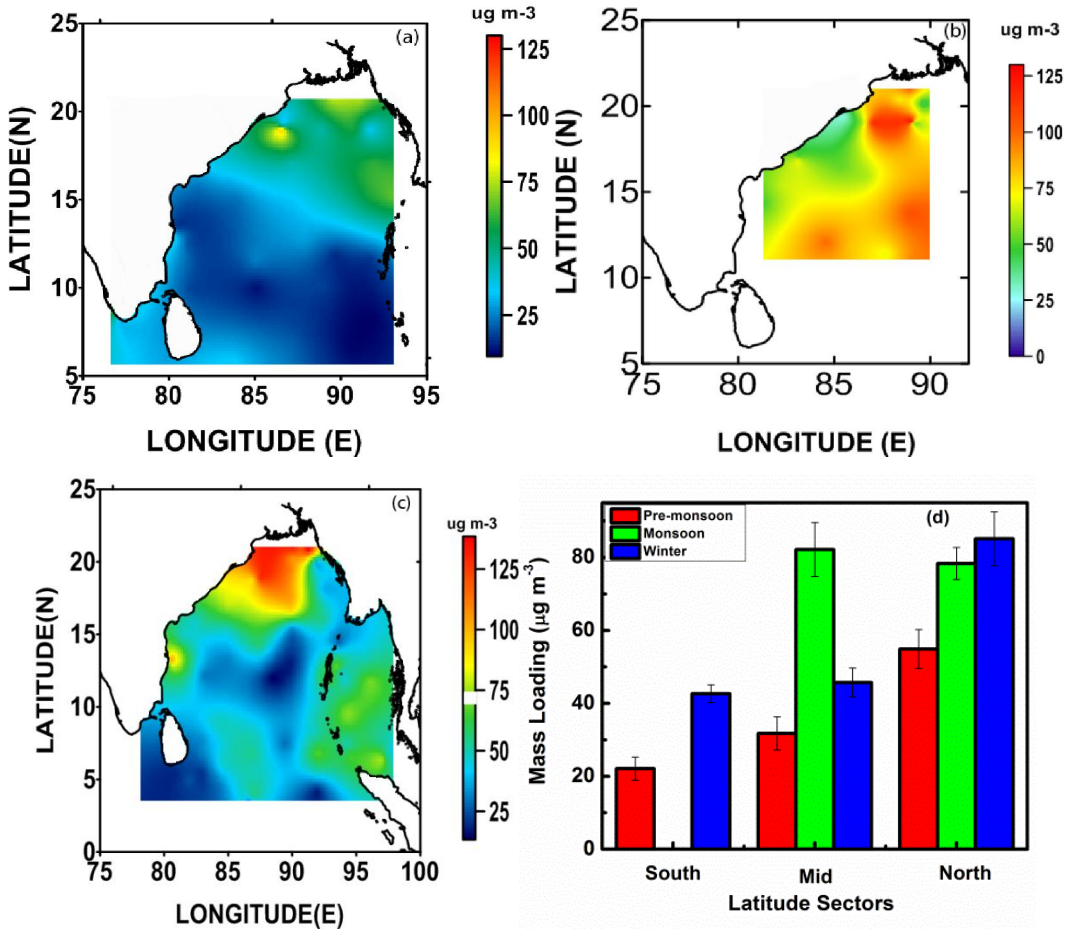

Figure 6.4. *Spatial patterns of near-surface aerosol mass loading (M_L) over BoB for different seasons (a) pre-monsoon, (b) monsoon and (c) winter seasons (d) Seasonal variation of aerosol mass loading for different regions of BoB.*

Among the three campaigns, the winter cruise had largest spatial coverage which included the South East-BoB (SE-BoB) for the first time. Significant aerosol loading (~55 ± 9μg m^{-3}) is observed over SE-BoB also. During pre-monsoon and winter, M_L showed a decreasing trend towards the south whereas for monsoon, the values increased towards south.

Figure 6.4 clearly shows that the aerosol mass loading is latitude-dependent. In order to have a quantitative assessment of the latitudinal patterns of M_L, the entire BoB region is broadly divided into three latitude sectors namely north-BoB (>15ºN), mid-BoB (10º-15ºN) and south-BoB (<10ºN) with longitudinal sector of 80°-92.5°E, where measurements were carried out during all the three cruises. The mean aerosol mass loading over north-BoB, mid BoB and south-BoB for the three seasons are depicted in Figure 6.4d. The SE-BoB covered only in winter is excluded in this regional analysis. Also, the monsoon cruise did not cover latitudes <10ºN. Figure 6.4d shows a northward increase of M_L from <10ºN (south) latitude to >15ºN (north) for the pre-monsoon and winter season. Highest M_L (~82µg m^{-3}) is observed in north-BoB during winter. The M_L values in monsoon are close to that in winter over north-BoB. Also, in winter, the M_L values are comparable over south and mid-BoB region probably due to the outflow from South-East Asia (Figure 6.3c and f). In monsoon season, M_L peaked over mid-BoB region with slightly lower or comparable values over north-BoB. This monsoonal enhancement in M_L can be attributed to in-situ production of sea-salt aerosols by the strong winds (seen in Figure 6.3a to f; Section 4.5.1.7 and 5.7 in Chapter 4 and 5) and hygroscopic growth due to high RH (Figure 6.2g to l). On the other hand, the winter peak in north-BoB can be attributed to continental advection (Chapter 5). Information on chemical nature of aerosols can throw more light into the sources and causative mechanisms in different seasons. More details on the wind induced production of aerosols in this region are discussed in section 5.2.

6.6 Seasonal changes in chemical composition over BoB

Chemical characterisation being the most potential tool for inferring the source characteristics of aerosols, the spatial distributions of the mass concentrations of various chemical components in aerosols during different seasons were compared.

As mentioned in the previous chapters, depending on their sources the chemical species quantified were classified into three categories namely, anthropogenic (SO_4^{2-}, NO_3^-, NH_4^+ and BC), crustal (e.g. Fe and Al) and marine/oceanic (e.g. Na and Cl^-). The seasonal variation of the mean mass concentration of these chemical species for the three latitude regions (south, mid and north-BoB) are shown in Figure 6.5a to c. The anthropogenic species showed maximum values in winter and minimum for monsoon with peak values over north BoB, and decreasing towards south, irrespective of season (Figure 6.5a).

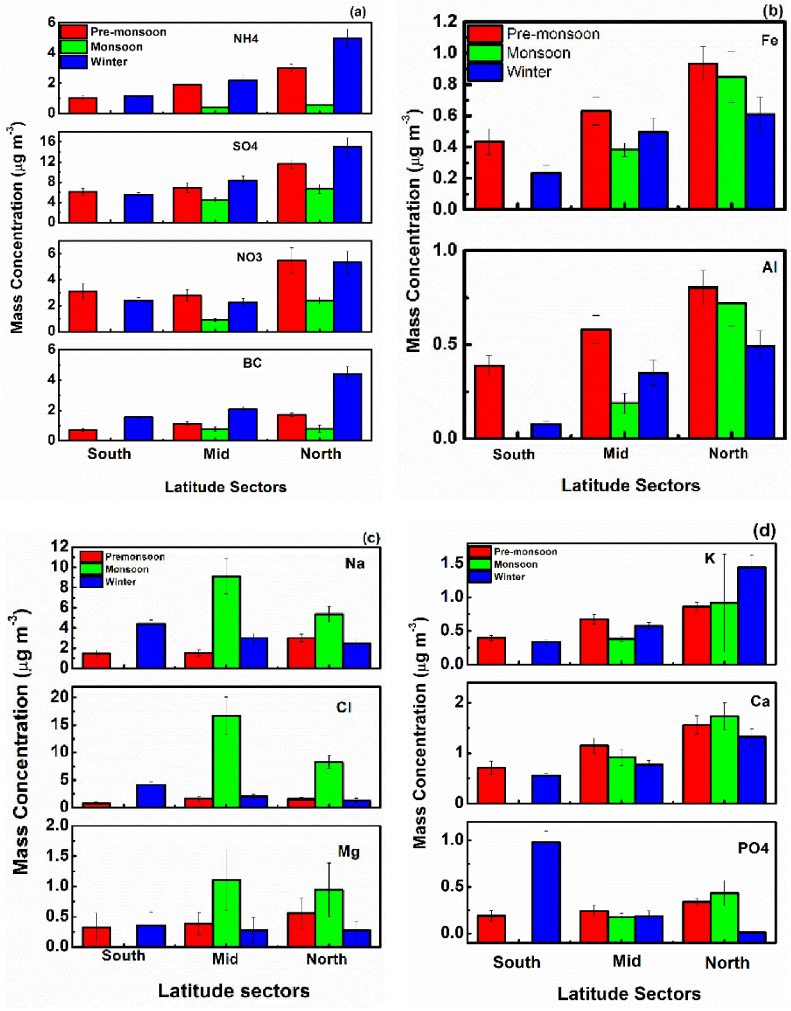

Figure 6.5. *Seasonal patterns of mass concentration of various aerosol chemical species (a) anthropogenic, (b) for crustal (c) marine and (d) mixed sources (K, Ca and PO_4) for different latitude sectors of BoB (South, Mid and North-BoB).*

The pre-monsoon pattern is also similar to that of winter, but with less magnitude. Monsoonal wet scavenging depletes the aerosol mass load of anthropogenic species to half the value during winter/pre-monsoon (NH_4^+ is depleted more) as can be seen from Figure 6.5a. Crustal species Fe and Al also peaked in north-BoB in all seasons and decreased towards south (Figure 6.5b). An interesting feature observed for the crustal species was that the higher loading of Fe and Al during the pre-monsoon season as compared to winter throughout BoB. Long range transport of dust aerosols from western arid regions over to IGP during this period is reported earlier [*Prijith et al*., 2012, 2013] based on the airflow pattern and dynamics. The enhancement in Fe and Al is an observational evidence for this. K (a tracer for biomass burning) was high over north-BoB for all the three seasons (Figure 6.5d) thus revealing the influence of the

biomass burning taking place over north and northeast regions of BoB as also revealed by MODIS retrieved fire counts [*David et al*., 2011]. Forest fires, agricultural slash burning and burning of wood for heating and cooking, taking place over surrounding landmass could be partially responsible for this. The dominance of the absorbing components like BC and crustal species over north-BoB in winter and pre-monsoon has serious implications on the regional radiative forcing. All species of continental origin shows a southward decrease in all the seasons. Thus, BoB is an outflow region to aerosols of continental origin, especially from IGP and SE Asian region.

The most striking feature revealed by Figure 6.5 is that the oceanic species depict a latitudinal pattern different from those of anthropogenic or crustal species. Unlike the continental species, dominance of the major oceanic species Na, Cl^- and Mg, is seen in the monsoon season with highest concentration towards mid-BoB (Figure 6.5c). Their loading increased upto 4 times in monsoon compared to that during winter and pre-monsoon. In winter also oceanic species showed an enhancement over south-BoB. The enhancement of M_L over southern part of BoB in winter has been attributed to wind induced production of sea salt which is exponential in nature, given as $M_{ss}=M_0 e^{bU}$ where M_{ss} is mass concentrationof seasalt, $M_0=1.68$, b=0.18 and U is the wind speed as discussed in Chapter 5. The high loading of Na and Cl^- as revealed by the chemical analysis confirmed the wind induced production of seasalt aerosols. The mean windspeed in monsoon over south BoB is twice that in winter (~16-20m s^{-1}), as recorded by the onboard AWS and also indicated by NCEP-NCAR reanalysis (Figure 6.3d and f). Assuming same functional dependence, the mean sea-salt contribution in monsoon is estimated to be 25µg m^{-3} accounting 30-35% of the total aerosol mass loading over BoB. During pre-monsoon, oceanic species Na and Cl^- which are less over south-BoB show a slight enhancement towards north. This high is attributed to crustal sources rather than sea-salt [*Nair et al*., 2014].

6.7 Air mass back trajectories

With a view to identify the source region of transported aerosols over the cruise region, the 7-day air mass back trajectories reaching the marine boundary layer (at 100m) of different parts of BoB during the three seasons were obtained by running the HYSPLIT model [*Draxler and Rolph*, 2003] and presented in Figure 6.6.

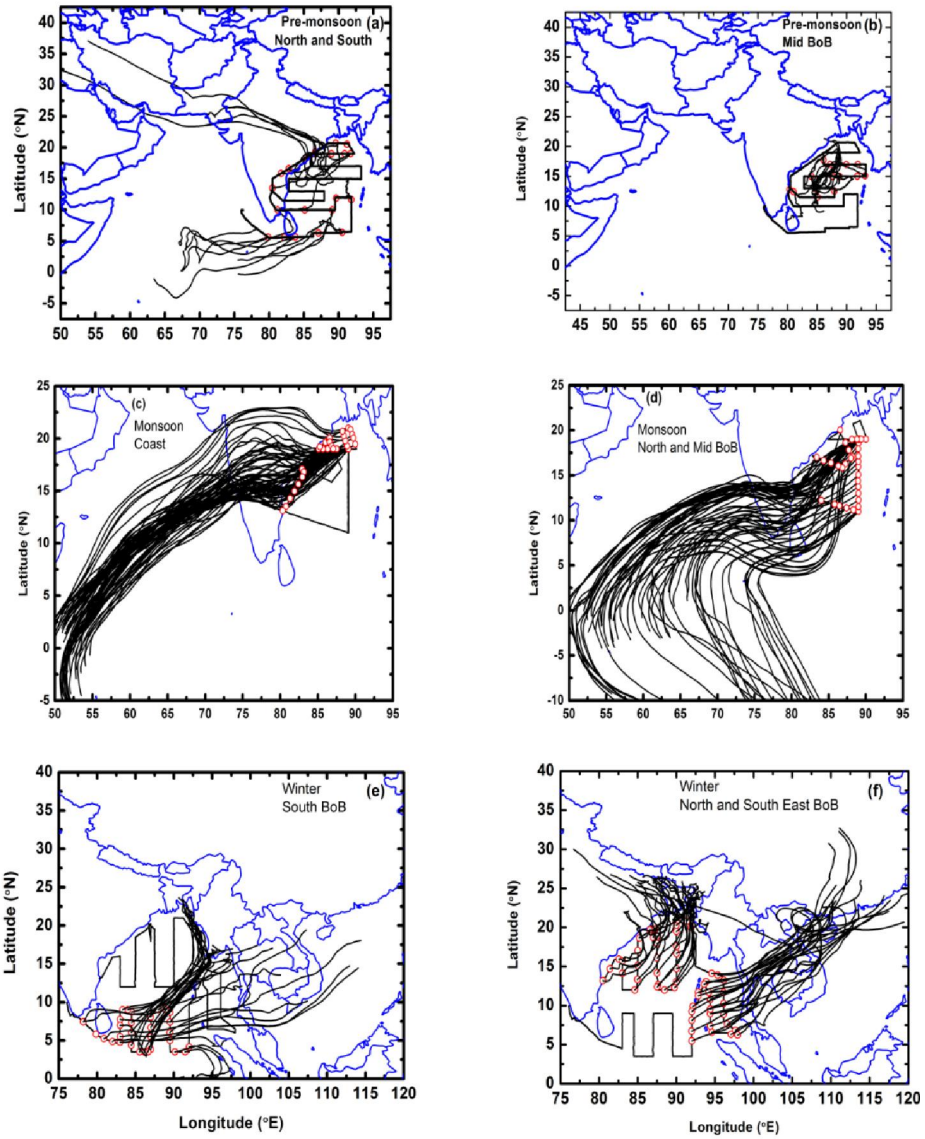

Figure 6.6. *Air mass back-trajectories reaching 100m AMSL at the mean sampling locations for the three seasons (a) North and South regions of BoB for the pre-monsoon (b) Mid BoB for the pre-monsoon (c) coastal region for monsoon (d) north and mid BoB for monsoon (e) South BoB for winter (f) North, mid and SE BoB for the Winter*

During pre-monsoon (Figure 6.6a and b) the air mass originating from IGP and Central India reaches the north-BoB and coastal regions and that over south-BoB is of purely marine origin. Moreover, the anti-cyclonic airflow existing over mid-BoB (as seen from wind pattern in Figure 6.3a) confines the air mass to that region (more explanation on Chapter 4). In monsoon, the origin of the trajectories is completely (South or Southwest) from oceanic regions. However, those reaching the north-BoB and coastal region travel considerable distance over land and hence show signatures of continental species. In winter, the air mass over north/mid BoB originates from IGP or crosses IGP and that over southeast-BoB is from South East Asia. Over the southern BoB, the trajectories have their origin from South East Asia or IGP. They travel long

distance over the marine environment, and hence they partly loose the continental aerosols and gain marine aerosols, particularly due to the strong winds over the region (Figure 6.2).

North-BoB and coastal region of BoB are regions of high aerosol loading for all the seasons where air mass with continental origin persists. This is confirmed by the presence of high levels of anthropogenic species SO_4^{2-}, NO_3^-, NH_4^+, etc. over these regions. The higher aerosol loading with dominance of anthropogenic over southeast-BoB shows the continental influence during winter. Moreover, presence of significant amounts of crustal species Fe and Al over the north-BoB shows the influence of long-range transport. Over southern parts of BoB, where oceanic species dominate, the marine air mass prevails during most of the periods. The stronger winds prevailing over southern region (Figure 6.3a to f) leading to production of sea-salt aerosols which are mostly in coarse mode and of relatively high mass [*Seinfeld and Pandis*, 1998]. The high concentrations of oceanic species like Na, Cl^-, Mg over these regions confirm this source.

6.8 Latitudinal gradients and scale distances for M_L and various species

The latitudinal variation of M_L and mass concentrations of various chemical species for the pre-monsoon and winter cruises (as scatter plot of mean mass concentration against latitude bins) are shown in Figure 6.7a -l and Figure 6.7m-x respectively, from which a quantitative estimate of the latitudinal gradient for each component was made. Since the latitudinal coverage of monsoon cruise was limited, this analysis was not done for that season. For the other two seasons it is observed that there is an exponential decrease of total aerosol mass loading M_L as well as mass concentration of individual species towards south.

The solid red curves represent the exponential fit of the form $M_X=k_0\exp(-k_xL)$ where M_X is the mass concentration of any species X (or M_L in Figure 6.7(a) and (m)) with k_0 and k_x being the respective constants. The red dots in Figure 6.7a to l represent the high values observed over the southern BoB (see Figure 6.4a), the source of which is different from that of outflow from IGP. These points are excluded in the curve fitting. In winter, the spatial distribution of oceanic species like Na, Cl^-, Mg etc. are random and hence no functional dependence could be attributed to the latitude variation (Figure 6.7q, r and s).

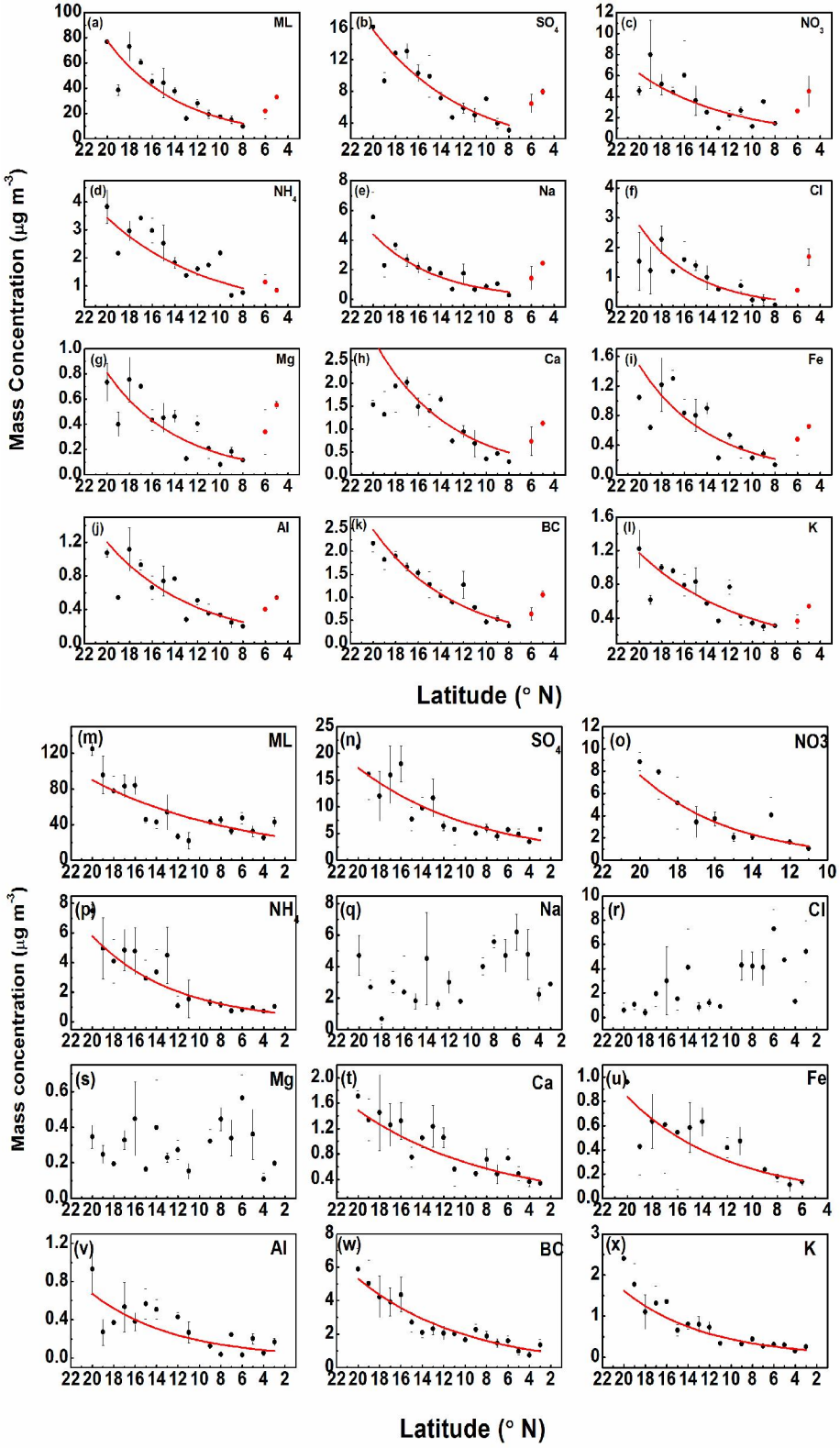

Figure 6.7. *Latitudinal variation of M_L and the various aerosol chemical species for pre-monsoon (a to l) and winter (m to x) season. The red solid curves represent the exponential fits.*

Table 6.1 lists k_0, k_x, correlation coefficient and scale distance ($D=1/k_x$) for M_L and the various species. The exponential decrease of M_L yields an e^{-1} scale distance of

688km in pre-monsoon and 1571km in winter indicating more penetration of continental pollution over to BoB during winter. During monsoon season, no such systematic latitudinal variation is observed due to the prevalence of marine air-mass over the entire Bay of Bengal as evident from the air flow and back trajectories in Figure 6.6c and d.

In pre-monsoon, the scale distance lies in the range 500-900km for the individual species, where as in winter, it often exceeds 1000km. The strong airflow from IGP is responsible for the large scale distance in winter. The overall loading also is higher in winter compared to pre-monsoon. In addition, the anthropogenic species SO_4^{2-}, NO_3^-, NH_4^+ and Ca, are in fine mode, and owing to their long life time (~1 week), get transported to longer distances as indicated by the large scale distances.

Species	**ICARB (pre-monsoon)**				**Species**	**WICARB (winter)**			
	k_0	**k_x**	**D (km)**	**R**		**k_0**	**k_x**	**D (km)**	R
M_L	3.49	0.16	688	0.74	**M_L**	3.10	0.07	1571	0.73
Na	0.12	0.18	611	0.63	**Na**				
Cl^-	0.05	0.20	550	0.51	**Cl^-**	No dependence observed			
Mg	0.04	0.16	688	0.51	**Mg**				
Ca	0.15	0.15	748	0.65	**Ca**	0.30	0.08	1375	0.85
K	0.13	0.11	1000	0.77	**K**	0.12	0.13	846	0.95
SO_4^{2-}	1.43	0.12	917	0.71	**SO_4^{2-}**	1.05	0.09	1222	0.89
NH_4^+	0.38	0.11	1000	0.85	**NH_4^+**	0.43	0.13	846	0.92
NO_3^-	0.56	0.12	917	0.49	**NO_3^-**	0.14	0.2	550	0.88
Fe	0.06	0.16	688	0.62	**Fe**	0.07	0.12	913	0.86
Al	0.09	0.13	846	0.69	**Al**	0.05	0.13	846	0.71
BC	0.15	0.14	786	0.81	**BC**	0.72	0.1	1100	0.93

Table 6.1 *The constants k_0, k_x, e^{-1} scale distance (D) and correlation coefficient (R) of the exponential fits of aerosol mass loading and concentrations of various species for pre- monsoon and winter.*

6.9 Columnar properties of aerosols retrieved from MODIS over BoB: seasonal patterns

Since almost all aerosol sources are confined to the earth's surface (land as well as ocean), the physico-chemical characteristics of near-surface aerosols should have influence on their properties in atmospheric column (columnar properties). In this section, the above discussed spatio-temporal features of near-surface aerosols are compared with those of columnar properties as observed by the satellite-borne MODIS.

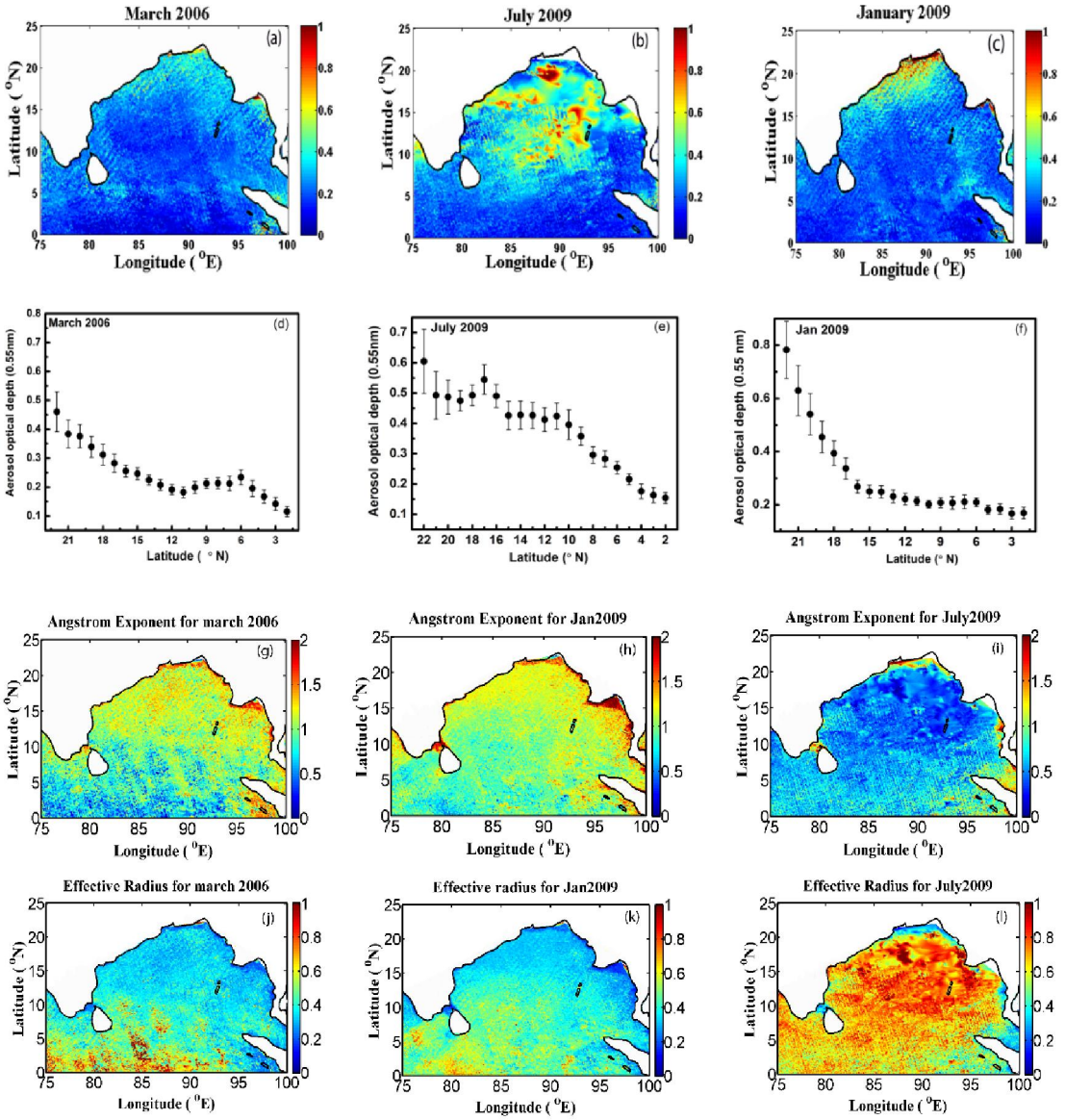

Figure 6.8 *a-c Spatial map of column AOD at 550nm from MODIS for pre-monsoon (March 2006), monsoon (July 2009) and winter (January 2009), d-f latitude variation of AOD, g-l spatial variation of Angstrom exponent and effective radius for the above seasons.*

The monthly mean values of AOD at 550nm, R_{eff}, α, column mass concentration M_c, fine mode AOD, large mode AOD and fine mode fraction were retrieved over BoB region for March 2006, January 2009 and July 2009, representative months of pre-monsoon, winter and monsoon season (corresponding to the three cruise periods during which the near-surface measurements were made). The column AOD, a measure of the depletion caused to the incoming solar radiation produced by the vertical column of aerosols, is one of the most important radiative forcing parameter. The Angstrom exponent α provides information on the particle size (larger the exponent, the smaller the particle size), phase function and the relative magnitude of aerosol scattering at

different wavelengths. R_{eff} indicates the relative abundance of large and small particles; and M_c is the critical parameter deciding the optical properties of aerosols. The month-to-month variation of the spatial pattern of all the parameters (not shown here) are more or less similar in both the years 2006 and 2009 (cruise periods), but with minor differences in magnitudes.

In Figure 6.8a to c are depicted the monthly mean spatial pattern of column AOD (at 550nm) over BoB for March 2006, July 2009 and January 2009 representing pre-monsoon, monsoon and winter respectively for a comparison. The AOD is invariably high over north BoB irrespective of season with peak values in monsoon and winter, similar to the near-surface aerosol loading. For winter and pre-monsoon AOD decreases from north to south while in monsoon AOD is high over mid and south-BoB. Figure 6.8d to f shows the latitudinal variation of AOD for the three seasons. The AOD presents an exponential decrease from north to south in winter and pre-monsoon (0.8 to 0.2 and 0.45 to 0.2 respectively). The most striking feature is that the enhancement of M_L seen in the latitude sector 6°-8°N in pre-monsoon (see Figure 6.4) is reflected in columnar AOD also revealing that near-surface aerosol loading has significant contribution to the columnar loading. In monsoon, the AOD remains high (~0.45) in a wide latitude sector from 10°N to 22°N and then decreases towards south. But the M_L measurements are limited to the latitude region, 11°N to 21°N (Figure 6.4) where it remains high. The ship-based sun photometric measurement of AOD over BoB during same cruises in winter and pre-monsoon has also shown decrease from north to south [*Nair et al.,* 2009; *Babu et al.,* 2012]. The AOD remained in the range 0.5-0.6 over north-BoB and 0.1 to 0.4 in the southern parts [*Nair et al.,* 2009] in pre-monsoon, and for winter it was 0.8 over north-BoB reaching 0.3 in south-BoB [*Babu et al.,* 2012].

In Figure 6.8g to i and j to l are shown the spatial patterns of α and R_{eff} respectively for the seasons corresponding to the AOD patterns in Figure 6.8a to c. Throughout BoB the values for α lies in the range of 1 and 1.5 for the pre-monsoon and winter season while it lowers to <0.5 for the south-BoB. For the monsoon season values remained low (<0.5) over entire BoB. Effective radius showed lower values <0.3 over the northern part of BoB for the pre-monsoon and winter season and it increased to >0.6 over the south. For the monsoon season R_{eff} showed higher values >0.8 throughout BoB. The high α values along with the low R_{eff} over BoB in pre-monsoon and winter indicate dominance of fine particles. In monsoon the entire BoB is covered by large particles as seen by the high α and low R_{eff}. Even though retrievals of α and R_{eff} are

independent of each other, it shows similar inferences on the size characteristics of aerosols.

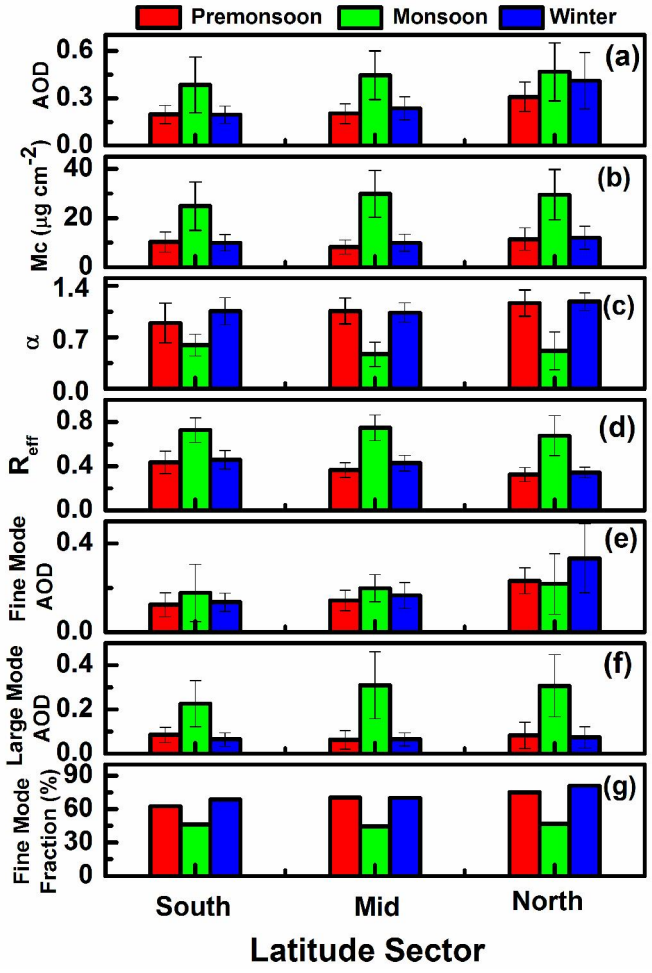

Figure 6.9. *Seasonal patterns of columnar (a) AOD, (b) mass concentration (M_c), (c) Angstrom exponent (α) (d) R_{eff} (e) fine mode AOD and (f) large mode AOD (g) fine mode fraction (%) for south, mid and north-BoB from MODIS.*

The columnar aerosol parameters viz. AOD (at 550nm), R_{eff}, α, M_c, fine mode AOD, large mode AOD and the fine mode fraction (%) for the three latitude sectors were averaged and presented in Figure 6.9a to g. In any latitude sector or throughout BoB, the mean AOD for winter and pre-monsoon is 50% of its monsoonal value (Figure 9a and b). AOD increases from south to north in all seasons, the increase being exponential in pre-monsoon and winter and linear in monsoon. The satellite retrieved M_c also depicts a similar spatial pattern which is expected. During pre-monsoon and winter M_c is 30% of its monsoonal value. The Angstrom exponent (α), the qualitative indicator of particle size, (larger the value, smaller the size) increases from south to north in pre-monsoon and winter and exhibits opposite behaviour during monsoon. On

the other hand, R_{eff} (indicative of abundance of large sized aerosols) decreases from south to north in pre-monsoon and winter while it increases towards north in monsoon.

6.10 Comparison of near-surface and columnar properties over BoB

An examination of the near-surface aerosol mass loading M_L (Figure 6.4d) shows a spatial pattern with the broad features matching with that of AOD and M_c, but there is no one to one correspondence. Both AOD and M_c peaks during monsoon throughout BoB. M_L is comparable in monsoon and winter over north-BoB as for AOD also. Significantly high M_L (~80μg m^{-3}) is observed over mid and north-BoB (M_L measurement is not available over south-BoB), during monsoon. The high levels of oceanic species Na and Cl^- (see Figure 6.5c), confirms that oceanic aerosols dominate throughout BoB during monsoon. Thus, the columnar mass loading has a bearing on the near-surface aerosol characteristics during monsoon. But the winter high is not contributed by sea-salt aerosols since sea-salt species Na and Cl^- exhibit low concentration of during this period (Figure 6.5). Besides, the Angstrom exponent α, is >0.8 during pre-monsoon and winter, over the entire BoB, indicative of the presence of significant amount of small particles, with highest value of 1.2 in winter. The abundance of small particles over north-BoB is also evident from the low R_{eff}. These patterns of α and R_{eff} were examined in conjunction with those of the anthropogenic species SO_4^{2-}, and NO_3^- (Figure 6.5a) which are formed through gas-to-particle conversion mechanism and comprise mostly of small particles. It is seen that the latitudinal variation of these species are similar to that of α and opposite in nature to that of R_{eff}, confirming the presence of significant amount of small particles during winter.

It may also be noted that the small particles may not contribute significantly to aerosol mass. In this context, the fine/small mode AOD contributed by fine particles (diameter < 1μm) was also examined (Figure 6.9e) which increases from south to north and peaks in winter over north-BoB like M_L. On the other hand, the large mode AOD reveals a different picture with high values in monsoon throughout BoB and remaining more or less same, during other seasons. The average percentage contribution of small mode AOD over BoB is 45% in monsoon, 69% in pre-monsoon and 73% in winter, the south to north increase being 62% to 75% and 68 to 81% in pre-monsoon and winter respectively. Thus, the AOD over BoB in winter and pre-monsoon has significant contribution from the fine mode aerosols, which are mostly of anthropogenic origin. The high column AOD towards north- BoB during pre-monsoon and winter with the

column mass concentration remaining low throughout, can be attributed partly to other characteristics of aerosols like their scattering or absorption coefficient which are decided by refractive index which in turn depends on the chemical nature of aerosols and their number density. Here it is worth noting that (1) major contribution of AOD over north-BoB during winter is from the fine mode aerosols which include anthropogenic species like SO_4^{2-}, NO_3^-, BC, NH_4^+, etc. (2) mass concentration of BC the major absorbing species peaks over north-BoB in winter and (3) mass concentration of dust aerosols containing Fe and Al peaks in pre-monsoon over north-BoB. The high AOD over north-BoB in winter is due to the presence of large amount of BC as well as other fine mode anthropogenic species like SO_4^{2-}, NO_3^-, etc. On the other hand the monsoon AOD is contributed significantly by sea-salt aerosols.

6.11 Estimation of column mass concentration from in situ-measured near-surface mass loading and comparison with MODIS retrieved M_c

In this section it is attempted to make an estimate of the columnar mass loading of aerosols over BoB based on the in situ measured near-surface mass loading, assuming an exponential decrease of the form $M(h) = M_0 \exp(-h/H)$ where M(h) is the mass loading at an altitude h, M_0 is near-surface mass loading (the measured M_L in this case), and H is the scale height; for which M fall by e^{-1} of M_0. Mass concentration at each height interval of 0.5km is estimated with the scale height H= 1.5 km, 2 km and 3 km and the respective column mass concentrations, M_c ($\mu g\ m^{-2}$) are obtained by integrating upto 16km (tropopause). The error in these estimates is due to error in M_L measurements and is estimated to vary from 2 to 15%, and dependent on M_L.

In Figure 6.10a, c and e are shown the column M_c retrieved from MODIS and those estimated from M_L for the sampling locations (with H=1.5km, which is best matching with the satellite retrievals) as discussed above for the three seasons. The corresponding scatter plots along with the linear fit obtained through regression analysis are also shown in Figure 6.10b, d and f.

All major spatial features appearing in M_c estimated from in-situ measured near-surface aerosol loading M_L matches well with the MODIS retrieved M_c in winter and pre-monsoon (Figure 6.10a and c). The correlation coefficients are 0.65 and 0.53 for pre-monsoon and winter respectively, with confidence level of $p \geq 0.0001$. But in monsoon no significant correlation exists between the two (Figure 6.10e and f).

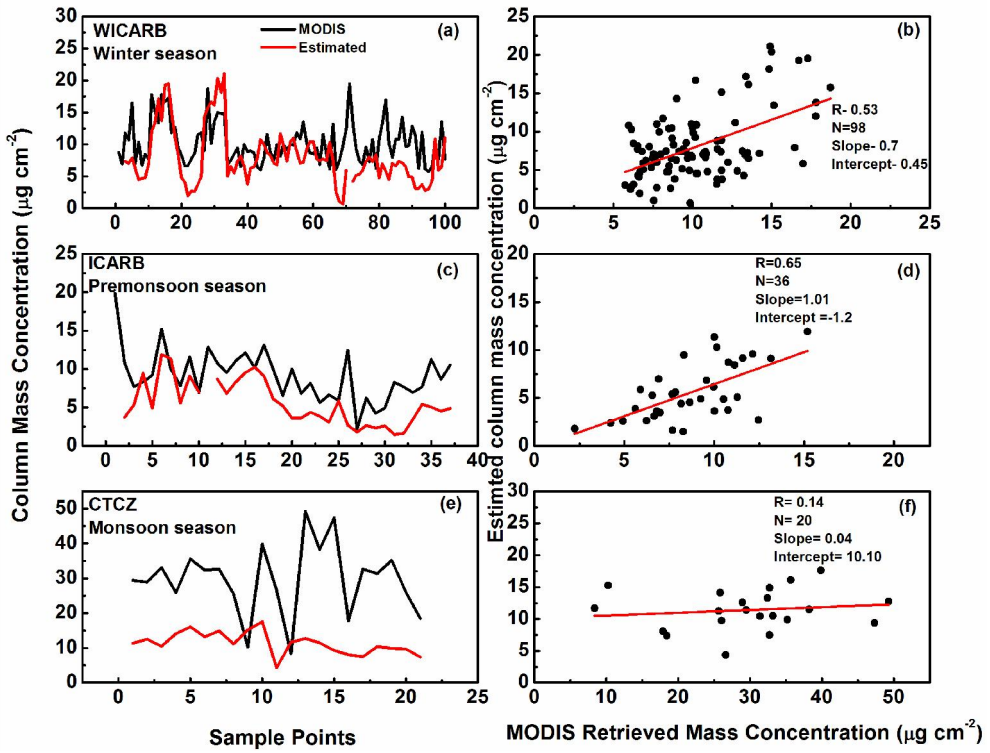

Figure 6.10. *(a,c,e) Comparison of MODIS-retrieved column mass concentration (M_c) of aerosols and that estimated based on in-situ measured near-surface aerosol mass loading over BoB and (b,d,f) the scatter plot between the two. The correlation coefficient (R), number of regression points (N), slope, y-intercept of the fitted line are also presented.*

Over south-BoB, where low M_L was observed, MODIS retrievals are found to be over-estimated, but over north and mid-BoB where high and moderate surface loading was observed they are in better agreement. During monsoon, the MODIS retrieved M_c values are over estimates and not at all correlated. This implies that the vertical distribution of aerosols does not follow exponential decrease in monsoon, instead there can be some layers present at higher levels. Moreover, this analysis shows that scale height over BoB is season and region-dependent and hence a uniform scale height cannot be assumed throughout the year and for the entire region.

6.12 Discussions on the relevance of the study in the context of Indian monsoon

The above observations on the spatial variations of near-surface and columnar loading of aerosols over BoB and the seasonal changes have relevance in strengthening our understanding of role of aerosols on the Asian monsoon system. It is well established that the monsoon system develops in response to the large scale land-sea thermal contrast from equator to ~ 30º N, and is a part of the natural cycle [*Rao 1976;*

Wang 2006]. This is controlled by the amount of solar radiation incident on the surface and the thermal capacity of the underlying surface. The ocean surrounding Indian landmass has a pivotal role in the development and sustenance of monsoon system. The strong ocean-atmosphere-land interaction in the northern Indian Ocean and Asian landmass during pre-monsoon is fundamental factor that induces the genesis and development of a monsoon onset vortex over the BoB, which in turn triggers the onset of the Asian summer monsoon [*GuoXiong et al.*, 2011]. Sea surface temperature (SST), being one of the parameter for deep convection over tropics, is positively correlated with surface air temperature [*Jaswal et al., 2012*]. It is also known that aerosols affect the incoming solar radiation through scattering and absorption (direct effect) or acting as CCN and controlling the microphysics and morphology of clouds (indirect effect) and modify the surface reaching solar flux [*Hansen et al., 1997; Kaufman and Koren, 2006; Tao et al., 2012*]. Even though the impact of aerosols on Asian monsoon is still disputed, several observational and modelling studies have shown that aerosols cause anomalies in the monsoon rainfall and their regional strengths [*Menon et al.,* 2002; *Ramanathan et al.,* 2001;*Gautam et al.,* 2009; *Jiang et al.,* 2013; *Ganguly et al.,* 2009; *Zhu et al.,* 2012; *Yi et al.,* 2015]. Both positive and negative direct radiative forcing by aerosols on Indian summer monsoon has been reported [*Wang et al.,* 2004, 2007; *Ramanathan et al.,* 2001; *Lau and Kim, 2006*; *Meehl et al.,* 2008; *D'Errico et al.,* 2012; *Jiang et al.,* 2013]. Experimental studies during INDOEX has shown aerosol induced surface cooling and lower tropospheric warming leading to large scale dynamical response like low level convergence [*Chung et al.,* 2002]. Heating of atmosphere by aerosols and consequent enhancement of upward motion over Indian region in winter leads to weak monsoon [*Menon et al.,* 2002; *Bollasina et al.,* 2008]. The tropospheric warming due to absorbing species like BC, eventually act as an elevated heat pump [*Lau and Kim.,* 2006] which leads to advancement and intensification of summer monsoon [*Gautam et al.,* 2009]. Satellite based measurement of aerosol absorption and their estimate of critical cloud factor (ccf) has indicated a shift in ccf indicative of change in aerosol type from post monsoon to winter and consequently from cooling to warming regime *Eswaran et al.,* (2014). The present study has revealed a change in chemical composition of aerosols from winter to monsoon from more absorbing species to more scattering type. The columnar AOD in pre-monsoon period is nearly half the value during monsoon and also exhibits north ward positive gradient. This low AOD enables more solar radiation to reach BoB which in turn is partially responsible for the pre-monsoon warming of the ocean surface and atmosphere. Even though this is part of

a natural cycle it can have impacts on the regional radiative forcing due to aerosols, depending on the amplitude of the seasonal variations. The inter-annual variation in aerosol characteristics could lead to anomalies in monsoon activity. The inter-annual variations in the onset date and intensity of rainfall and associated anomalies depend on the regional forcing. In addition, it was also reported that the impact of monsoon rainfall in reducing the aerosol load has impact on the north-east monsoon. Since the westward moving depressions (low pressure system) in BoB is responsible for a considerable amount of monsoonal rainfall, the large seasonal changes in aerosols characteristics has regional climate implications [*Sumanth et al.,* 2004]. The present analysis has also revealed that the columnar properties of aerosols in any season have strong dependence on the physical and chemical characteristics of near-surface aerosols, which are controlled by continental advection and wind-induced sea-salt generation.

6.13 Summary

This chapter presents the seasonal changes in the in-situ measured near-surface features of aerosols over the marine boundary layer of BoB based on the ship-based experiments conducted as part of three field campaigns along with the corresponding changes in the satellite retrieved columnar properties. The measured near-surface properties include total aerosol loading (M_L) and mass concentrations of various chemical species and the MODIS retrieved columnar properties are aerosol optical depth (AOD), column mass concentration (M_c), Angstrom exponent (α), effective radius (R_{eff}) and fine mode AOD and fine mode fraction. The highlights of results are given below.

1. Irrespective of the season, the M_L exhibited high values over north-BoB and decreased towards south. This is mainly due to transport of aerosols from IGP to BoB as observed by the analysis of wind patterns and air mass back trajectories. Highest aerosol loading of ~83μg m^{-3} was observed over north-BoB in winter with close-by values in monsoon over north (~81μg m^{-3}) and mid-BoB (~78μg m^{-3}).
2. Enhancement in column AOD and α over north-BoB during winter (~0.8 and >0.8 respectively) decreases towards south. Mean AOD over north-BoB in winter and monsoon are comparable (~0.5). The low R_{eff} and large (α) over north for winter and pre-monsoon indicating dominance of fine aerosols.

3. Column AOD and M_c showed similar spatial pattern, increasing from south to north. While column AOD in winter and pre-monsoon is ~50% of that in monsoon, the column mass loading shows a reduction of 30%.

4. There is a change in chemical composition of aerosols over BoB for more absorbing species in winter to scattering type in monsoon.

5. Presence of absorbing species like BC and mineral dust is partially responsible for the high AOD over north-BoB during pre-monsoon and winter.

6. Chemical composition of aerosols over north-BoB shows that the high column aerosol loading and AOD in winter are due to anthropogenic aerosols and those in monsoon are due to sea-salt aerosols. The size characteristics of aerosols revealed by α and R_{eff} confirmed the dominance of fine aerosols in winter and coarse particles in monsoon, supporting the above inference.

7. Total aerosol loading as well as individual species showed an exponential decrease from north to south. The e^{-1} scale distance for total aerosol loading were estimated to be of 668km and 1567km in pre-monsoon and winter respectively. The scale distances for individual species varied from 550km to 1375km with longer distances in winter facilitating intrusion of pollutants to larger distances.

8. In any season, considerable loading of anthropogenic/crustal aerosols is observed over BoB. The fine mode AOD contributes to 45% in total AOD during monsoon 69% in pre-monsoon and 73% in winter.

9. The column aerosol mass concentration estimated based on near-surface loading and that retrieved from MODIS revealed similar spatial patterns over BoB and in fairly good agreement. However, over regions of low near-surface loading, MODIS-retrieved mass concentration is found to be over-estimate by 40 to 140%.

10. The columnar properties of aerosols over the marine environment of BoB depend strongly on the physical and chemical characteristics of near-surface aerosols as seen from the in-situ measured near-surface properties and satellite retrieved columnar properties.

11. The regional changes in aerosol characteristics like AOD can influence regional weather systems and inter-annual variations can affect the monsoon systems. This aspect needs to be investigated further using models.

Chapter 7

Summary and future scope

7.1 Summary

This thesis presents the results of a comprehensive study on the physical, chemical and radiative/optical properties of near-surface aerosols at the coastal environment of Thiruvananthapuram(TVM) and the marine environments of Arabian Sea (AS) and Bay of Bengal (BoB) based on collocated simultaneous measurements of physical and chemical characteristics. This thesis is organized in seven chapters. The highlights of the major outcome of this research activity and the future scope of this work are presented in this chapter.

Chapter 1 gives an overview of the atmospheric aerosol system. Brief descriptions of the production and removal mechanisms, aerosol residence time, their physical and chemical characteristics, spatio-temporal variations and the major natural and anthropogenic sources of aerosols are included in this chapter. The climatic and environmental impacts of aerosols are also discussed. Different measurement and analytical techniques used world-wide to characterise aerosols are also outlined in this chapter. This chapter also highlights the importance of concurrent and simultaneous measurements of both physical and chemical properties of aerosols to bring out a realistic picture on the radiative/optical characteristics of aerosols. Results of a detailed literature survey of the scientific studies carried out on the physical, chemical and radiative characteristics of atmospheric aerosols all over the globe with emphasis on Indian scenario are also presented. This chapter concludes with a brief discussion of the scope of the present study in the above context.

A detailed description of various instruments and techniques used for characterizing the physical and chemical properties of atmospheric aerosols is presented in **Chapter 2**. The measurement of near-surface aerosol number density and size distribution were carried out by using an Aerosol Spectrometer and for aerosol sample collection, a High Volume aerosol Sampler was employed. For the chemical characterization of aerosols, state-of-the-art analytical techniques like Ion Chromatography, Inductively Coupled Plasma-Atomic Emission Spectroscopy and Atomic Absorption Spectroscopy were used. The principle of operation and other

technical details of these instruments are also included in this chapter. In addition, the satellite-based data of columnar aerosol optical depth (AOD), mass concentration, Angstrom exponent and effective radius retrieved by MODIS also was used in this work. A brief account of the retrieval methods along with uncertainties is also presented. Highlights of supplementary data used for interpreting the observed aerosol features, like meteorological data (from Automatic Weather Station), NCEP/NCAR reanalysis of wind and airmass back trajectories from HYSPLIT model, are also presented in this chapter. Apart from this, a brief account of OPAC used for the computation of optical/radiative parameters of aerosols is also included.

In Chapter 3 is presented the results of the first time comprehensive physico-chemical characterization of aerosols at the tropical coastal site Thiruvananthapuram based on simultaneous and collocated measurement of total aerosol number density (particles of aerodynamic diameter >0.3μm) (N), number density size distribution (NSD) and chemical composition during the period 2011-2013. The chemical species quantified in the present analysis include SO_4^{2-}, Cl^-, NO_3^-, F^-, PO_4^{2-}, HCO_3^-,Na, K, Ca, Mg, Fe, Al, Pb, etc. In addition, data on BC and OC from this location are also utilized for chemical closure. The major findings are summarized in the following.

a) The physical properties such as number density, size distribution and mass loading showed diurnal changes associated with mesoscale meteorological features like sea-breeze (SB) and land breeze (LB) and monthly/ seasonal changes associated with synoptic scale meteorology and transport. Aerosols number density remained invariably high during LB regime (night time) in all months except in June when it is comparable with that during SB (daytime).On the other hand, M_L during SB exceeded that during LB in monsoon months whereas it remained high during LB in all other seasons. The mean M_L obtained for the study period is 67±30μg $m^{-3}$and total number density is $(2.05\pm0.8)\times10^8 m^{-3}$.

b) The source identification based on Principal Component Analysis showed three prominent sources of aerosols over TVM namely anthropogenic, crustal and marine which varied seasonally. Strong mixing of aerosols from these sources is also observed in different seasons.

c) The NSDs are of multi-modal in nature with two prominent modes one at radius Ò 0.175μm and other ~0.7-0.9μm with indication of less pronounced modes in fine particle and coarse particle regimes. While the small particle mode becomes prominent in winter due to advection of inland aerosols, the coarse mode gets pronounced in monsoon due to wind-induced sea salt production.

d) Correlation analysis between the mass concentrations of various chemical species and size-resolved number density indicated that the anthropogenic species like NH_4^+, SO_4^{2-} are mostly in fine mode (diameter <1µm) for all the seasons while Na, Cl, Fe and Al in coarse mode (diameter>1µm). Species Fe, Ca, NO_3^-, K and Mgare present in both the modes showing multiple sources or production mechanism for these species.

e) First-cut chemical models of aerosols were evolved on seasonal basis including components of sea salt (SS) other Water-Soluble non-seasalt (WSN), Mineral dust (MD), Particulate Organic Matter (POM) and Black Carbon (BC). SS contributes maximum in monsoon (~40%) minimum in winter (with 6%) with 20% and 25% in pre-monsoon and post-monsoon respectively. WSN mostly comprising of anthropogenic species are found to beminimum in monsoon (13%) and lies in the range 20-22% in other seasons. MD peaks in pre-monsoon (29%) and showed least for winter (10%) with monsoon and post-monsoon values being 25% and 17% respectively. BC and POM were highest in winter (~5% and 34 % respectively), POM remaining more or less same (~23-24%) in all other seasons.

f) Based on the measured aerosol properties,the aerosol radiative characteristics namely scattering coefficient ($б_{sc}$), absorption coefficient ($б_{ab}$)extinction coefficient ($б_{ex}$),single scattering albedo (SSA), and phase function (P(θ)) were estimated on seasonal basis for TVM for the first time. The ($б_{sc}$) varied from 0.04 to 0.14 km^{-1} and ($б_{ab}$) between 0.01 and 0.05 km^{-1}. There is strong seasonal variation insingle scattering albedo(SSA)being 0.71 for winter indicating the presence of more absorbing aerosols and 0.89 for monsoon season.

g) Making use of the measured aerosol number density-size distribution and mass loading, an approximateestimate of the density of aerosols over the location was made on monthly basis. The density varied in the range of 1.4 to 2.6g cm^{-3} annually.

h) Over a span of ~10 years from 2004 to 2013, the aerosol number density over TVM showed a mean increase of 19% and aerosol mass loading increased by 29%. These long-term changes are found to be season dependent.

Chapter 4 deals with the spatial features of N, NSD, M_L and mass concentrations of various chemical species measured over the marine environment of AS and BoB during pre-monsoon (March to May),revealed by ship-based measurements conducted as part of ICARB.Based on the measurements of chemical composition of aerosols, region-specific first-cut chemical models were evolved for AS as well as BoB and used for the estimation of the radiativeparameters $б_{sc}$, $б_{ab}$, $б_{ex}$,SSA and P(θ). Compared to AS, BoB was found to be anthropogenically more affected in

view of aerosols number density, total aerosol mass loading and mass concentrations of anthropogenic species like SO_4^{2-},NO_3^-,$NH_4^+$and trace metals. Both fine mode and coarse mode number density of aerosols over BoB are one order higher than those over AS. The high aerosol loading over BoB is reflected in the scattering and extinction coefficients also.Associated with anti-cyclonic air flow, both N and M_L showed low values over AS and BoB.While aerosols of natural origin like sea salt, mineral dust etc dominated over AS, continental species wheremore predominant over BoB. The mean % contribution of anthropogenic aerosols over AS is estimated as ~21%, and that over BoB is found to be ~64%.Significant mineral dust loading was observed over AS and BoB (being 15-37% and ~25% respectively) thus revealing the role of long range transport from arid/semi-arid regions.Mineral dust (Fe and Al) was found to be in both fine and coarse mode over AS and BoB. The SSAvaried in the range 0.88 to 0.95 over AS and 0.81 to 0.89 over BoB indicating the presence of more aerosols over BoB.

The winter-time aerosol characteristics obtained through the ship-based measurements over the entire marine environment of BoB covering South East-BoB for the first time are presented in **Chapter 5**. During winter, the spatial distribution of M_L showed two prominent high regions, one over north BoB and other over South East-BoB. While the high over north BoB is caused by transport from the populated and industrialized IGP, that over SE BoB is due to transport from the anthropogenically active SE Asian region as revealed by the backtrajectory analysis and chemical composition. $M_L$was minimum over the mid BoB. The oceanic species (Na, Cl, Mg, etc), crustal species (Al and Fe) and anthropogenic species (SO_4^{2-}, NH_4^+, BC, etc) showed distinctly different spatial patterns. For the species like Ca, K and SO_4^{2-} having both sea-salt (ss) and non-sea-salt (nss) components, the ss and nss components showed distinctly different patterns, with ss component peaking over SW-BoB and nss component exhibiting maximum over N-BoB.The anthropogenic species (SO_4, NO_3, NH_4, BC, etc) peaked over north BoB and the crustal components were high near to the eastern coastal regions of India with isolated hotspots away from the coast.The anthropogenic aerosol mass load is estimated to vary from 60% to 98% over north-BoB. Significant loading of natural aerosols (upto 60%) was noted over south BoB. The accumulated rainfall of ~15mm occurred close to cruise track produced 85% reduction in total aerosol mass loading and species dependent depletion. The percentage contributions of the major aerosol components SS, WSN, MD, POM and BC over different regions of BoB were found to be region dependent.The scattering and absorption coefficients were highest over north BoB($0.22km^{-1}$ and $0.045km^-$

[1]respectively) followed by the coast (0.15km^{-1} and 0.025km^{-1} respectively) at 0.55µm wavelength. These estimated aerosol scattering and absorption coefficient were higher compared those estimated for pre-monsoon. The estimated SSA ranged from 0.76-0.86 revealing the presence of more absorbing aerosols in this season. The influence of surrounding anthropogenically active landmass increases the aerosol loading in the marine boundary layer which can directly and indirectly affect the environment and regional climate.

Chapter 6presents the results of a detailed study on the seasonal changes in the in-situ measured near-surface aerosol characteristics in the marine boundary layer of BoB as revealed by the ship-based experiments and the corresponding changes in the satellite-retrieved columnar properties of aerosols. The measured near-surface properties include total aerosol loading (M_L) and mass concentrations of various chemical species and theMODIS retrieved columnar properties are aerosol optical depth (AOD), column mass concentration (M_c), Angstrom exponent (Ŭ), effective radius (R_{eff}) and fine mode AOD and fine mode fraction. Irrespective of the season, M_L exhibited high values over north BoB and decreased towards south indicative of an outflow from IGP to BoB extending to southern BoB. Highest aerosol loading of ~83 µg m^{-3} was observed over north BoB in winter with close-by values in monsoon over north and mid BoB. Column AOD also peaked over north BoB in winter (~0.8) decreasing towards south. Mean AOD over north BoB in winter and monsoon are comparable (~0.5). The large Ŭvalues and low R_{eff} over north-BoBduring winter and pre-monsoon, indicated dominance of fine aerosols.The high AOD over North BoB in winter is attributed to anthropogenic aerosols and those in monsoon to sea-salt aerosols as revealed by their chemical composition.A seasonal change in the chemical composition of aerosols over BoB from more absorbing species in winter to scattering type in monsoon is seen.Presence of absorbing species like BC and mineral dust is partially responsible for the high AOD over north BoB during pre-monsoon and winter.Column AOD and M_c showed similar spatial pattern, decreasing from northto south.While column AOD in winter and pre-monsoon is ~50% of that in monsoon, the column mass loading shows a reduction of 30%.Total aerosol loading as well as individual species showed an exponential decrease from north to south. The e^{-1} scale distances for total aerosol loading were estimated to be of 668km and 1567km in pre-monsoon and winter respectively whereas those estimated for individual species varied from 550km to 1375km with longer distances in winter facilitating intrusion of pollutants to larger distances. In any season, considerable loading of

anthropogenic/crustal aerosols is observed over BoB. The fine mode AOD contributes to 45% in total AOD during monsoon, 69% in pre-monsoon and 73% in winter. The column aerosol mass concentration estimated based on near-surface loading and that retrieved from MODIS revealed similar spatial patterns over BoB and in fairly good agreement. However, over regions of low near-surface loading, MODIS-retrieved mass concentration is found to be over-estimate by 40 to 140%. It is observed that the columnar properties of aerosols over the marine environment of BoB have bearing on the physical and chemical characteristics of near-surface aerosols.The regional changes in aerosol characteristics can influence regional weather systems and inter-annual variations may play role in creating monsoon anomalies. This aspect needs to be investigated further using models.

7.2 Future Scope

The present study has brought out several new results on the physical, chemical and radiative characteristics of aerosols at the tropical coastal site Thiruvananthapuram and over the marine environments of AS and BoB. At the same time, this work has opened up new themes for future research in the areas of aerosol chemistry and the role of aerosols in regional radiative forcingand their role in Indian monsoon.The highlight of future directions in which the research activities to be focused in view of the outcome of the present work are given below.

Quantification of carbonaceous aerosols in atmospheric aerosols over different geographical environments is essential for more realistic assessment of the radiative and environmental impacts.Region specific models for the chemical composition of aerosols needs to be brought out including particulate organic matter through systematic long-term measurements.

Since the radiative impacts of aerosols dependent on both size and chemical nature, studies on size-resolved chemical composition of aerosols is to be focussed.The present study also brought out the need for evolving regional aerosol models combining the physical characteristics like size-distribution, mass loading and density along with size-resolved chemical composition.

A comprehensive picture on the near-surface and columnar properties of aerosols over Indian land mass and surrounding oceanic regions to be brought out making use of in-situ measurements and available satellite data. Based on this, realistic radiative forcing estimates are to be made.

Another major aspect to be addressed is the altitude dependent aerosol chemical composition. This can provide better understanding of long range transport and the source characteristics.

The role of aerosols in the Asian monsoon is still a topic of debate.The radiative forcing caused by aerosols on regional scales is to be estimated using radiative transfer codes and in depth analysis of the monsoonal anomalies needs to be carried out.

References

Achtert, P., Karlsson Andersson, M., Khosrawi, F., and Gumbel, J.: On the linkage between tropospheric and Polar Stratospheric clouds in the Arctic as observed by space–borne lidar, *Atmos. Chem. Phys*., 12, 3791-3798, doi:10.5194/acp-12-3791-2012, 2012.

Ackerman, A. S., et al., (2000), Reduction of tropical cloudiness by soot, *Science*, 288,1042-1047.

Afifi, A., V. A. Clark, and S. May (2004), Computer-aided multivariate analysis. London and New York: Chapman & Hall/CRC.

Alam, M. M., M. A. Hossain, and S. Shafee (2003), Frequency of Bay of Bengal cyclonic storms and depressions crossing different coastal zones, *Int. J. Climatol*., 23, doi:10.1002/joc.927.

Alfaro, S.C., L. Gomes, J.L.Rajot, S. Lafon, A. Gaudichet, B.Chatenet,M.Maillé, G.Cautenet, F.Lasserre, H. Cachier, and X.Y.Zhang (2003), Chemical and optical characterization of aerosols measured in spring 2002 at the ACE-Asia supersite, Zhenbeitai, China, *J.Geophys. Res.,*108 (D23):8641, doi:10.1029/ 2002JD003214.

Aloysius M, M. Mohan, K. Parameswaran, S.K. George, P.R. Nair (2008), Aerosol transport over the Gangetic basin during ISRO-GBP land campaign-II, Ann Geophys 26:431-440.

Anderson, C., R. Bergstrom, and C. Johansson (2009), Populationexposure and mortality due to regional backgroundPM in Europe – Long-term simulations of source regionand shipping contributions, *Atmos. Environ*., 43, 3614–3620,doi:10.1016/j.atmosenv.2009.03.040.

Andreae, M. O. (1995), Climate effects of changing atmospheric aerosols levels, in World Survey of Climatology , vol. 16, Future Climate of the World, edited by A. Henderson- Sellers, pp. 341-392, Elsevier, New York

Andreae, M. O., W. Elbert, R. Gabriel, D. W. Johnson, S. Osborne, and R. Wood (2000), Soluble ion chemistry of the atmospheric aerosol and SO2 concentrations over the eastern North Atlantic during ACE-2, Tellus, 52B, 1066-1087.

Andreae, M. O., and P. Merlet (2001), Emission of trace gases and aerosols from biomassburning, *Global Biogeochem. Cyc*.,12, 955-966.

Andreae, T. W., M. O. Andreae, C. Ichoku, W. Maenhaut, J. Cafmeyer, A. Karnieli, and L. Orlovsky, Light scattering by dust and anthropogenic aerosol at a remote site in the Negev desert, Israel, *J.Geophys. Res.,* 107(D2), doi:10.1029/2001JD900252, 2002.

Andreae, M. O. (2007), Atmospheric aerosols versus greenhouse gases in the twenty-firstcentury, *Phil. Trans. R. Soc*., doi: 10.1098/rsta.2007.2051, 1915-1923.

Arimoto, R., R. A. Duce, D. L. Savoie, J. M. Prospero, R. Talbot, J. D. Cullen, U. Tomza, N. F. Lewis, and B. J. Ray (1996), Relationship among aerosol constituents

from Asia and the North Pacific during PEM-West A, *J. Geophys. Res.,*101(D1), 2011-2023.

Aryasree. S., P. R. Nair, I. A. Girach, S. Jacob (2015), Winter time chemical characteristics of aerosols over the Bay of Bengal: continental influence, *Environ. Sci. Pollut. Res*., doi.10.1007/s11356-015-4700-7.

Asmi, Aet al., (2011), Number size distributions and seasonality of submicronparticles in Europe 2008–2009, Atmos. Chem. Phys., 11, 5505–5538, doi:10.5194/acp-11-5505-2011, 2011.

Asmi, A., et al., (2013), Aerosol decadal trends – Part 2: In-situ aerosol particlenumber concentrations at GAW and ACTRIS stations, Atmos.Chem. Phys., 13, 895–916, doi:10.5194/acp-13-895-2013.

Asnani, G.C., Tropical Meteorology (1993), Vol.1 and Vol.2, Indian Institute of Tropical Meteorology, Pashan, Pune, 1012 pp.

Athanasopoulou,E., M. Tombrou, S. N. Pandis, and A. G. Russell (2008), The role of sea-salt emissions and heterogeneous chemistry in the air quality of polluted coastal areas, *Atmos. Chem. Phys*., 8, 5755–5769.

Avino, P., S. Casciardi, C. Fanizza, and M. Manigrasso(2011). Deep Investigation of Ultrafine Particles inUrban Air,*Aerosol Air Qual. Res*.,11: 654–663.

Babu, S. S., K. K. Moorthy, and S. K. Satheesh (2004), Aerosol black carbon overArabian Sea during intermonsoon and summer monsoon seasons, *Geophys. Res. Lett*.,31, L06104, doi:10.1029/2003GL018716.

Babu, S.S. (2005), Investigations of atmospheric aerosol characteristics and shortwave radiative forcing over distinct environments of India. Ph.D Thesis, University of Kerala.

Babu, S.S., M.M. Gogoi, V.H. Arun, V.S. Nair, K.K. Moorthy (2012), Radiative properties of Bay of Bengal aerosols: Spatial distinctiveness and source impacts, *J Geophys Res.,*117, doi:10.1029/2011JD017355.

Babu, S. S., et al. (2013), Trends in aerosol optical depth over Indian region: Potential causes and impact indicators, *J. Geophys. Res. Atmos*., 118, 11,794–11,806, doi:10.1002/2013JD020507.

Barren P.A., and K. Willeke (2001), Aerosol Measurements: Princples, Techniqes and Applications, A John Wiley & Sons Inc, USA.

Bates, T. S., B. J. Huebert, J. L. Gras, F. B. Griffiths, and P. A. Durkee (1998),International Global Atmospheric Chemistry (IGAC) Project's First AerosolCharacterization Experiment (ACE 1): Overview, *J. Geophys. Res*., 103, 16297-16318.

Bates, T. S., P. K. Quinn, D. J. Coffman, J. E. Johnson, T. L. Miller, D. S. Covert, A.Wiedensohler, S Leinert, A. Nowak, and C. Neusüss (2001), Regional physical andchemical properties of the marine boundary layer aerosols across the Atlantic duringAerosols99: An overview, *J. Geophys. Res*., 106(D18), 20767-20782.

Bates T.S, et al., (2002), Regional marine boundary layer aerosol size distributions in the Indian, Atlantic, and Pacific Oceans: A comparison of INDOEX

measurements with ACE-1, ACE-2 and Aerosols99,*J. Geophys. Res*, 107. doi:10.1029/2001JD001174.

Bates, T. S., et al. (2004), Marine boundary layer dust and pollutant transport associated with the passage of a frontal system over eastern Asia, *J. Geophys. Res*., 109, D19S19, doi:10.1029/2003JD004094.

Bates, T. S., et al. (2006), Aerosol direct radiative effects over the northwestern Atlantic, northwestern Pacific, and North Indian Oceans: estimates based on in situ chemicaland optical measurements and chemical transport modelling, *Atmos. Chem. Phys*., 6,1657-1732.

Beegum, S.N., K. K.Moorthy, S. S.Babu(2009),Aerosol microphysics over a tropical coastal station inferred from the spectral dependence of Angstrom wavelength exponent and inversion of spectral aerosol optical depths, *J. Atmos.Solar Terr. Phys*., 71,1846–1857, doi:10.1016/j.jastp.2009.07.004.

Beegum, S.N.,(2010), Multi-station Synthesis of Aerosol Characteristics over India: Spatio-temporal Heterogeneity and Natural Variabilities,Ph.D. Thesis, University of Kerala.

Berg, W. W. Jr, and J. W. Winchester (1978),Aerosol chemistry of marine atmosphere.InChemical Oceanography, 7th ed., edited by J. P. Riley and R. Chester, pp. 173-231,Academic Press, London.

Bergstrom, R. W., Schmidt, K. S., Coddington, O., Pilewskie, P., Guan, H., Livingston, J. M., Redemann, J., and Russell, P. B.: Aerosol spectral absorption in the Mexico City area: results from airborne measurements during MILAGRO/INTEX B, Atmos. Chem. Phys., 10, 6333-6343, doi:10.5194/acp-10-6333-2010, 2010.

Bhanarkar, A.D., Rao, P.S., Gajghate, D.G. and Nema, P (2005). Inventory of SO2, PM and Toxic Metals Emissions from Industrial Sources in Greater Mumbai, India,*Atmos.Environ*.,39: 3851–3864

Bhat, G. S., et al (2001), BOBMEX: The Bay of Bengal Monsoon Experiment, *Am. Meteo. Soc*., 82, 2217-2243.

Bindu G., P. R. Nair, S.Aryasree and S. Jacob(2015), Pattern of aerosol mass loading and chemical composition over the atmospheric environment of an urban coastal station, *Journal of Atmospheric and Solar-Terrestrial Physics*, 138-139(2016) 121–135, doi.org/10.1016/ j.jastp.2016.01.004.

Blanchard, D. C. (1983), The production, distribution, and bacterial enrichment of the sea-salt aerosol, in Air-Sea Exchange of Gases and Particles, edited by P. S. Liss and W. G. N. Slinn, pp. 299-405, D.Reidal Publishing Co., Dordrecht, Holland.

Bollasina, M., and S. Nigam (2008), Absorbing Aerosols and Summer Monsoon Evolution over South Asia: An Observational Portrayal, *Am. Met. Soc.*, doi: 10.1175/2007JCLI2094.1.

Boucher, O. (1998), On aerosol direct shortwave forcing and Henyey-Greenstein phase function, J. Atmos. Sci., 55, 128–134.

Born M., and Wolf E (1996), Principles of Optics.Third edition. Pergamon Press, Oxford 1965.Brink et al., 1996,

Brito, J., L. V. Rizzo, W. T. Morgan, H. Coe, B. Johnson, J. Haywood, K. Longo, S. Freitas, M. O. Andreae, and P. Artaxo (2014), Biomass Burning Analysis (SAMBBA) field experiment, *Atmos. Chem. Phys*., 14, 12069–12083, ,doi:10.5194/acp-14-12069-2014.

Bullrich, K., (1964), Scattered Radiation in the Atmosphere and Natural Advan. Aerosols, Geophysics *10* (1964).

Cachier, H., J. Ducret, M. P. Brémond, A. Gaudichet, J.P. Lacaux, V. Yoboué, and J Baudet (1991), Biomass burning in a savannaregion of the Ivory Coast, in: Global Biomass Burning: Atmospheric,Climatic and Biospheric Implications, edited by: Levine,J. S., MIT Press, Cambridge, Mass., 174–180,.

Cachier, H., C. Liousse, P. Buat-Menard, and A. Gaudichet (1995), Particulatecontent of savanna fire emissions, *J. Atmos. Chem*., 22,123–148,.

Cariolle, D., S. M¨uller, and F. Cayla (1989), Mountain waves, polar stratospheric clouds, and the ozone depletion over Antarctica, *J. Geophys.Res*., 94, 11233–11240, doi:10.1029/JD094ID09.

Carlson, T. N., and P. Wendling (1977), Reflected radiance measured by NOAA 3 VHRR as a function of optical depth for Saharan dust, *J. Appl. Meteorol*., 16, 1368-1371.

Chakraborthy, A., and T.Gupta (2009), Chemical Characterization of SubmicronAerosol in Kanpur Region: a SourceApportionment Study, *International Journal of Civil and Environmental Engineering*, 1:2.

Chan, Y. C., R. W. Simpson, , G. H. Mctainsh, P. D. Vowles, D. D. Cohen, and G. M. Bailey (1999), Source apportionment of visibility degradation problems in Brisbane (Australia) using the multiple linear regression techniques, *Atmos. Environ*., 33(19), 3237–3250.

Charlson, E.J., W.M. Porch, A.P. Waggoner, N.C Ahlquist (1974), Background aerosol lightscattering characteristics: nephelometric observations at Mauna Loa Observatory compared with results at other remote locations, *Tellus.,* XXVI (3), 345-359.

Charlson, R. J., J. E. Lovelock, M. O. Andreae, and S. G. Warren (1987), Oceanic phytoplankton, atmospheric sulfur, cloud albedo and climate, *Nature.*, 326, 655-661.

Charlson, R.J., S.E. Schwartz, J.M. Hales, R.D. Cess, J.A. Coakley, J. E. Hansen, and D.J.

Chen, Y.S., P.C Sheen, E. Chen, Y.K Liu, T.N Wu, C.Y. Yang (2004), Effects of Asian dust storm events on daily mortality in Taipei, Taiwan(2004), *Environmental Research*.,95, Issue 2, 151–155, doi:10.1016/j.envres.2003.08.008.

Cheng, Y.H. and Y.L. Lin (2010), Measurement of ParticleMass Concentrations and Size Distributions in anUnderground Station,*Aerosol Air Qual. Res*.,10: 22–29.

Chiapello I, G. Bergametti, B. Chatenet, F. Dulac, I. Janokowiak, C. Liousse, E. S. Soares (1999), Contribution of the different aerosol species to the aerosol mass load

and optical depth over the northeastern tropical Atlantic, *J Geophys Res.*,104: 4025-4036.

Chinnam N., S. Dey, S.N.Tripathi,M.Sharma (2006), Dust events in Kanpur, northern India: Chemical evidence forsource and implications to radiative forcing, *Geophys. Res. Lett*. 33, L08803 (2006).doi:10.1029/2005GL025278.

Choobari A.O., Zawar-Reza P, Sturman A (2013) The global distribution of mineral dust and its impacts on the climate system: a review. Atmos Res 138:152–165

Chow C., J. G. Watson, H. Kuhns, V. Etyemezian, D. H. Lowenthal, D. Crow, S. D. Kohl, J. P. Engelbrecht, M. C. Green (2004), Source profiles for industrial, mobile, and area sources in the Big Bend Regional Aerosol Visibility and Observational study Judith, *Chemosphere*., 54 ,185–208.

Chow, J. C., and J. G.Watson (2004), PM2.5 carbonate concentrations at regionally representative Interagency Monitoring of Protected Visual Environment sites, *J. Geophys. Res.,* 107, doi: 10.1029/2001JD000574.

Chow, J.C., (1995), Measurement methods to determine compliance with ambient air quality tandards for suspended particles, *Journal of the Air and Waste Management Association*, 45 (5), 320-382

Christopher SA, Johnson B, Jones TA, Haywood J. 2009. Vertical andspatial distribution of dust from aircraft and satellite measurements during the GERBILS field campaign, *Geophys. Res. Lett*., **36**: L06806,DOI: 10.1029/2008GL037033.

Chun, Y., K. O. Boo, J. Kim, S.U. Park, and M. Lee (2001), Synopsis, transport, and physical characteristics of Asian dust in Korea, *J. Geophys. Res*., 106, 18461-18469.

Chung, C. E., S. Nigam, and J. T. Kiehl (2002), Effects of the South Asian absorbing haze on the northeast monsoon and surface–air heat exchange. *J. Climate*., 2462–2476.

Clarke, A. D., and J. N. Porter (1993), Pacific marine aerosol: 2. Equatorialgradients in chlorophyll, ammonium, and excess sulfate during Saga-3, *J. Geophys. Res*., 98, 16,997–17,010.

Clarke, A.G., G.A. Azadi-Boogar and G.E. Andrews (1999), Particle size and chemical composition of urban aerosols, *The Science of the Total Environment*., 235, 15-24.

Clegg S.L., P. Brimblecombe (1985), Potential degassing of hydrogen chloride from acidified sodium chloride droplets, *Atmos Environ*., 19: 465-470.

Coe, H., Allan, J. D., Alfarra, M. R., Bower, K. N., Flynn, M. J., Mc-Figgans, G. B., Topping, D. O., Williams, P. I., O'Dowd, C. D.,Dall'Osto, M., Beddows, D. C. S., and Harrison, R. M.: Chemicaland physical characteristics of aerosol particles at a remotecoastal location, Mace Head, Ireland, during NAMBLEX, *Atmos.Chem. Phys*., 6, 3289–3301, doi:10.5194/acp-6-3289-2006,

Colbeck I.,(Editor)(2008), Environmental Chemistry of Aerosols, ISBN: 978-1-4051-3919-9268 pages February 2008, Wiley-Blackwell.

Crippa, M., et al. (2013), Identification of marine and continental aerosol sources in Paris using high resolution aerosol mass spectrometry, *J. Geophys. Res. Atmos.*, 118, 1950–1963, doi:10.1002/jgrd.50151.

Curtius (2006), Nucleation of atmospheric aerosol particles, 10.1016/j.crhy.2006.10.018.

D'Errico. M., C. Cagnazzo, P. Fogli , W. K. M. Lau, and J. von Hardenberg (2012), Asian Monsoon and Elevated Heat Pump Mechanism in coupled aerosol-climate model simulations, 3rd International Conference on Earth System Modelling, 3ICESM-361-3.

Dahl, E.E., Yvon-Lewis, S.A., Saltzman, E.S.: Saturation anomalies of alkyl nitrates in the tropical Pacific Ocean,*Geophys. Res. Lett*.,**32**, (20), L20817.

d'Almeida, G. A., P. Koepke, and E. P. Shettle (1991), Atmospheric Aerosols: GlobalClimatology and Radiative Characteristics, 561 pp., A. Deepak, Hampton, Va

Das, P.K (1986), Monsoons (Monograph), World Meteorological organisation. pp155.

Das, N., S. S. Baral, S. K. Sahoo, R. K. Mohapatra, T. S. Ramulu, S. N. Das, and G. R. Chaudury (2009), Aerosol physical characteristics at Bhubaneswar, East coast of India, *Atmos. Res*., 93, 897–901, doi:10.1016/j.atmosres.2009.04.013.

Das, S., S. Dey, S.K.Dash (2014), Impacts of aerosols on dynamics of Indian summer monsoon using a regional climate model, *Clim Dyn*., DOI 10.1007/s00382-014-2284-4

David L.M., I.A. Girach, P.R. Nair (2011), Distribution of ozone and its precursors over Bay of Bengal during winter 2009: role of meteorology, *Ann Geophys*, 29:1613-1627.

David, L. M. and Nair, P. R (2011), Diurnal and seasonal variability of surface ozone and NOx at a tropical coastal site:Association with mesoscale and synoptic meteorological conditions, *J. Geophys. Res*., 116, D10303,doi:10.1029/2010JD015076, 2011.

De Leeuw G., (1986), Vertical profiles of giant particles close above the sea surface, *Tellus*.,38:51-61.

Deepak, A., and G. P. Box (1982), Representation of aerosol size distribution data by analytic models, in Atmospheric aerosols: Their formation, optical properties and effects, pp. 79-110, Spectrum Press, Hampton, Virginia.

Deepak, A., and H. E. Gerber, Eds., 1983: Report of the experts meeting on aerosols and their climatic effects. WCP-55, 107 pp. [Available from World Meteorological Organization, Case Postale No. 5, CH-1211 Geneva, Switzerland.]

Deirmendjian, D. (1969), Electromagnetic scattering on spherical polydispersions, Elsevier, New York.

Denjean, C., et al., (2016), Size distribution and optical properties of African mineral dust after intercontinental transport, *J.Geophys.Res.Atmos*., 121, 7117–7138, doi:10.1002/2016JD024783.

Dentener, F. J., G. R. Carmichael, Y. Zang, J. Lelieveld, and P. J. Crutzen (1996), Role of mineral aerosol as a reactive surface in the global troposphere, *J. Geophys. Res.*, 101, 22869-22889.

Stevens, J. (1996). *Applied Multivariate Statistics for the Behavioral Sciences (3rd ed.)*. Mahwah, Erlbaum, NJ.

Devara, P. C. S., Raj, P. E., and Pandithurai, G (1995), Aerosol-profile measurements in the lower troposphere with four-wavelength bistatic argon-ion lidar, Appl. Opt. 34(21), 4416–4425.

Dey, S., Di Girolamo, L., (2010), A climatology of aerosol optical andmicrophysicalproperties over the Indian subcontinent from 9 years (2000–2008) of Multiangle Imaging Spectroradiometer (MISR) data,*J. Geophys. Res*. 115(D15), 1–22. http://dx.doi.org/10.1029/2009JD013395.

Dey, S., S. N. Tripathi, R. P. Singh, and B. N. Holben (2004), Influence of dust storms on the aerosol optical properties over the Indo-Gangetic basin, *J. Geophys. Res*., 109, D20211, doi:10.1029/2004JD004924.

Dey, S., Tripathi, S.N., (2008),Aerosol direct radiative effects over Kanpur in the Indo-Gangetic basin, northern India, Long-term (2001-2005) observations and implications to regional climate,*J. Geophys. Res*. 113, D04212. http://dx.doi.org/10.1029/2007JD009029.

Diapouli, E.,K. Eleftheriadis , A. A. Karanasiou , S. V.Ove Hermansen , I. Colbeck , M. Lazaridis (2011), Indoor and Outdoor Particle Number and Mass Concentrations in Athens. Sources, Sinks and Variability of Aerosol Parameters ,*Aerosol and Air Quality Research*, 11: 632–642, doi: 10.4209/aaqr.2010.09.0080

Dillner, A. M., J. J. Schauer, Y. Zhang, L. Zeng, and G. R. Cass (2006), Size-resolvedparticulate matter composition in Beijing during pollution and dust events, *J. Geophys.Res.*, 111, D05203, doi:10.1029/2005JD006400.

Diner et al., 1998 Multi-angle Imaging SpectroRadiometer (MISR) Instrument Description and Experiment Overview, IEEE TRANSACTIONS ON GEOSCIENCE AND REMOTE SENSING, VOL. 36, NO. 4, JULY 1998.

Ding, A. J., et al. (2016), Enhanced haze polltuion by black carbon in megacities in China, *Geophys. Res. Lett*., 43, 2873–2879, doi:10.1002/2016GL067745,

Draxler R.R., G.D. Rolph (2003), HYSPLIT (HYbrid Single-Particle Lagrangian Integrated Trajectory)Model access via NOAA ARL READY Website (http://www.arl.noaa.gov/ready/hysplit4.html). NOAA Air Resources Laboratory, Silver Spring, MD.

Draxler, R.R., 1996. Trajectory optimization for balloon flight planning. Weather and Forecasting, 11, 111-114.

Dubovik, O., et al. (2002a), Variability of absorption and optical properties of key aerosol types observed in worldwide locations, *J. Atmos. Sci*., 59, 590– 608.

Duce, R. A., R. Arimoto, B. J. Ray, C. K. Unni, and P. J. Harder (1983), Atmospherictrace elements at Enewetak Atoll 1. Concentrations, sources and temporal variability, *J.Geophys. Res*., 88, 5321-5342.

Koulouri E., S.Saarikoski, C. Theodosi , Z. Markaki , E. Gerasopoulos, G. Kouvarakisa, T. Ma¨kela, R. Hillamo, N. Mihalopoulos (2008), Chemical composition and sources of fine and coarse aerosol particles in the Eastern Mediterranean, *Atmospheric Environment*., 42, 6542–6550,doi:10.1016/j.atmosenv.2008.04.010.

Eastman, R., and S. G. Warren(2013): A 39–yr survey of cloud changes from landstations worldwide 1971–2009: Long-term trends, relation to aerosols, andexpansion of the tropical belt. *J. Clim*., **26**, 1286–1303.

Edgerton, E.S.,Benjamin E. Hartsell, Rick D. Saylor, John J. Jansen, D. Alan Hansen, and George M. Hidy 2006 The Southeastern Aerosol Research and Characterization Study, Part 3: Continuous Measurements of Fine Particulate Matter Mass and Composition,*Journal of the Air & Waste Management Association*.,Vol. 56 , Iss. 9,

Eleftheriadis K. et al., (2006), Size distribution, composition and origin of the submicron aerosol in the marine boundary layer during the eastern Mediterranean "SUB-AERO" experiment, *Atmos Environ*, 40:6245-6260.

Elias, T., Haeffelin, M., Drobinski, P., Gomes, L., Rangognio, J.,Bergot, T., Chazette, P., Raut, J.-C., and Colomb, M.: Particulate contribution to extinction of visible radiation: pollution, haze, and fog, *Atmos. Res.,* 92, 443–454, 2009.

Englert, N. (2004), Fine particles and human health- a review of epidemiological studies,*Toxicol. Lett*.,149, 235-242.

Eswaran, K., S. K. Satheesh, and J. Srinivasan (2014), Dependence of 'critical cloud fraction' on aerosol composition, *Atmos. Sci. Lett*., DOI: 10.1002/asl2.571.

Exton, H. J., J. Latham, P. M. Park, S. J. Perry, M. H. Smith, and R. R. Allan (1985), The production and dispersal of marine aerosol, *Q. J. Roy. Meteorol. Soc*., 111, 817-837.

Finlayson-Pitts, B. J. ., J. N. Pitts, 2000, Chemistry of the Upper and Lower Atmosphere, Academic Press, San Diego.

Fishman, J., J. M. Hoell, R. D. Bendura, R. J., McNeil, and V. W. J. H. Kirchhoff, NASA GTE TRACE A experiment (September-October 1992): Overview, *J. Geophys. Res*.,101, 23,865-23,879.

Fitzgerald, J. W. (1991), Marine aerosols: A review, *Atmos. Environ*., 25A, 533-545.

Flossman, A. I., and H. R. Pruppacher (1988), A theoretical study of the wet removal of atmospheric pollutants Part-III: The uptake, redistribution and deposition of (NH4)2SO4 particles by a convective cloud using a two-dimensional cloud dynamics model, *J. Atmos. Sci*., 45, 1857-1871

Flossman, A. I., W. D. Hall, and L. R. Pruppacher (1985), A theoretical study of the wet removal of atmospheric pollutants Part-II: The redistribution of aerosol particles captured through nucleation and impaction scavenging by growing cloud drops, *J. Atmos. Sci*., 42, 582-606.\

Fomba, K. W., K. M¨ uller, D. van Pinxteren, and H. Herrmann (2013), Aerosol size-resolved trace metal composition in remote northerntropical Atlantic marine

environment: case study Cape Verdeislands, *Atmos. Chem. Phys*., 13, 4801–4814, www.atmos-chem-phys.net/13/4801/2013/doi:10.5194/acp-13-4801-2013

Ford, B. and C. L. Heald, (2013,: Aerosol loading in the Southeastern United States: reconciling surface and satellite observations, *Atmos. Chem. Phys*., 13, 9269-9283, doi:10.5194/acp-13-9269-2013, 2013.

Fraser, M.P., K Lakshmanan, S.G Fritz, B Ubanwa Variation in composition of fine particulate emissions from heavy-duty diesel vehicles. *Journal of Geophysical Research*., 107 (D21) (2002), p. 8346

Fraser R. S. (1976) Satellite measurements of mass of Sahara dust in the atmosphere. Appl. e

Frierl, G. R., and A. R. Robinson (1972), Deadly Surges in the Bay of Bengal: Dynamics and Storm-tide Tables, *Nature*, 239, doi:10.1038/239213a0.

Fritz J.S.,and D.T. Gjerde, 2009 Ion Chromatography, 4th, Completely Revised and Enlarged Edition, ISBN: 978-3-527-32052-3, John Wiley & Sons

Fuzzi, S., Baltensperger, U., Carslaw, K., Decesari, S., Denier van der Gon, H., Facchini, M. C., Fowler, D., Koren, I., Langford, B., Lohmann, U., Nemitz, E., Pandis, S., Riipinen, I., Rudich, Y., Schaap, M., Slowik, J. G., Spracklen, D. V., Vignati, E., Wild, M., Williams, M., and Gilardoni, S (2015), Particulate matter, air quality and climate: lessons learned and future needs, *Atmos. Chem. Phys*., 15, 8217-8299, doi:10.5194/acp-15-8217-2015, 2015.

Galloway, J. N., Thornton, J. D., Norton, S. A., Volchok, H. L., andMclean, R. A. N.: Trace-Metals in Atmospheric Deposition – aReview and Assessment, *Atmos. Environ.*, 16, 1677–1700, 1982.

Ganguly, D., A. Jayaraman, and H. Gadhavi (2005), In situ ship cruise measurements ofmass concentration and size distribution of aerosols over Bay of Bengal and theirradiative impacts, *J. Geophys. Res*., 110, D06205, doi:10.1029/2004JD005325.

Ganguly. D., P. J. Rasch, H. Wang, and J. Yoon (2009) Fast and slow responses of the South Asian monsoon systemto anthropogenic aerosols, *Geophys. Res. Lett*., 39, doi:10.1029/2012GL053043.

Gantt, B., and Meskhidze, N (2013), The physical and chemical characteristics of marine primary organic aerosol: a review, *Atmos. Chem. Phys*., 13, 3979-3996, doi:10.5194/acp-13-3979-2013, 2013.

Gantt, B., Xu, J., Meskhidze, N., Zhang, Y., Nenes, A., Ghan, S. J., Liu, X., Easter, R., and Zaveri, R.: Global distribution and climate forcing of marine organic aerosol – Part 2: Effects on cloud properties and radiative forcing, *Atmos. Chem. Phys*., 12,6555–6563, doi:10.5194/acp-12-6555-2012, 2012

Gautam. R., N. C. Hsu, K. M. Lau, and M. Kafatos (2009) Aerosol and rainfall variability over the Indian monsoon region: distributions, trends and coupling, *Ann. Geophys*., 27, 3691–3703.

Gebhart, J., (1993) Optical direct-reading techniques: light intensity systems. In: Willeke, K., Baron, P.A. (Eds.), Aerosol Measurement: Principles, Techniques, and Applications. Van Norstrand Reinhold, New York, pp. 313-344.

Gelencser, A., (2004) Carbonaceous Aerosol, Springer, Dordrecht.

Geng, H., F. Cheng, and C. Ro (2011), Single-Particle Characterization of Atmospheric Aerosols Collected at Gosan, Korea, during the Asian Pacific Regional Aerosol Characterization Experiment Field Campaign Using Low-Z (Atomic Number) Particle Electron Probe X-ray Microanalysis,*Journal of the Air & Waste Management Association*Vol. 61 , Iss. 11.

George S,K, P.R. Nair, K. Parameswaran, S. Jacob, A. Abraham (2008), Seasonal trends in chemical composition of aerosols at a tropical coastal site of India, *J. Geophys. Res*. 113., doi:10.1029/2007JD009507.

George S.K and P.R. Nair (2008), Aerosol mass loading over the marine environment of Arabian Sea during ICARB: Sea-salt and non-sea-salt components, *J. Earth. Syst. Sci*, 117: 333-344.

George S.K, P.R. Nair, K. Parameswaran, S. Jacob (2011), Wintertime chemical composition of aerosols at a rural location in the Indo-Gangetic Plains, *J. Atmos. Solar Terr. Phys.,* 73. doi:10.1016/j.jastp.2011.04.005.

Gillette, D. (1978), Wind tunnel simulation of erosion of soil: Effect of soil texture,sandblasting, wind speed and soil consolidation on dust production, *Atmos. Environ*.,12, 1735-1743.

Ginoux, P., J. M. Prospero, T. E. Gill, C. Hsu, and M. Zhao (2012), Global scale attribution of anthropogenic and natural dust sources and theiremission rates based on MODIS Deep Blue aerosol products, *Rev. Geophys*., 50, RG3005, doi:10.1029/2012RG000388.

Girach IA., and PR Nair (2010),Spatial distribution of near-surface CO over Bay of Bengal during winter: role of transport,*J Atmos Solar TerrPhys.,* 72:1241–1250. doi:10.1016/j.jastp.2010.07.025

Girach I.A., P.R. Nair (2014), On the vertical distribution of carbon monoxide over Bay of Bengal during winter: Role of water vapour and vertical updrafts, *J. Atmos. Solar. Terr. Phy*s., 117: 31-47.

Girolamo, L., T. C. Bond, D. Bramer, D. J. Diner, F. Fettinger, R. A. Kahn, J. V. Martonchik, M. V. Ramana, V. Ramanathan, and P. J. Rasch (2004), Analysis of Multiangle Imaging Spectroradiometer (MISR) aerosol optical depths over greater India during winter 2001-2004, *Geophys. Res. Lett*., 31, L23115,doi:10.1029/2004GL021273.

Glantz, P., Nilsson, E. N., and Hoyningen-Huene, W (2009), Estimating a relationship between aerosol optical thickness and surface wind speed over the ocean, *Atmos. Res*., 92, 58–68.

Gogoi, M. M., K. K. Moorthy, S. S. Babu, and P. K. Bhuyan (2009),Climatology of columnar aerosol properties and the influence of synopticconditions: First-time results from the northeastern region of India,*J. Geophys. Res*., 114, D08202, doi:10.1029/2008JD010765.

Granier C, Bessagnet B, Bond T, D'Angiola A, van der Gon HG, Frost G, Heil A, Kainuma M, Kaiser J, Kinne S et al (2011) Evolution of anthropogenic and biomass burning emissions at global and regional scales during the 1980–2010 period. Climatic Change. doi: 10.1007/s10584-011-0154-1

Grey, W.M.F., North, P.R.J., Los, S.O., 2006a. Computationally efficient method for retrieving aerosol optical depth from ATSR-2 and AATSR data,*Appl. Opt*., 45, 2786–2795.

Guenther, A. B.: Upscaling biogenic VOC emissions from leaves tolandscapes, in: Biology, Controls and Models of Tree Volatile Organic Compound Emissions, edited by: Niinemets, U. and Monson, R., Springer Tree Physiology series, 2012.

GuoXiong. W., G. Yue, W. TongMei, L. YiMin, Y. JingHui and M. JiangYu (2011),Vortex genesis over the Bay of Bengal in spring and its role in the onset of the Asian Summer Monsoon, *Science* China,54, doi: 10.1007/s11430-010-4125-6.

Hadley, O. and Kirchstetter, W.: Black-carbon reduction of snow albedo, *Nat. Clim. Change*, 2, 437–440, 2012.

Hand, J. L., and S.M Kreidenweis (2002), A New Method for Retrieving Particle Refractive Index and Effective Density from Aerosol Size Distribution Data, *Aerosol Science and Technology*., 36: 1012–1026.

Hand, J. L., B. A.Schichtel,., W. C.Malm,., and M.L. Pitchford, (2012), Particulate sulfate ion concentration and SO2 emission trends in the United States from the early 1990s through 2010, *Atmos. Chem.* Phys., 12, 10353–10365, doi:10.5194/acp-12-10353-2012, 2012.

Hansen, A.D.A., H. Rosen, and T. Novakov, The Aethalometer, an instrument for the realtime measurement of optical absorption by aerosol particles, *Sci. Total Environ.*, 36, 191- 196, 1984.

Hansen, J., M. Sato, and R. Ruedy (1997), Radiative forcing and climate response, *J. Geophys. Res*., 102(D6), 6831–6864.

Harrison and vanGrieken J. Wiley, (1998) ISBN; 0471959359, 9780471959359; University of Michigan Atmospheric particles, Volume 5.

Hansen, J. E., M. Sato, R. Ruedy, A. Lacis, and V. Oinas (2000), Global warming in thetwenty-first century: An alternative scenario, *Proc. Nat. Acad. Sci*., 97, 9875-9880.

Haywood, J. and O. Boucher (2000), Estimates of the direct and indirect radiativeforcing due to tropospheric aerosols: a review, *Rev. Geophys*., 38, 513-543.

Haywood, J. M., et al. (2008), Overview of the Dust and Biomass burning Experiment andAfrican Monsoon Multidisciplinary Analysis Special Observing Period, *J. Geophys. Res*., 113, D00C17, doi:10.1029/2008JD010077.

Hegde, P., A. K. Sudheer, M. M. Sarin, and B. R. Manjunatha (2007), Chemical characteristics of atmospheric aerosols over southwest coast of India, *Atmos. Environ.*, 41, 7751-7766.

Hegde, P., and K. Kawamura (2012), Seasonal variations of water-soluble organic carbon, dicarboxylic acids, ketocarboxylic acids, and dicarbonyls in Central

Himalayan aerosols, *Atmos. Chem. Phys*, 12, 6645–6665, doi:10.5194/acp-12-6645-2012.

Hegde P., K. Kawamura, I. A. Girach and P. R. Nair (2015), Characterisation of water-soluble organic aerosols at a site on the southwest coast of India, *Journal of Atmospheric Chemistry*, 73, 181-205, http://dx.doi.org/10.1007/s10874-015-9322-4.

Hegde P., K. Kawamura, H. Joshi and M. Naja (2015), Organic and inorganic components of aerosols over the central Himalayas: Winter and summer variations in stable carbon and nitrogen isotopic composition, *Environmental Science and Pollution Research.*, 23, 6102-6118, http://dx.doi.org/10.1007/s11356-015-5530-3.

Hegg, D. A., L. F. Radke, and P. V. Hobbs (1991), Measurement of Aitken nuclei andcloud condensation nuclei in the marine atmosphere and their relation to the DMSCloud-Climate hypothesis, *J. Geophys. Res*., 96, 8727-8733.

Heintzenberg J. 2009. The SAMUM-1 experiment over southern Morocco: overview and introduction, *Tellus* B 61(1): 2–11, doi: 10.1111/j.1600-0889.2008.00403.x.

Heintzenberg, J., D. S. Covert, and R. Van Dingenen (2000), Size distribution and chemical composition of marine aerosols: A compilation andreview, *Tellus*, Ser. B, 52, 1104–1122.

Hess, M., Koepke, P., Schult, I., (1998), Optical properties of aerosols and clouds: thesoftware package OPAC, *Bull. Amer. Meteor. Soc*., 79 (5), 831e842.

Hidy, G. M. (1984), Aerosols: An industrial and environmental science, 774 pp., Academic Press Inc., Orlando, Florida.

Hidy, G. M., Blanchard, C. L., Baumann, K., Edgerton, E., Tanenbaum, S., Shaw, S., E. Knipping, I. Tombach, J. Jansen, and J. Walters (2014), Chemical climatology of the southeastern United States, 1999–2013, *Atmos. Chem. Phys*., 14, 11893–11914, doi:10.5194/acp-14-11893-2014,.

Hidy, G.M., and W. Pennell (2010), Multipollutant air quality management: A critical review. *J. Air Waste Manage. Assoc*. 60:645–74. doi:10.3155/1047-3289.60.6.645.

Hildemann, L. M., G. R. Markowski, and G. R. Cass, Chemical composition of emissions from urban source of fine organic aerosol, *Environ. Sci. Technol*., 25, 744-759, 1991.

Hinds, W. C 1999.Aerosol Technology, 2nd Ed. New York: John Wiley & Sons.

Ho, K.F., S. S. Hang.Ho, Ru-. J. Huang, S.X. Liu , Jun-Ji Cao, T. Zhang , Hsiao-Chi Chuang, C.S. Chan, D. Hu, and L. Tian (2015), Characteristics of water-soluble organic nitrogen in fine particulate matter in the continental area of China *Atmospheric Environment* 106 (2015) 252e261.

Hobbs, P. V. (2000), Introduction to Atmospheric Chemistry, 262 pp., Cambridge

Hoffman, D. J. (1988), Aerosols and climate, Ed. P.V. Hobbs and M. P. McCormick, A.Deepak publishing, Virginia, USA, 486 pp.

Hofmann, (1992), Climate forcing by anthropogenic aerosols, *Science*, 255, 423-430, 1992.

Hondula, D.M., L. Sitka, R. E. Davis, D. B. Knight, S. D. Gawtry, M. L. Deaton, T. R. Lee, C. P. Normile, and P. J. Stenger (2010), A back-trajectory and air mass climatology for the Northern Shenandoah Valley, USA *Int. J. Climatol*., 30: 569 – 581 (2010), DOI: 10.1002/joc.1896.

Hoppel,W. A., and G. M. Frick (1990), Submicron aerosol size distributionsmeasured over the tropical and South-Pacific, *Atmos. Environ*., Part A, 24,645–659.

Hoppel, W. A., G. M. Frick, and R. E. Larson (1986), Effect of nonprecipitatingclouds on the aerosol size distribution in the marine boundary-layer, *Geophys. Res. Lett*., 13, 125– 128.

Hsu, N. C., Tsay, S. C., King, M. D., and Herman, J. R (2004), Aerosol Properties Over Bright-Reflecting Source Regions, *IEEE T. Geosci. Remote.*, 42, 557–569, doi:10.1109/TGRS.2004.824067, 2004.

Hsu, N. C., Tsay, S. C., King, M. D., and Herman, J. R.: Deep blue retrievals of Asian aerosol properties during ACE-Asia, *IEEE T. Geosci. Remote*, 44, 3180–3195, doi:10.1109/TGRS.2006.879540, 2006.

Huang, H., G. E. Thomas, and R. G. Grainger (2009)Relationship between wind speed and aerosol optical depth over remote ocean,*Atmos. Chem. Phys. Discuss*., 9, 24511–24529.

Huebert BJ, Bates T, Russell PB, Shi G, Kim YJ, Kawamura K, Carmichael G, Nakajima T (2003) An overview of ACE-Asia: Strategies for quantifying the relationships between Asian aerosols and their climatic impacts, *J Geophys Res.*, 108.doi:10.1029/2003JD003550

Huebert, B. J., S. G. Howell, L. Zhuang, J. A. Heath, M. R. Litchy, D. J. Wylie, J. L. Kreidler-Moss, S. Coppicus, and J.E. Pfiffer (2009), Filter and Impactor measurements of anions and cations during the First Aerosol Characterization Experiment (ACE 1), *J. Geophys Res*., 103, 16,493-16,509,

Hurley, P., (1994), PARTPUFF - A Lagrangian particle-puff approach for plume dispersion modeling applications, *J. Appl. Meteorol*., 33, 285-294.

Hussein, T., A.Karppinen, J.Kukkonen,J.Härkönen, P. P. Aalto,K.Hämeri, V.M.Kerminen, and M.Kulmala (2006), Meteorological dependence of size-fractionated number oncentrations of urban aerosol particles, *Atmos. Environ*., 40, 1427–1440, 2006.

Ignatov, A., et al. (2005), Two MODIS aerosol products over ocean on the Terra and Aqua CERES SSF datasets, *J. Atmos. Sci*., 62, 1008–1031.

IPCC, 2007: *Climate Change 2007*: The Physical Science Basis. Contribution of Working Group I to the Fourth Assessment Report of the Intergovernmental Panel on Climate Change [Solomon, S., D. Qin, M. Manning, Z. Chen, M. Marquis, K.B. Averyt, M.Tignor and H.L. Miller (eds.)]. Cambridge University Press, Cambridge, United Kingdom and New York, NY, USA.

IPCC, 2013: *Climate Change 2013:* The Physical Science Basis. Contribution of Working Group I to the Fifth Assessment Report of the Intergovernmental Panel on Climate Change [Stocker, T.F., D. Qin, G.-K. Plattner, M. Tignor, S.K. Allen, J. Boschung, A. Nauels, Y. Xia, V. Bex and P.M. Midgley (eds.)]. Cambridge University Press, Cambridge, United Kingdom and New York, NY, USA, 1535 pp, doi:10.1017/CBO9781107415324.

Jacob, D., J. Crawford, M. Kleb, V. Connors, R. J. Bendura, J. Raper, G. Sachse, J. Gille,L. Emmons, and C. Heald (2003), The Transport and Chemical Evolution over thePacific (TRACE-P) aircraft mission: design, execution, and first results, *J. Geophys. Res*., 108, 9000, 10.1029/2002JD003276.

Jacobson, M. C., H. -C. Hansson, K. J. Noone, and R. J. Charlson (2000), Organicatmospheric aerosols: Review and state of the science, *Rev. Geophys*., 38, 267-294.

Jacobson, M. Z., (2012), Investigating cloud absorption effects: Global absorptionproperties of black carbon, tar balls, and soil dust in clouds and aerosols. *J. Geophys. Res*., **117**, D06205.

Jaenicke R. and L.Schütz (1978), Comprehensive study of physical and chemical properties ofthe surface aerosol in the Cape Verde Islands region, *J. Geophys. Res*., 83, 3585-3599, 1978.

Jaenicke, R. (1984), Physical aspects of atmospheric aerosol, in Aerosols and their Climatic Effects, edited by H. E. Gerbard and A. Deepak, pp. 7-34, A. Deepak,Hampton, Va..

Jaenicke, R., (1993), Tropospheric Aerosols in Aerosol-Cloud-Climate Interactions, edited by P.V.Hobbs, Academic Press.

Tomlinson, J.M., R. Li, and D. R. Collins (2007), Physical and chemical properties of the aerosol within thesoutheastern Pacific marine boundary layer, *J. Geophys. Res,* VOL. 112, D12211, doi:10.1029/2006JD007771, 2007.

Jaswal, A. K., V. Singh and S. R. Bhambak (2012). Relationship between sea surface temperature and surface air temperature over Arabian Sea, Bay of Bengal and Indian Ocean, *J. Ind. Geophys.Union*., 16, 41-53.

JayaramanA.,Y. B. Acharya, B. H. Subbaraya,H. Chandra (1996),Laser radar study of the middle atmosphere over Ahmedabad, *Indian Journal of Radio and Space Physics.,* 25(6):318-327.

Jayaraman, A., D. Lubin, S. Ramachandran, V. Ramanathan, E. Woodbridge, W. Collins and K.S Zalpuri (1998), *J.Geophys.Res*., 103,13827-13836.

Jayaraman, A., H. Gadhavi, D. Ganguly, A. Misra, S. Ramachandran, and T. A. Rajesh (2006), Spatial variations in aerosol characteristics and regional radiative forcing overIndia: Measurements and modeling of 2004 road campaign experiment, *Atmos. Environ*., 40, 6504-6515.

Jethva, H., S. K. Satheesh, and J. Srinivasan (2005), Seasonal variability of aerosols over the Indo-Gangetic basin, *J. Geophys. Res*., 110, D21204, doi:10.1029/2005JD005938.

Jiang, X., M. C. Barth, C. Wiedinmyer, and S. T. Massie (2013), Influence of anthropogenic aerosolsthe Asian monsoon: a case studythe WRF-Chem model, *Atmos. Chem. Phys.*, 13,doi:10.5194/acpd-13-21383-2013.

Johansen A.M, R.L. Siefert, M.R. Hoffman (2000), Chemical composition of aerosols collected over the tropical North Atlantic Ocean*, J. Geophys. Res*. 105:15277-15312.

Junge, (1982), Physical aspects of the atmospheric aerosol Chemistry of the Unpolluted and polluted Troposphere, 341-373,10.1007/978-94-009-7918-5_14, Springer, Netherlands.

Junge, C. E. (1963), Air Chemistry and Radioactivity, Academic Press, New

Junge, C. E., and J. E. Manson (1961), Stratospheric aerosol studies, *J. Geophys. Res.*, 66(7), 2163–2182, doi:10.1029/JZ066i007p02163.

Satheesh S.K., (1998), Seasonal and long term variation of aerosol content in theatmospheric mixing region at a tropical station on the Arabian Sea coast, *J. Atmos. Solar Terr. Phys*., 60, 17-25.

Kaiser H F.The varimax criterion for analytic rotation in factor analysis (1958) *Psychometrika* **23**:187-200.

Kanakidou, M., et al. (2005), Organic aerosol and global climate modelling: A review, *Atmos. Chem. Phys*., 5(4), 1053–1123.

Kandler. K et al., (2009), Size distribution, mass concentration, chemical and mineralogical composition and derived optical parameters of the boundary layer aerosol at Tinfou, Morocco, during SAMUM 2006, *Tellus B*., 61, 32–50, doi:10.1111/j.1600-0889.2008.00385.x.

Kanlay et al., (1996), The NCEP/NCAR 40-year reanalysis project, *Bulletin of American Meteorological Society,* Volume 77, pp. 437-470.

Kapoor, R. K., and S. K. Paul (1980), A study of the chemical components of aerosolsand snow in the Kashmir region, *Tellus*., 32, 33-41.

Kapoor, R. K., L. T. Khemani, and BH. V. Ramanamurty (1972), Chemical compositionof rain water and rain characteristics at Delhi - II, *Tellus*, 24, 575-580.

Kaskaoutis, D.G., et al., 2013. Aerosol properties and radiative forcing over Kanpur during severe aerosol loading conditions, *Atmos. Environ*., 79, 7–19.

Kaufman, Y. J., D. Tanre, H. R. Gordon, T. Nakajima, J. Lenoble, R. Frouin, H. Grassl,B. M. Herman, M. D. King, and P. M. Teillet (1997), Passive remote sensingof tropospheric aerosol and atmospheric correction for the aerosol effect, *J.Geophys. Res.,* 102, 16815-16830.

Kaufman, Y. J., D, Tanre, L. A. Remer, E. F. Vermote, A. Chu, and B. N. Holben, (1997) Operational remote sensing of tropospheric aerosol over land from EOS moderate resolution imaging spectroradiometer, *J. Geophys. Res*., 102, 17051–17068, doi:10.1029/96JD03988, 1997a.

Kaufman, Y., A. Smirnov, B. Holben, and O. Dubovik (2001), Baseline maritime aerosol: methodology to derive the optical thicknessand scattering properties, *Geophys. Res. Lett*., 17, 3251–3254, doi:10.1029/2001GL013312, 2001.

Kaufman, Y.J., and I. Koren (2006), Smoke and pollution aerosol effect on cloud cover, *Science*, 313, DOI: 10.1126/science.1126232.

Kaufman, Y.J., P. V. Hobbs, V. W. J. H. Kirchhoff, P. Artaxo, L.A. Remer, B. N. Holben, M. D. King, D. E. Ward, E. M. Prins,K. M. Longo, L. F. Mattos, C. A. Nobre, J. D. Spinhirne, Q. Ji,A. M. Thompson, J. F. Gleason, and S. A. Christopher, (1998), Smoke, clouds, and radiation—Brazil (SCAR-B) experiment, *Journal of Geophysical Research*., **103**, 31783-31808

Kedia, S., S. Ramachandran, A. Kumar, and M. M. Sarin (2010),Spatiotemporal gradients in aerosol radiative forcingand heating rate over Bay of Bengal and Arabian Seaderived on the basis of optical, physical, and chemicalproperties, *J. Geophys. Res*., 115, D07205, doi:10.1029/2009JD013136.

Kedia, S., S. Ramachandran, T.A. Rajesh, R. Srivastava (2012), Aerosol absorption over Bay of Bengal during winter: Variability and sources, *Atmospheric environment*, 54,738-745.

Kedia, S., and S. Ramachandran (2008), Features of aerosol optical depthsover the Bay of Bengal and the Arabian Sea during premonsoon season: Variabilities and anthropogenic influence, *J. Geophys. Res*., 113, D11201, doi:10.1029/2007JD009070.

Keene, W. C., and D. L. Savoie (1998), The pH of deliquesced sea-salt aerosol inpolluted marine air, *Geophys. Res. Lett*., 25, 2181–2184, 1998.

Keene, W. C., R. Sander, A. A. P. Pszenny, R. Vogt, P. J. Crutzen, and J. N. Galloway (1998), Aerosol pH in the marine boundary layer: A review and model evaluation, *J. Aerosol Sci*., 29, 339–356.

Kerminen, V.-M., L. Pirjola, and M. Kulmala (2001), How significantly does coagulational scavenging limit atmospheric particle production?, *J. Geophys. Res*., 106(D20), 24119–24125, doi:10.1029/2001JD000322.

Khemani, L. T., M. S. Naik, G. A. Momin, R. Kumar, R. N. Chatterjee, G. Singh, and Bh.V. Ramanamurty (1985), Trace elements in the atmospheric aerosols at Delhi, NorthIndia, *J. Atmos. Chem*., 2, 273-285.

King MD, Kaufman YJ, Tanre D and Nakajima T (1999) Remote sensing of tropospheric aerosols from space: past, present, and future, *Bulletin of the American Meteorological Society.,* 80: 2229-2259.

Kleefeld, C., C. D. O'Dowd, S. O'Reilly, S. G. Jennings, P. Aalto,E. Becker, G. Kunz, and G. de Leeuw (2002), Relative contribution of submicron and supermicron particles to aerosol light scattering in the marine boundary layer, *J. Geophys. Res*., 107(D19), 8103, doi:10.1029/2000JD000262.

Kline, (1994), An Easy Guide to Factor Analysis Psychology Press, 19940415094909, 9780415094900.

Koepke, P., Hess, M., Schult, I., Shettle, E.P (1997), Global Aerosol Data Set, MPI Meteorologie Hamburg Report No. 243, 44 pp.

Kok, J. F., (2011), A scaling theory for the size distribution of emitted dust aerosolssuggests climate models underestimate the size of the global dust cycle. *Proc.Natl. Acad. Sci*. U.S.A., **108**, 1016–1021.

Kokhanovsky A., (2008), Aerosol optics: light absorption and scattering by particles in the atmosphere, Springer Science & Business Media.

Kompalli, S. K., S. S. Babu, K. K. Moorthy, M. M. Gogoi, V. S. Nair, and J. P. Chaubey (2013), Seasonal variation of aerosol black carbon distribution over the Bay of Bengal: multi-campaign measurements. *Atmos. Environ*., 64,366–373. http://dx.doi.org/10.1016/j.atmosenv.2012.09.073.

Kompalli, S.K., K. Krishna Moorthy and S. Suresh Babu (2013), Rapid response of atmospheric BC to anthropogenic sources: observational evidence, *Atmos. Sci. Let*. 15: 166–171 (2014)DOI: 10.1002/asl2.483.

Kondo, Y., Y. Miyazaki, N. Takegawa, T. Miyakawa, R. J. Weber, J. L. Jimenez, Q. Zhang, and D. R. Worsnop (2007),Oxygenated and water-soluble organic aerosols in Tokyo. *J. Geophys. Res*., 112, D01203, doi:10.1029/2006JD007056.

Konwar, M., R. S. Maheskumar, J. R. Kulkarni, E. Freud, B. N. Goswami, and D. Rosenfeld (2012), Aerosol control on depth of warm rain in convective clouds, *J. Geophys. Res*., 117, D13204, doi:10.1029/2012JD017585.

Kreyszig, E., 1968. Advanced Engineering Mathematics. 2nd Ed., J. Wiley and Sons, New York, 898 pp.

Kulmala, M., et al., (2011) General overview: European Integrated project on Aerosol Cloud Climate and Air Quality interactions (EUCAARI) – integrating aerosolresearch from nano to global scales. *Atmos. Chem. Phys*., **11**, 13061–13143.

Kulshrestha A., D. D. Massey, J. Masih, A. Taneja (2014), Source Characterization of Trace Elements in Indoor Environments at Urban, Rural and Roadside Sites in a Semi Arid Region of India. *Aerosol and Air Quality Research*, 14: 1738–1751,doi: 10.4209/aaqr.2013.05.0147.

Kulshrestha, U. C., L. Granat, M. Engardt, and H. Rodhe (2005), Review of precipitation monitoring studies in India - a search for regional patterns, *Atmos. Environ*., 39, 7403-7419.

Kulshrestha, U. C., A. Saxena, N. Kumar, K. M. Kumari, and S. S. Srivastava (1998), Chemical composition and association of size-differentiated aerosols at a suburban site in a semi-arid tract of India, *J. Atmos. Chem*., 29, 109-118.

Kumar, A., and M. M. Sarin (2009), Mineral aerosols from western India: Temporal variability of coarse and fine atmospheric dust and elemental characteristics. *Atmos. Environ*., 43, 4005-4013.

Kumar, A., M. M. Sarin, and A. K. Sudheer (2008), Mineral and anthropogenic aerosols in Arabian Sea atmospheric boundary layer: Sources and spatial variability, *Atmos. Environ*., 42(21), 5169-5181.

Kunhikrishnan, P. K., K. Sen Gupta, R. Radhika, J. W. J. Prakash, J., Nair, and K.Narayanan (1993), Study on thermal internal boundary layer structure over Thumba, India. *Ann. Geophys*, 11, 52–60.

Larssen, S., Gram,F., Hagen,L.O., Jansen,H., Olsthoorn, X., Aundhe,R.V., Joglekar, U.,1997. In: Shah,J., Nagpal,T. (Eds.),URBA IR—Urban Air Quality Management Strategy in Asia: Greater Mumbai Report. The International Bank of Reconstruction and Development, The World Bank, Washington DC,231pp.

Lau, K. M., and K. M. Kim (2006), Observational relationships between aerosol and Asian monsoon rainfall, and circulation, *Geophys. Res. Lett*., doi:10.1029/2006GL027546.

Lau, K. M., M. K. Kim, and K. M. Kim (2006), Asian summer monsoon anomaliesinduced by aerosol direct forcing: The role of the Tibetan Plateau*, Clim. Dyn.,* 26, 855-864, doi:10.1007/s00382-006-0114-z.

Lau, K.-M., et al. (2008), The Joint Aerosol-Monsoon Experiment: A new Challenge for monsoon climate research, *Bull. Am. Meteorol. Soc*., 89, 369 – 383, doi:10.1175/BAMS-89-3-369.

Lau, K.-M., K.-M. Kim, Y. C. Sud et al., 2009a: A GCM study of the response of the atmospheric water cycle of West Africa and the Atlantic to Saharan dust radiative forcing. *Ann. Geophys*., **1**, 4023–4037, doi: 10.51941/angeo-27-4023-2009.

Lau, W. K. M., and K.-M. Kim (2010), Fingerprinting the impacts of aerosols on long-term trends of the Indian summer monsoon regional rainfall,Geophys. Res. Lett., 37, L16705, doi:10.1029/2010GL043255.

Lawrence M.G, J. Lelieveld (2010), Atmospheric pollutant outflow from Southern Asia: a review, *Atmos Chem Phys*., 10.doi:10.5194/acp-10-11017.

Lee et al., (2003), Airborne measurement of inorganic ionic components of fine aerosol particles using the particle-intoliquid sampler coupled to ion chromatography technique during ACE-Asia and TRACE-P, *J. Geophys. Res.*, 108(D23), 8646, doi:10.1029/2002JD003265, 2003.

Lehahn, Y., Koren, I., Boss, E., Ben-Ami, Y., and Altaratz, O.: Estimating the maritime component of aerosol optical depth and its dependency on surface wind speed using satellite data, *Atmos. Chem. Phys*., 10, 6711–6720, doi:10.5194/acp-10-6711-2010, 2010.

Lelieveld, J., P. J. Crutzen, V. Ramanathan, et al., (2001), The Indian Ocean Experiment:Widespread air pollution from south and souteast Asia, *Science*, 291, 1031-1036

Leon, J.-F. et al., (2001), Large scale advection of continental aerosols during INDOEX*, J. Geophys. Res*., 106(D22), 28,427– 28,440.

Levy, R. C., L. A. Remer, S. Mattoo, E. F. Vermote, and Y. J Kaufman (2007), Second generation operational algorithm: Retrieval of aerosol properties over land from inversion of Moderate Resolution Imaging Spectroradiometer spectral reflectance, *J. Geophys Res.,* 112(13), 1–21.

Levy, R. C., S. Mattoo, L. A. Munchak, L. A. Remer, A. M. Sayer, F. Patadia, and N. C. Hsu (2013), The Collection 6 MODIS aerosol products over land and ocean, *Atmos. Meas. Tech*., 6,doi:10.5194/amt-6-2989-2013.

Lewis, E. and Schwartz, S (2004), Sea salt aerosols production: mechanisms, methods, measurements and models: a critical review, American Geophysical Union, Washington, DC.

Li H., F. Duan, K. He, Y. Ma, T. Kimoto and T. Huang (2016), Size-Dependent Characterization of Atmospheric Particles during Winter in Beijing Atmosphere 2016, 7, 36; doi:10.3390/atmos7030036.

Li X., L. Wang, D. Ji , T. Wen , Y. Pan, Y. Sun, Y. Wang (2013), Characterization of the size-segregated water-soluble inorganic ions in the Jing-Jin-Ji urban agglomeration: Spatial/temporal variability,size distribution and sources, *Atmospheric Environment.,* 77, 250e259, http://dx.doi.org/10.1016/j.atmosenv.2013.03.042b

Li, F., and V. Ramanathan (2002), Winter to summer monsoon variation of aerosol optical depth over the tropical Indian Ocean. *J. Geophys. Res*., 107, 4284, doi:10.1029/ 2001JD000949.

Li, R. R., Kaufman, Y. J., Gao, B. C., and Davis, C. O.: Remote sensing of suspended sediments and shallow coastal waters, *IEEE T. Geosci. Remote*, 41, 559–566, 2003.

Li, X., S. Wang, L. Duan, J. Hao, C. Li, Y. Chen, L. Yang, (2007) Particulate and tracegas emissions from open burning of wheat straw and corn stove in China. *Environ. Sci. Technol*. 41, 6052e6058.c

Lin, C.I., M. Baker, R.J. Charlson (1973), Absorption coe$cientof atmospheric aerosol: a method for measurement. *Applied Optics,* 12 (6), 1356}1363.

Lindesay, J. A., M. O. Andreae, J. G. Goldammer, G. Harris, H. J. Annegarn, M. Garstang, R. J. Scholes, and B. W. van Wilgen (1996), International Geosphere-Biosphere Programme/International Global Atmospheric Chemistry SAFARI-92 field experiment: Background and overview, *J. Geophys. Res*., 101, 23,521 – 23,530

Lovett R.F., (1978), Quantitative measurement of airborne sea-salt in the North Atlantic. Tellus 30: 358–363.

Mahadevan, T. N., B. S. Negi, and V. Meenakshy (1989), Measurements of elementalcomposition of aerosol matter and precipitation from a remote background site in India, *Atmos. Environ*., 23, 869-874.

Malm, W. C., J. F. Sisler, D. Huffman, R. A. Eldred, and T. A. Cahill (1994), Spatial andseasonal trends in particle concentration and optical extinction in the United States, *J.Geophys. Res*., 99(D1), 1347-1370.

Manoli, E., D. Voutsa, and C. Samara, (2002), Chemical Characterization and Source Identification/Apportionment of Fine and Coarse Air Particles in Thessaloniki, Greece. *Atmos. Environ*., 36: 949–961.

Maring, H., D. L. Savoie, M. A. Izaguirre, C. McCormick, R. Arimoto,J. M. Prospero, and C. Pilinis, Aerosol physical and optical propertiesand their relationship to aerosol composition in the free troposphere atIzan˜a, Tenerife, Canary Islands during July 1995, *J. Geophys. Res*., 105,14,677– 14,700, 2000

Mark, D. (1998), Atmospheric Aerosol Sampling, in Atmsopheric Particles, edited byR.M. Harrison and R. Van Grieken, pp. 29-94, John Wiley & Sons.

Markowicz, P. J., J. Fltau, R. Zewska, M. Witek, E. A. Reid, J. S. Reid, A. Bucholz, and B. Holben, Observations and Modeling of the Surface Aerosol Radiative Forcing during UAE2 K. M. DOI: 10.1175/2007JAS2555.1 © 2008 American Meteorological Society.

Matsuki, A., B. Quennehen, A. Schwarzenboeck, S. Crumeyrolle, H. Venzac, P. Laj, and L. Gomes, (2010), Temporal and vertical variations of aerosol physical and chemical properties over West Africa: AMMA aircraft campaign in summer 2006, *Atmos. Chem. Phys.,* 10, 8437–8451, doi:10.5194/acp-10-8437- 2010.

McCormick, M. P., L. W. Thomason, and C. R. Trepte (1995), Atmospheric effects of theMt. Pinatubo eruption, *Nature*, 373, 399-404.

McCormick, M.P., J.M. Zawodny, R.E. Veiga, J.C. Larsen, P.H. Wang (1989), An overview of sage I and II ozone measurements, *Planetary and Space Science*, , 37, 12, 1567

McCartney, E. J (1976), Optics of the atmosphere, John Wiley, New York.

McMurry, P. H. (2000), A review of atmospheric aerosol measurements, *Atmos. Environ.*, 34(12– 14), 1959– 1999.

McMurry, P. H., X. Wang, K. Park, and K.Ehara (2002), The RelationshipBetween Mass and Mobility for Atmospheric Particles: A New Technique for Measuring Particle Density, *Aerosol Sci. Technol*., 36:227–238.

Meehl, G. A., J.M. Arblaster, and W.D. Collins (2008), Effects of black carbon aerosols on the Indian monsoon, *J. Climate*, 21, doi:10.1175/2007JCLI1777.1.

Mekler, Y., H. Quenzel, G. Ohring, and I. Marcus (1977), Relative atmospheric aerosol content fromERTS observations*, J. Geophys.Res*., 82, 967-970,.

Menon. S., J. Hansen, L. Nazarenko, and Y. Luo (2002), Climate effects of black carbon aerosols in China and India, *Science*, 297, 5590, 2250–2253.

Mie, G., 1908. Beitraege zur Optik trueber Medien, speziell kolloidaler Metalosungen. Annales de Physik 25, 377-445.

Mishra, M.K., K. Rajeev, B.V. Thampi, A.K.M. Nair (2013), Annual variations of the altitude distribution of aerosols and effect of long-range transport over the southwest Indian Peninsula, *Atmos. Environ.*, 81, 51e, http://dx.doi.org/10.1016/j.atmosenv.2013.08.066.

Mohanty, U. C. (1994), Tropical cyclones in the Bay of Bengal and deterministic methods for prediction of their trajectories, *Sadhana*., 19, 567-582.

Monahan, E. C., K. L. Davidson, and D. E. Spiel (1982), White cap aerosol productivity deduced from simulation tank measurements, *J. Geophys. Res*., 87, 8898-8904.

Moore, R. M., and N. V. Blough (2002), A marine source of methyl nitrate, *Geophys. Res. Lett*., 29(15), doi:10.1029/2002GL014989.

Moorthy, K. K., P. R. Nair, B. V. K. Murthy (1991), Size distribution of coastal aerosols: effects of local sources and sinks, *J. Appl. Meteorol*. 30, 844–852.

Moorthy, K. K. and S.K. Satheesh (2000), Characteristics of aerosols over a remote island,Minicoy in the Arabian Sea: optical properties and retrieved size characteristics, *Q. J.Roy. Meteorol. Soc*., 126, 81–109.

Moorthy, K. K., et al. (1999), Aerosol climatology over India. 1 – ISRO GBP MWR network and database, ISRO/GBP, SR-03-99.

Moorthy, K. K., S. K. Satheesh and B.V .Krishna Murthy (1997), Investigations of Marine Aerosols over the Tropical Indian Ocean, *J. Geophys. Res*., 102, 18,827-18,842, doi: 10.1029/97JD01121.

Moorthy K.K, S.K. Satheesh (2002), Characteristics of aerosols over a remote island, Minicoy in the Arabian Sea: Optical properties and retrieved size characteristics, *Q J Roy Meteorol Soc*., 126: 81– 109.

Moorthy, K. K., Pillai, P.S., Babu, S. S. (2003), Influence of changes in the prevailing synoptic conditions on the response of aerosol characteristics to Land-and Seabreeze circulations at a coastal station, *Boundary Layer Meteorol.*108, 145–161.

Moorthy, K. K., S. S. Babu, S. V. Sunilkumar, P. K. Gupta, and B. S. Gera (2004), Altitude profiles of aerosol BC, derived from aircraft measurements over an inlandurban location in India, *Geophys. Res. Lett*., 31, L22103, doi:10.1029/2004GL021336.

Moorthy, K. K., et al., (2005), Wintertime spatial characteristics of boundary layer aerosols over peninsular India, *J. Geophys. Res*., 110, D08207, doi:10.1029/2004JD005520.

Moorthy K.K, S.K. Satheesh, S.S. Babu, C.B.S. Dutt (2008), Integrated Campaign for Aerosols, gases and Radiation Budget (ICARB): An overview, *J Earth Sys Sci*., 117: 243–262

Moorthy, K. K., S. K. Satheesh, S. S. Babu and C. B. S Dutt (2008), Integrated Campaignfor Aerosols, gases and Radiation Budget (ICARB): An Overview, *J. Earth. Sys. Sci*., 117, 243-262.

Moorthy, K. K., et al. (2010), Optical and physical characteristics of Bay of Bengal aerosols during WICARB: Spatial and vertical heterogeneities in the marine atmospheric boundary layer and in the vertical column. *J. Geophys. Res.*, 115, doi:10.1029/2010jd014094.

Moorthy, K.K., S. S. Babu, M. R. Manoj and S. K. Satheesh (2013), Buildup of aerosols over the Indian Region, *Geophys. Res. Lett*, 40, 1011–1014, doi:10.1002/grl.50165, 2013

Morlok, A., M. Kohler, J. E. Bowey, and M. M. Grady (2006), FT–IR microspectroscopy of extraterrestrial dust grains: Comparison of measurement techniques, Planet. Space

Mouli, P. C., S. V. Mohan, V. Balaram, M. P. Kumar, and S. J. Reddy (2006), A study ontrace elemental composition of atmospheric aerosols at a semi-arid urban site usingICP-MS technique, *Atmos. Environ*., 40, 136-146.

Mouli , P.C., K. Kawamura, T. Swaminathan, E. Tachibana (2011), Stable carbon isotopic composition of total carbon, dicarboxylic acids and glyoxalic acid in

tropical Indian aerosols: Implications for sources and photochemical processing of organic aerosols. *J. Geophys. Res.*, 116, D18307.

Mulcahy, J. P., O'Dowd, C. D., Jennings, S. G., and Ceburnis, D.: Significant enhancement of aerosol optical depth in marine air under high wind conditions, *Geophys. Res. Lett.*, 35, L16810, doi:10.1029/2008GL034303, 2008.

Murty, A. S. R., and Bh. V. Ramanamurty (1969), Chemical composition of rain wateracross western ghats, *Indian J. Meteorol. Geophys*.,20, 395-400.

Nagai, T., Liley, B., Sakai, T., Shibata, T., and Uchino, O.: Postpinatubo evolution and subsequent trend of the stratospheric aerosol layer observed by mid-latitude lidars in both hemispheres, SOLA, 6, 69–72, 2010.

Nair, P. R. (1993), Studies on atmospheric aerosols, Ph.D. Thesis, University of Kerala.

Nair, P. R, K. Parameswaran, A. Abraham, and S. Jacob (2005), Wind-dependence of sea-salt and non-sea-salt aerosols over the oceanic environment, *J. Atmos. Solar Terr. Phys*., 67, 884-898.

Nair, P.R., S.K George, S.V. Sunilkumar, K. Parameswaran, S. Jacob, A. Abraham, (2006), Chemical composition of aerosols over peninsular India during winter. *Atmos. Environ.,* 40,6477–6493.

Nair P.R., S.K. George, K. Parameswaran, M. Aloysius, D.P. Alappattu, M. Mohan, P.K. Kunhikrishnan (2009), Short-term changes in the aerosol characteristics at Kharagpur (22°19′N, 87°19′E) during winter, *J Atmos Sol Terres Phys* 71: 1771–1783.

Nair, P. R., S. K. George, S. Aryasree, and S. Jacob (2014), Chemical composition of aerosols over Bay of Bengal during pre-monsoon: Dominance of anthropogenic sources, *J. Atmos. Sol. Terr.Phy*., 109, doi:10.1016/201401004.

Nair, V. S., K. K. Moorthy, S. S. Babu and S. K Satheesh (2009), Optical and physical properties of atmospheric aerosols over the Bay of Bengal during ICARB, *J. Atmos. Sci.,* 66, 2640–2658,.

Nair, V. S., K. K. Moorthy, D. P. Alappattu, P. K. Kunhikrishnan, S. George, P. R. Nair,S. S. Babu, B. Abish, S. K. Satheesh, S. N. Tripathi, K. Niranjan, B. L. Madhavan, V.Srikant, C. B. S. Dutt, K. V. S. Badarinath, and R. R. Reddy (2007), Wintertime aerosol characteristics over the Indo-Gangetic Plain (IGP): Impacts of local boundary layer processes and long-range transport, *J. Geophys. Res*., 112, D13205, doi:10.1029/2006JD008099.

Nair, V. S., S. S. Babu, and K. K. Moorthy (2008), Aerosol characteristics in the marine atmospheric boundary layer over the Bay of Bengal and Arabian Sea during ICARB: Spatial distribution and latitudinal and longitudinal gradients, *J. Geophys. Res.,* 113, D15208, doi:10.1029/2008JD009823.

Nair, V.S., Moorthy, K.K. and Babu, S.S. (2008).Size Segregated Aerosol Mass Concentration measurements over the Arabian Sea during ICARB. *J. Earth Syst. Sci.*

Nair,V.S., S.K. Satheesh, K.K. Moorthy, S.S. Babu, P.R. Nair, S.K. George, (2010), Surprising observation of large anthropogenic aerosol fraction over the "near-

pristine" southern BayofBengal: climateimplications, *J. Geophys. Res*., 115, D21201, http://dx.doi.org/10.1029/2010JD013954.

Nakajima, T., et al., 2007: Overview of the Atmospheric Brown Cloud East AsianRegional Experiment 2005 and a study of the aerosol direct radiative forcing inEast Asia. *J. Geophys. Res*., **112**, D24S91.

Nambi, K. S. V., R. Raghunath, R. M. Tripathi, and R. N. Khandekar (1997), Scenario ofPb pollution and children in Mumbai: current air quality standard vindicated, *Energy Enivron. Monitor*, 13(2), 53-60.

Niranjan, K., B. Melleswara Rao, P. S. Brahmanandam, B. L. Madhavan,V. Sreekanth, and K. Krishna Moorthy (2005), Spatial characteristics ofaerosol physical properties over the northeastern parts of peninsular India, *Ann. Geophys*., 23, 3219–3227.

Niranjan, K., V. Sreekanth, B. L. Madhavan, and K. K. Moorthy (2007), Aerosol physical properties and Radiative forcing at the outflow region from the Indo-Gangetic plains during typical clear and hazy periods of wintertime, *Geophys. Res. Lett.*, 34, L19805, doi:10.1029/2007GL031224.

Norstrand Reinhold, New York, pp. 260}295.

Norton, C.C., F.R. Mosher, B. Hinton, D.W. Martin, D. Santik and W. Kuhlow, (1980), A model for calculating desert aerosol turbidity over ocean from geostationary satellite data. *J. Applied Meteorol.*, 19: 633-644.

O'Dowd, C. D., M. H. Smith, and S. G. Jennings (1993), Submicron particle, radon, and soot carbon characteristics over the northeast Atlantic, *J. Geophys. Res*., 98, 1123–1135.

O'Dowd, C. D., and M. C. Smith (1993), Physiochemical properties of aerosols over the northeast Atlantic: Evidence for wind speed related submicron sea-salt aerosol production, *J. Geophys. Res*., 98, 1137-1149.

O'Dowd, C. D., M. H. Smith, I. E. Consterdine, and J. A. Lowe (1997), Marine aerosol, sea-salt, and the marine sulphur cycle: A short review, *Atmos. Environ*., 31, 73–80.

O'Dowd, C. D., J. A. Lowe, and M. H. Smith (1999), Observations and modelling of aerosol growth in marine stratocumulus – Case study, *Atmos. Environ*., 33, 3053– 3062.

O'Dowd, C. D. (2001), Biogenic coastal aerosol production and its influence on aerosol radiative properties, *J. Geophys.Res.,* 106, 1545– 1550.

O'Dowd, C. D., et al. (2002a), A dedicated study of New Particle Formation and Fate in the Coastal Environment (PARFORCE): Overview of objectives and achievements, *J. Geophys. Res*., 107(D19), 8108,doi:10.1029/2001JD000555.

O'Dowd, C. D., et al. (2002b), Coastal new particle formation: Environmental conditions and aerosol physicochemical characteristics during nucleation bursts, *J. Geophys. Res*., 107(D19), 8107, doi:10.1029/ 2000JD000206

O'Dowd, C. D. and de Leeuw, G (2007), Marine aerosol production: a review of the current knowledge*, Phil. Trans. R. Soc. A*, 365,1753–1774.

O'Dowd, C. C. Scannell, J. Mulcahy, and S. G. Jennings (2010), Wind Speed Influences onMarine Aerosol Optical Depth, *Advances in Meteorology*, 830846, doi:10.1155/2010/830846

Ogorodnikov, B. I. (2002), Origin and components of radioactive aerosols on the coversite at the Chernobyl nuclear power plant, *Atomic Energy*, 93, 917-922.

Orellana, M. V., Matrai, P. A., Leck, C., Rauschenberg, C. D., Lee,A. M., and Coz, E (2011), Marine microgels as a source of cloud condensationnuclei in the high Arctic, *P. Natl. Acad. Sci.* USA, 108,13612–13617, doi:10.1073/pnas.1102457108, 2011.

Ott, L., B. Duncan, S. Pawson, P. Colarco, M. Chin, C. Randles, T. Diehl, and E. Nielsen (2010), Influence of the 2006 Indonesian biomass burning aerosols on tropical dynamics studied with the GEOS□5 AGCM, *J. Geophys. Res*., 115,D14121, doi:10.1029/2009JD013181.

Owega, S., B. U. Z. Khan, R. D'Souza, G. J. Evans, M. Fila, and R. E. Jervis, (2004), Receptor modeling of Toronto, PM2.5 characterizedby aerosol laser ablation mass spectrometry, *Environ. Sci. Tech*., 38, 5712–5720.

Williams, P. I., G. McFiggans, and M. W. Gallagher (2007), Latitudinal aerosol size distribution variation in the Eastern Atlantic Ocean measured aboard the FS-Polarstern, *Atmos. Chem. Phys*., 7, 2563–2573, 2007.

Shrestha, P., A. P. Barros, and A. Khlystov (2010), Chemical composition and aerosol size distribution of the middle mountain range in the Nepal Himalayas during the 2009 pre-monsoon season, *Atmos. Chem. Phys*., 10, 11605–11621, 2010, doi:10.5194/acp-10-11605

Pachauri T., A. Satsangi, V. Singla, A. Lakhani, K.M. Kumari (2013), Characteristics and sources of carbonaceous aerosols in $PM_{2.5}$ during wintertime in Agra, India, *Aerosol Air Qual Res* 13:977–991.

Pacyna, J. M. and Pacyna, E. G.: An assessment of global and regional emissions of trace metals to the atmosphere from anthropogenic sources worldwide, Environmental Reviews, 9, 269–298, 2001.

Pacyna, E. G., Pacyna, J. M., Fudala, J., Strzelecka-JastrzabE., Hlawiczka, S., Panasiuk, D., Nitter, S., Pregger, T., PfeifferH., and Friedrich, R.: Current and future emission of selected heavy metals to the atmosphere from anthropogenic sources in Europe*, Atmos. Environ*., 41, 8557–8566doi:10.1016/j.atmosenv.2007.07.040, 2007.

Pandithurai G, Dipu S, Dani KK, Tiwari S, Bisht DS, Devara PCS, Pinker RT (2008) Aerosol radiative forcing during dust events over New Delhi, India. *J. Geophys. Res.,* 113: D13209, doi:10.1029/2008JD009804.

Pant, P., P. Hegde, U. C. Dumka, R. Sagar, S. K. Satheesh, K. K. Moorthy, A. Saha, andM. K. Srivastava (2006), Aerosol characteristics at a high-altitude location in centralHimalayas: Optical properties and radiative forcing, *J. Geophys. Res.,* 111, D17206,doi:10.1029/2005JD006768.

Papastefanou, C., (2008), Radioactive aerosols, RADIOACTIVITY IN THE ENVIRONMENT, vol. 12, Elsevier, Series Editor

Parameswaran K., (1995), Influence of micrometeorological features on coastalboundary layer aerosol characteristics at the tropical station, Trivandrum, *Proc Indian Acad Sci (Earth Planet. Sci.*).,110, 247-265.

Parameswaran, K., R. Rajan, G. Vijayakumar, K. Rajeev, K. K. Moorthy, P. R. Nair and S. K. Satheesh, Seasonal and long term variation of aerosol content in the atmospheric mixing region at a tropical station on the Arabian Sea coast, *J. Atmos. Soalar Terr. Phys*., 60, 17- 25, 1998.

Parameswaran, K., (2001), Influence of micrometeorological features on coastal boundarylayer aerosol characteristics at the tropical station, Trivandrum, *Proc. Ind. Acad. Sci.*, 110(3), 247-265.

Parameswaran, K., S. V. Sunilkumar, K. Rajeev, Prabha R. Nair, and K. K. Moorthy (2004), Boundary layer aerosols at Trivandrum tropical coast, *Adv. Space Res*., 34, 838–844.

Parameswaran K., S.K Nair, K. Rajeev (2008), Impact of aerosols from the Asian continent on the adjoining oceanic environments, *J. Earth. Syst. Sci*., 17: 83–102.

Parashar, D. C., R. Gadi, T. K. Mandal, and A. P. Mitra (2005), Carbonaceous aerosolemissions from India, *Atmos. Environ*., 39, 7861-7871.

Paredes-Miranda, G., W. P. Arnott, J. L. Jimenez, A. C. Aiken, J. S. Gaffney, and N. A. Marley, (2009), Primary and secondary contributions to aerosol light scattering and absorption in Mexico City during the MILAGRO 2006 campaign, *Atmos. Chem. Phys*., 9, 3721–3730, doi:10.5194/acp-9-3721-2009.

Philippin, S., Laj, P., Putaud, J.-P.,Wiedensohler, A., de Leeuw,G., Fjaeraa, A., Platt, U., Baltensperger, U., and Fiebig, M.: EUSAARAn Unprecedented Network of Aerosol Observation in Europe, Earozoru Kenkyu, 24, 78–83, 2009

Pillai, P. S. (2003), Investigations on the physical characteristics of near surface aerosolsat a coastal station, Ph.D. Thesis, University of Kerala.

Pillai, P. S., and K. K. Moorthy (2001), Aerosol mass-size distributions at a tropicalcoastal environment: response to mesoscale and synoptic processes, *Atmos. Environ*., 35, 4099-4112.

Pillai, P. S., and K. K. Moorthy (2004), Size distribution of near-surfaceaerosols and its relation to the columnar aerosol optical depths, *Ann.Geophys*., 22, 3347– 3351.

Pio, C. A., et al., (2007), Climatology of aerosol composition (organic versus inorganic)at nonurban sites on a west-east transect across Europe, *J. Geophys. Res*., 112, D23S02,doi:10.1029/2006JD008038.

Pope, C. and Dockery, D (2006), Health effects of fine particulate air pollution: Lines that connect, *J. Air. Waste Manage. Assoc*., 56, 709–742.

Pope, C., Brook, R., Burnett, R., and Dockery, D (2011), How is cardiovascular disease mortality risk affected by duration and intensity of fine particulate matter exposure? An integration of the epidemiologic evidence, *Air. Qual. Atmos. Health*, 4, 5–14,doi:10.1007/s11869-010-0082-7,.

Pöschl, U., et al., (2005), Atmospheric aerosols: Composition, transformation,climate and health effects, *Angew. Chem.-Int. Edit*., 44, 7520–7540, 2005.

Pöschl, U., et al. (2010), Rainforest aerosols as biogenic nuclei of clouds andprecipitation in the Amazon, *Science*., 329(5998), 1513–1516.

Prakash, J. W. J. (1993), Atmospheric boundary layer studies at Thumba, Ph.D. Thesis,University of Kerala.

Price, C., J. Penner, and M. Prather (1997), NOx from lightning 1. Global distributionbased on lightning physics, *J. Geophys. Res*., 102(D5), 5929-5941.

Prijith, S. S., M. Aloysius, M. Mohan, N. Beegum, and K. K. Moorthy (2012), Role of circulation parameters in long range aerosol transport: Evidence from Winter-ICARB, *J. Atmos. Sol. Terr. Phys*., 77, 144-151.

Prijith, S. S., K. Rajeev, B. V. Thampi, S. K. Nair, and M. Mohan (2013), Multi-year observations of the spatial and vertical distribution of aerosols and the genesis of abnormal variations in aerosol loading over the Arabian Sea during Asian summer monsoon season, *J. Atmos. Sol. Terr. Phys*., 105–106,142-151.

Prospero, J. M., R. J. Charlson, V. Mohnen, R. Jaenicke, C. Delany, J. Moyere, W. Zoller, and K. Rahn (1983), The atmospheric aerosol system: An overview, *Rev. Geophys. and Space Phys*., 21(7), 1607-1629.

Prospero, J. M., M. Uematsu, and D. L. Savoie (1989), Mineral aerosol transport to the Pacific Ocean, in Chemical Oceanography, 10, 187-218, edited by J. P. Riley, Academic Press, New York.

Prospero, J. M. (2002), The Chemical and Physical Properties of Marine Aerosols: AnIntroduction, in Chemistry of Marine Water and Sediments, edited by A. Gianguzza, E.Pellizzetti and S. Sammarano, pp. 35-82, Springer-Verlag Berlin, Heidelberg.

Pruppacher, H.R., and J.D Klett, (1997), Microphysics of Clouds and Precipitation. Kluwer Acad., Norwell, Mass, 954 pp.

Putaud, J., et al., (2010), A European aerosol phenomenology-3: Physical and chemicalcharacteristics of particulate matter from 60 rural, urban, and kerbside sites across Europe, *Atmos. Environ*., 44, 1308–1320,doi:10.1016/j.atmosenv.2009.12.011, 2010.

Quinn, P. K., D. J. Coffman, V. N. Kapustin, T. S. Bates, and D. S. Covert (1998), Aerosoloptical properties in the marine boundary layer during ACE 1 and the underlying chemical and physical aerosol properties, *J. Geophys. Res*., 103, 16457-16563.

Quinn P.K., T.S Bates, D.J Coffman, T.L Miller, J.E Johnson, D.S Covert, J.P Putaud, C. Neusüß, and T. Novakov (2000), A comparison of aerosol chemical and optical properties from the 1st and 2nd Aerosol Characterization Experiments, *Tellus*., 52B: 239-257.

Quinn P.K., T.L Miller, T.S Bates, J.A Ogren, E. Andrews, G.E Shaw (2002), A 3-year record of simultaneously measured aerosol chemical and optical properties at Barrow, Alaska. *J. Geophys. Res.,* 107. doi:10.1029/2001JD001248.

Quinn, P. K., D. J. Coffman, T. S. Bates, T. L. Miller, J. E. Johnson, E. J. Welton, and C.Neusüß (2002), Aerosol optical properties during INDOEX 1999: Means, variability, and controlling factors, *J. Geophys. Res*., 107(D19), 8020, doi:10.1029/2000JD000037.

Quinn, P. K. and Bates, T. S (2011), The case against climate regulation via oceanic phytoplankton sulphur emissions, *Nature,* 480, 51–56, doi:10.1038/nature10580, 2011.

Radhakrishnan S.R., M. Satyanarayana. V. Krishnakumar, V. P. Mahadevan, and K.Reghunath (2009), Lidar measurements on aerosol characteristics at the tropical stations Trivandrum (8.330 N, 770 E) and Gadanki (13.50 N, 79.20 E), *IEEE*, 9781-4244-3941-6/09.

Raes, F., T. Bates, F.M. McGovern, and M. van Liederkerte, The second Aerosol Characterization Experiment (ACE-2): General overview and main results, *Tellus,* 52B, 111-126, 2000.

Rajeev, K., V. Ramanathan, and J. Meywerk (2000), Regional aerosol distribution and itslong-range transport over the Indian ocean, *J. Geophys. Res*., 105, 2029-2043

Rajeev, K., K. Parameswaran, B. V. Thampi, M. K. Mishra, A. K. M. Nair, S. Meenu (2010), Altitude distribution of aerosols over Southeast Arabian Sea coast during premonsoon season: Elevated layers, long-range transport and atmospheric radiative heating, *Atmos Environ*., 44, 2597-2604.

Ram, K., and Sarin, M.M. (2011). Day-night Variability ofEC, OC, WSOC and Inorganic Ions in Urban Environmentof Indo-Gangetic Plain: Implications to Secondary AerosolFormation. *Atmos. Environ*. 45: 460–468.

Ram, K., M.M. Sarin, and P. Hegde, (2008), AtmosphericAbundances of Primary and Secondary CarbonaceousSpecies at Two High-altitude Sites in India: Sources andTemporal Variability. *Atmos. Environ*. 42: 6785–6796.

Ram, K., M.M. Sarin, and S.N. Tripathi (2012), Temporal Trends in Atmospheric PM2.5, PM10, EC, OC, WSOCand Optical Properties of Aerosols from Indo-Gangetic Plain: Impact of Biomass Burning Emissions*. Environ.Sci. Technol*. 46: 686–695.

Ramachandran, S and A. Jayaraman (2002), Pre-monsoon aerosol mass loadings and size distributions over the Arabian sea and the tropical Indian ocean, *J.Geophys. Res*.,

Ramachandran, S. (2005), Aerosol radiative forcing over Bay of Bengal and Chennai: comparison with maritime, continental, and urban aerosolmodels, J. Geophys. Res., 110, D21206, doi:10.1029/2005JD005861.

Ramachandran S., and T.A Rajesh (2007), Black carbon aerosol mass concentrations over Ahmedabad and urban location in western India: Comparison with

urban sites in Asia, Europe, Canada and the United State, *J Geophys Res*., 112. doi:10.1029/2006JD007488.

Ramachandran, S., S. Ghosh, A.Verma, and P.K. Panigrahi (2013), Multiscale periodicities in aerosol optical depth over India Environ. *Environ. Res. Lett*. 8, 014034.

Ramachandran, S., and Kedia, S., (2012), Radiative effects of aerosols over Indo-Gangeticplain: environmental (urban vs. rural) and seasonal variations. *Environ. Sci*.

Ramanathan V et al., (2001), Indian Ocean experiment: An integrated analysis of the climate forcing and effects of the great Indo Asian haze, *J Geophys Res* 106: 28,371–28,398.

Ramanathan V., P. J. Crutzen, J. T. Kiehl, D. Rosenfeld (2001), Aerosols, Climate, and the Hydrological Cycle, *Science* 294, 2119 (2001); DOI: 10.1126/science.10.

Ramanathan, V and G. Carmichael (2008), Global and regional climate changes due to black carbon, *Nature geoscience* 1 (4), 221-227.

Rao, Y. P (1976), Southwest Monsoon, Meteorol. Monogr. SynopticMeteorol.1/1976, 367 pp., India Meteorol. Dep., Delhi.

Rastogi, N., and M. M. Sarin (2005), Long-term characterization of ionic species inaerosols from urban and high-altitude sites in western India: Role of mineral dust andanthropogenic sources, *Atmos. Environ*., 39, 5541-5554.

Rastogi, N., Oakes, M., Schauer, J.J., Shafer, M.M., Majestic, B. and Weber, R.J. (2009). New Technique forOnline Measurement of Water-soluble Fe(II) in Atmospheric Aerosols. *Environ. Sci. Technol.* 43: 2425–2430, doi: 10.1021/es8031902

Reid, J. S., and H. B. Maring (2003), Foreword to special section on the Puerto Rico Dust Experiment (PRIDE), *J. Geophys. Res*., 108(D19), 8585,doi:10.1029/2003JD0035102003.

Reid, J. S., E. A. Reid, A. Walker, S. Piketh, S. Cliff, A. A. Mandoos, S.-C. Tsay, and T. F. Eck (2008), Dynamics of southwest Asian dust particle sizecharacteristics with implications for global dust research, *J. Geophys. Res*., 113, D14212, doi:10.1029/2007JD009752.

Reist P. C.: Aerosol Science and Technology (second edition). McGraw-Hill, NewYork 1993.

Remer, L.A., S. Gasso, D.A. Hegg, Y.J. Kaufman, and B.N. Holben (1997) , Urban/industrial aerosol:Ground-based Sun/sky radiometer and airborne in situ measurements, *J. Geophys.Res.,*102, 16 849-16 859, 1997.

Remer, L. A., et al. (2002), Validation of MODIS aerosol retrieval over ocean. *Geophys. Res. Lett*., 29 (12), 1-4.

Remer, L. A., Tanre, D., Kaufman, Y. J., Ichoku, C., Mattoo, S., Levy, R., Chu, D. A., Holben, B., Dubovik, O., Smirnov, A., Martins, J. V., Li, R. R., and Ahmad, Z. (2002), Validation of MODIS aerosol retrieval over ocean, *Geophys. Res. Lett*., 29, MOD3.1– MOD3.4, doi:10.1029/2001GL013204, 2002.

Remer, L. A., Kaufman, Y. J., Tanre, D., Mattoo, S., Chu, D. A., Martins, J. V., Li, R. R., Ichoku, C., Levy, R. C., Kleidman, R. G., Eck, T. F., Vermote, E., and Holben, B. N (2005), The MODIS aerosol algorithm, products, and validation*, J. Atmos. Sci*., 62, 947–973, doi:10.1175/JAS3385.1, 2005.

Remer, L. A., Kleidman, R. G., Levy, R. C., Kaufman, Y. J., Tanré, D., Mattoo, S., Martins, J. V., Ichoku, C., Koren, I.,Yu, H. and Holben, B. N (2008), Global aerosol climatology from the MODIS satellite sensors, *J. Geophys. Res.-Atmos*., 113, D14S07, doi:10.1029/2007JD009661, 2008.

Rengarajan, R., M. M. Sarin, and A. K. Sudheer (2007), Carbonaceous and inorganicspecies in atmospheric aerosols during wintertime over urban and high-altitude sites inNorth India, *J. Geophys. Res*., 112, D21307, doi:10.1029/2006JD008150.

Rosenfield, J.E., (1992), Radiative effects of polar stratospheric clouds during the Airborne Antarctic Ozone Experiment and the Airborne Arctic Stratospheric Expedition10.1029/91JD02019.

Ruellan S. and Cachier H. (2001), Characterization of fresh particulate vehicular exhausts near a Paris high flow road. *Atmos. Environ*., 35: 453-468.

Russell, P. B., P. V. Hobbs, and L. L. Stowe (1999), Aerosol properties and radiativeeffects in the United States East Coast haze plume: An overview of the TroposphericAerosol Radiative Forcing Observational Experiment (TARFOX), *J. Geophys. Res*.,104(D2), 2213–2222.

Russell, P. B., M. Kacenelenbogen, J. M. Livingston, O. P. Hasekamp, S. P. Burton, G. L. Schuster, M. S. Johnson, K. D. Knobelspiesse, J. Redemann, and S. Ramachandran (2014), A multiparameter aerosol classification method and its application to retrievals from spaceborne polarimetry, *J. Geophys. Res. Atmos*., 119, 9838–9863, doi:10.1002/2013JD021411.

Russo, R., et al., (2003), Chemical composition of Asian continental outflow over the western Pacific: Results from Transport and Chemical Evolution over the Pacific (TRACE-P), *J. Geophys. Res*., 108(D20), 8804, doi:10.1029/2002JD003184.

Ryder , E. J. Highwood , P. D. Rosenberg , J. Trembath , J. K. Brooke , M. Bart, A. Dean , J. Crosier , J. Dorsey , H. Brindley , J. Banks , J. H. Marsham , J. B. McQuaid , H. Sodemann, and R. Washington (2013), Optical properties of Saharan dust aerosol and contribution from the coarse mode as C. L. measured during the Fennec 2011 aircraft campaign, *Atmos. Chem. Phys*., 13, 303–325, 2013 www.atmos-chem-phys.net/13/303/2013/ doi:10.5194/acp-13-303-2013

Sakerin S. M. et al., (2015), On measurements of aerosol-gas composition of the atmosphereduring two expeditions in 2013 along the Northern Sea Route. *Atmos. Chem. Phys.,* 15, 12413–12443, 2015, www.atmos-chem-phys.net/15/12413/2015/doi:10.5194/acp-15-12413.

Sadasivan, S., and B. S. Negi (1990), Elemental characterization of atmospheric aerosols, *Sci. Total Environ.,* 96, 269-279.

Safai P.D., P.S.P. Rao, G.A. Momin, K. Ali, S.Tiwari, M.S. Naik and J.C. Kuniyal (2004), Chemical composition of size - separated aerosols at two rural locations in the Himalayan region. *Ind. J. Radio and Space Phys*. 30: 270-277.

Safai, P.D., P.S.P. Rao, G. A. Momin, K. Ali, D. M. Chate, P. S. Praveen and P. C. S. Devara. (2005), Variation in the Chemistry of Aerosols in two Different Winter Seasons at Pune and Sinhagad, India Aerosol and Air Quality Research, Vol. 5, No. 1, pp. 115-126, 2005

Sahu L.K., and V. Sheel (2013), Saptio-temporal variation of biomass burning sources over South and South East Asia, *J. Atmos .Chem.,* 71. doi:10.10007/s10874-013-9275-4.

Salcedo et al., (2006), Characterization of ambient aerosols in Mexico City during the MCMA-2003 campaign with Aerosol Mass Spectrometry: results from the CENICA Supersite, *Atmos. Chem. Phys*., 6, 925–946, 2006, http://www.atmos-chem-phys.net/6/925/2006/.

Salomonson, V. V., Barnes, W. L., Maymon, P. W., Montgomery, H. E., and Ostrow, H.: MODIS: Advanced facility instrument for studies of the Earth as a system, *IEEE T. Geosci. Remote*, 27, 145–153, 1989.

Sanderson P, Delgado-Saborit JM, Harrison RM. A review of chemical and physical characterization of atmospheric metallic nano particles. *Atmos Environ.* 2014;94:353–65

Satheesh, S. K., V. Ramanathan, X. Li-Jones, J. M. Lobert, I. A. Podgorny, J. M.Prospero, B. N. Holben, and N. G. Loeb (1999), A model for the natural andanthropogenic aerosols over the tropical Indian Ocean derived from Indian OceanExperiment data, *J. Geophys. Res*., 104(D22), 27421-27440.

Satheesh, S. K., and J. Srinivasan (2002), Enhanced aerosol loading over Arabian Seaduring the pre-monsoon season: Natural or anthropogenic?, *Geophys. Res. Lett.,* 29, 1874, doi:10.1029/ 2002GL015687.

Satheesh, S. K., K. K. Moorthy, and I. Das (2001), Aerosol spectral optical depths overthe Bay of Bengal, Arabian Sea and Indian Ocean, *Curr. Sci*., 81(12), 1617-1625.

Satheesh, S.K., et. al., (2002), Physical, chemical, and radiative properties of Indian Ocean aerosols. *J. Geophys. Res.,* 10.1029/2002JD002463.

Satheesh K, J. Srinivasan, K.K Moorthy (2006), Spatial and temporal heterogeneity in aerosol properties and radiative forcing over Bay of Bengal: Sources and role of aerosol transport, *J. Geophys. Res* .,111. doi:10.1029/2005jd006374.

Sato, M., James E. Hansen,M. Patrick McCormick,James B. Pollack (1993), Stratospheric aerosol optical depths, 1850–1990, 10.1029/93JD02553 *J. Geophys. Res.,* Atmospheres.

Savoie, D. L., J. M. Prospero, and E. S. Saltzman (1989), Nitrate, non-seasalt sulfate and methanesulfonate over the Pacific Ocean, in Chemical Oceanography, 10th ed., edited by J. P. Riley, pp. 219-250, Academic Press, New York.

Savoie D.L, J.M Prospero, R. Arimoto, R.A Duce (1994), Non-sea-salt sulfate and methane sulfonate at American Samoa, *J. Geophys. Res* .,99:3587–3596.

Savoie, D. L., R. Arimoto, W. C. Keene, J. M. Prospero, R. A. Duce, and J. N. Galloway, Marine biogenic and anthropogenic contributions to non-sea-salt sulfate in the marine boundary layer over the North Atlantic Ocean, *J. Geophys. Res*., 107(D18), 4356,doi:10.1029/2001JD000970, 2002

Schwartz, S. E., Arnold, F., Blanchet, J.-P., Durkee, P.A., Hofmann, D. J., Hoppel, W. A., King, M. D., Laos, A. A., Nakajima, T., Ogren, J. A., Toon, O. B., and Wendisch, M.: Group Report: Connections between aerosol properties and forcing of climate, John Wiley, Hoboken, N. J., pp. 251–280, 1995.

Seinfeld, J. H., and S. N. Pandis (2006), Atmospheric Chemistry and Physics, John Wiley, New York.

Shettle, E. P., and R. W. Fenn (1979), Models for the aerosols of the lower atmosphere andthe effects of humidity variations on their optical properties, AFGL TR 79-0214,Environmental research paper No. 676, Air Force Geophysics Laboratory, MA, USA.

Shindell et al., (2013), Radiative forcing in the ACCMIP historical and future climate simulations, *Atmos. Chem. Phys*., 13, 2939-2974, 2013 ,doi:10.5194/acp-13-2939-2013

Shrestha, A. B.,Wake, C. P., Dibb, J. E., Mayewski, P. A., Whitlow,S. I., Carmichael, G. R., and Ferm, M (2000), Seasonal variations inaerosol concentrations and compositions in the Nepal Himalaya, *Atmos. Environ*., 34, 3349–3363, 2000.

Sikka, D. R. (2002), Developments in tropospheric aerosols studies inIndia, *Indian J. Radio Space Phys*., 31, 391– 403.

Singh, A., Neeraj Rastogi2, Anil Patel2, R.V. Satish2, Darshan Singh1Size-Segregated Characteristics of Carbonaceous Aerosols over the Northwestern Indo-Gangetic Plain: Year Round Temporal Behavior, *Aerosol and Air Quality Research*, 16: 1615–1624, doi: 10.4209/aaqr.2016.01.0023.

Singh, R.P., Dey, S., Tripathi, S.N., Tare, V., 2004. Variability of aerosol parametersover Kanpur, northern India. *J. Geophys. Res.* 109 http://dx.doi.org/10.1029/2004JD004966.

Singh, S., Nath, S., Kohli, R., and Singh, R (2005) Aerosols over Delhi during pre-monsoon months: Characteristics and effectson surface radiation forcing, *Geophys. Res. Lett.,* 32, L13808, doi:10.1029/2005GL023062, 2005.

Slinn, A., and W.G. N. Slinn (1980), Predictions for particle deposition on natural waters, Atmos. Environ., Vol 14. pp. 1013. 1016. Pergamon Press Ltd. 1980. Printed in Great Britain.

Smith M.H, I.E Consterdine, P.M Park (1989), Atmospheric loadings of marine aerosol during a Hebridean cyclone, *Q J Roy Meteorol Soc*.,115: 383-395.

Smith S.R., M.A Bourassa, R.J Sharp (1999), Establishing more truth in true winds, *J Atmos Ocean Technol* 16: 939–952.

Soni, V. K. and Sarkar, J. (2006), Long term variation in precipitation acidity over the Indian Global Atmosphere Watch (GAW) stations, *Asian. J. Water, Env. and Poll*., 3, 2, 35-41.

Srinivas B., A. Kumar, M.M Sarin, A.K Sudheer (2011), Impact of continental outflow on chemistry of atmospheric aerosols over tropical Bay of Bengal, *Atmos Chem Phys Dis.*,11: 20667–20711.

Srivastava, A. K., P. C. S. Devara, Y. J.Rao, Y.Bhavani kumar,and D. N.Rao (2008), Aerosol optical depth, ozone and water vapour measurements over Gadanki, a tropical station in peninsular India, *Aerosol Air Qual. Res*., 8(4), 459–476.

Srivastava, A.K., S. Singh, P. Pant, U.C. Dumka (2012), Characteristics of black carbon over Delhi and Manora Peak — a comparative study, *Atmos. Sci. Lett*. 13, 223–230.

Srivastava, M. K., Srivastava, S. K., Saha, A., Tiwari, S., Singh, S., Dumka, U. C., Singh, B. P., Singh, N. P (2005), Aerosol opticalproperties over Delhi and Manora Peak during a rare dust event in early April 2005, *Int. J. Remote Sens*.

Steigvileˇcenkien˙e, VidmantasUlevicius,NinaProkopˇciuk, Dalia Jasinevi˘cien˙e, Observations of the aerosol particle number concentration in the marine boundary layer over the south-eastern Baltic Sea, OCEANOLOGIA, 55 (3), 2013. pp. 573–597doi:10.5697/oc.55-3.573

Stone, E.A., Yoon, S. and Schauer, J.J. (2011).Chemical Characterization of Fine and Coarse Particles in Gosan, Korea during Springtime Dust Events. *Aerosol Air Qual. Res.*, 11: 31–43.

Stull, R. B. (1988), An Introduction to Boundary Layer Meteorology, Springer, New York.

Sturges W.T., and G.E Shaw (1993), Atmospheric Environment. Part A. General Topics, Volume 27, Issues 17–18, December 1993, Pages 2969-2977doi:10.1016/0960-1686(93)90329-W.

Subrahamanyam, D. B., Gupta, K. S., Ravindran, S., and Krishnan,P.: Study of sea breeze and land breeze along the west coast ofIndian sub-continent over the latitude range 15_ N to 8_ N duringINDOEX IFP-99 (SK-141) cruise, *Curr. Sci. India*, 80, 85–88,2001.

Subrahamanyam D.B., N.V.P.K. Kumar, C.B.S. Dutt, T.J. Anurose, P.K. Kunhikrishnan, and M. Mohan (2011), Characterization of air-sea interaction processes over the Bay of Bengal during the winter phase of ICARB field experiment, *Atmos Res.*, 99(1): 97–111.

Sudheer AK, Rengarajan R, Sheel V (2015) Secondary organic aerosol over an urban environment in a semi–arid region of western India, *Atmos Pollut Res.,* 6:11–20.

Sudheer, A.K. and Rengarajan, R (2012), Atmospheric Mineral Dust and Trace Metals over Urban Environment in Western India during Winter, *Aerosol Air Qual Res*.,12: 923–933.

Sudheer. A. K, and M. M. Sarin (2008), Carbonaceous aerosols in MABL of Bay of Bengal, Influence of continental outflow, *Atmos Environ*., 42(18), 4089-4100.

Sumanth. E., K. Mallikarjuna, J. Stephen, M. Moole, V. Vinoj, S. K. Satheesh, and K. K. Moorthy (2004), Measurements of aerosol optical depths and black carbon over Bay of Bengal during post-monsoon season, *Geophys. Res. Lett.*, 31, doi:10.1029/2004GL020681.

Takami , A., T. Miyoshi, A. Shimono, S. Hatakeyama (2005), Chemical composition of fine aerosol measured by AMS at Fukue Island, Japan during APEX period**,** *Atmos. Environ.,* 39, Issue 27, Pages 4913–4924.

Tanré, D., Y. J. Kaufman, M. Herman, and S. Mattoo (1997), Remote sensing of aerosol properties over oceans using the MODIS/EOS spectral radiances, *J. Geophys. Res*., 102, 16971-16988.

Tanr´e, D., F. M. Br´eon, J. L. Deuz´e, O. Dubovik, F. Ducos, P. Franc¸ois, P. Goloub, M. Herman, A. Lifermann and F. Waquet (2011), Remote sensing of aerosols by using polarized, directional and spectral measurements within the A-Train: the PARASOL mission, *Atmos. Meas. Tech*., 4, 1383–1395, 2011, doi:10.5194/amt-4-1383-2011.

Tao, W.K., J.P. Chen, Z. Li, C. Wang, and C. Zhang (2012), Impact of aerosols on convective clouds and precipitation, *Rev. Geophys*., 50, RG2001, doi:10.1029/2011RG000369.

Tare, V., et al., (2006), Measurement of atmospheric parameters during ISRO/GBP Land Campaign II at a typical location in the Ganga Basin: 2. Chemical properties, *J. Geophys. Res*., 111, D23210,doi:10.1029/2006JD007279.

Taylor S.R., and S.M. McLennan (1995), The geochemical evolution of the continental crust, *Rev Geophys*., 33: 241-265.

Timmreck, C., 2012: Modeling the climatic effects of large explosive volcaniceruptions, *Climate Change*, **3**, 545–564.

Tindale, N., and P. Pease (1999), Aerosols over the Arabian Sea: Atmospheric transport pathways and concentrations of dust and sea salt. Deep Sea Research Part II: Tropical Studies in Oceanography, 46(8-9), 1577-1596, doi:10.1016/S0967-0645(99)00036-3.

Tiwari, S., Srivastava, A.K., Bisht, D.S., Parmita, P., Srivastava, M.K., Attri,S.D., 2013. Diurnal and seasonal variations of black carbon and PM2.5 over New Delhi, India: influence of meteorology, *Atmos. Res*. 125–126,50–62.

Tripathi, S. N., S. Dey, V. Tare, S. K. Satheesh, S. Lal, and S. Venkataramani (2005),Enhanced layer of black carbon in a north Indian industrial city, *Geophys. Res. Lett*., 32, L12802, doi:10.1029/2005GL022564.

Tsigaridis, M. Kroll, F. J. Dentener, Y. Balkanski, J. Lathi`ere, S. Metzger, D. A. Hauglustaine, and M. Kanakidou (2006), Change in global aerosol composition since preindustrial times, *Atmos. Chem. Phys*., 6, 5143–5162, 2006

Tunved, P., H. C. Hansson, V. M. Kerminen, J. Strom, M. Dal Maso,H. Lihavainen, Y. Viisanen, P. P. Aalto, M. Komppula, and M. Kulmala(2006), High natural aerosol loading over boreal forests, *Science.*, 312(5771), 261–263.

Tunved, P., J.Str¨om, and H.C. Hansson (2004), An investigation of processes controlling the evolution of theboundary layer aerosol size distribution properties at the Swedish background station Aspvreten, *Atmos. Chem. Phys*., 4, 2581–2592, 2004www.atmos-chem-phys.org/acp/4/2581/.

Turpin B.J.,and H.J. Lim (2001), Species contributions to $PM_{2.5}$ mass concentrations: revisiting common assumptions for estimating organic mass, *Aerosol Science and Technology.*, 35, 602–610.

Turpin BJ, Ho-Jin Lim (2000) Species contribution to $PM_{2.5}$ Mass Concentrations: Revisiting Common Assumptions for Estimating Organic Mass, *Aero. Sci. Tech*., 35: 602-610

Twomey, S. (1977), The influence of pollution on the shortwave albedo of clouds, *J.Atmos. Sci.,* 34, 1149-1152.

Tyson P.D., M. Garstang, R. Swap, P. Kallberg, and N. Edwards, An air transport climatologyfor subtropical southern Africa, *Int. J. Climatol*., 16, 256-291, 1996.

Usher C R, Michel A E, and Grassian V H, 2003. Reactions on mineral dust. *Chemical Review*, 103: 4883--4940.

Veefkind, J. P., de Leeuw, G., and Durkee, P. A.: Retrieval of Aerosol Optical Depth over Land using two angle view Satellite Radiometry during TARFOX, *Geophys. Res. Lett*., 25, 3135–3138, 1998.

Venkataraman, C., C. K. Reddy, S. Josson, and M. S. Reddy (2002), Aerosolsize and chemical characteristics at Mumbai, India during INDOEX-IFP(1999), *Atmos. Environ.*, 36, 1979–1991.

Verma, S., O. Boucher, C. Venkataraman, M. S. Reddy, D. Mu¨ ller, P. Chazette, and B. Crouzille (2006), Aerosol lofting from sea breeze during the Indian Ocean Experiment, *J. Geophys. Res,* 111, D07208, doi:10.1029/2005JD005953.

Vernier, L. W., J.P. Thomason, A. Pommereau, J. Bourassa, A. Pelon, A. Garnier, L. Hauchecorne, C. Blanot, Trepte, D. Degenstein, and F. Vargas (2011), Major influence of tropical volcanic eruptions on the stratospheric aerosol layer during the last decade, *Geophys. Res. Lett*., VOL. 38, L12807, doi:10.1029/2011GL047563.

Verver, G. H. L., Sikka, D. R., Lobert, J. M., Stossmeister, G., andZachariasse, M.: Overview of the meteorological conditions andatmospheric transport processes during INDOEX 1999, *J. Geophys.Res*., 106, 28399–28413, 2001.

Vignati, E., Facchini, M. C., Rinaldi, M., Scannell, C., Ceburnis, D.,Sciare, J., Kanakidou, M., Myriokefalitakis, S., Dentener, F., andO'Dowd, C. D.: Global scale emission and distribution of seaspray aerosol: sea-salt and organic enrichment, *Atmos. Environ.*,44, 670–677, 2010.

Vinoj, V., S. S. Babu, S. K. Satheesh, K. K. Moorthy, and Y. J. Kaufman (2004),Radiative forcing by aerosols over the Bay of Bengal region derived from shipborne,island-based, and satellite (Moderate-Resolution Imaging Spectroradiometer)observations, *J. Geophys. Res*., 109, D05203, doi:10.1029/2003JD004329

Waggoner, M. B. Baker, and R. J. Charlson, "Optical Absorption by Atmospheric Aerosols," Appl. Opt. 12, 896-896 (1973) http://www.opticsinfobase.org/ao/abstract.cfm?URI=ao-12-4-896

Wallace, J. V., and P. V. Hobbs (1977), Atmsopheric Science - An Introductory Survey,Academic Press, New York.

Wang, B (2006), The Asian Monsoon, Praxis publishing, Springer, Chichester, UK.

Wang, C (2004), A modeling study on the climate impacts of black carbon aerosols, *J. Geophys. Res*., 109, doi:10.1029/2003JD004084.

Wang, C (2007), Impact of direct radiative forcing of black carbon aerosols on tropical convective precipitation, *Geophys. Res. Lett*., 34, doi:10.1029/2006GL028416.

Warneck, P., (1988), Chemistry of the Natural Atmosphere, Academic Press Inc., San Diego, California, U.S.A., pp. 432–531.

Weber, R.J., M.R. Stolzenburg, S.N. Pandis, and P.H. McMurry (1998), Inversion of ultra"ne condensation nucleus counter pulse height distributions to obtain nanoparticle (3 to 10 nm) size distributions. *Journal of Aerosol Science*., 29 (5/6), 601}615.

Whitby, K. T. (1978), The physical characteristics of sulphur aerosols, *Atmos. Environ*., 12, 135-159.

Wilson, et al., 2015 A marine biogenic source of atmospheric ice-nucleating particles, *Nature*, 525, 234–238 (10 September 2015) doi:10.1038/nature14986

Winquist, A., J.J. Schauer, J.R. Turner, M. Klein, S.E. Sarnat (2015), Impact of ambient fine particulate matter carbon measurement methods on observedassociations with acute cardiorespiratory morbidity, *J. Expo. Sci. Environ. Epidemiol*., 25 (2), pp. 215–221

Witt, M., Baker, A. R., and Jickells, T. D.: Atmospheric tracemetals over the Atlantic and South Indian Oceans: Investigationof metal concentrations and lead isotope ratios in coastaland remote marine aerosols (2006), *Atmos. Environ*., 40, 5435–5451,doi:10.1016/j.atmosenv.2006.04.041.

Wolf, M. E., and G. M. Hidy (1997), Aerosols and climate: Anthropogenic emissionsand trends for 50 years, *J. Geophys. Res*., 102, 1113-1121.

Woodcock A.H., (1953), Salt nuclei in marine air as a function of altitude and wind force, *J Meteorol*., 10: 362-371.

Wu, Y. L., C. I. Davidson, D. A. Dolske, and S. I. Sherwood (1992), Dry depositiono f atmospheric ontaminantst:h e relative importance of aerodynamic, boundary layer, and surface resistances, *Aerosol Sci. Technol.,* 16, 65-81.

Wu, J. (1993), Production of spume drops by wind tearing of wave crests: The search for quantification, *J. Geophys. Res.*, 98, 18221-18227.

Xing, L., T.M. Fu, J. J. Cao, S. C. Lee, G. H. Wang, K. F. Ho, M.C. Cheng, C.F. You, and T. J. Wang (2013), Seasonal and spatial variability of the OM/OC mass ratios and high regional correlation between oxalic acid and zinc in Chinese urban organic aerosols, *Atmos. Chem. Phys*., 13, 4307–4318,doi:10.5194/acp-13-4307-2013.

Yi. B., P. Yang, A. Dessler, and A. M. da Silva (2015), Response of Aerosol Direct Radiative Effect to the East Asian Summer Monsoon, *IEEE Geoscience and Remote Sensig Letters*, 12, 10.1109/LGRS.2014.2352630.

Yoon, Y.J., D. Ceburnis, F. Cavalli, O. Jourdan, J.P. Putaud, M.C. Facchini, S. Descari, S. Fuzzi, , S.G. Jennings and C.D. O'Dowd. 2007. Seasonal characteristics of the physico-chemical properties of North Atlantic marine atmospheric aerosols. *J.Geophys. Res*., doi:10.1029/2005JD007044.

Young, S. A. and Vaughan, M. A.: The retrieval of pro- files of particulate extinction from Cloud-Aerosol Lidar Infrared Pathfinder Satellite Observations (CALIPSO) data: Algorithm description, *J. Atmos. Ocean. Technol*., 26, 1105–1119, doi:10.1175/2008JTECHA1221.1, 2009.

Yu, H., et al. (2006), A review of measurement-based assessments of the aerosol direct radiative effect and forcing, *Atmos. Chem.Phys*., 6, 613-666.

Zalpuri, K.S., Direct observations of aerosol radiative forcing over the tropical IndianOcean during the Jan-Feb 1996 Pre-INDOEX Cruise, *J. Geophys. Res*., **103**, 13827-13836, 1998.

Zhang, D., and Y. Iwasaka (1999), Nitrate and sulfate in individual Asian dust-storm particles in Beijing, China in spring of 1995 and 1996, *Atmos. Environ*., 33, 3213-3223.

Zhang, F., Y. Chen, C. Tian, X. Wang, G. Huang, Y. Fang, and Zong, Z (2014), Identificationand quantification of shipping emissions in Bohai Rim, China, *Sci. Total Environ*., 497–498, 570-577,10.1016/j.scitotenv.2014.08.016, 2014.

Zhang, Y.X., Shao, M., Zhang, Y.H., Zeng, L.M., He, L.Y., Zhu, B., Wei, Y.J., Zhu, X.L.,2007. Source profiles of particle organic matters emitted from cereal strawburnings. *J. of Environ. Sci.,* 19, 167e175.

Zhu L, Huang X, Shi H, Cai X, Xong Y (2011), Transport pathways and potential sources of PM10 in Beijing. *Atmos. Environ.,* 45:594–604.

Zhu. J., H. Liao, and J. Li (2012), Increases in aerosol concentrations over eastern China due to the decadal-scale weakening of the East Asian summer monsoon, *Geophys. Res. Lett*., VOL. 39, L09809, doi:10.1029/2012GL051428.

Zhuang, B.L., S. Li, T.J. Wang, J.J. Deng, M. Xie, C.Q. Yin, J.L. Zhu (2013), Direct radiative forcing and climate effects of anthropogenic aerosols with different mixing states over China, 79, 2013, 349–361,doi:10.1016/j.atmosenv.2013.07.004**.**

Zong, Z., X. Wang, C. Tian, Y. Chen, L. Qu, L. Ji, G. Zhi, J. Li, and G. Zhang (2016), Biomass burning contribution to regional $PM_{2.5}$ during winter in the North China, *Atmos. Chem. Phys. Discuss*., doi:10.5194/acp-2016-97, in review, 2016.